TÉCNICO LISBOA

UNIVERSIDADE DE LISBOA
INSTITUTO SUPERIOR TÉCNICO

Kinetic mechanisms in non-equilibrium plasmas: influence of N_2 on CO_2 dissociation and sensitivity analysis of computational models

Loann Terraz

Supervisor: Doctor Vasco António Dinis Leitão Guerra
Co-Supervisor: Doctor Olivier Guaitella

Thesis approved in public session to obtain the PhD Degree in

Technological Physics Engineering

Jury final classification: Pass with Distinction

2020

TÉCNICO LISBOA

UNIVERSIDADE DE LISBOA
INSTITUTO SUPERIOR TÉCNICO

Kinetic mechanisms in non-equilibrium plasmas: influence of N_2 on CO_2 dissociation and sensitivity analysis of computational models

Loann Terraz

Supervisor: Doctor Vasco António Dinis Leitão Guerra
Co-Supervisor: Doctor Olivier Guaitella

Thesis approved in public session to obtain the PhD Degree in

Technological Physics Engineering

Jury final classification: Pass with Distinction

Jury

Chairperson: Doctor Luís Paulo da Mota Capitão Lemos Alves, Instituto Superior Técnico, Universidade de Lisboa, Portugal

Members of the Committee:

Doctor Jan van Dijk, Faculty of Applied Physics, Eindhoven University of Technology, Netherlands

Doctor Vasco António Dinis Leitão Guerra, Instituto Superior Técnico, Universidade de Lisboa, Portugal

Doctor Gianpiero Colonna, Consiglio Nazionale delle Richerche - Istituto per la Scienza e Tecnologia dei Plasmi, Italy

Doctor Nuno Rombert Pinhão, Instituto Superior Técnico, Universidade de Lisboa, Portugal

2020

Acknowledgments

I first arrived in Portugal in September 2016, to deliver the final version of this PhD thesis in September 2020. Seeing the compilation of four years of work is something new to me and I cannot deny a certain satisfaction. On the other hand, four years ago I was imagining my current self as, somehow, more confident than I feel in my topic. But this is how research works: the more your learn, the more you discover about the knowledge you still lack. One thing is for sure, I did learn a lot during this period.

The realization of this work was only possible thanks to Vasco Guerra, who accepted to turn his project into a PhD thesis. During these last four years, he was elected 'Best supervisor of the world' by a totally-biased comity of fans. The explanation, in a few words, lies in an incredible availability for his students, excellent advice on substance and form, an endless motivation and, of course, a vast knowledge of red wines. I am also indebted to my second supervisor, Olivier Guaitella, who shares the above-mentioned qualities but cannot remove the fish bones from his plate alone. Hopefully, he was supervising Ana Sofia, who fixed his fish issues and greatly contributed to the results presented in this thesis. From the Lisbon team, I am very grateful to the other professors/post-docs who shared their experience with me, Luís Lemos Alves, Antonio Tejero-del-Caz, Nuno Pinhão, Mário Lino da Silva and Carlos Pintassilgo. Within this team, Tiago Silva certainly deserves a special mention for the large amount of time he spent to help me (and others at the same time!) and the numerous restaurants/drinks/fado/setas/pétanque we had. May MaxiCoco be with you. I must thank the students I met in Lisbon as well, Polina, Ridhima, Domenica, Fábio, Egor, João and Francisco, for their friendship, time, jokes and many more.

I could not have done this work without the help of my family. I am truly glad that they trusted me for this experience abroad and that they contributed so much to offer me the best chances. As a reward, and although the temptation is great, I will not risk a bad joke about their poor mental support here :) My last thanking words go to Flavia, who is sharing my life and undergoing my changing mood since a few years now. Merci pour tout ce que tu m'as apporté et ce que tu as supporté Doudou.

These four years were a very good experience. I especially enjoyed the opportunity to meet many different people, because sharing with them enriches my conception of things. Thanks to this, I fully realize how lucky I was to have this working and social environments[1]. I sincerely wish the best to all the people I mentioned above.

Toulouse, September 2020

Loann Terraz

[1] See, I am not pessimistic at all!

Resumo

A motivação por trás desta tese de doutoramento vem de duas questões cruciais que têm preocupado a sociedade atual: (i) o aquecimento global, devido à quantidade enorme de gases de efeito estufa libertada pelas atividades humanas e (ii) a rarefação de fontes de energia fóssil. O primeiro problema pode ser minimizado pela redução das emissões de CO_2, pois o dióxido de carbono é responsável por mais de metade do aquecimento global. A última questão é parcialmente resolvida pelo desenvolvimento de energias renováveis, que atualmente sofrem de uma produção intermitente e uma escassa rede de distribuição. Portanto, alcançar uma produção de energia com emissões líquidas nulas de CO_2 é uma etapa obrigatória, mas não suficiente. Ambas as questões seriam resolvidas capturando CO_2 da atmosfera e utilizando o CO resultante de sua dissociação como matéria-prima para converter, armazenar e distribuir eletricidade verde via combustíveis sintéticos, uma forma estável de energia que beneficiaria de uma rede de distribuição já bem desenvolvida. Um dos principais problemas para se desenvolver tal tecnologia em escala industrial é o alto custo energético da dissociação de CO_2, porque as reações que levam à criação de CO são altamente endotérmicas.

Este trabalho faz parte de um vasto esforço de modelação desenvolvido pela equipe N-PRiME do Instituto de Plasmas e Fusão Nuclear (IPFN), Instituto Superior Técnico (IST), para estudar plasmas de CO_2. O projeto geral do grupo aborda a questão da eficiência da dissociação de CO_2 com a perspectiva de se utilizar o CO produzido para formar combustíveis à base de hidrocarbonetos. Este estudo é motivado pela alta eficiência energética obtida por Fridman *et al.* e concentra-se na cinética de plasmas não térmicos, especialmente na viabilidade da dissociação baseada no mecanismo de *ladder-climbing*. Assume-se muitas vezes que o bombeamento (*pumping-up*) do modo de alongamento linear assimétrico do CO_2 é uma maneira de aumentar a eficiência da dissociação. De facto, é provável que as moléculas altamente excitadas por vibração se dissociem uma vez impactadas por um electrão, outra partícula pesada ou ”simplesmente” vibrando-as com amplitude suficiente. O modo de alongamento assimétrico é preferível em comparação ao modo de alongamento simétrico e ao modo de flexão, devido ao seu longo tempo de relaxação e às menores quantidades de energia necessária para alcançar a dissociação. Os plasmas não térmicos são considerados mais adequados porque podem conter uma fração maior de moléculas altamente vibrantes do que os plasmas térmicos.

A primeira parte deste trabalho investiga a influência do azoto na cinética de CO_2 em plasmas não térmicos. Curiosamente, o N_2 é bem conhecido desde a tecnologia de lasers de CO_2 pela sua capacidade de trocar facilmente quanta de vibrações com o modo de alongamento assimétrico do CO_2. O azoto também é uma impureza comum resultante da captura de CO_2 do ar e, portanto, a sua influência na cinética deve ser investigada. Os resultados apresentados nesta tese mostram que a inclusão de N_2 no plasma de CO_2 aumenta a fração de CO_2 que se dissocia. Um modelo físico, contando com 72 níveis vibracionais de CO_2, 10 de N_2 e $\sim$3000 reações diferentes foi desenvolvido para investigar os mecanismos dominantes em descargas luminiscentes de CO_2-N_2 DC. Tais descargas têm a vantagem de criar um plasma homogéneo, adequado para modelos 0-D. Além disso, a excitação vibracional é suficientemente baixa, o que permite uma validação passo a passo dos coeficientes de reação. Como

o rendimento da dissociação não é muito alto, o efeito dos produtos de dissociação (CO, O_2, etc.) pode ser a priori negligenciado. No entanto, verificou-se que as trocas de energia de conversão de vibrações nas colisões de CO_2-O e N_2-O podem ter uma forte influência na cinética vibracional e devem ser levadadas em consideração. O modelo foi validado comparando-se as simulações com medições temporais das concentrações de moléculas de CO_2 excitadas vibracionalmente. Os experimentos foram realizadas no Laboratoire de Physique des Plasmas (LPP), França, por A.-S. Morillo-Candas, em descargas luminescentes nanopulsados em correntes contínuas. O acordo entre os resultados é bom e dá-nos confiança no esquema cinético implementado no código. O aumento da dissociação resultante da adição de azoto é analisado, bem como a influência das paredes do reator e o efeito de desativação (*quenching*) dos átomos O. Paralelamente, eu tive a oportunidade de realizar experimentos extras no LPP, concentrando-me em descargas luminescentes em corrente contínuas constantes para diferentes misturas de plasmas de CO_2-N_2. As medições obtidas foram utilizadas para concluir a análise sobre a conversão aprimorada de CO_2 na presença de N_2 e definir uma base interessante para comparações numéricas, uma vez que o modelo será adaptado para descargas em correntes contínuas constantes.

A segunda parte deste trabalho é dedicada à criação de uma ferramenta de Análise de Sensibilidade (AS). Atualmente, o uso de simulações numéricas está se espalhando amplamente, com uma complexidade crescente permitida por progressos recentes nas ciências da computação. No entanto, à medida que a complexidade do modelo aumenta, a análise dos resultados pode também tornar-se mais difícil. Na comunidade dos plasmas não térmicos, é comum o uso de modelos físicos que contêm milhares de reações e dezenas de espécies. Devido à complexa interdependência que caracteriza esses sistemas, identificar os mecanismos mais ou menos influentes torna-se é uma tarefa desafiadora. Por isso, nós criámos uma ferramenta numérica capaz de classificar os parâmetros/inputs por ordem de influência, relativamente a um determinado output. Os interesses são múltiplos: remover as reações mais desprezáveis para simplificar o sistema, uma melhor compreensão da física subjacente, a identificação das seções eficazes mais críticas que frequentemente sofrem de grandes incertezas, etc. A AS realizada é baseada no método de amostragem de Morris, além de recentes melhorias sugeridas por outros autores. Em resumo, ele consiste em medir as variações nos outputs enquanto os parâmetros são tirados aleatoriamente dentro de um intervalo bem definido de valores. O procedimento foi testado num modelo de plasma frio de oxigénio cujas equações governantes são resolvidas pela ferramenta Lisbon KInetics (LoKI). Esse modelo considera 51 espécies distintas e 179 reações. A cinética do oxigénio é semelhante à cinética do CO_2, no sentido que compreende o mesmo tipo de mecanismos, porém é mais simples de modelar, o que a torna mais adequada para a fase de teste da ferramenta AS. Diferentes parâmetros da AS foram testados para otimizar o custo computacional mas mantendo uma classificação suficientemente precisa. Os resultados são consistentes com as reações reconhecidas como mais influentes, como mostrado por uma comparação com outro ranking de um modelo semelhante. Além disso, a ferramenta AS permitiu a identificação de reações indiretas muito influentes, onde a espécie, cuja variação é considerada, não aparece nas próprias reações. A capacidade deste método para classificar a influência dos inputs em sistemas complexos, o sua adaptabilidade a diferentes misturas e o seu custo computacional relativamente baixo fazem dele uma abordagem sistemática muito interessante

para a comunidade de plasmas frios.

A questão-chave que conduz o trabalho apresentado nesta tese é: como contribui o azoto para a dissociação de CO_2 em plasmas não térmicos? Responder a essa pergunta naturalmente exigirá investigações mais detalhadas, tais como: (i) acontece dissociação vibracional pura de CO_2? (ii) quais são os principais mecanismos cinéticos nos plasmas não térmicos de CO_2-N_2? (iii) como podemos identificá-los com confiança, considerando a alta complexidade do meio? A primeira parte da tese trata de (i) e (ii), embora limitada a condições operacionais específicas. A segunda parte da tese trata de (iii) através do desenvolvimento de uma ferramenta de análise global, testada pela primeira vez em um modelo de oxigênio.

Palavras-chave: Plasma não térmico, CO_2 conversão, N_2, Função de Distribuição de Vibração, Modelação, Análise de sensibilidade

Abstract

The motivation behind this PhD thesis comes from two critical concerns that all societies have to face nowadays: (i) global warming, due to the tremendous amount of greenhouse gases released by human activities and (ii) the rarefaction of fossil energy sources. The former issue can be minimized by reducing the CO_2 emissions, as carbon dioxide is responsible for more than half of the increase of the global warming. The latter issue is partially solved by the development of renewable energies, which are currently suffering from an intermittent production and a scarce distribution network. Therefore, reaching a production of energy with 0-net CO_2 emissions is a mandatory step but not a sufficient one. Both issues would be partially solved by capturing CO_2 from the atmosphere and using the CO resulting from its dissociation as a raw material to convert, store and distribute green electricity *via* synthetic fuels, a stable form of energy which benefits from an already well-developed distribution network. One of the main problems to develop such technology at an industrial scale is the high energy cost of CO_2 dissociation, as the reactions leading to CO creation are highly endothermic.

This work is part of a vast modeling effort developed by the N-PRiME team of Instituto de Plasmas e Fusão Nuclear (IPFN), Instituto Superior Técnico (IST), to study CO_2 plasmas. The overall group project addresses the issue of the CO_2 dissociation efficiency, in the perspective of using the CO produced to form hydrocarbon-based fuels. Motivated by the high energy efficiency obtained by Fridman *et al.*, the research focuses on the kinetics of non-thermal plasmas, especially on the viability of a ladder-climbing-based dissociation. Pumping-up the asymmetric stretching mode of CO_2 is assumed to be an efficient way to increase the dissociation efficiency. Indeed, highly vibrationally excited molecules are likely to dissociate once impacted by an electron, another heavy particle or 'simply' by vibrating strongly enough. The asymmetric stretching mode is favored because of its long relaxation time and smaller amounts of energy required to reach dissociation, as compared with the symmetric stretching mode and the bending mode. Non-thermal plasmas are suitable environments because they can contain a larger fraction of molecules highly vibrating than thermal plasmas.

The first part of this work focuses on the influence of nitrogen on CO_2 kinetics in non-thermal plasmas. Interestingly, N_2 is well-known since CO_2 lasers technology for its ability to easily exchange vibrational quanta with the asymmetric stretching mode of CO_2. Nitrogen is also a common impurity resulting from CO_2 capture from the air, hence its influence on the kinetics should be investigated. The results presented in this thesis show that including N_2 in a CO_2 plasma increases the fraction of CO_2 that dissociates. A physical model, accounting for 72 vibrational levels of CO_2, 10 of N_2 and ~ 3000 different reactions was developed to investigate the driving mechanisms in CO_2-N_2 DC glow discharges. Such discharges have the advantage of creating a homogeneous plasma, suitable for 0-D modeling. Moreover, the vibrational excitation is rather low, which allows a step-by-step validation of the reaction rate coefficients. As the dissociation yield is not very high, the effect of the dissociation products (CO, O_2, etc.) can *a priori* be neglected. However, it is found that vibration-translation energy exchanges in CO_2-O and N_2-O collisions can have a strong influence on the vibrational kinetics and should be taken into account. The model was validated by comparing the simulations with time-resolved measurements of the vibrationally excited CO_2

molecules. The experiments were performed at Laboratoire de Physique des Plasmas (LPP), France, by A.-S. Morillo-Candas, in nanosecond pulsed direct-current glow discharges. The agreement is good and gives us confidence in the kinetic scheme implemented in the code. The enhanced dissociation resulting from nitrogen addition is analyzed, as well as the influence of the reactor walls and the quenching effect from O atoms. In parallel, I had the opportunity to perform experiments at LPP, focusing on continuous direct-current glow discharges for different mixtures of CO_2-N_2 plasmas. The measurements obtained were used to complete the analysis about the enhanced CO_2 conversion in presence of N_2 and set an interesting basis for numerical comparisons once the model will be adapted to continuous discharges.

The second part of this work is dedicated to the creation of a Sensitivity Analysis (SA) tool. The use of numerical simulations is widely spreading nowadays, with a growing complexity allowed by recent progress in computing sciences. However, as model complexity grows, the analysis of the results may also become more difficult. In the non-thermal plasma community, it is common to use physical models with thousands of reactions and dozens of species. Due to the complex interdependence characterizing such systems, it is often a hard task to identify the most/least influential mechanisms. Therefore, we created a numerical tool able to rank the parameters/inputs by order of influence, relatively to a specific output. The interests are multiple: removing the most negligible reactions to simplify the system, a better understanding of the underlying physics, an identification of the most critical cross-sections often suffering from great uncertainties, etc. The SA performed is based on the Morris screening method, plus recent improvements suggested by other authors. In brief, it consists in measuring the variations in the outputs when parameters are randomly sampled within a well-defined range of values. The procedure was tested on an oxygen cold plasma model whose driving equations are solved by the Lisbon KInetics (LoKI) tool suite. This model accounts for 51 distinct species and 179 reactions. Oxygen kinetics are similar to CO_2 kinetics in the sense it comprises the same type of mechanisms, yet simpler to model, which is suitable for the testing phase of the SA tool. Different SA parameters were tested to optimize the computational cost while keeping an accurate-enough ranking. Results are consistent with the well-known most influential reactions, as shown by a comparison with another ranking from a similar model. In addition the SA tool allowed to identify indirect very influential reactions, where the species whose variation is considered does not appear in the reactions themselves. The capacity of this method to rank inputs' influence in very complex systems, its adaptability to different mixtures and its relatively low computational cost make it a very interesting systematic approach for the cold plasma community.

The key question driving the work presented in this thesis is: how does nitrogen contribute for CO_2 dissociation in non-thermal plasma? Answering this question will naturally ask for more detailed investigations, such as: (i) does pure vibrational CO_2 dissociation occur, (ii) what are the main kinetic mechanisms in CO_2-N_2 non-thermal plasmas, (iii) how can we trustfully identify them considering the high complexity of the medium? The first part of the thesis addresses (i) and (ii), albeit limited to specific operating conditions. The second part of the thesis addresses (iii) *via* the development of a global analyzing tool, first tested on an oxygen model.

Keywords: Non-Thermal Plasma (NTP), CO_2 conversion, N_2, Vibration Distribution Function (VDF), Modeling, Sensitivity Analysis

Contents

Chapter 1

Introduction

1.1 Motivation

1.1.1 The role of CO_2 in climate change

One of the main challenges of the 21st century is to limit the global temperature increase to a maximum of 1.5 $^\circ$C, as advised by the Intergovernemental Panel on Climate Change (IPCC) [1], to avoid dramatic consequences on the ecosystems and on our societies. For instance, the melting of the ice cap not only impacts the animals/plants living there: it also increases the overall warming, as less light from the Sun is reflected to space. Among the causes of the global warming, carbon dioxide (CO_2) is infamously known for being one of the main greenhouse gas. Its contribution to *radiative forcing*, a measure representing the increase of the global warming effect, is evaluated at 66% [2] among all other gases. Although the presence of CO_2 is mandatory to ensure a certain heat balance of the atmosphere, its concentration drastically increased since the last centuries: it has grown by 145% since 1750 [3, 4], to reach the highest concentration in the past 3 million years. The situation is so alarming that, at the United Nations Climate Action Summit (2019), about 70 countries have pledged to drastically reduce their net CO_2 emissions by 2030, some of them aiming for a 0 net emission by 2050 [5]. This goal cannot be reached without drastic societal and economical transformations. Human activity is widely recognized as the major source of CO_2 emissions [3], mainly *via* the use of fossil energies, representing $\sim$82% [6] of the world energy consumption (cf. fig 1.1). Therefore, a prerequisite for a 0 net CO_2 emission is the existence of alternative energy sources, and/or of efficient carbon capture and utilization techniques.

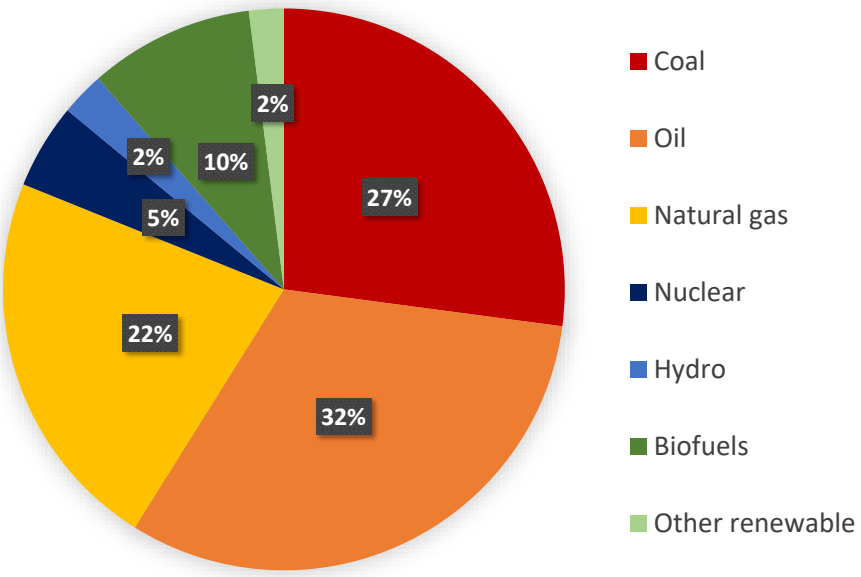

Figure 1.1: Data extracted from IEA [6], representing the Total Primary Energy Supply (TPES) in 2019. As changes in energy storage are small in a year, the TPES is a good estimation of the world energy consumption. The world TPES in 2019 was equal to 13972×10^6 tonne of oil equivalent (toe)

1.1.2 Renewable energies and CO_2 capture

The last decades have seen a tremendous development of renewable energies, most of them also called 'green energies', as they emit relatively low CO_2 quantities during their production lifecycle. The alternative they represent is however restricted to power production. Yet, the greenhouse gas emissions for electricity account for only a quarter of the total emissions related to energy. Therefore, it is important to keep in mind that even if the entire world power production had a 0 net CO_2 footprint, agriculture and transportation would still be the greatest sources of greenhouse gases. That being said, reaching this step is somewhat necessary and constant progress is made to achieve it.

The median CO_2 emissions of the main electricity supply technologies are evaluated in a report of IPCC [7], measured in equivalent grams of CO_2 released per kilowatt hour (gCO_2eq/kWh). With the exception of the cofiring biomass (740 gCO_2eq/kWh), all commercialized electricity supply technologies from renewable sources emit low quantities of CO_2, from $\sim$10 gCO_2eq/kWh for wind onshore/offshore to $\sim$40 gCO_2eq/kWh for geothermal and solar panels. It is much less than for coal and gas, at 820 gCO_2eq/kWh and 490 gCO_2eq/kWh respectively. Nuclear technologies are also well ranked, with 12 gCO_2eq/kWh, as only the supply chain releases CO_2 in the atmosphere.

Consequently, replacing coal and gas power production by green and nuclear technologies seems to be a promising way to reduce efficiently greenhouse gas emissions. However, many issues are still to be solved to reach this step. For instance, nuclear fission technologies go along with a potential risk of large and permanent disaster at human scale. The nuclear wastes are also a problem, because of their important activity and long lifetime. Renewable energies do not include such risks, but they are globally less powerful than coal, gas or nuclear power plants, hence requiring more infrastructures and maintenance. Solar and wind technologies also suffer from intermittent production and decentralization, as they depend on the weather conditions to reach their full capacity and as their full-capacity location is

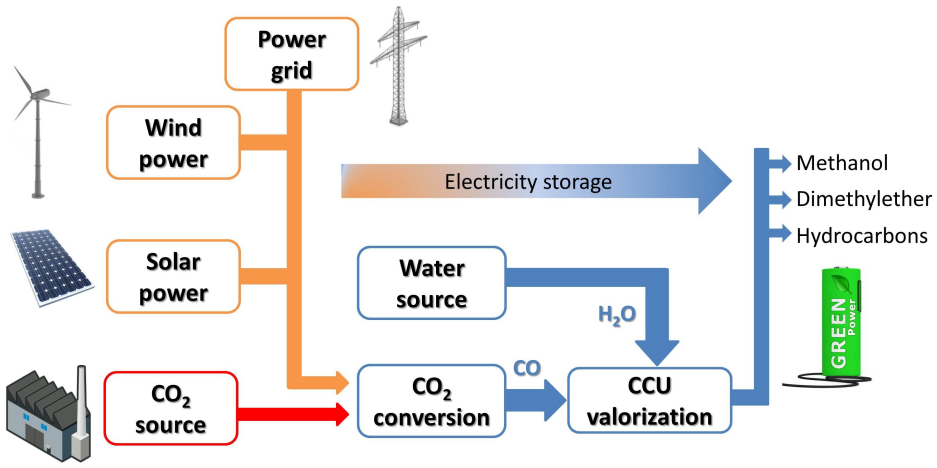

Figure 1.2: Figure extracted from [9]. Idealized scheme of CO_2 utilization, taking advantage of the surplus of electricity produced from green technologies.

often far from the densely populated areas. They lack a well established distribution network and the electricity overproduced is not easily stored and transported.

These drawbacks are overcome if the surplus of electricity is used to form hydrocarbons. The synthetic gases obtained this way will indeed benefit from well developed transportation and distribution grids. Moreover, they are suitable for a long term storage, without the cons of using capacitors. However, their combustion will release CO_2 in the atmosphere. Hence, the idea is to use CO_2 as a raw material to form the synthetic gases, aiming for a neutral CO_2 balance. Carbon capture technologies are being developed to remove greenhouse gases from our atmosphere and control human emissions, but the captured CO_2 is currently considered as a waste. The underlying idea, depicted in fig 1.2, is to dissociate CO_2 into CO at high energy efficiencies, taking advantage of the non-used electricity produced from low-carbon emitters, like nuclear power plants or renewable technologies. Then, the carbon monoxide is mixed with hydrogen to form synthetic gases, like in the Dry Reforming of Methane (DRM) process [8]. Overall, nuclear and renewable technologies would gain in flexibility and distribution range by storing the excess electricity into hydrocarbons, without increasing their low carbon footprint. The main limitation to reach this goal lies in the difficulty to dissociate the CO_2 molecule, which is very stable. Besides, most of the CO_2 emission sources contain dinitrogen, due to its abundance in the atmosphere. Investigating its influence on CO_2 dissociation mechanisms is therefore mandatory to determine if further CO_2 gas purification steps are necessary.

In this work we investigate CO_2 dissociation in non-thermal plasmas, extensively described in subsection 1.1.5 and in chapter 2. The thesis focuses on the influence of nitrogen, the most common gas in our atmosphere, to verify whether it helps CO_2 dissociation or not and what effect it may have in CO_2 plasmas. The main characteristics of both molecules are described hereafter.

1.1.3 The CO_2 molecule: main properties

Compared to other gases like nitrogen or oxygen, the concentration of carbon dioxide in our atmosphere is relatively low: 0.035% of its volume only. Nonetheless, CO_2 is responsible for more than half of the increase of the global warming effect. An issue relative to CO_2 emissions is the lifetime of the molecule in the atmosphere. Approximately a quarter is absorbed by the oceans, the biggest CO_2 tank on our planet, and another quarter is absorbed by the biosphere, *i.e.* mainly by the plants. These processes take several decades, which is faster than the lifetime of the 50% of CO_2 left in the air: typically from hundreds to thousands years. Hence, current anthropic emissions are having an impact on our climate that will last for the next centuries. This feature is specific to CO_2 as the lifetimes of the other main greenhouse gases are shorter: $\sim$114 years for nitrous oxide (N_2O), $\sim$12 years for methane (CH_4) and water vapor (H_2O) is rapidly condensed into rain or snow.

The CO_2 molecule has a triatomic structure, consisting in 1 carbon atom double bonded to 2 oxygen atoms, as illustrated in figure 1.3. At ground state, it is a linear and symmetric molecule. It can be electronically, rotationally or vibrationally excited, or in a mixed state. Note that the rotational excitation can be measured by rotational Raman spectroscopy, a technique using the scattering properties of a medium to characterize it (cf. chapter 3). However the rotational excitation is out of the scope of this work, hence will not be further detailed. The electronic excitation corresponds to larger orbits of electrons around the nuclei, in a Newtonian perspective. The vibrational excitation is seen as the motion of the atoms one to another, keeping the center of mass constant, like an oscillator. Like all symmetric triatomic molecules, 4 normal vibration modes can be defined: a symmetric stretching mode, an asymmetric stretching mode and 2 bending modes, represented schematically in figure 1.3. The symmetric and the asymmetric stretchings are characterized by the quantum numbers v_1 and v_3, associated to the frequency of the vibration. The 2 bending modes have the same energy, so they are considered as a unique degenerate mode characterized by 2 quantum numbers v_2 and l_2, where v_2 is associated to the frequency of the vibration and l_2 is associated to the angular momentum. Overall, the vibrational state of CO_2 is written following Herzberg's [10] notation: $CO_2(v_1, v_2^{l_2}, v_3)$. Normal modes are independent, which means that without perturbation they do not exchange energy between each other. This statement is however mitigated by the existence of a Fermi resonance [11] between the levels $(v_1, v_2^{l_2}, v_3)$ and the levels $((v_1 - 1), (v_2 + 2)^{l_2}, v_3)$, due to an 'accidental degeneracy'. Consequently, these levels cannot be differentiated unambiguously.

The physical properties of CO_2 change with the mode vibrating because its dipole moment or its polarisability are modified. While symmetrically stretching, the modification of the electric field induced by the motion of one oxygen atom is compensated by the second one, so the dipole moment is not modified. A CO_2 molecule at ground state or symmetrically vibrating is hence not visible with InfraRed (IR) light. If symmetrically vibrating, the total length of the molecule is however modified, so is its polarisability. As a consequence, it is detectable with Raman spectroscopy, detailed in chapter 3. On the contrary, only the dipole moment is modified while asymmetrically stretching or bending. A a result, the molecule absorbs IR light, which is the main reason why CO_2 is a potent greenhouse gas. Figure 1.4 shows the IR light absorbed by an air background from a Fourier Transform InfraRed (FTIR) spectroscopy, detailed

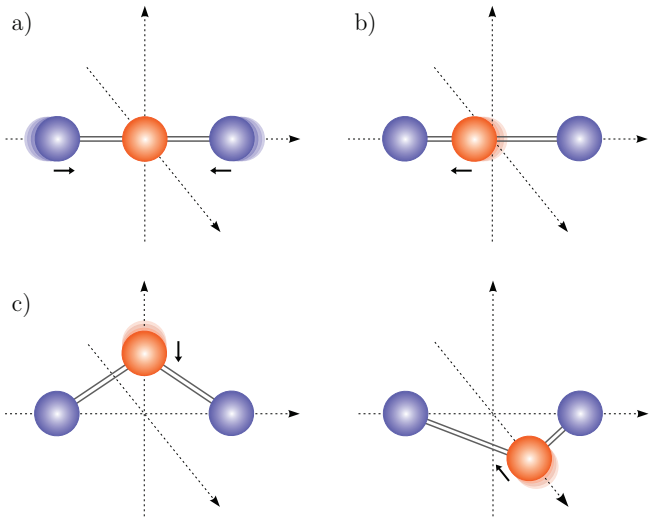

Figure 1.3: CO_2 molecule and its 4 normal vibration modes, extracted from [12]. The symmetric stretching (a), the asymmetric stretching (b), and the bending in two orthogonal planes (c).

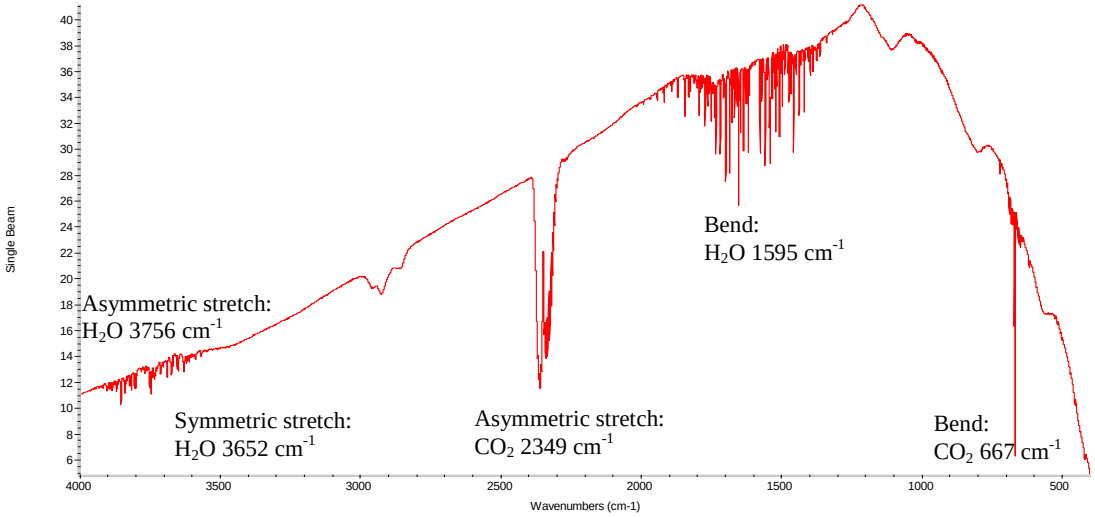

Figure 1.4: Air background spectrum, extracted from [13]. It shows the frequencies absorbed by water and carbon dioxide in the infrared range, according to their vibration modes.

in chapter 3. Because they are both symmetric triatomic molecules, CO_2 and H_2O are IR active for the bending mode and the asymmetric stretching mode. However, even at ground state H_2O is not linear, hence it is also IR active for the symmetric stretching mode.

1.1.4 The N_2 molecule: main properties

Dinitrogen (N_2), shortened to nitrogen in this work, is the most common pure element on Earth. The volume of our atmosphere consists in $\sim$78% of N_2, hence it is likely to find nitrogen while capturing CO_2 from air. It naturally raises the question of knowing if the presence of N_2 impurities would favor CO_2 conversion, or not. If nitrogen worsens the energy efficiency of CO_2 dissociation, then the gas mixture used as a raw material would need to be pure enough to get rid of the nitrogen effects. In this case, the need for additional purification would probably increase the overall cost and the carbon footprint, which is

not desirable.

Apart from potential impurities, nitrogen has other interesting characteristics for CO_2 dissociation. As a stable, inert and cheap gas it is widely used in laboratories to provide a chemical neutral background or as a cooler. However, N_2 most particular feature is related to its vibration frequencies. As a diatomic molecule, it has only one vibration mode, characterized by the quantum number v. While vibrating, the dipole moment remains unchanged, but the polarisability is modified, hence N_2 is detectable by Raman spectroscopy but not by IR light absorption. The energies of the first levels $v = 1, 2, 3$ for $N_2(v)$ (red) and $v_1 = 1, ..., 5, v_2 = 1, ..., 5, v_3 = 1, 2, 3$ for $CO_2(v_1, v_2^{l_2}, v_3)$ (blue and black) are represented in figure 1.5. The energies of the asymmetric stretching $CO_2(0, 0^0, v_3)$ almost match the energies of $N_2(v)$, although the discrepancy increases with the higher levels. Such levels with very close energies are said to be 'quasi-resonant' one with the other. **It implies that the energy stored under vibration form in one molecule can be easily exchanged to the corresponding resonant level of another molecule.** As a consequence, one can think about excited N_2 as an energy reservoir for the asymmetric mode of CO_2. This property of nitrogen is of interest to reach an efficient CO_2 conversion, especially in a medium taking advantage of vibrational processes, such as non-equilibrium plasmas introduced hereafter. The vibrational processes are further detailed in chapters 2 and 4.

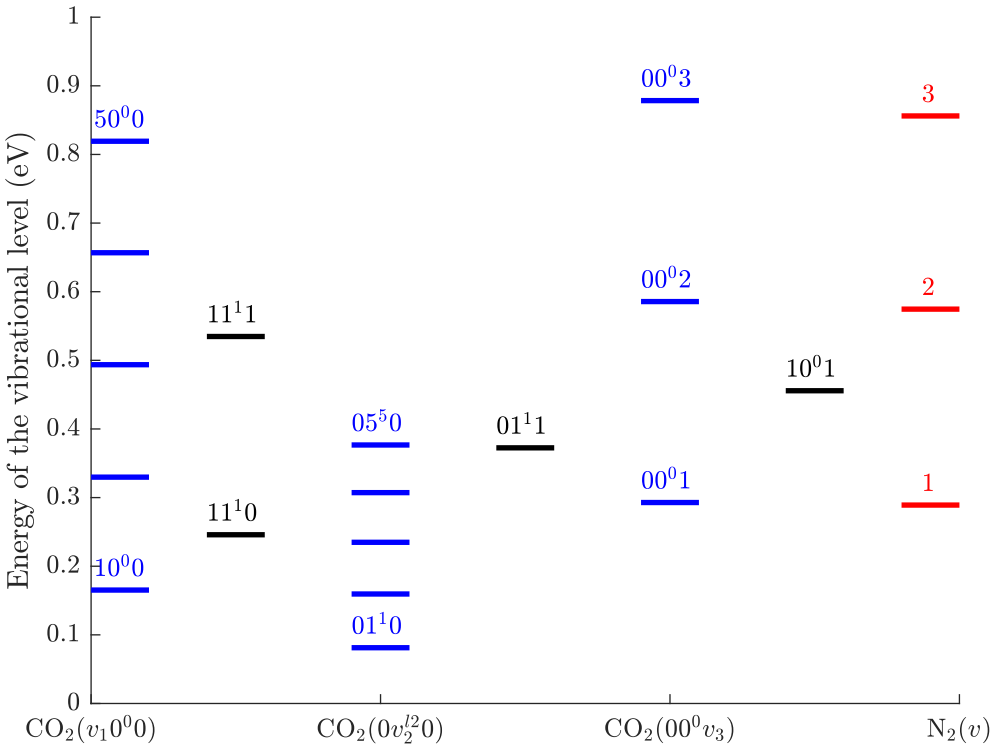

Figure 1.5: Energies of the first vibrational levels for N_2 (red) and CO_2 (blue and black). The blue lines show energies for only one mode excited at a time, while the black lines correspond to mixed excited modes.

1.1.5 Non-thermal plasma assisted dissociation [1]

A brief introduction to plasmas

Plasma was first identified as 'radiant matter' by W. Crookes in 1879, and further investigated by J. J. Thomson in 1897. The term of plasma was first used by I. Langmuir in 1928 in analogy with the blood plasma, while he was working on thermionic emissions in vacuum tubes. In these experiments, I. Langmuir was heating a wire enough to release electrons from the metallic particles, hence charging negatively the neighborhood of the wire. A current is then created through the gas of the tube if there is another electrode at the other edge, charged positively.

Plasma is often referred to as the 4^{th} state of matter. While neutral gases are good electrical insulators, plasmas are very sensitive to electromagnetic fields. They consist in ionized gases, *i.e.* a relevant part of electrons have been pulled out from their molecules/atoms and are free to travel. The quasi-totality of ordinary matter, for instance stars, pulsars, nebula, etc. is actually plasma, although it is not abundant on Earth. Natural plasmas on our planet can be found in the lightnings, auroras or very hot fires. However, industrial plasmas are very common due to the specific physical and chemical properties of this state of matter. Among the numerous possible applications one would find: high accuracy etching of electrical circuits, agriculture enhancers, (de)activation of specific tissues for medical applications, energy production *via* nuclear fusion, modern televisions, etc.

Non-thermal plasmas in the context of CO_2 dissociation

Plasmas can be defined as 'thermal' or as 'non-thermal' depending on the kinetic energy of electrons compared to the kinetic energy of heavy species, *i.e.* ions and neutrals. If both respective kinetic energies are similar, then electrons and heavy species are in thermal equilibrium, and their kinetic properties will be determined by thermodynamic theories. On the other hand, if the neutral species have a relative kinetic energy about one order of magnitude smaller than the electrons, or less, the plasma is said to be a Non-Thermal Plasma (NTP), or similarly a 'cold plasma'. Note that in this work we refer to energy distributions, and more specifically to the Electron Energy Distribution Function (EEDF). Another property of NTPs is the possibility to have Vibrational Distribution Function (VDF) different from the classic Maxwell-Boltzmann ones. Typically, NTPs can contain a larger fraction of highly vibrationally excited molecules than thermal plasmas. This is of interest to reach an energy-efficient CO_2 dissociation, as explained below. More details about NTP modeling are given in chapter 2.

The reactions leading to CO_2 dissociation by direct electron impact require a high amount of energy, typically about 7 eV and 10.5 eV for the main dissociative channels, above the CO_2 dissociation energy of 5.5 eV. However, it is possible to reduce the energy cost, hence improving the overall energy efficiency, by taking advantage of non-equilibrium plasma processes. Fridman [15] listed experimental results exhibiting high energy dissociation efficiencies, reporting that Legasov [16] reached energy efficiencies up to 80% and Asisov [17] up to 90%, both in non-equilibrium microwave plasmas operating at pressures between 50 and 200 Torr. Recently, van Rooij [18] obtained an energy efficiency of 45% under industrial conditions,

[1] Parts of this sub–section are based on [14]

approaching the theoretical thermodynamical limit. This limit represents the maximum efficiency one can reach with a fully thermalized plasma, and overcoming it involves non-equilibrium processes. It is claimed that dissociation in [16, 17] was obtained precisely taking advantage of non-equilibrium conditions, resulting mainly from collisions of highly vibrating molecules previously excited by the electrons from the discharge [15], hence benefiting from the energy stored in the vibrational levels. The asymmetric mode v_3 is of major interest here to reach an efficient dissociation by molecular collisions: though any highly excited mode can in principle lead to dissociation, the relaxation of the asymmetric strech is much slower than that of the symmetric stretch and bending modes [15]. Moreover, dissociation into C+O+O or C+O_2, associated with the symmetric and bending vibration, respectively, requires higher energies than dissociation into CO+O [19]. Hence the necessity to pump-up the density of CO_2 molecules vibrating at high v_3, for example by a fine tuning of the operating conditions (type of discharge, pressure, temperature, etc.). This process is called "ladder-climbing" and is illustrated in figure 1.6 together with the dissociation from direct electron impacts. Note that, however, electrons also transfer their energy to the bending and the symmetric vibration modes, as well as they excite the electronic states of CO_2, resulting in a loss of efficiency. A potential way to favor the asymmetric vibration mode is the addition of molecular nitrogen, as it is known in the context of CO_2 laser technologies [20]. Indeed, the first excited levels of N_2 have respective energies very close to the first asymmetric levels of CO_2 (see figure 1.5), allowing **nitrogen to exchange easily vibration quanta with the asymmetric mode of CO_2.** At low pressure and low temperature, *i.e.* typical conditions in NTPs, the vibration-vibration (V-V) exchanges are faster than the relaxation (V-T) reactions and, therefore, nitrogen molecules can transfer vibration quanta to the v_3 mode of CO_2 before thermalization occurs. In such plasmas, during a time scale of a few milliseconds, the VDF of the molecules shows a higher tail in the highly excited levels than in a classic Boltzmann distribution [21, 22]. Under these circumstances, the ladder climbing process depicted by the red arrow in figure 1.6 is likely to occur.

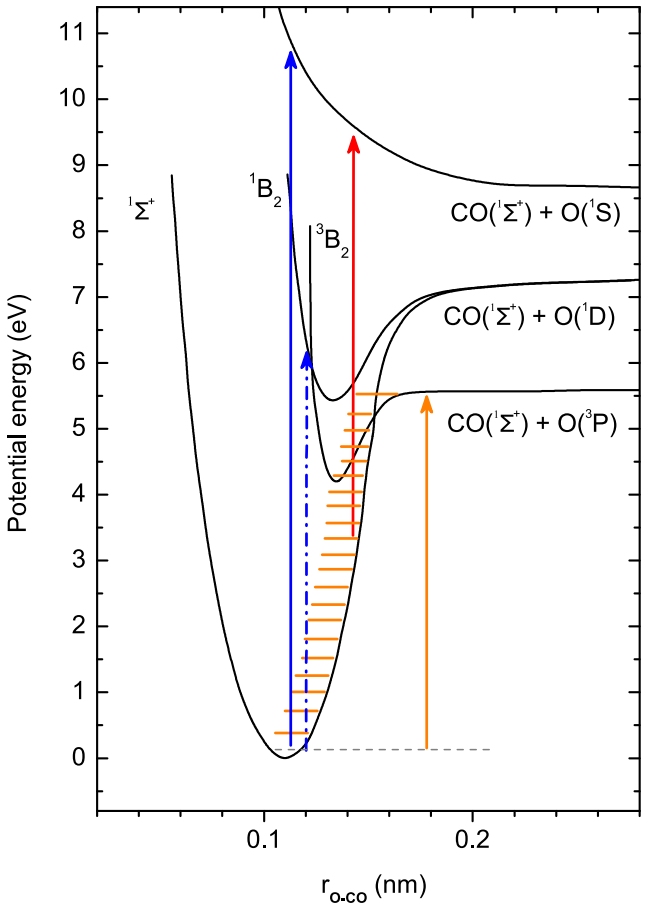

Figure 1.6: Figure extracted from [12]. It shows the potential energy of CO_2 molecule as a function of the distance between O and CO. The blue arrows represent the dissociation from direct electron impacts, at 7 eV and 10.5 eV. The orange arrow represents the dissociation from pure vibrational excitation. The red arrow is an example of a dissociation *via* a mix of vibrational excitation and electron impact.

The particular case of the Direct Current (DC) glow discharge

The following paragraphs focus on a well-known plasma discharge, the DC glow discharge, suitable to obtain non-thermal plasmas. All the experimental results presented in this thesis were measured in DC glow discharges, in **nanosecond pulsed regime** for the measurements of A. S. Morillo-Candas and in **continuous regime** for my measurements.

A glow discharge is a plasma formed by running an electric current in a neutral gas. Above a certain voltage threshold, known as the striking voltage, the ionization of the gas molecules becomes self-sustained. Indeed, if the electrons have enough energy, they can produce enough secondary electrons while colliding with the gas particles. This requires high voltages, typically several hundreds of Volts. It also requires low pressures, as the electron mean free path increases when pressure drops (less collisions), allowing electrons to gain more energy. However, the pressure cannot be decreased to too low values, as a minimum number of ionizing collisions before the electrons are lost must be ensured.

The easiest way to obtain a glow discharge is to run a DC discharge, having two electrodes placed at each side of a tube. Figure 1.7 schematizes the main regions created in a glow discharge, in this case in a so-called Crookes tube. The blue regions correspond to space where light is emitted. The following list describes very briefly the characteristics of each region, from the cathode to the anode. Note that the tube is separated into two layers: the cathode layer, positively charged, and the anode layer, negatively charged. More details about this setup can be found in the litterature, for example in [15].

- **Aston Dark space**: the electrons emitted from the cathode do not have enough energy to excite or ionize atoms.
- **Cathode glow**: electrons may have enough energy to excite atoms, which emit light while going back to the ground state.
- **Cathode dark space**: electrons gain energy, to the point that they ionize the gas atoms more than they excite them. The ions and electrons do not recombine immediately so there is no emission of light.
- **Negative glow**: electron density increases but their energy decrease, so they can more easily recombine with positive ions, emitting light in the process.
- **Faraday space**: the electrons keep losing energy, they recombine less than in the previous region, so there is no more light emitted. The end of this regions marks the end of the so-called Cathode layer.
- **Positive column**: the electric field increases so electrons gain enough energy to excite the atoms again. Increasing the length of the plasma tube results in an increase of the Positive column region (*e.g.* the neon signs), while the cathode layer length remains the same.
- **Anode glow**: the electric field still increases, so electrons excite more atoms.
- **Anode dark space**: electrons recombine on the anode, their density lowers, hence there is no more light.

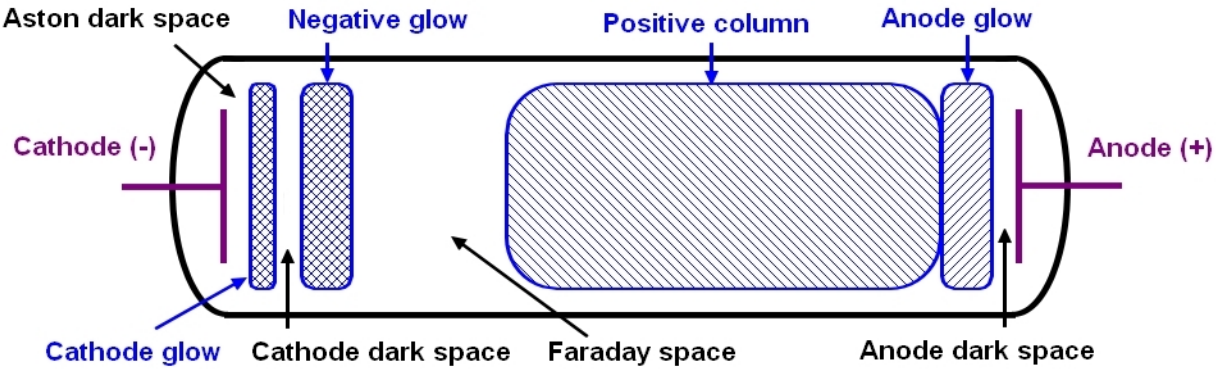

Figure 1.7: Simple scheme of glow discharge in a Crookes tube. The blue regions correspond to light emission. The scale is not respected for a clarity purpose.

Plasma offers an interesting medium for CO_2 dissociation, yet requiring a better understanding

Working with plasmas offers other interesting advantages when compared to existing dissociation technologies. The kinetic reactions occurring in plasmas have typical time-scales equal or lower than a few milliseconds, allowing quasi-instantaneous on/off switch, specifically suitable for intermittent electricity supply sources. Plasma technologies are also relatively easy to scale up to fit industrial standards. The current solutions investigated do not require expensive or rare materials, which is the case of electrolysis for instance. Nonetheless, the very high 90% energy-efficiency once reached by Fridman *et al.* [15] was never reached again so far, and plasma-assisted CO_2 dissociation remains a rather new and unknown field. Developing accurate physical models and gathering measurements from new experiments are the core of a deeper, necessary understanding, towards an efficient CO_2 dissociation.

1.1.6 The growing importance of numerical simulations [2]

The rapid development of computers in the last fifty years had a huge impact in various fields, typically thanks to the use of numerical simulations to solve the equations of physical models. Among these fields, one would find physics and biology in general, but computer modeling also greatly influenced economics or sociology, and decisions made out of simulations can have important repercussions on our society. The increase of computational power allowed models to become more and more complex, although depending on the level of detail some simulations still cannot be run in a decent time. For instance, simulations of a combustion flame would typically require a few minutes to be performed for a 0D (volume-averaged) model, while passing to a 3D particle-in-cell model extends the running time to several weeks. In order to reduce the computational time, one might want to reduce the complexity of the model, for example by getting rid of any implemented species/reaction whose influence on the results would be negligible.

In the cold plasma community, it is common to see models including dozens of species and hundreds to thousands of reactions. Typically, species are discriminated if they are ionized, but also according to their excitation level (*e.g.* $CO_2(02^21)$, $O_2(b^1\Sigma_g^+)$, etc.), each state often corresponding to one full

[2] Parts of this sub–section are based on [23]

species in the model. Reactions are even more diversified as they describe numerous types of processes (*e.g.* $CO_2(00^00) + N_2(1) \rightarrow CO_2(00^01) + N_2(0)$, $CO_2(00^00) + e^- \rightarrow CO_2(00^01) + e^-$, etc.). The sub–sections 2.3.4 and 2.3.5 in chapter 2 give more details about the most common species and reactions, respectively, one usually finds in CO_2-N_2 cold plasmas. In these complex non-linear systems, assumptions made 'by hand' about their relative importance might prove to be impossible or even lead to important errors. It is then desirable to have an objective procedure measuring the effect of the reactions on the outputs, rather than relying only on one's intuition. Sensitivity Analysis (SA) methods were developed to answer this issue: they aim at providing a ranking of the inputs' influence, while keeping a compromise between accuracy and computational cost. Various procedures are described in the literature [24–29] with different reported efficiencies, and the best suited method can vary from one model to another. It is worth mentioning that applying such procedures is relatively recent in the cold plasma community [30–37], as compared for example with the combustion community [38, 39].

Models in general can be developed according to two different aims. The first one is to reproduce experimental results accurately and to predict correctly quantities that are still to be observed. A model will be considered validated if it can reproduce outputs comparable with experimentally measured quantities within a prescribed precision. The second one is to understand which are the main phenomena governing the behavior of a complex system and to predict its response in conditions yet to be explored. In either case, to understand, control and/or optimize the system operation, one might want to identify the main mechanisms related to a specific output. This identification also provides information about the most sensitive inputs, whose values often suffer from great uncertainties. It is a typical situation in cold plasma modeling, as the reaction rate coefficients can vary up to two orders of magnitude from one database to another. It is also the case here, as the results presented along the thesis were mainly derived from complex physical models.

1.2 Methodology and original publications

As discussed in section 1.1, there are many reasons to study CO_2 plasmas, the main one dealing with efficient CO_2 conversion technologies. The work presented here intends to contribute to a better understanding of the main mechanisms responsible for dissociation. It constitutes as well a necessary preliminary step towards a future optimization of the operating conditions of the plasma. A global methodology was defined to achieve these goals in a delay of three years, according to the data/resources available at the time. The first part of the thesis mainly focuses on the influence of N_2 in a CO_2 plasma. The second one leaves the CO_2-N_2 mixtures to set the basis of a sensitivity analysis tool, helpful to identify the most/least important mechanisms in complex systems. It is worth mentioning that, although the work described here results from personal efforts, none of the presented results would have been obtained without the past and current efforts of the whole CO_2 groups from Instituto Superior Técnico (IST) in Portugal and Laboratoire de Physique des Plasmas (LPP) in France.

The starting point to study CO_2-N_2 plasmas was the physical model developed by T. Silva *et al.* to model pure CO_2 NTP (see chapter 2 for details). The model was tested against experimental

measurements and validated in previous publications [40–43]. Consequently, an important initial step consisted in implementing all the reactions/species linked to nitrogen. This is not trivial from a theoretical point of view as, often, databases for reaction rate coefficients are either scarce, or giving very different results for similar conditions. The work realized on some specific N_2 reaction rate coefficients was presented as a poster, during the conference ICPIG 2017 in Estoril, Portugal [44], and is extensively detailed in section 4.2. Once the physical model adapted, it has to be validated by reproducing accurately experimental measurements, which was possible thanks to new measurements (presented in [14, 45]) from Morillo-Candas *et al.* at LPP. A satisfactory agreement was reached for validation, and presented on a few occasions: as a poster for the conference ESCAMPIG 2018, in Glasgow, Scotland [46], and as talks for a workshop in Ericeira (2018), Portugal [47], and the conference CESPC 2019, in Gozd Martuljek, Slovenia [48]. Finally, it was also the object of a publication [14] in the Journal of Physics D: Applied Physics. Meanwhile, a short-period mission of 2 months was set at LPP in order to gather new measurements (cf. section 3.4). Being there personally was a good opportunity for me to learn more about experiments and data treatment. Although the personal measurements obtained during this short period were not crucial for the investigations, such a crossover between numerical simulation and experimental practice is always of great interest to get a more global picture and to facilitate communication between modelers and experimentalists.

Due to the complexity of plasma chemistry models and the numerous approaches allowed, the second part of the thesis did not focus on predictions nor optimizations of CO_2-N_2 systems. Instead, the attention was dedicated to another code, the Lisbon KInetics (LoKI) [49] tool suite, in development at IST, Portugal, and described in section 5.4. In brief, it describes the coupled electron and heavy particle kinetics, solving the two-term homogeneous Boltzmann equations and the rate balance equations. The kinetics implemented in LoKI are fairly complex: for the case of oxygen plasmas, simpler to model than CO_2 plasmas, the particles are distinguished into dozens of specific species, and the number of possible reactions between them approach 200. That being said, the O_2 kinetics are very similar to those of CO_2 in terms of electronic and vibrational processes. Such situations, where assessing the respective influence of each process on the outputs is difficult, correspond to the ones described in sub–section 1.1.6. Therefore, the second part of the thesis dealt with the creation of a Sensitivity Analysis (SA) tool, based on the Morris method and applied to the specific case of an oxygen cold plasma model. The validation of this approach, enriched by some refinements, and the results obtained are detailed in chapter 5 and were the object of a publication [23]. It corresponds to a preliminary step towards the integration of a generalized SA tool into the LoKI simulation suite, to be used in the investigation of more complex mixtures, including CO_2-N_2 systems.

1.3 Literature overview: starting point

This section intends to provide the context in which the PhD was started by listing some of the most useful publications used for this work. The reader can find more details about the state-of-the-art and relevant literature for pure CO_2 and CO_2-N_2 modeling in section 2.2, while those about sensitivity analyzes are

given in section 5.2.

As mentioned in the previous section, the starting point dealt with the implementation of N_2-related reactions in an already-developed model for pure CO_2 DC glow discharges [40–43]. To do so, we started from the work of Guerra *et al.* [50, 51] on nitrogen and compared the reaction rate coefficients to the calculations of Billing *et al.* [52], Blauer *et al.* [53], Smith *et al.* [54], Plönjes *et al.* [55], Kozák *et al.* [56], Capitelli *et al.* [57] and Kurnosov *et al.* [58–60]. The deactivation by O atoms was implemented later on by considering the atmospheric model of Puertas *et al.* [61] and the deactivation at the walls relied on the work of Guerra *et al.* [62], Kutasi *et al.* [63], supported by the database of physics parameters from Hirschfelder *et al.* [64], Marinov *et al.* [65] and Black *et al.* [66]. The validation of the new model for CO_2-N_2 mixtures was discussed thanks to comparisons with recent measurements performed by Morillo-Candas *et al.* [45].

The second part of the thesis was dedicated to the creation of a sensitivity analysis tool, based on the so-called Morris method. Evidently, the work of M. D. Morris [25] was extensively used, together with recent improvements of his method provided by Campolongo *et al.* [26, 27] and J. Norton [28]. The sensitivity analysis tool was applied to an oxygen kinetic scheme whose driving equations are solved by the numerical code LoKI [67–69]. The reliability of the tool developed was checked by comparing our results with those obtained by Annušová *et al.* [70] in a quasi-identical context. Finally, similar analyzes from M. M. Turner [30–32] and Obrusník *et al.* [71] were extensively investigated for their interesting discussions.

1.4 Thesis Outline

The thesis is structured in 6 chapters, including the current one for the Introduction. The content of the next chapters is given below.

Chapter 2: CO_2-N_2 theoretical kinetic scheme
The main mechanisms responsible for CO_2 dissociation in cold plasmas are described in this chapter, as well as the initial results which motivated extra research in the first place. A state-of-the-art of CO_2-N_2 physical models is presented. The last part of this chapter deals with the driving equations of cold plasma and describes the physical model used in the chapter 4.

Chapter 3: Experimental work
This chapter gives a global description of the experimental setup, the operating conditions and the diagnostics used for all the measurements presented in the thesis. They were performed at LPP, where I spent 2 months and obtained some results, presented in this chapter.

Chapter 4: Exploitation of the physical model for CO_2-N_2 plasmas in pulsed DC discharges
This chapter explains how the reactions implying N_2 are implemented in the physical model described in chapter 2. It details how some reaction rate coefficients were refined to be consistent on larger temperature/vibrational energy ranges. The results obtained with the new set of CO_2-N_2

reactions are compared to new experimental measurements, to check the validity of the model and gain further insight into the underlying kinetics.

Chapter 5: Sensitivity Analysis: the Morris method and refinements

The work described in this chapter presents the concept of sensitivity analysis, as well as a state-of-the-art of the existing SA in the cold plasma community. The sections of the chapter explain step-by-step how the SA, starting from the original Morris method, was refined and applied to the simulation tool LoKI. Results are analyzed and compared, when possible, to other existing sensitivity measures.

Chapter 6: Conclusions

The last chapter summarizes the work done and the main points of interest. The relevance of the approach is globally discussed. Some ideas for further development are given as well.

Chapter 2

CO_2-N_2 kinetic scheme

2.1 Introduction

The very high energy efficiency for CO_2 dissociation obtained by Fridman *et al.* [15–17] in supersonic non-equilibrium microwave plasmas motivated numerous investigations of CO_2 Non-Thermal Plasmas (NTPs). They were greatly helped by the parallel development of numerical tools, allowing to solve the equations driving complex systems. In the context of this thesis, the stress is put on the non-equilibrium characteristics of CO_2-N_2 plasmas. Indeed, vibrational excitation of CO_2 – and more specifically the asymmetric stretching – is assumed to be responsible for the high energy efficiency. Therefore, a detailed description of the vibrational levels of the main species is required, as well as a consistent set of reactions creating and removing those levels. Some other parameters are also crucial: for instance, an accurate description of the electrons' energy, representing the discharge characteristics, as they are the source of energy provided to the CO_2 molecules.

Global features of CO_2-N_2 cold plasma modeling are detailed in this section. The main species and reaction mechanisms for CO_2-N_2 plasmas are presented in section 2.3. Section 2.4 gives further insight on how the model is implemented in the code developed by Silva *et al.* to simulate Direct Current (DC) glow discharges in a pure CO_2 gas, with time-resolved calculations. It uses 0D (volume-averaged) model, thanks to a relative homogeneity of the plasma modeled and for the sake of simplicity and computational cost. Nonetheless, surface interactions cannot be neglected and radial diffusion of species towards the walls is taken into account. Detailed information about more complex surface interactions can be found in the PhD thesis of A.S. Morillo-Candas [45].

2.2 State-of-the-art of pure CO_2 and CO_2-N_2 NTPs models

This section intends to provide a detailed database of pure CO_2 and CO_2-N_2 models available in the literature. It is not meant to be exhaustive but includes the majority of the most recent models to our knowledge.

The first models including vibrational levels for pure CO_2 and CO_2-N_2 NTPs were initially designed for

the investigation of CO_2 lasers [20, 72–74]. On the one hand, models developed specifically for CO_2-N_2 mixtures are still rare nowadays [75–77]. On the other hand, pure CO_2 models are far more common in the literature, motivated by the recent interest in CO_2 conversion. Dealing with the numerous vibrational levels existing in CO_2 is not trivial and recent publications proposed alternative ways to consider them. Among them, the lumping method which treats levels of similar energies as one pseudo-level [78], a fluid mechanics view describing all levels as a continuum (based on the Fokker-Planck equation) [79, 80] and Particle-In-Cell (PIC) Monte-Carlo-based simulations [81]. However, most of the models use a State-to-State (StS) description of the vibrational levels of CO_2. Because of remaining uncertainties regarding the reaction rate coefficients/cross-sections and high computational cost, these models often include only the very first levels of $CO_2(v_1, v_2^{l_2}, v_3)$, typically $v_1, v_2, v_3 \leq 5$. The most complete StS CO_2 models were developed mainly for atmospheric entry and include between 1500 and 10000 levels and states [82–84]. As the energy is initially transmitted to CO_2 molecules by electron impacts, an accurate description of the electron energy distribution and of the electron density (in time and/or space) is necessary and strongly depends on the type of discharge used to ignite the gas. Therefore, most models are specific to a certain type of discharge. The most common ones are Dielectric Barrier Discharge (DBD) [56, 85–90], MicroWave (MW) discharge [56, 78, 88, 89, 91–94] and DC glow discharge [40–43, 89]. Among the less common ones, one can find micro-hollow cathode discharge [95], gliding arc [96], pulsed corona discharge [97] or more global considerations about how the Electron Energy Distribution Function (EEDF) varies with the reduced electric field [98–100].

2.3 Modeling cold CO_2 plasmas

2.3.1 Introduction

Natural plasmas may be rare on Earth, but man-made ones are frequent in industries or in laboratories. The most common way to create a plasma is to run an electrical discharge in a tube filled with gas, typically thanks to electrodes placed at each edge of the tube. Above a certain voltage threshold, some electrons are pulled out from the molecules they were bond to. If their velocity is high enough, or equivalently their kinetic energy, they can pull out new electrons by colliding with the molecules in the gas. On the contrary, if their energy is too low, the electrons recombine with the ions and the plasma-state of the gas is lost. The degree of ionization, α_{ioni}, measures the proportion of charged particles to the total number of particles:

$$\alpha_{ioni} = \frac{n_+}{n_0 + n_+} \tag{2.1}$$

where n_+ is the density (or number) of charged particles and n_0 is the density (or number) of neutral particles. To exhibit plasma properties, a gas usually requires a degree of ionization greater than 10^{-7} [15].

The following sections present the main features, equations, species and reactions typically encountered while modeling cold CO_2-N_2 plasmas. Details about the numerical implementation of such models

are given in section 2.4 and in chapter 4.

2.3.2 Non-thermal plasmas properties

Plasmas are classified into different categories, depending on their degree of ionization, the density of the neutral species (or the pressure), the gas temperature, etc. Generally speaking, the thermal motion of ions can be ignored in a non-thermal plasma. Therefore, only the electric force acts on the charged species, the pressure gradients and magnetic forces being negligible. This can only be achieved in plasmas with a low degree of ionization, typically from 10^{-6} to 10^{-3}, otherwise the ion motion cannot be ignored anymore. Another characteristic of cold plasmas is the presence of species, namely ions and neutrals, that are not in equilibrium with the electrons. Let us define 3 temperatures reflecting averaged kinetic energies, T_e, T_i and T_0 for the electrons, the ions and the neutrals respectively. While in NTPs the electrons have typical temperatures above 1 eV, ion and neutral temperatures are usually much smaller [15]. The following relation is observed in NTPs:

$$T_e \gg T_i \gtrsim T_0 \tag{2.2}$$

This characteristic is reached if the ions and the neutrals do not collide often enough to thermalize with each other. The term of 'cold' plasma comes from the temperature of the neutral species, ranging from the classic room temperature (~ 300 K) up to 10000 K. This temperature T_0 also corresponds to the so-called gas temperature, and is denoted T_g in the rest of the thesis.

A temperature can be defined for each type of excitation, rotational, vibrational or electronic. Working with a scalar value rather than a full distribution allows easy comparisons between different results, at the cost of a loss of information on the states. Indeed, passing from a distribution to a temperature requires an assumption about the shape of the distribution. Distributions (velocities, vibrations, etc.) are often assumed to be Boltzmann, which is fairly correct to compute the densities of the low excited states in general, but could lead to great errors for the most excited states. Note that other velocity distributions may be used in cold plasmas, for instance the Druyvesteyn [101] and the bi-Maxwellian [102] distributions. In NTPs, it was shown in [21] that the Rotational-Translational (R-T) processes are so fast ($\simeq$ 1 ns) compared to others (from μs to milliseconds) that the rotational temperature is very often assumed to be equal to the translational one, *i.e.* to the gas temperature for the neutrals.

Triatomic molecules, like CO_2, technically require 3 different temperatures to describe their vibrational state: one for each vibration mode. However, the interplay between the symmetric stretching temperature T_1 and the bending temperature T_2 is very complex due to the 'accidental degeneracy' [11] between the levels $(v_1, v_2^{l_2}, v_3)$ and the levels $((v_1 - 1), (v_2 + 2)^{l_2}, v_3)$. As a result, it is impossible to unambiguously distinguish two resonant levels. Here we adopted a common measure and notation T_{12} representing both modes at the same time. Note that this assumption was verified to hold in the present conditions, by fitting the spectra without imposing the temperatures T_{12} and T_3 and letting the populations of all the individual levels as free parameters to the fitting [45].

2.3.3 Main mechanisms taking place

In a cold plasma, most of the energy stored by the molecules is primarily given *via* electron collisions. Therefore, it is important to properly assess the electron kinetic energy. The Electron Energy Distribution Function (EEDF) $f_e(E)$, expressed in $\text{eV}^{-3/2}$, illustrated in figure 2.1, gives the proportion of electrons at a given kinetic energy E. When electrons are considered thermalized, their energy distribution is described by a Maxwellian distribution of parameter T_e:

$$f_e(E) = A \cdot \exp\left(\frac{-E}{T_e}\right) \tag{2.3}$$

where T_e is in eV. The coefficient A comes from the normalization $\int_0^\infty \sqrt{E} \cdot f_e(E) \cdot dE = 1$, and is equal to $A = 2(k_B T_e)^{-3/2}/\sqrt{\pi}$. As shown in figure 2.1, a Maxwellian distribution has a linear shape in logarithmic scale, with a slope defined by $-1/T_e$.

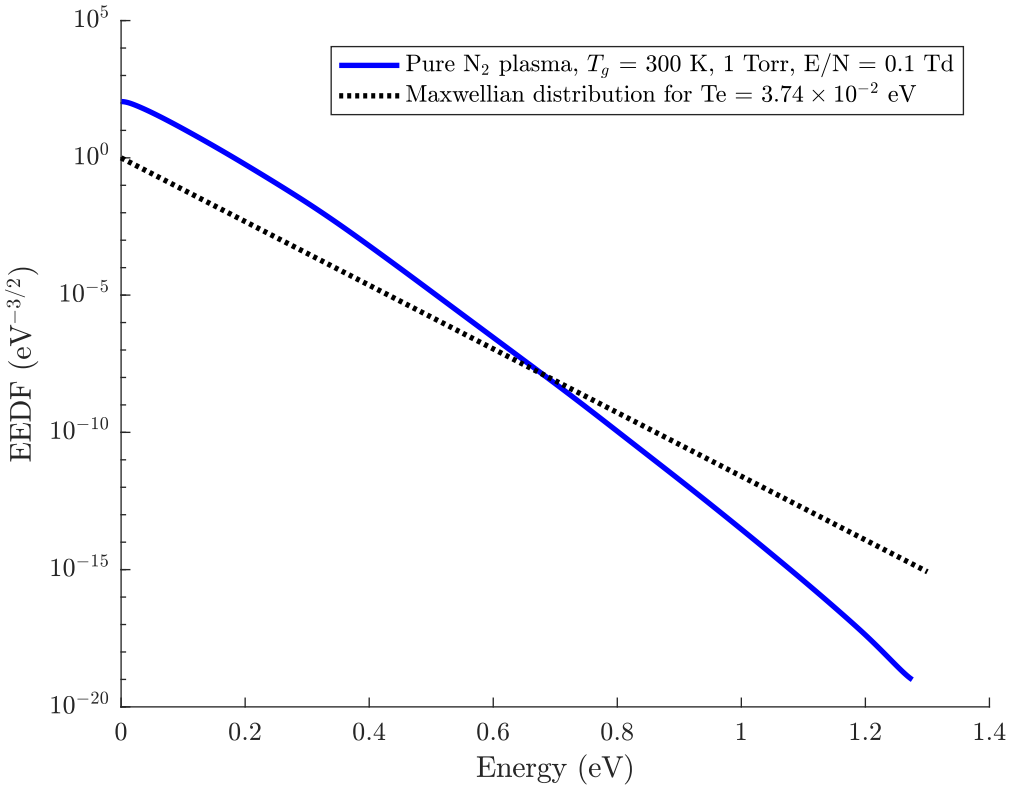

Figure 2.1: EEDF of a vibrationally excited pure N_2 plasma, compared to a Maxwellian distribution. The EEDF was obtained with the LoKI-Boltzmann solver.

Electron-electron collisions are often neglected in cold plasma modeling because of the low degree of ionization. However, they collide with other particles, ions or neutrals, in many ways. Particles may be electronically, vibrationally, or rotationally excited. Electron collisions can also induce ionization, recombination, etc. All these collisional processes have different probabilities to happen, depending on the state/energy of the incoming particles and the resulting products. In modeling, these probabilities are usually assessed *via* a cross-section σ. Using a theoretical example of a 2-body collisional process

$A + B \rightarrow C + D$, and assuming that only this collisional process takes place in the plasma, one can define the mean free path λ that particles A travel in between two collisions as:

$$\lambda = \frac{1}{n_B \cdot \sigma} \tag{2.4}$$

where n_B is the density of particles B. The reaction rate $R_{AB\rightarrow BC}$, measuring the number of collisional processes taking place in a unit of time and volume, is expressed as:

$$R_{AB\rightarrow CD} =< \sigma v > n_A n_B \tag{2.5}$$

where $< \sigma v >$ is called reaction rate coefficient and depends on the cross-section σ and the relative velocity v. It is calculated as:

$$k_{AB\rightarrow CD} =< \sigma v >= \int f(v) \cdot v \cdot \sigma(v) \cdot dv \tag{2.6}$$

where $f(v)$ is the velocity distribution function of the incoming particles and v is their relative velocity. Note that in general the cross section depends on the relative velocity, $\sigma = \sigma(v)$

Collisional processes can be sorted into two categories: elastic collisions when the total kinetic energy of the particles interacting is conserved and inelastic collisions otherwise. Assuming an inelastic collision for the reaction $A + B \rightarrow C + D$, the energy difference is denoted $\Delta E = E_A + E_B - (E_C + E_D)$, where E_M denotes the energy of the particle M. The reaction rate coefficient corresponding to the *superelastic* reaction $A + B \leftarrow C + D$ (backward reaction) can be estimated using the reaction coefficient $k_{AB\rightarrow CD}$ by assuming that in steady-state and in Local Thermodynamic Equilibrium (LTE) the forward and backward reactions must balance each other. For instance, the net balance (creation minus destruction) of species C over time can be expressed as:

$$\frac{dn_C}{dt} = n_A n_B k_{AB\rightarrow CD} - n_C n_D k_{CD\rightarrow AB} \tag{2.7}$$

where n_M denotes the density of species M. At steady-state, $\frac{dn_M}{dt} = 0$, which leads to:

$$k_{CD\rightarrow AB} = \frac{n_A n_B}{n_C n_D} k_{AB\rightarrow CD} \tag{2.8}$$

When A, B, C and D refer to internal states of a certain molecule/atom, the LTE assumption can be expressed as:

$$\frac{n_A}{n_{tot}} = \frac{g_A \exp(-E_A/(k_B T))}{\sum_{i=0}^{\infty} g_i \exp(-E_i/(k_B T))} \tag{2.9}$$

where g_i corresponds to the statistical weight of the species of number i, k_B is the Boltzmann constant, and T is the characteristic temperature of the concerned species, in K. For the ratio $n_A n_B/(n_C n_D)$ it turns into:

$$\frac{n_A n_B}{n_C n_D} = \frac{g_A g_B}{g_C g_D} \exp(-\Delta E/(k_B T)) \tag{2.10}$$

Finally, assuming for this example that all statistical weights are equal to 1, the reaction rate coefficient of the superelastic collision is computed as:

$$k_{CD\to AB} = k_{AB\to CD}\exp(-\Delta E/(k_B T)) \tag{2.11}$$

2.3.4 Species involved in CO_2-N_2 plasmas

The complexity of plasma chemistry in CO_2-N_2 plasmas is well illustrated by considering the number of species involved. An initial pure CO_2 gas can result in more than 30 species, even without discriminating the vibrational states. Including nitrogen further increases the number of possible combinations. As an example, the non-exhaustive list below sums up some of the main species one is likely to find in a CO_2-N_2 NTP [76, 77]. The presence of these species in non-negligible quantities depends on many parameters, such as the type of discharge and the operating conditions. The species taken into account for the results presented in this thesis are discussed in section 2.4 of this chapter and in chapter 4. Note that the electronic states e_1 and e_2 from the list below correspond to the excitation of groups of electronically excited states with thresholds around 7 eV and 10.5 eV, respectively. Some of these electronically excited states are assumed to lead to dissociaiton [40]. It is important to mention that the rotational states are not detailed in this thesis. Indeed, it was shown in [21] that Rotational-Translational (R-T) processes have a characteristic time of ~ 1 ns, while the other ones described here are of the order of 1 μs up to few milliseconds.

- **Molecules:** CO_2, CO, O, O_2, O_3, N_2, N_2O, N_2O_3, N_2O_4, N_2O_5, ONCN, C_2N_2, NCN, etc.
- **Radicals:** C_2O, C_2, C, O, N, NO, NO_2, NO_3, CN, NCO, etc.
- **Positive ions:** CO_2^+, $C_2O_2^+$, $C_2O_3^+$, $C_2O_4^+$, C_2^+, C^+, CO^+, CO_4^+, O_2^+, O^+, O_4^+, N^+, N_2^+, N_3^+, N_4^+, NO^+, N_2O^+, NO_2^+, $N_2O_2^+$, etc.
- **Negative ions:** CO_3^-, CO_4^-, O_2^-, O^-, O_3^-, O_4^-, NO^-, N_2O^-, NO_2^-, NO_3^-, etc.
- **Electronically excited:** $CO_2(e_1)$, $CO_2(e_2)$, CO($a^3\Pi$), CO(a'$^3\Sigma^+$), CO($A^1\Pi$), CO($b^3\Sigma^+$), CO($B^1\Sigma^+$), CO($C^1\Sigma^+$), CO($E^1\Pi$), O_2($a^1\Delta_g$), O_2($b^1\Sigma_g^+$), O(^{1}D), O(^{3}P), O($a^1\Delta_g$), O($b^1\Sigma_g^+$), N_2($C^3\Pi_u$), N_2($A^3\Sigma_u^+$), N_2(a'$^1\Sigma_u^-$), N_2($B^3\Pi_g$), N(^{2}D), N(^{2}P), etc.
- **Vibrationally excited:** $CO_2(00^01)$, $CO_2(100)$, $CO_2(01^10)$, CO(1), CO(2), $O_2(1)$, $O_2(2)$, $N_2(1)$, $N_2(2)$, etc.

2.3.5 The different types of reaction

One characteristic of cold plasmas is the number of collisional processes which can take place. The list hereafter gives the main categories which matter in CO_2 NTPs, with an example of a reaction. Note that a non-specified state corresponds to the sum of all existing states, including the ground state. For a model with a state-to-state approach, such as the one described in the next sub–section, the reaction rate coefficients have to be assessed for any state of the reacting particles.

- **Electronic reactions:**
  - Ionization: $CO_2(00^00) + e \rightarrow CO_2^+ + 2e$
  - Dissociative attachment: $CO_2 + e \rightarrow CO + O^-$
  - Dissociative recombination: $CO_2^+ + e \rightarrow CO + O$
  - Electronic excitation: $CO_2(00^00) + e \rightarrow CO_2(e_1) + e$
  - Vibrational excitation (e-V) : $CO_2(00^00) + e \rightarrow CO_2(00^01) + e$
- **Vibrational-Translational (V-T):** $CO_2(00^01) + CO_2 \rightarrow CO_2(00^00) + CO_2$
- **Vibrational-Vibrational (V-V):** $CO_2(00^01) + CO_2(00^00) \rightarrow CO_2(02^20) + CO_2(01^10)$
- **Dissociation:** $CO_2(00^00) + CO_2 \rightarrow CO + O + CO_2$
- **Radiation:** $CO_2(00^01) \rightarrow CO_2(00^00) + h\nu$
- **De-excitation at the walls:** $CO_2(00^01) +$ wall $\rightarrow CO_2(00^00) +$ wall

2.3.6 Driving equations of a State-to-State (StS) model

Our approach towards an energy-efficient CO_2 conversion is to investigate the non-equilibrium mechanisms occurring in cold plasmas. More specifically, CO_2 molecules highly vibrating (asymmetrically) are suspected to dissociate easily when they collide with another particle [15]. When it comes to modeling, a rather intuitive idea is to discriminate each vibrational state, in order to investigate its density or the mechanisms responsible for its creation/destruction. Let us denote n_v the density of a certain molecule/atomic state, for instance $n_v = [CO_2(02^21)]$. The term 'species' in this work has to be understood in its most detailed meaning: any specific state implemented in the code is considered as a species, hence $CO_2(10^00)$ is a different species than $CO_2(01^10)$. The total number of species is denoted N_S in this work. The N_S rate balance equations of a state-to-state model are written:

$$\frac{dn_v}{dt} = \left(\frac{dn_v}{dt}\right)_{e-V} + \left(\frac{dn_v}{dt}\right)_{V-T} + \left(\frac{dn_v}{dt}\right)_{V-V} + \left(\frac{dn_v}{dt}\right)_{h\nu} + \left(\frac{dn_v}{dt}\right)_{\text{Wall}} \tag{2.12}$$

where the left hand side represents the variations of the density n_v over time, and the right hand side sorts the creation/destruction terms into different reaction categories. The $e - V$ term stands for the vibrational excitation from electron impact, $V - T$ stands for the vibrational relaxation due to collisions with atoms/molecules, $V - V$ stands for the exchange of vibrational quanta, $h\nu$ stands for the radiations and Wall stands for de-excitation at the walls (cf. chapter 4).

2.4 The model of Silva *et al.* and its numerical implementation

Silva *et al.* developed a consistent 0-D (volume-averaged) kinetic StS model for CO_2 plasma, described in detail in [42, 43]. Implemented in Wolfram Mathematica, it computes the time-evolution of excited states

of CO_2, for different conditions of pressure, intensities, etc. The model and its numerical implementation were previously validated for pure CO_2 DC glow discharges (cf. chapter 1) by comparing the simulations with experimental results measured at LPP. Therefore, it was considered as an excellent basis for new investigations on CO_2-N_2 plasmas. The sub–sections hereafter describe the main features of the physical model and its corresponding numerical implementation for pure CO_2. Chapter 4 focuses on the specific implementation of nitrogen-related processes and their validation as a new kinetic scheme.

2.4.1 Global features

Solving the rate balance equations

At each time step Δt, the code developed by Silva *et al.* solves the N_S rate balance equations, using the previously computed densities n_V and the associated rate coefficients. The time step Δ_t is derived from a time vector specified by the user. It is usually a logarithmic vector which may start as low as 10^{-9} second to end typically around 1 second. Therefore, the time step value varies during a simulation. Albeit it was not tested, one should avoid using time vectors with large time steps as the fastest reactions would be underestimated. The functions used to solve the equations are inherent to the Wolfram Mathematica software and no problem of convergence was ever reported. Note that an informal benchmark against calculations from MATLAB gave identical results. The simulations' results consist in a set of N_S **time-resolved** densities, or equivalently the time-resolved vibrational temperatures if a certain distribution shape is assumed.

Reproducing a single-pulsed discharge

The physical model was initially developed to reproduce DC single-pulsed discharges. In such discharges, the plasma is generally homogeneous and the low degree of ionization is suitable for a step-by-step validation. A single-pulsed discharge is divided into two regimes: (i) the 'active part', a period t_{on} with a constant voltage applied in the reactor, followed by (ii) the 'post-discharge' or 'afterglow', a period t_{off} with no voltage applied. From a numerical point of view, such discharges were divided into two different simulations: (i) one with all the electronic reactions enabled during a time t_{on} and (ii) one with all the electronic reactions disabled during a time t_{off}. The inputs for the simulation of the post-discharge are derived from the outputs of the simulation of the active part, or alternatively from experimental data when available. The adequacy of the model to the experiments is further discussed in chapter 4.

2.4.2 Species, states and reactions considered

Species and states

A state-to-state modeling approach goes with some drawbacks, especially concerning the lack of reliable data about reaction rate coefficients or cross-sections. Therefore, a step-by-step validation method seems reasonable, if not mandatory: rather than working with the most detailed kinetic scheme available, it is better to keep the overall complexity of the model low enough to have it compared to existing

measurements. If the agreement is satisfactory, the model is said to be validated and can be further developed. A first advantage is the possibility to compare directly the outputs from the simulations to the outputs of the experiments, without any further transformation required. Another advantage, in case of a strong disagreement with the measurements, lies in an easier identification of the most influential reactions, in order to check/tune them. However, it may also go with drawbacks in some specific cases. For instance, Colonna *et al.* [103] claimed that working with a restrictive model may lead to important errors. Nonetheless, the step-to-step approach proved to give satisfying results for pure CO_2 plasmas, hence the same approach was adopted for the N_2 implementation. From this perspective, the vibrational states of CO_2 are limited to $v_1^{\text{max}} = 2$, $v_2^{\text{max}} = 5$ and $v_3^{\text{max}} = 5$, corresponding to the upper levels currently measurable at LPP. It results in a total of 72 vibrational levels for CO_2. Similarly, the N_2 levels are limited to $v^{\text{max}} = 10$, resulting in 11 states for nitrogen with the ground state. No excited electronic state was considered in this work.

Reactions

An exhaustive list of the considered reactions is given in Appendix A, with explicit formula and their corresponding coefficients. Note that the list also includes the newly-implemented N_2 reactions, detailed in chapter 4.

2.4.3 Self-consistent calculations and required inputs

Gas temperature

The simulations require a certain number of previous calculations to be consistent. At the time of N_2 implementation, there was no self-consistent calculation of the gas temperature. Instead, a time profile was provided as an input to the code. This gas temperature profile is, most often, corresponding to experimental measurements provided by LPP. It is worth mentioning that the current version of the code now includes a self-consistent way of computing the gas temperature, giving results in good agreement with the measured profiles [104].

Electrons and reduced electric field

As it focuses on the vibration kinetics, the model does not take into account any electronically excited state. The electron collisions are restricted to the e-V processes and ionization. The reduced electric field value E/N, main parameter determining the electron rate coefficients, is provided as an input during the simulations and kept constant all along. The electron density is set to 0 during the afterglow regime of a pulsed discharge. To mimic the active part, the electron density is derived from an empirical formula, whose parameters are provided by measurements:

$$n_e(t) = n_e^{\infty} + (n_e^0 - n_e^{\infty}) \exp\left(-\frac{t - T_{\text{shift}}}{\tau}\right) \tag{2.13}$$

where n_e^∞ is the saturated electron density, n_e^0 is an arbitrary measured electron density, τ characterizes the temporal growth and T_{shift} corrects the shift between the simulations' starting point and the measurements. The saturated electron density n_e^∞ is derived from:

$$n_e^\infty = \frac{I_{exp}}{S v_d e} \tag{2.14}$$

where I_{exp} is the steady-state value of the current, S is the cross-section of the experimental tube, v_d is the electron drift velocity and e is the absolute value of the electron charge.

The EEDF, the drift velocity v_d and the rate coefficients for e-V processes depend on the reduced electric field E/N, and are first determined thanks to the Boltzmann solver Lisbon KInetics Boltzmann (LoKI-B) solver [49]. LoKI-B is one of the two modules constituting the LoKI tool suite, extensively used and presented in chapter 5. Note that Silva's code also includes an option allowing a self-consistent calculation of the reduced electric field E/N, by comparing the electron density n_e with the number of positive ions created from CO_2, according to the global neutrality assumption. However, there is no Boltzmann solver included, hence the e-V reaction rates can not be updated during a simulation. Note also that the diffusion of ions is driven by a Lieberman-type diffusion, detailed and adapted in [70, 105, 106].

Gas mixture

The initial mixture composition is another important input. It allows the user to have mixtures of CO_2-N_2 in any proportions. So far, only CO_2 and N_2 are fully considered as particles in the model, while other species like CO, O_2 and O are just treated as extra collision partners with no discrimination of their vibrational states. It is possible to have already-excited populations *via* a vibrational temperature parameter, which is used to determine the VDF of the molecules according to a Maxwell-Boltzmann distribution. The total density of species depends on the pressure set as an input.

Geometry

Finally, the last inputs are geometrical parameters, representing the length L and the radius R of the tube where the discharge occurs. As the model is volume-averaged, the results do not depend on space, but the diffusion towards the walls will be greatly influenced by L and R.

Workflow of Silva's code

Figure 2.2 summarizes how Silva's code works, with the required database in green diamonds, the inputs and outputs in blue circles and the rate balance equations solver in the yellow rectangle. 'Mixture' denotes the ratio of CO_2-N_2 as well as their vibrational excitation, I_{exp} is the steady-state current used to derive the electron density over time, T_{gas} is the gas temperature (potentially updated thanks to recent features of the code), $(E/N)_0$ is the constant reduced electric field used to derive the electron-Vibration (e-V) reaction rates thanks to LoKI-B, R is the radius and L is the length of the reactor. The V-V and V-T notations stand for Vibration-Vibration and Vibration-Translation, respectively.

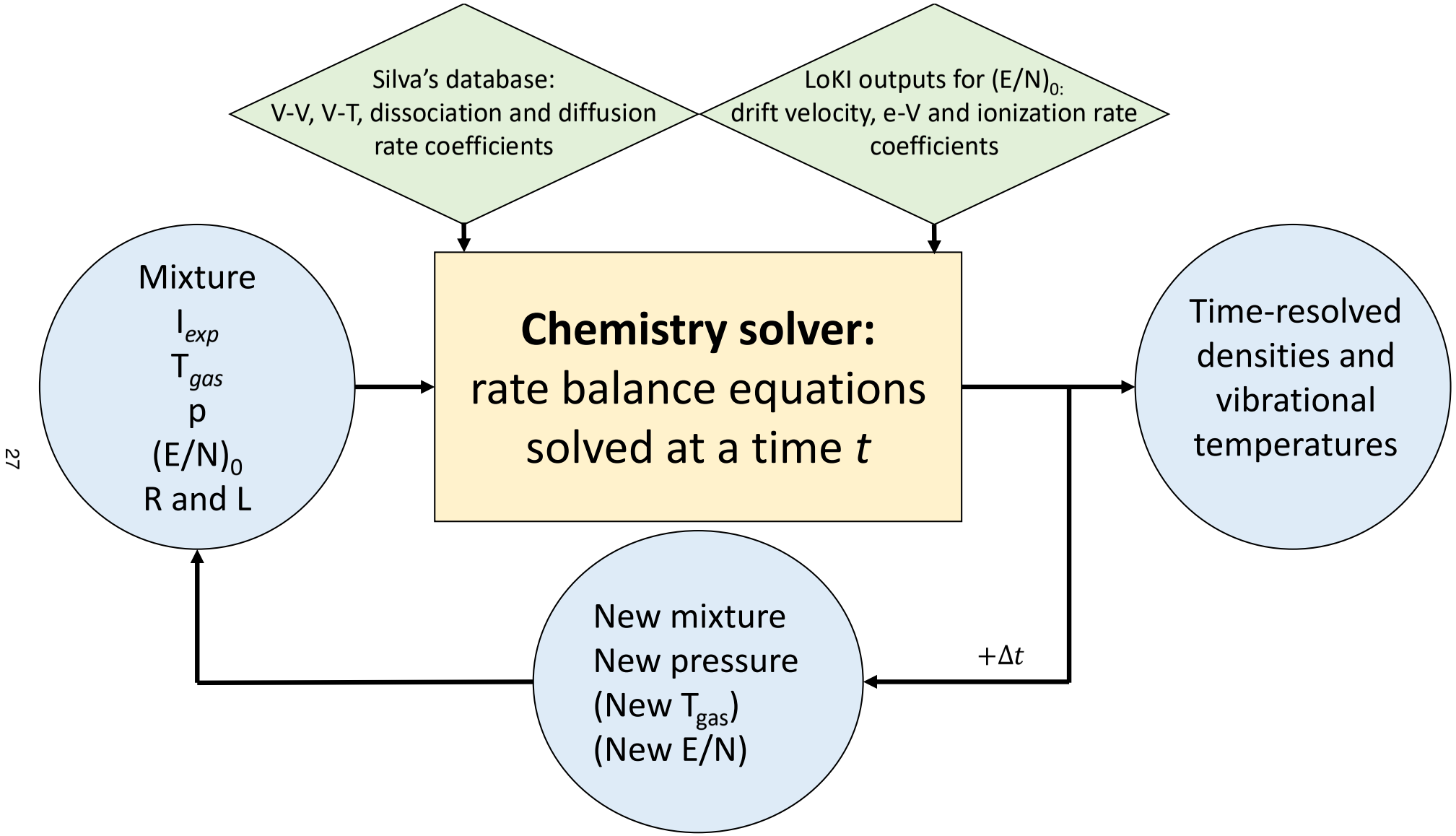

Figure 2.2: The workflow of Silva's code. Blue circles refer to inputs/outputs, green diamonds refer to required databases and the yellow rectangle refers to rate balance equations solver.

Chapter 3

Experimental work

3.1 Introduction

The motivations and the details of modeling CO_2-N_2 NTPs are presented in the previous chapters. They briefly recall the importance of comparing simulations results to 'real' data, *i.e.* measurements from actual experimental setups, in order to confirm the reliability of the model. However, existing measurements of vibrationally excited CO_2 and N_2 in cold plasmas are scarce. They most often come from the context of laser technology [20, 72], with data acquired only for the lowest levels of carbon dioxide. Having said that, the issue of the lack of data was partially solved by a collaboration between the modeling effort from Lisbon (at IST[1]) and the experiments from Paris (at LPP[2]). A. S. Morillo-Candas [45] was able to measure the time-resolved densities of CO_2 up to the 5^{th} vibrational level, for all modes, in CO_2-N_2 Direct-Current (DC) glow discharges. Measurements detailing so much the vibrational states were never obtained before in CO_2-N_2 cold plasmas, hence they represent a great new set of data for any modeler. Working together with LPP was also the occasion for me to go for a 2-months mission at the laboratory. While A. S. Morillo-Candas performed **pulsed** DC discharges in CO_2-N_2 plasmas, presented in chapter 4, I performed **continuous** DC discharges in CO_2-N_2 plasmas, presented in this chapter.

Global features about DC glow discharges were previously presented in chapter 1. There are many other types of discharge, using either DC or Alternate-Current (AC) power sources, but a detailed description is beyond the scope of this work. In this chapter, section 3.2 details the 2 diagnostics used for measurements, *i.e.* Fourier Transform Infra-Red (FTIR) spectroscopy and Raman spectroscopy. Section 3.3 presents the experimental setup with the typical operating conditions, for both the **pulsed** discharges performed by A.S. Morillo-Candas and the **continuous** discharges I performed. The results I acquired during the 2-month mission at LPP in **continuous** discharges are discussed in section 3.4 and partial conclusions are given in section 3.5.

[2]IST: Instituto Superior Técnico, Lisboa, Portugal.
[2]LPP: Laboratoire de Physique des Plasmas, Paris, France.

3.2 Diagnostics

This section presents the main diagnostic technique used for the measurements presented in this chapter and in chapter 4, *i.e.* the Fourier-Transform InfraRed (FTIR) spectroscopy [107]. The Raman spectroscopy [10] is also briefly described, as it was used by Morillo-Candas *et al.* to confirm the results from the FTIR measurements. The thesis is more focused on modeling than on experimental work, therefore this section does not intend to provide exhaustive explanations to the reader. One can find more details, if necessary, in the publications of B. Klarenaar *et al.* [108–110], in the thesis PhD of A. S. Morillo-Candas [45] and in the PhD thesis of M. Grofulović [12] where FTIR spectroscopy, Raman spectroscopy, actinometry and Two-photon Absorption Laser Induced Fluorescence (TALIF) in the context of CO_2 and CO_2-N_2 plasmas are extensively described.

As mentioned in chapter 1, the CO_2 molecule is active in the infrared when the bending and the asymmetric stretching modes are excited, and Raman active when the symmetric stretching mode is excited. As such, the two diagnostics described hereafter are complementary to assess vibrationally excited densities of CO_2. Note that some other techniques exist, for instance Quantum Cascade Lasers (QCL) [111] or Tunable Diode Lasers (TDL) (both using infrared absorption), but they are not used nor investigated in this work.

3.2.1 Fourier Transform Infra-Red (FTIR) spectroscopy

Global features

The setup of a FTIR spectrometer relies on a Michelson interferometer structure (see figure 3.1). As for any absorption techniques, the goal is to obtain a spectrum of the light after it passed through the medium of interest, in this case the plasma contained in the reactor. If the resulting spectrum exhibits a drop of intensity for a specific wavelength, it means that one species in the plasma is absorbing it. Its density is then related with the intensity loss thanks to the Beer-Lambert law, expressed under its general form for N absorbing species as:

$$T(\nu) = \frac{\Phi(\nu)}{\Phi_0(\nu)} = \exp\left(-\sum_{i=1}^{N} \sigma_i \int_0^L n_i(z)dz\right) \tag{3.1}$$

where $T(\nu)$ is the transmittance of the plasma for the frequency ν (or wavelength), Φ is the radiant flux transmitted by the plasma, Φ_0 is the radiant flux received by the plasma, σ_i is the attenuation cross-section of the species i, n_i is the density of the attenuating species i and L is the path length of the beam in the plasma.

The incoming source of light is a broadband IR source, containing many wavelengths. In short, one mirror can be moved to vary the length of one of the arms of the interferometer, to scan interferometric fringes for all the wavelength emitted by the IR source. This beam is then sent through the absorbing medium, in this case the plasma, where part of the light is absorbed by the molecules. The resulting light intensity obtained on the detector is measured for many mirror positions, to be finally Fourier-transformed to an actual spectrum. Figure 3.1 shows a scheme of the plasma reactor with a FTIR spectrometer. As

illustrated, the light goes through the length of the plasma L, which is assumed to be homogeneous under the operating conditions. The integral term in equation 3.1 is then simplified into $\int_0^L n_i(z)dz = n_i L$.

Some pre-treatments are required to have an exploitable spectrum with FTIR spectroscopy, requiring additional spectrum measurements:

- The 'background' of the FTIR source, required to obtain Φ_0 in equation 3.1. It is measured without gas in the reactor, while the source is on.
- The 'gas mixture' to verify if the imposed conditions, namely mixture, flow and pressure, are respected. It is measured with source on and plasma off (no voltage). In this case there is no energy supplied to the gas, hence all molecules are in thermal equilibrium. An example of a fitted thermal spectrum is illustrated in figure 3.2. Without excitation from the electrons the CO_2 does not dissociate into CO, as correctly assessed by the fitting script.
- The 'plasma emission': the plasma itself emits IR light even in the absence of the FTIR source. Some of this light goes directly to the spectrometer detector, while another part of it enters the interferometer before reaching the detector. Therefore, an extra measurement must be performed without the IR source, while the plasma is on, to take the reflected light into account.

It is worth mentioning that many other effects may occur and modify the results with spectroscopy techniques, such as temperature or pressure broadening of the emitted transition lines. Nevertheless, it is beyond the scope of this work to detail them here.

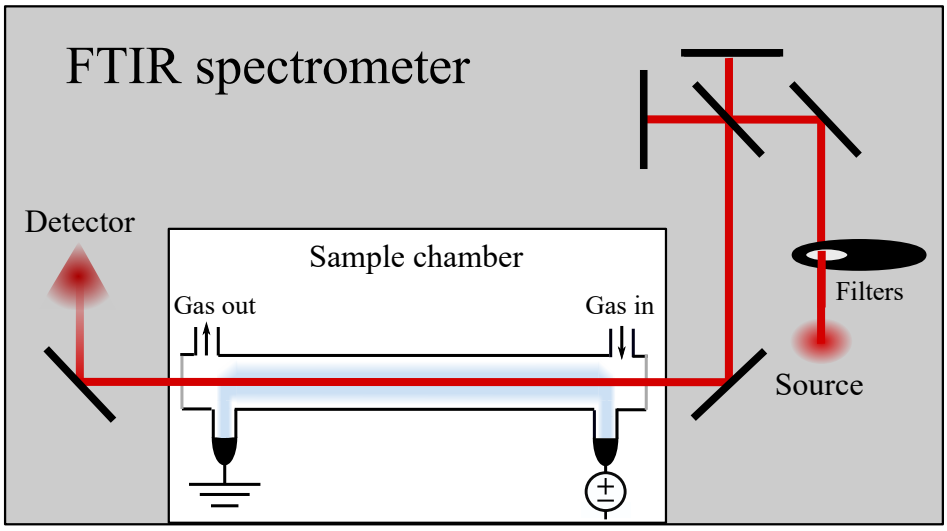

Figure 3.1: Scheme of a plasma reactor with a FTIR spectrometer, extracted from [45]

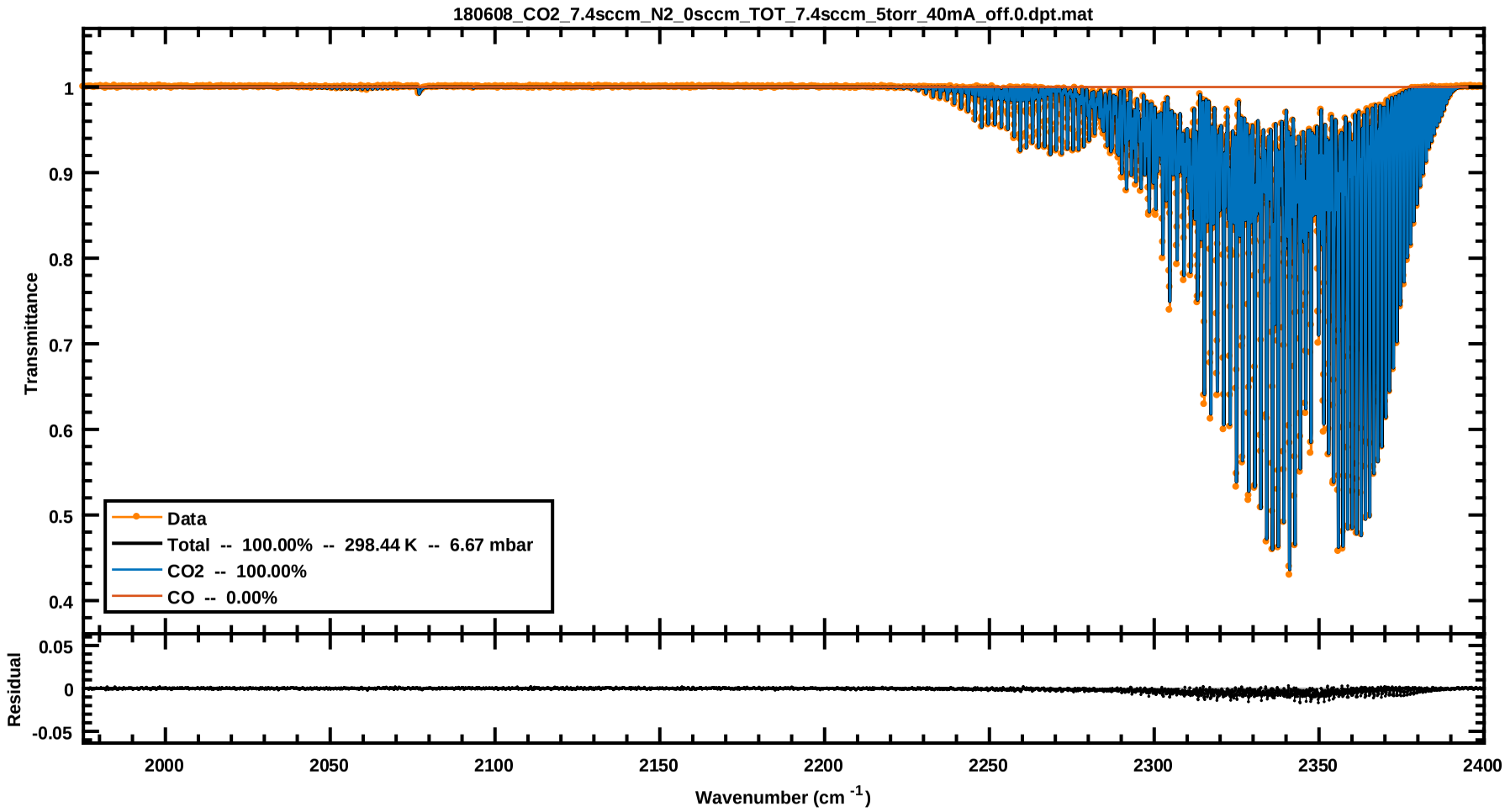

Figure 3.2: Example of a spectrum of the IR light source, plasma off, for 100% CO_2 at 5 Torr. The lines are fitted thanks to a script developed by Klarenaar *et al.* [112].

Data treatment

An IR spectra obtained from FTIR spectroscopy still requires post-treatment to give information about the excited populations. Under some assumptions, it is possible to relate the strength of the (absorbed) lines appearing on the spectra to the densities of the species. Typically, absorption between $\sim$2200 cm^{-1} and $\sim$2400 cm^{-1} correspond to the asymmetric stretch of CO_2, while lines appearing between $\sim$2000 cm^{-1} and $\sim$2250 cm^{-1} are a signature of vibrationally excited CO. The MATLAB scripts used to fit the lines and to compute the corresponding densities were developed by B. Klarenaar, and are extensively detailed in his PhD thesis and in the publication [112]. Here, we just briefly describe the 3 main options available:

- Thermal script: assumes thermal equilibrium. It is used when plasma is off. It is the case for the characterization of the 'gas mixture' to check the experimental conditions, or for post-discharges. The script relies on HITRAN database [113] for all the spectroscopic parameters.
- Out of equilibrium script: does not assume any equilibrium nor vibrational distribution. The rotational levels are assumed to have a Maxwellian distribution. The script determines the densities of the excited levels v_1, v_2 and v_3 for CO_2, v for CO, from the line strength. It also computes the conversion factor α and the rotational temperature T_{rot}, assumed to be equal to the gas temperature T_{gas}. It assesses the change in the pressure resulting from CO_2 dissociation. The script relies on HITEMP-2010 database [114].
- Out of equilibrium with imposed distributions: assumes Treanor distributions [22] for the vibrational populations of CO_2. Similar to the previous script for the rest, but assuming a specific distribution also allows to compute an equivalent vibrational temperature: T_{12} for the symmetric stretching and the bending (Fermi-coupled) and T_3 for the asymmetric stretching. It is worth mentioning that the results between this script and the previous one are in very good agreement, which implies that there is indeed an observable Fermi-coupling between v_1 and v_2, at least for low levels.

3.2.2 Raman spectroscopy

The basic mechanism of Raman spectroscopy consists in sending a monochromatic (*i.e.* one wavelength) light on a sample and in collecting the light scattered at 90° or 180°. From a wave point of view, the electromagnetic field of the incoming beam transfers energy to the field produced by the electron cloud of the molecules, inducing a dipole moment P. Under some assumptions, it is possible to express this dipole moment P as:

$$P = \alpha_0 E_0 \cos(2\pi\nu_0 t) + \frac{1}{2}\left(\frac{\partial\alpha}{\partial q}\right)_0 q_0 \left[\cos(2\pi(\nu_0 - \nu_p)t) + \cos(2\pi(\nu_0 + \nu_p))\right] \tag{3.2}$$

where α is the polarizability, E_0 is the vibration amplitude of the field, ν_0 is the laser frequency, q_0 is the equilibrium position and ν_p is the vibration frequency of the phonon (*i.e.* an energy quantum of vibration). The 3 terms of equation 3.2 correspond to different scatterings, explained hereafter. From a particle point of view, the molecules can be seen as excited by the incoming photons to an upper virtual state than their initial state. They then de-excite rapidly to a lower state, which characterizes the type of scattering:

- **Rayleigh scattering**: the molecule goes back to its initial state, hence there is no change of energy (elastic process) when the photo is re-emitted. This is the most probable type of scattering.
- **Stokes Raman scattering**: the molecule goes to an upper vibrational state than the initial one, hence there is a change of energy (inelastic process). Due to the law of energy conservation, the re-emitted photon has less energy than the incoming one.
- **Anti-Stokes Raman scattering**: the molecule goes to an lower vibrational state than the initial one, hence there is a change of energy (inelastic process). Due to the law of energy conservation, the re-emitted photon has more energy than the incoming one. This is the least probable scattering to occur.

Consequently, the laser beam has its energy shifted. The scattered light is collected and the shift is measured, using a notch filter to eliminate the very intense Rayleigh scattering. Figure 3.3 shows a typical collection of fitted Raman-shifts (Stokes only), giving information on the vibrational populations of CO_2-N_2 plasmas. The measurements were performed by M. Grofulović [12] in pulsed DC glow discharges with on-off time of 5-10 ms, for different types of mixtures and at different times. As for the FTIR spectroscopy, the collected data still require treatment to be exploitable. The scripts used at the University of Technology, Eindhoven (TU/e) were written by Klarenaar *et al.* [109]. More information is available about Raman spectroscopy in [10], about data treatment and results for pure CO_2 plasmas in [108–110] and results for CO_2-N_2 plasmas in [12, 115].

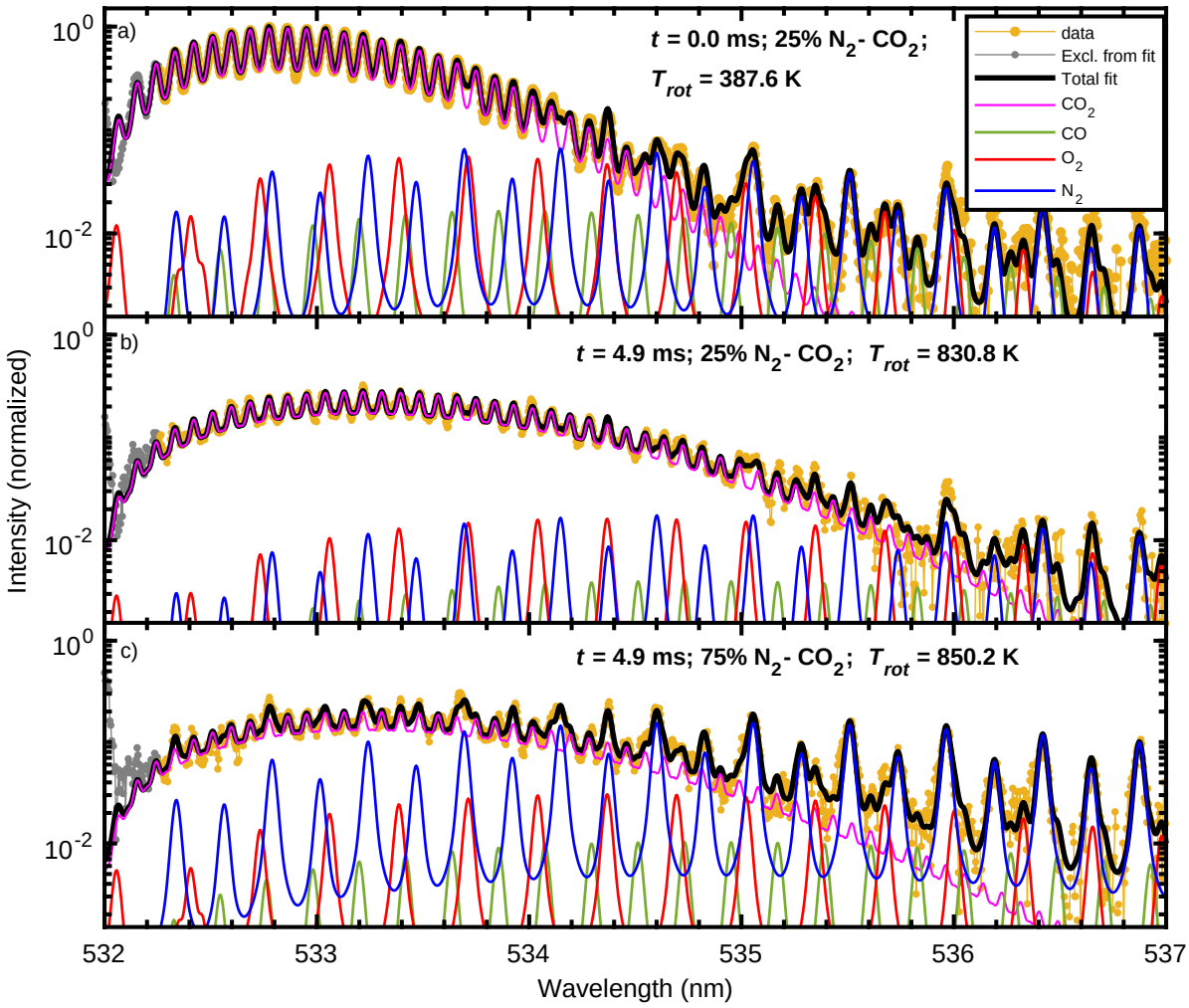

Figure 3.3: Extracted from [12]. The abscissa represent the Raman-shifts from the Stokes scattering, expressed in nm. The measurements were performed in pulsed DC glow discharges, at the middle of a 17 cm-long plasma.

3.3 Experimental setup

3.3.1 Plasma reactors at LPP

Results acquired in **continuous** and **pulsed** DC discharges (cf. chapter 1) were run onto 3 reactor facilities: (i) a reactor with an *in situ* FTIR spectrometer (see figure 3.4), suitable for measuring vibrationally excited populations, (ii) a reactor with a downstream FTIR spectrometer (see figure 3.5) and (iii) a straight reactor similar to (i) with tungsten pins, suitable for measuring electric fields. The electrodes consist in two metallic cylinders placed perpendicularly to the reactor tube, in order to ensure that the IR beam goes only through the **positive column** (cf. figure 1.7 in chapter 1) of the plasma, in the case of an *in situ* measurement. However, with this configuration the beam also goes through neutral gas at each edge of the tube, hence the plasma length is slightly shorter than the tube length.

All tubes are in Pyrex, which has an importance for surface interactions (see [45]). The L-shape reactor allows to perform measurements in the post-discharge without any influence of the materials of the gas line downstream the plasma, since both the plasma part and the downstream are in one single

piece made of Pyrex. The water injections were used to control the walls temperature. The dimensions of the reactor tube change from one facility to the other, but the measured electric field is assumed to be spatially uniform, so the electrical measurements do not depend on the tube length. Note that, concerning dimensions, the ratio between plasma length L_p and the reactor length L plays a role for the FTIR fitting scripts, while the reactor radius R is an important parameter for the diffusion of species towards the walls.

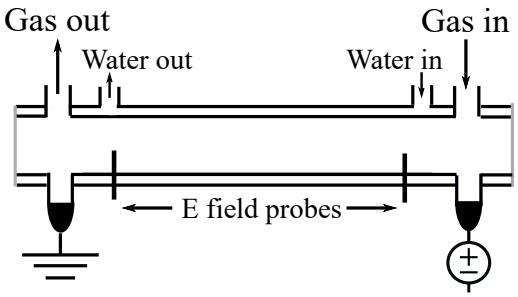

Figure 3.4: Figure extracted from [45]. Basic reactor for *in situ* FTIR and Raman measurements at LPP. Two reactors of different lengths but similar setup were used during the 2-months mission.

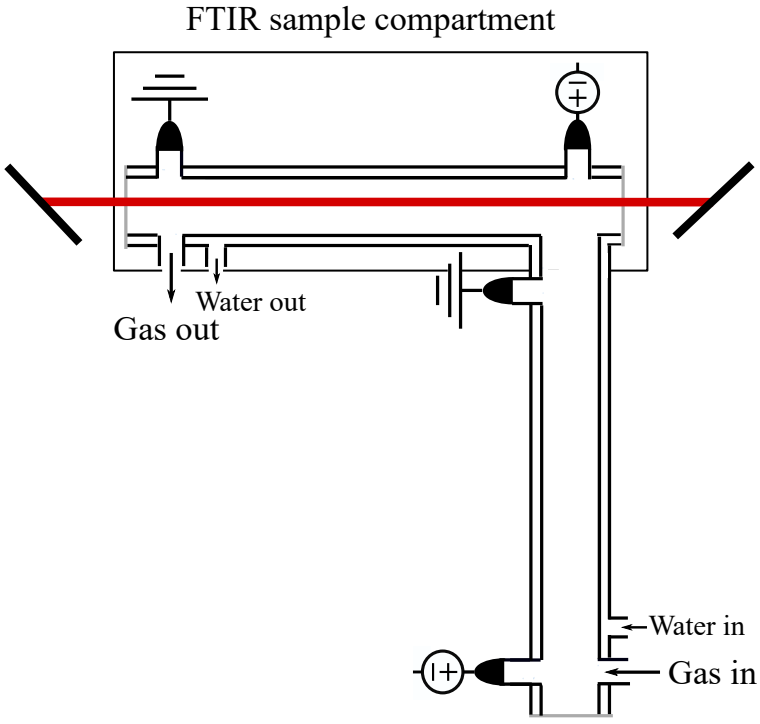

Figure 3.5: Figure extracted from [45]. L-shape reactor for downstream FTIR measurements at LPP. The red line represents the IR beam from a FTIR spectrometer. This setup was used to assess the influences of the walls and the gas residence time.

3.3.2 Operating conditions

The typical operating conditions for both the **continuous** and the **pulsed** regimes are summarized hereafter. The operating conditions needed to be restricted compared to the initial plan, due to time limitations and because some experimental data could not be fitted out of the ranges given below.

- **Initial gas pressure:** from 1 Torr to 5 Torr (133 Pa to 667 Pa). Depending on the pressure, the time required to stabilize the electric current may be long. The pressure gauge becomes very sensitive to any user modifications for the highest pressures.

- **Total flow:** 7.4 sccm (cf. text in sub–section 3.3.3), except for a few measurements where the flow was varied between 2 sccm and 20 sccm. The corresponding data is not presented in this work. See the work presented in [45] for details about the evolution of T_{rot}, α, and the vibrational temperatures against the flow/residence time.

- **Initial gas temperature:** room temperature at $\sim$20 $^\circ$ C, hence 293 $^\circ$ K.

- **Electric current:** from 10 mA to 50 mA. It is difficult to 'ignite the gas' into plasma for values below 10 mA.

- **Gas mixture:** from 30%-70% CO_2-N_2 to 100%-0% CO_2-N_2. It is possible to measure electric field in plasmas with lower CO_2 percentage than 30%, but the signal to noise ratio on the absorption spectra becomes doubtful and does not allow for accurate fitting of the vibrational temperatures and dissociation fractions. This issue is still questioned as some measurement in CO_2-O_2 plasmas were possible with lower percentage than 30% CO_2.

3.3.3 Total flow

All the measurements are done with a total mixture flow of 7.4 sccm (standing for *Standard Cubic Centimeters per Minute*). It corresponds to the 'reference' flow chosen at LPP. Its value may have an impact on the plasma kinetics: the fastest the flow, the shortest the residence time of the gas in the tube, hence some of the slowest reactions may not occur. The relation is given by:

$$\tau_{res} = \frac{N}{f} = 60 \cdot \frac{pV/k_B T_{gas}}{f_{(sccm)} \cdot (p^o V^o / k_B T^o)} \tag{3.3}$$

where 60 is a conversion factor from minutes to seconds, N is the number of particles, f is the flow in particles per unit of time, p is the pressure, V is the volume of the plasma, k_B is the Boltzmann constant, T_{gas} is the gas temperature, $f_{(sccm)}$ is the flow in sccm units and the superscript ^{o} denotes the *standard* parameters used as a reference for the flow, *i.e.* $p^o = 1$ atm$= 1.01 \times 10^5$ Pa and $T^o = 273$ $^\circ$ K. With pressures ranging from 1 Torr to 5 Torr, we observed gas temperatures ranging from $\sim 450^\circ$ K (at the lowest pressure) to $\sim 750^\circ$ K (at the highest pressure). With these values, equation 3.3 - appropriate for continuous discharges - gives residence times between 0.36 s and 1.1 s. Considering a characteristic time of $\lesssim 10$ ms for the slowest vibrational processes, the residence time of the gas is then long enough to ensure that the main kinetic reactions occur. It means, in this context, the kinetic reactions responsible for enhancing the VDF tail of $CO_2(00^0v_3)$, followed by the quenching reactions responsible for thermal equilibrium. Note, however, that some slower chemical reactions have been evidenced in such plasmas, depending strongly on the surface material [45]. The dependence of the dissociation parameter α on the flow/residence time was verified in [45]. It is shown there that α increases to a saturation value when the

flow lowers down to $\simeq 0.3$ sccm when the L-shape reactor (Pyrex tube) is used, *i.e.* when the surface interactions downstream are disabled. On the contrary, long residence times in metallic tubes tend to exhibit a drop of α, due to reactions on the walls. Therefore, the results presented in the next section for continuous discharges show a **lower** dissociation than for **a static gas undergoing continuous discharges** in similar conditions. When compared to the **pulsed DC glow discharges, for a 7.4 sccm flow** they show an **upper** limit instead.

Equation 3.3 is divided into two parts to approximate the residence time in pulsed discharges. For a on-time of 5 ms and an off-time of 10 ms, it becomes:

$$\tau_{res} = \frac{1}{3}\tau_{res}^{plasma} + \frac{2}{3}\tau_{res}^{gas} \tag{3.4}$$

where the τ_{res}^{plasma} is computed with $450°$ K$\leq T_{gas} \leq 750°$ K and τ_{res}^{gas} is computed with the room temperature. Note also that the plasma length, used to determine V, is actually shorter than the length of the reactor tube because of the position of the perpendicular electrodes. The plasma length is evaluated at 17 cm for a tube of 23 cm.

3.4 Results in continuous DC discharges

This section presents a part of the data I acquired during a 2-months mission at LPP. These results form a first set of data in **continuous** CO_2-N_2 plasmas. With the model validated from the comparison of simulations and experiments in **pulsed** plasmas (cf. chapter 4), this set will be used in the near future by the team at IPFN[3]/IST for further investigation of plasma kinetics.

3.4.1 Reduced electric field E/N

The floating potential is measured by 2 tungsten pins immersed in the plasma. It is corrected to take into account the resistors, the oscilloscope and the probe resistances. The tension measured is then divided by the distance inter-pins, which is 8.5×10^{-2} m on this facility, to give an electric field E expressed in V.m^{-1}. The electric field is finally divided by the gas density N deduced from the gas temperature measurements to obtain the reduced electric field E/N, in V.m^2, using the well-known ideal gas law $p = N \cdot k_B \cdot T\_gas$:

$$E/N = \frac{E \cdot k_B \cdot T_{rot}}{p} \tag{3.5}$$

where k_B is the Boltzmann constant in J.K^{-1}, $T_{rot} = T_{gas}$ is the rotational temperature in K derived from FTIR measurements in equal conditions, and p is the pressure in Pa imposed in the gas. For convenience, the reduced electric field E/N is converted from V.m^2 to Townsend (Td) while the electric field E is expressed in V.cm^{-1} instead of V.m^{-1} in the results hereafter. Note that, in chapter 4, the reduced electric fields E/N from **continuous** discharges were used as no equivalent measurement existed for

[3]IPFN: Instituto de Plasmas e Fusão Nuclear.

pulsed discharges. Indeed, the tungsten pins used to measure the floating potential of the plasma have to be connected to high resistances ($R =\sim 500$ MΩ), so the characteristic time $\tau = RC$ (C being the capacitance) is too large for the pulsed regime. The differences of electric current were not considered for the evaluation of E/N, *i.e.* the values derived at 40 mA were used for the 20 mA and the 50 mA cases presented in the next chapter. This is justified by considering the results from A. S. Morillo-Candás, who showed in figure 3.11 in Ref. [45] that the discrepancy is below 8%.

The measurements were done for different ratios of CO_2-N_2 mixtures, for pressures ranging from 1 Torr to 5 Torr, at constant current (40 mA) and constant total flow (7.4 sccm), in continuous DC discharges. As expected, lower CO_2 fractions required a higher electric field to reach the imposed 40 mA. This is explained by: (i) the lower ionization energy of CO_2 as compared to nitrogen, 13.78 eV vs 15.58 eV, respectively, and (ii) both molecules have 'similar' electronic cross-sections, in the sense that they both undergo inelastic processes with electrons whose energy is ≥ 0.1 eV. It is worth mentioning that, although Argon also has a higher ionization energy than CO_2 (*i.e.* 15.76 eV), the voltage required to sustain the plasma is nonetheless decreasing when the Ar fraction increases. This is due to the absence of relevant inelastic processes between argon and electrons below 11 eV, allowing low-energy electrons to travel longer without undergoing collisions, hence acquiring more energy from the field than in a pure CO_2 plasma. On the contrary, in CO_2-N_2 plasmas, more energy has to be provided when the N_2 fraction increases, which explains the decreasing trend of the E field measurements when plotted against CO_2 fraction at constant pressure (see figure 3.6). For the same reasons the E field curve has an increasing trend when plotted against the pressure, at constant CO_2 fraction: more energy is required to obtain a 40 mA plasma when the pressure raises (see figure 3.7). Note, however, that this trend is reversed for the **reduced** electric field E/N vs pressure, as the density denominator also increases (see figure 3.9). As shown in figure 3.8, the reduced electric field E/N increases when the fraction of N_2 increases. It is the opposite behavior of CO_2-Ar plasmas, where the reduced electric field decreases when the fraction of Ar increases [116]. The outcome of an E/N variation is not trivial, as many different processes can take place. Increasing E/N tend to increase the dissociation *via* the e_1 and e_2 excitation channels, at the cost of pumping up the asymmetric stretching mode. Such situation is illustrated and discussed more extensively in chapter 4, figure 4.7.

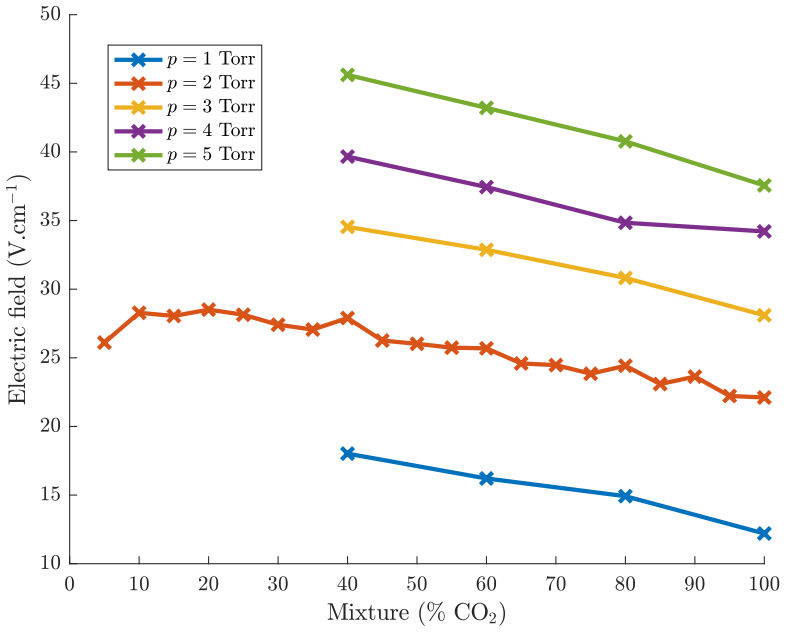

Figure 3.6: E field measurements vs mixture of CO_2-N_2 plasmas, in continuous DC glow discharges, at different pressures and at I $= 40$ mA.

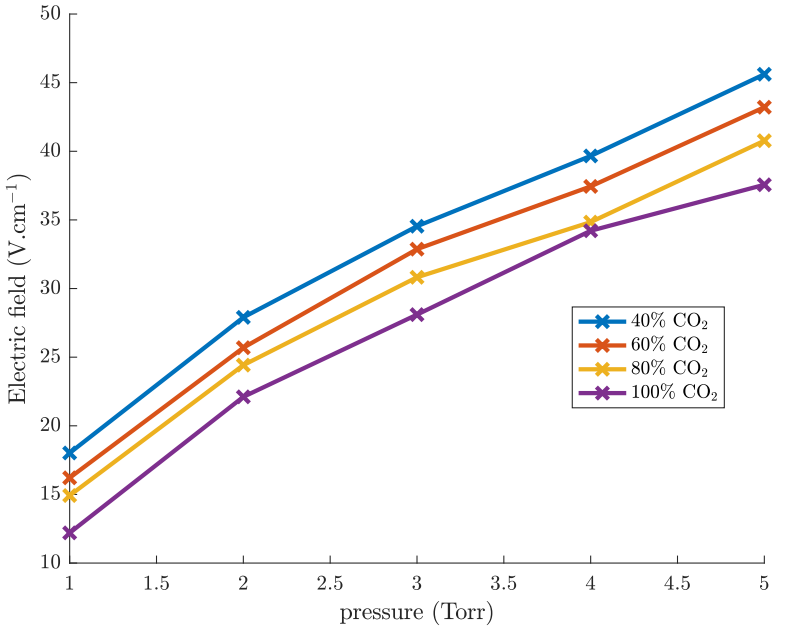

Figure 3.7: E field measurements vs pressure of CO_2-N_2 plasmas, in continuous DC glow discharges, at different mixtures and at I $= 40$ mA.

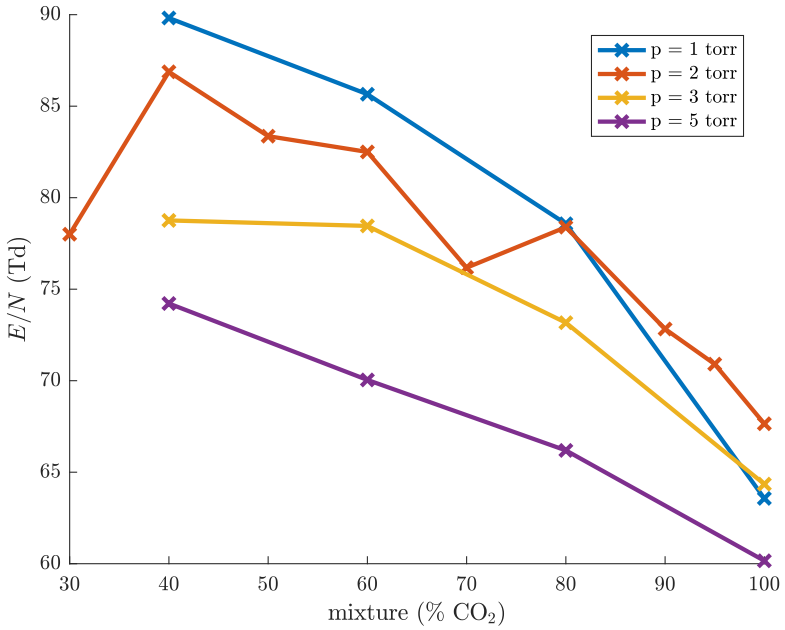

Figure 3.8: E/N reduced field measurements vs mixture of CO_2-N_2 plasmas, in continuous DC glow discharges, at different pressures and at I $= 40$ mA. Data for lower fraction than 30% CO_2 are not available as the corresponding FTIR spectroscopy failed.

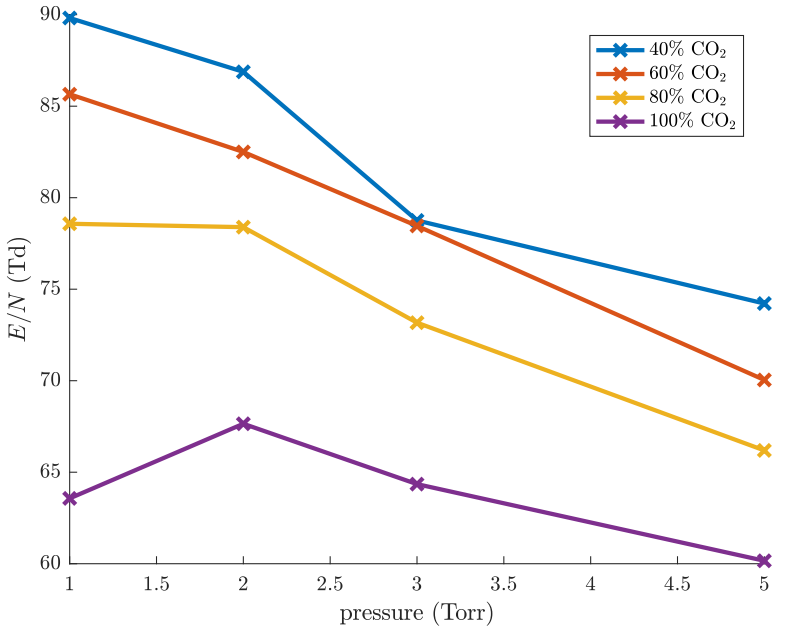

Figure 3.9: E/N reduced field measurements vs pressure of CO_2-N_2 plasmas, in continuous DC glow discharges, at different mixtures and at I $= 40$ mA.

3.4.2 FTIR measurements

The reactor (Pyrex walls) used for the FTIR measurements is illustrated in figure 3.4. It is 23 cm-long, with an electrode gap (hence approximate plasma length) of 17 cm. The setup for the FTIR spectrometer

is schematized in figure 3.1. Many measurements for different mixtures of CO_2-N_2 were taken, at a constant total flow of 7.4 sccm, electric currents of 20 and 40 mA, for 1, 2, 3 and 5 Torr (cf. the operating condition ranges described in sub–section 3.3.2). The duration of the data acquisition was fairly fast in these conditions, *i.e.* about a few seconds. Comparatively, more time was dedicated to modify the operating conditions, especially above 3 Torr as the pressure requires more time to stabilize. It is worth mentioning that data acquisition for time-resolved densities in pulsed DC glow discharges, performed by A. S. Morillo-Candas, takes on the contrary a few hours for one set of conditions only.

The measured and fitted quantities are the vibrational/gas temperatures of CO_2 (T_{12} and T_3) and CO (T_{CO}), the rotational temperature T_{rot} (assumed to be the same as the gas temperature T_{gas}), the dissociation parameter α and the fitted pressure (the pressure increases with dissociation). The script used for the data treatment is the 'Out of equilibrium with imposed distributions', described in sub–section 3.2.1, assuming Treanor distributions for the VDFs. It allows to compare vibrational temperatures rather than level-to-level densities, which makes the analysis easier. As mentioned in sub–section 3.3.3, the residence time is not long enough for α to reach its saturation value, hence the values given here are lower than for a static gas. Note that the dependence of the vibrational temperatures on the gas flow is indirect: they are modified due to the change in the mixture (measured by α) but the variations are very small as compared to the pressure effect.

Vibrational/gas temperatures as a function of CO_2 fraction

The FTIR measurements for the vibrational/gas temperatures are plotted versus the CO_2 fraction. The reason for it is to observe the influence of molecular nitrogen on the potential enhancement of the asymmetric stretching of CO_2, in order to increase the ladder-climbing dissociation. Consequently, varying the mixture was favored as compared with other parameters. As shown in figures 3.10 and 3.11, increasing the fraction of N_2 goes together with an increase of T_3 and T_{CO}, implying that the asymmetric stretching of CO_2 is indeed more excited when N_2 is added. Note that the values of T_{CO} have to be considered with caution, as it is the noisiest parameter, which is especially visible for the 1 Torr cases. The accuracy of T_{CO} fitting relies on weak absorption lines that are more difficult to fit properly out of the noise level than the other absorption lines. A comparison with [45] in pure CO_2 shows that the values of T_{CO} are similar, except for the 1 Torr cases where T_{CO} seems to be underestimated in the present results. Contrarily to T_3 and T_{CO}, the rotational temperature T_{rot} is very constant with N_2 fraction. This effect is not due to a poor accuracy of the measurements, as the expected slight increase of T_{rot} while the pressure increases is indeed captured by the measurements. The trend of T_{12} is a bit different: it is fully thermalized with T_{rot} in pure CO_2 but slowly increases with the fraction of N_2, an effect which may be attributed to the dilution of the very-effective O atoms quenchers. Consequently, adding nitrogen does not enhance the 'energy wastes', *i.e.* does not further excite the bending and the symmetric stretching of CO_2. Similarly, the fact that T_{rot} (hence T_{gas}) does not increase implies that the quenching reactions, leading to the thermalization of all species, is not accelerated by the addition of nitrogen. As expected, the non-equilibrium state of the plasma is stronger at low pressures, as too many collisions lead to the thermalization of the species with each other. A typical 'measure' β of the non-equilibrium strength

can be defined as the ratio of T_3 over T_{rot}: $\beta = T_3/T_{rot}$. Maximum values of β are $\lesssim 4$, obtained for mixtures of $30\%$$CO_2$-$70\%$$N_2$, at the lowest pressures for both currents. The evolution of the temperatures with the electric current is also interesting. Doubling the current implies a higher electron density in the plasma, so at first glance one would expect all the temperatures to raise. Although it is the case, there are differences between T_{rot} and T_{12} as compared with T_{CO} and T_3. In average, the relative increase of temperature from 20 mA to 40 mA is about 19% and 22% for T_{rot} and T_{12}, respectively, while it is about 11% for both T_3 and T_{CO}. From these results, it appears that an increase of electron density favors the 'energy wastes' rather than exciting favorably the asymmetric stretching mode, hence not interesting for an efficient ladder-climbing-based CO_2 dissociation. However, this conclusion is questioned when considering directly the dissociation parameter α.

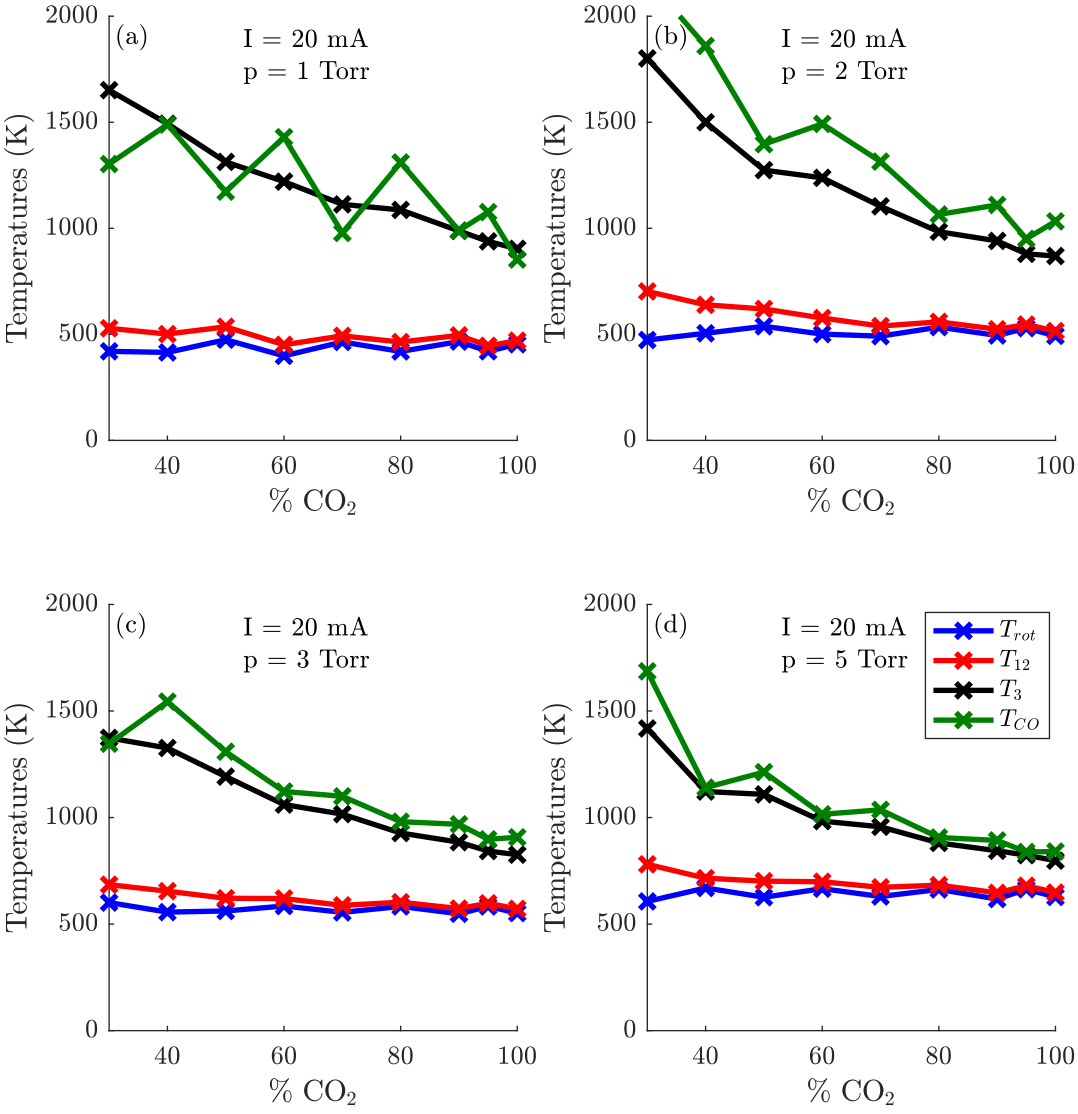

Figure 3.10: Vibrational temperatures derived from FTIR measurements in continuous DC glow discharges, at 20 mA. Temperatures are plotted versus different CO_2-N_2 fractions. Panels (a), (b), (c) and (d) show results for different pressures.

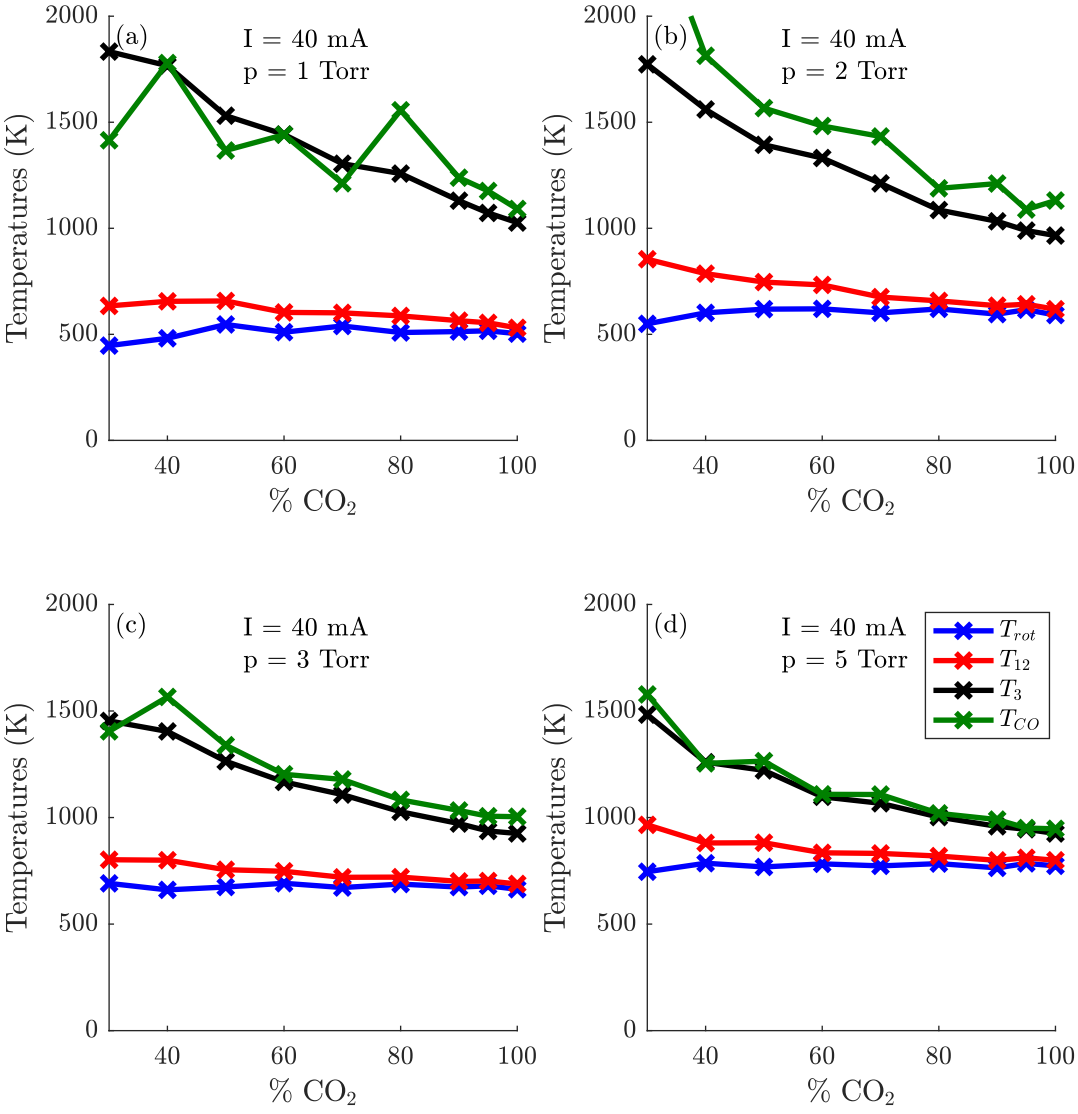

Figure 3.11: Vibrational temperatures derived from FTIR measurements in continuous DC glow discharges, at 40 mA. Temperatures are plotted versus different CO_2-N_2 fractions. Panels (a), (b), (c) and (d) show results for different pressures.

Dissociation parameter α as a function of CO_2 fraction

Figure 3.12 shows the dissociation parameter $\alpha = [CO]/([CO] + [CO_2])$ as a function of the CO_2 fraction in the plasma. As the results for both currents are plotted on the same graphs, it is evident that increasing the current leads to more dissociation. Surprisingly, the α increase is roughly constant, about 0.10 whatever the pressure conditions and the fractions of CO_2. Because molecules have a low vibrational excitation, the larger value of α may be attributed to an increase of the rate of dissociation due to processs e_1. This assertion is discussed hereafter with the help of additional simulations, for the representative case $p = 3$ Torr.

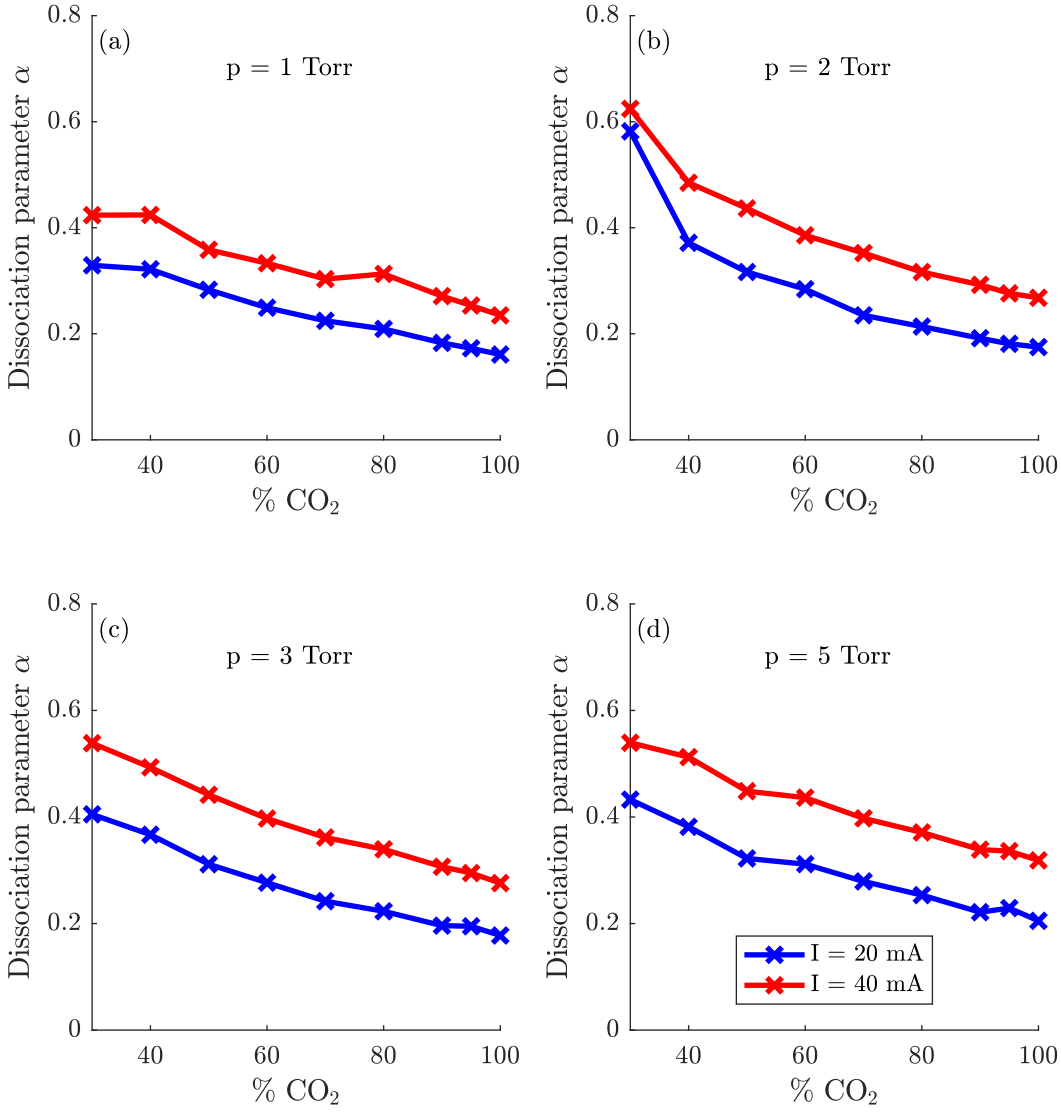

Figure 3.12: Dissociation parameter α derived from FTIR measurements in continuous DC glow discharges. It is plotted versus different CO_2-N_2 fractions. The blue line (—) corresponds to I = 20 mA and the red line (—) corresponds to I = 40 mA. Panels (a), (b), (c) and (d) show results for different pressures.

Figure 3.13 shows 4 EEDFs computed by the Lisbon KInetics Boltzmann (LoKI-B) solver. The

solid lines correspond to the conditions for 60% CO_2 - 40% N_2 (no CO included), at 3 Torr, for 20 and 40 mA. The gas temperature corresponds to the measured rotational temperature and the experimental temperatures are used to define the vibrational populations (Boltzmann distribution) of CO_2 and N_2, assuming $T_{N2} = T_3$. The electron densities are determined from equation 2.14, the drift velocities being derived from [117], so $n_e^{40\text{ mA}} = 2 \cdot n_e^{20\text{ mA}}$. Note that electron density plays a role on the EEDF's shape only if the electron-electron collisions are activated. These collisions may have a non-negligible effect only when $n_e/N > 1 \times 10^{-4}$ [70], while in our conditions we have $n_e/N < 1 \times 10^{-6}$, hence electron-electron collisions were not considered. The dotted lines in figure 3.13 were calculated using the exact same inputs as for the solid lines, with the exception of the mixture, set at 100% CO_2. As this set of parameters does not correspond to any experiment performed at LPP, it is denoted as 'Fake 100% CO_2' in the figure. The interest is to observe the variations induced by the modification of only one parameter, namely the mixture. By contrast, the dotted lines in figure 3.14 are denoted as 'Real 100% CO_2' because the inputs are derived from the experiments in pure CO_2, at 3 Torr, for 20 and 40 mA. The input parameters used to generate both figures are summarized in tables 3.1 and 3.2.

Table 3.1: Input parameters for LoKI-B simulations, for the 20 mA case at 3 Torr.

20 mA	**Mixture**	**E/N (Td)**	n_e **(m^{-3})**	T_{gas} **(K)**	T_{12} **(K)**	T_3 **(K)**	T_{N2} **(K)**
Default case	60% CO_2 - 40% N_2	78.46	1.04E+16	585	620	1061	1061
Fake case	100% CO_2	78.46	1.04E+16	585	620	1061	
Real case	100% CO_2	65	1.02E+16	552	552	826	

Table 3.2: Input parameters for LoKI-B simulations, for the 40 mA case at 3 Torr.

40 mA	**Mixture**	**E/N (Td)**	n_e **(m^{-3})**	T_{gas} **(K)**	T_{12} **(K)**	T_3 **(K)**	T_{N2} **(K)**
Default case	60% CO_2 - 40% N_2	78.46	2.08E+16	691	748	1167	1167
Fake case	100% CO_2	78.46	2.08E+16	691	748	1167	
Real case	100% CO_2	65	2.04E+16	663	688	925	

Concerning the 60% CO_2 - 40% N_2 mixture (solid lines in figures 3.13 and 3.14), the EEDF calculated at 40 mA has a higher tail than at 20 mA, *i.e.* a higher fraction of electrons at high energies. This is due to larger excited populations, imposed in the simulations *via* a Boltzmann distribution. Therefore, a larger fraction of high-energy electrons is required to reach a state with more excited molecules, explaining the tail enhancement. From 20 mA to 40 mA, the fraction of electrons at $E = e_1 = 7$ eV increases of $\sim 11\%$. Consequently, the e_1 dissociation rate coefficient is also modified (see equation 2.6 or equivalently equation 4.2), the model predicting an increase of $\sim 15\%$ the reaction rate coefficient. Together with the fact that there are twice more electrons at 40 mA than at 20 mA, it is likely that the increase in α is mainly due to an e_1 dissociation-like reaction.

In both figures 3.13 and 3.14, it seems that including N_2 strongly deforms the EEDFs' shape, resulting in a larger concentration of low-energy electrons. The energy range $[0\ ;\ 2]$ eV concentrates the vast majority of the vibrational excitation cross-sections from elecron impact, according to the IST-Lisbon database on LXCat [118]. Therefore, it would *a priori* imply that including N_2 results in higher excitation of both N_2 and CO_2 molecules. Although this is observed for T_3, which drastically increases with the N_2 fraction, it is not the case for T_{12} which remains almost constant. Indeed, while the *inelastic* rate

coefficients for vibrational excitation increase with the N_2 fraction, it also the case of their *superelastic* counter-part, resulting in a quasi-constant net rate. Consequently, the increase of T_3 and T_{12} is not likely to be explained by the modification of the EEDF's shape. Instead, it may be due to very efficient Vibrational-Vibrational (V-V) transfers from the excited N_2 molecules towards the asymmetric stretching mode of CO_2. This hypothesis is supported by the fact that T_3 increases far more than T_{12}, as if N_2 was acting as an 'energy reservoir' for $CO_2(00^0v_3)$. Let us now consider the EEDFs in figure 3.14, at 40 mA, from the 60% CO_2 mixture (solid red line) and the 100% CO_2 mixture (dotted red line). It appears that the fraction of electrons having an energy greater than 7 eV is roughly the same in both cases. Moreover, the rate coefficient for the e_1 dissociation reaction is equal in both cases. Therefore, the large difference in the dissociation parameter α cannot be explained by the e_1 dissociation reaction alone. In such low-excitation regimes, it is unlikely that the ladder-climbing-based dissociation plays a significant role, hence it does not explain the enhanced dissociation neither. A possible explanation lies in a 'dilution effect' of the very-efficient O atoms quenchers, as their relative density compared to the total gas density lowers with the addition of N_2. This question is addressed in chapter 4 in more detail.

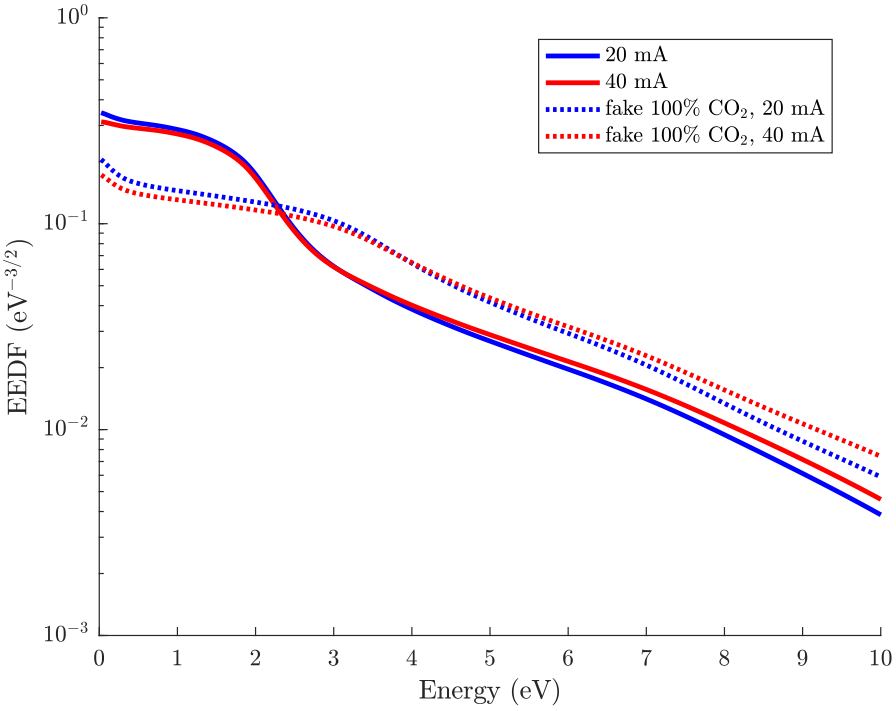

Figure 3.13: EEDFs computed by LoKI-B, for two different currents, with inputs derived from the measurements made at 60% CO_2 - 40% N_2 and 3 Torr. The solid lines correspond to the real 60% CO_2 - 40% N_2 mixture while the dotted lines correspond to an artificial 100% CO_2 mixture.

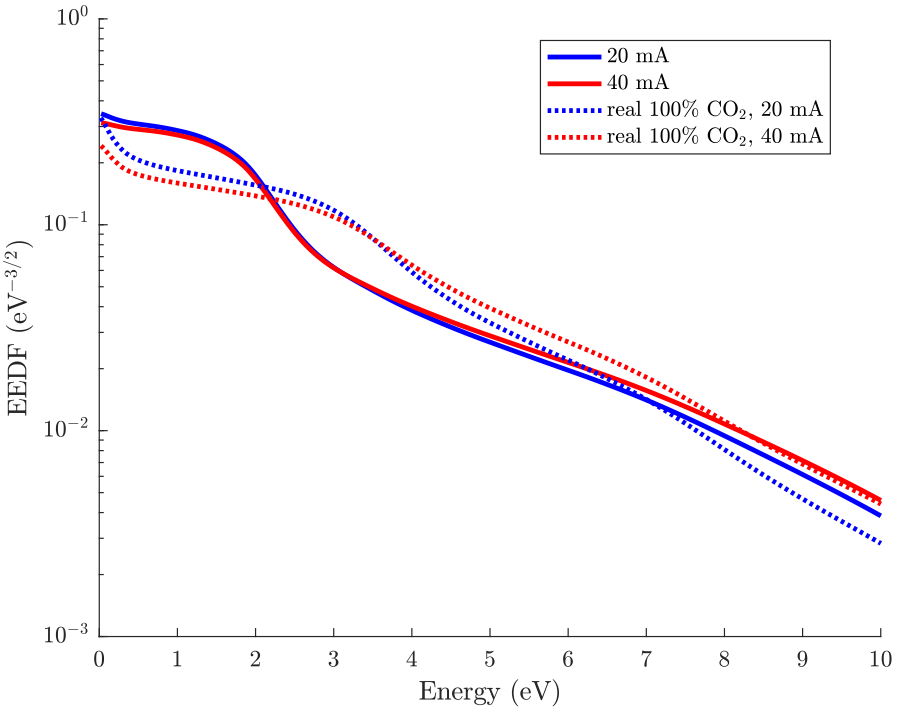

Figure 3.14: EEDFs computed by LoKI-B, for two different currents, with inputs derived from the measurements made at 3 Torr, for two mixtures. The solid lines correspond the 60% CO_2 - 40% N_2 mixture while the dotted lines correspond to the 100% CO_2 mixture.

Nevertheless, an interesting fact is that even in such low-excitation regimes the dissociation parameter α increases with the proportion of N_2. In our conditions, dissociation proceeds mainly by direct electron impact and the contribution of the ladder-climbing mechanism to dissociation is small. Consequently, the increase of α may be even larger in discharges with larger VDF tails, taking fully advantage of vibrational processes (see orange and red arrow in figure 1.6). However, in the present results, the CO produced slowly decreases with the proportion of N_2 in the gas. If one's goal is the absolute quantity of CO production, then the best mixture correspond to 100% CO_2 for the conditions under study. On the other hand, if the goal is to have an efficient conversion of CO_2 into CO, then the higher N_2 fraction the better. Taking more advantage of vibrational processes by tailoring the VDFs may help to dissociate more, to the point that the absolute CO produced may actually increase with the nitrogen fraction.

3.5 Conclusions

The 2-month mission at LPP was a great opportunity to learn more about experiments in general and helped, for instance, to understand existing difficulties that a modeler may not think about. A typical example, worth to mention due to its unexpected nature, deals with the time-resolved measurements from FTIR spectroscopy. Indeed, such measurements are actually impossible to acquire in summer, for room temperature reasons. As the data acquisition time lasts hours, the setup initially cooled with liquid nitrogen warms up too much to provide exploitable results. Adding more nitrogen during the experiments

perturbs the diagnostic too much as well, as it is very sensitive.

The results acquired in continuous discharges at LPP show that, when the N_2 fraction increases, the asymmetric mode of CO_2 is getting more energy and the CO produced is more vibrationally excited. These observations are very interesting for the investigation of ladder-climbing processes, although there is no direct evidence of such phenomena here. It is nonetheless promising for a high-excitation regime, where N_2 would potentially be preliminary excited. As discussed in section 3.4, the increase of T_3 and T_{CO} when the N_2 fraction increases may be attributed to 3 main mechanisms: (i) a modified EEDF shape, which is found to have a minor influence, (ii) important V-V exchanges between excited N_2 and $CO_2(00^0v_3)$ and (iii) a 'dilution effect' of efficient quenchers, especially the O atoms produced from CO_2 dissociation. Providing an accurate analysis of the dominant processes is not trivial and requires the use of dedicated physical models, such as done in chapter 4. Note that future simulations will also take into account the electronic reactions for CO and O species, a feature recently allowed by the development of the LoKI tool suite.

From the perspective of nitrogen impurities resulting from CO_2 capture, there is confirmation that N_2 would help the CO_2 conversion efficiency. Indeed, the results clearly show an enhancement of CO_2 dissociation, relative to its initial concentration, when the N_2 fraction increases. Even the absolute CO production is only slightly reduced when the nitrogen fraction increases until 70%. However, the mechanisms responsible for this enhanced conversion require more data and modeling investigations to be correctly identified. In the future, data acquired at LPP will be further used to validate the physical model, once its numerical implementation is adapted to DC **continuous** discharges. For the present work, the model from Silva *et al.* presented in chapter 2 simulates DC **pulsed** discharges, more suitable for a step-by-step validation of the kinetic scheme. The version enriched with N_2 reactions and the comparison with experimental results in DC **pulsed** discharges are detailed in chapter 4.

Chapter 4

Exploitation of the physical model for CO_2-N_2 plasmas in pulsed DC discharges [1]

4.1 Introduction

In order to better understand the driving mechanisms behind vibration kinetics, reproduce and interpret experimental results, and later on optimize the energy efficiency or the yield of dissociation, a modelling effort is being pursued at Instituto Superior Técnico (IST), Lisboa, supported by dedicated experiments in DC pulsed discharges undertaken at the Laboratoire de Physique des Plasmas (LPP), Ecole Polytechnique, Palaiseau, and at the Technische Universiteit Eindhoven [40–43]. The non-equilibrium state-to-state kinetic model developed at IST couples the electron Boltzmann equation with a system of rate balance equations describing the creation and loss of several vibrational levels and positive ions. It is used to obtain the time-evolution of the densities of each vibrationally excited level, depending on various input parameters. However, the complexity of state-to-state models can grow very fast with the number of vibrational or electronic states considered for each species, a growth accompanied by a loss of reliability due to the lack of experimental measurements and of accurate information on the required rate coefficients.

The strategy followed in [40–43] consists in a step-by-step validation of the kinetic scheme and the relevant rate coefficients, keeping on purpose a fairly low complexity of the system. To do so, the vibrational levels considered had been limited to $v_1^{max} = 2$, $v_2^{max} = 5$ and $v_3^{max} = 5$, resulting in 72 levels for CO_2. The CO_2 levels considered correspond to the measurable densities of vibrationally excited molecules in pulsed DC discharge experiments at pressures around 1 Torr [41–43]. In these previous publications, M. Grofulović [40, 41] and T. Silva [42, 43] established the validity of the model for low excitation conditions, in which the role of dissociation products (mainly O, O_2 and CO) and of high

[1] Parts of this chapter are based on [14]

vibrational levels is negligible, by comparing model predictions and experimental data in single-pulse discharges in pure CO_2 [109]. More details about the model and its implementation can be found in chapter 2.

Herein, we focus on the addition of molecular nitrogen to the model and on its validation, while maintaining a low excitation regime, by further accounting for levels up to $v_{N_2}^{max} = 10$ for N_2. This upper limit is high enough to reproduce adequately the main vibrational mechanisms of a low-excitation regime, since in the present conditions the relative population of this level is always below 10^{-5}, comparable with the population of the highest CO_2 vibrational level considered, $CO_2(25^55)$. This was further confirmed by running simulations extending the upper limit to either $v_{N_2}^{max} = 48$ or $v_{N_2}^{max} = 59$, depending on the N_2 potential chosen [62], with no noticeable changes in the results. Additionally, keeping the number of levels fairly low helps reducing the computational cost and avoids the propagation of errors introduced by classic scaling theories [62]. The modelling effort is complemented by new experiments performed in DC pulsed discharges in CO_2-N_2 mixtures, using *in situ* time-resolved step-scan Fourier Transform Infrared Spectroscopy (FTIR) to accurately access the CO_2 vibrational state densities, using the experimental setup and diagnostics described in detail in [108, 109] and the chapter 3 herein. Despite the focus on a low-excitation regime, the possible influence of the deactivation of vibrationally excited N_2 and CO_2 by atomic oxygen is evaluated, since in the experiments presented in this work a non-negligible density of atoms may be present due to its accumulation in the reactor from pulse to pulse. Note that the FTIR measurements were done after that the density of O atoms stabilized. Hence, their population does not evolve on time during the measurements.

The current formulation avoids the description of higher vibrational levels and of a complex chemistry. Nevertheless, it constitutes an additional step in the validation roadmap initiated in [40], as it now includes many processes where N_2 is implied, namely vibration excitation from electron impact, V-T and V-V exchanges, deactivation at the walls, as well as a parametric quenching from O atoms for both N_2 and CO_2. It brings a major advance when compared with the studies of the laser system, which typically account only for ~ 5 CO_2 vibrational levels and a single N_2 vibrational level [20].

The structure of this chapter is as follows. Section 4.2 describes how the reactions including molecular nitrogen and quenching of CO_2 by atomic oxygen are implemented in the model. The former include electron impact reactions, vibration-translation and vibration-vibration exchanges, and diffusion towards the walls. Section 4.3 briefly reviews the setup used for the pulsed DC discharge FTIR measurements. The comparison between the experiments and the simulations is presented and discussed in section 4.4. Finally, section 4.5 summarizes the main results of the work.

4.2 Reaction rates refinements

The procedure adopted to validate the model is the same followed in [41–43], here with the addition of molecular nitrogen. The simulations in [41–43] reproduce very well the experiments available in pure CO_2. Hence, the next validation step consists in including vibrational energy transfer processes involving molecular nitrogen and in comparing the model predictions with measurements in CO_2-N_2 mixtures.

Keeping a low dissociation degree is desirable to establish the reliability of the rate coefficients involved in the N_2 and CO_2-N_2 kinetics. In fact, having a high dissociation rate asks additionally for an accurate description of the processes involving CO, O_2, O, NO, etc, not considered here. These mechanisms are relevant for a real plasma processing reactor and will be systematically investigated in the future.

The simulations performed when establishing a reaction mechanism for pure CO_2 describe accurately the 'single-pulse experiment' from [109], where only one on-off cycle of length 5 ms-150 ms takes place during the gas residence time, with a pressure $p = 5$ Torr and a discharge current $I = 50$ mA [41–43]. The CO_2 gas is initially at room temperature and the simulations in [41–43] were divided into two time ranges: one corresponding to the active part of the discharge, when a voltage is applied during 5 ms; and another one to the afterglow, when no voltage is applied. Having only one pulse ensures a negligible dissociation, so that only V-T and V-V CO_2-CO_2 processes and electron impact excitation and de-excitation of CO_2 vibrational levels (e-V) are at play, as accounted for in the model. An adequate agreement with experiments in a 'multi-pulse' regime (several on-off cycles take place during the gas residence time) in CO_2 was also obtained in [42], showing that even in these conditions the simplified model provides a powerful tool to interpret the experimental results.

New multi-pulse experiments for CO_2-N_2 mixtures, performed for discharge operating parameters similar to those in [41–43], are described in detail in section 4.3. They are used to characterize the discharge and for model validation. In these conditions, a non-negligible dissociation is usually present (*cf.* table 4.2 in section 4.4). Therefore, the influence of the deactivation of vibrationally excited N_2 and CO_2 by O atoms in the results is also evaluated parametrically in the model. The reliability of the present CO_2-N_2 model is discussed in section 4.4, where further insight into the importance of dissociation in a multi-pulse case is also given.

In the non-thermal plasmas under study the gas temperature remains relatively low as compared with the vibrational ones, typically between 300 and 900 K, with a maximum occurring during the discharge. On the other hand, approximating the population of the vibrational states of CO_2 by a Boltzmann or a Treanor distribution leads to vibrational temperatures of the asymmetric mode v_3 between 1000 and 2000 K [41–43], which are suitable to enhance vibrational kinetics. The following paragraphs describe in detail how the mechanisms involving vibrationally excited N_2 and the quenching of vibrationally excited CO_2 and N_2 by O atoms are added to the model.

4.2.1 General formulation

The physical model and its numerical implementation are extensively detailed in sections 2.3 and 2.4 of chapter 2, where one can find information about the main equations solved and the required inputs. Here, we briefly recall the main principles: (i) to identify the main reactions driving the cold plasma kinetics, (ii) pairing a reaction with a reaction rate coefficient, or alternatively with a cross-section and (iii) using this reaction rate coefficients to solve the rate balance equations for each individual vibrational level n_v, at each time step (cf. eq 2.12).

The base model includes V-T and V-V exchanges in collisions N_2-N_2, CO_2-CO_2 and CO_2-N_2. However,

vibrational relaxation induced by collisions with oxygen atoms can be significant and its influence is studied parametrically, by considering constant values for the gas phase atomic oxygen concentration and including V-T deactivation in N_2-O and CO_2-O collisions. This procedure is suited for the purpose of the present investigation, as it allows to avoid a complex O-based chemistry and to asses separately the role of different phenomena. It is worth mentioning that according to [53, 61], in the range of [200 K ; 1500 K], the rate coefficients for the deactivation $N_2(v)$+O are at least five orders of magnitude higher than $N_2(v)$+CO or $N_2(v)$+O_2 processes, however remaining about one order of magnitude lower than those of CO_2 deactivation by O atoms. For the CO_2, the quenching from CO and O_2 becomes comparable with the quenching from O atoms only for gas temperatures above 1000 K, hence their effect was not included in the present work.

While chapter 2 gives a global picture of the main features of the physical model, the next subsections focus on the implementation of the processes involving N_2 molecules and O atoms, *i.e.* the personal contribution to the base pure CO_2 code. The presented work is divided into three main mechanisms: electron impact collisions, V-V and V-T energy transfers and, finally, deactivation at the wall.

4.2.2 Electron impact (e-V) rate coefficients

There is always a flow of electrons gaining their energy from the applied electric field, whatever the type of discharge under study. This energy is unevenly shared by the electrons, most of them having low velocities, while a smaller fraction is much faster. They interact *via* not only electron-electron collisions but also electron-heavy particle collisions, for instance exciting a molecule to an upper vibrational state. This latter process can lead to a consequent amount of energy stored in a gas under vibrational form, but there are other channels where electrons can lose their energy, like ionization, excitation to an upper electronic state and molecular dissociation.

The probability for a specific reaction to happen is strongly dependent on the electron kinetic energy. Thus, modelling requires an accurate description of the electron energy distribution function (EEDF). Its calculation is achieved here using the LisbOn KInetics Boltzmann tool (LoKI-B) [68], which numerically solves a space-independent form of the two-term electron Boltzmann equation. Most of the required electron scattering cross-section data can be found at the open-access website LXCat [118]. For this work we use the IST-Lisbon database both for N_2 [119] and CO_2 [40]. To obtain the rate coefficients for electronic excitation $N_2(v)$+$e^- \rightarrow N_2(v+n)$+e^- for any $v > 0$, where v and $v+n$ denote vibrationally excited states, required to solve equation (2.12) for N_2 vibrationally excited states, the scaling law given by Colonna in [103] for nitrogen is applied,

$$k_{v,v+n} = \frac{k_{0,n}}{1+av} \ , \tag{4.1}$$

where k_{v_1,v_2} is the rate coefficient associated to the excitation $N_2(v_1) + e^- \rightarrow N_2(v_2) + e^-$, $k_{0,n}$ is calculated from the corresponding cross-section for $\{v = 0, n \leq 10\}$ all known, and a is a fitting parameter equal to 0.15 [103].

Once the EEDF is known, the rate coefficient associated to a specific process can be obtained from

$$k = \sqrt{\frac{2}{m_e}} \int_0^\infty \sigma(u) f(u) u \, du \, , \tag{4.2}$$

where m_e is the electron mass, $f(u)$ is the EEDF with the normalization $\int_0^\infty f(u)\sqrt{u}\, du = 1$, u is the electron kinetic energy and σ is the cross-section associated with the process considered. It was verified that, for fixed E/N and in the range of parameters corresponding to the experimental conditions under study (see section 4.3), the dependences of the e-V rates with the gas temperature, initial vibrational distribution, pressure and mixture composition are all negligible. Thus, we considered averaged values of pressures and temperatures derived from the experimental measurements for our calculations.

4.2.3 Vibration-Vibration (V-V) and Vibration-Translation (V-T) rate coefficients

V-V and V-T energy exchanges occur both in the discharge and in the afterglow. Their influence is especially emphasised in the latter case, as the electron contribution can be neglected. Various sources are available in the literature compiling rate coefficients derived either from theory [52, 53] or experiment [20, 120]. However, considering the number of vibrational levels to take into account, the diversity of species involved, as well as the difficulty to obtain accurate measurements, no reference can be exhaustive. Furthermore, depending on the experimental results and the type of scaling with vibrational level applied, the rates given for the same process can vary over several orders of magnitude.

In this work, we focus on the datasets from Blauer [53] and Plönjes [55], who based their work partly on the quantum calculations of Billing [52] and Capitelli [121]. Various rate coefficients are fitted versus the gas temperature in these reports. For the missing reactions, two types of scaling laws were applied, depending on the corresponding process (see below): the classic SSH (Schwartz, Slawsky, Herzfeld) theory [122–124], accounting for short-range contributions, and the Sharma-Brau (SB) scaling [125], describing transitions dominated by long-range interactions. It is important to mention that even if the processes involving low-vibration states seem to be accurately described by these scaling laws, this is often not the case for the highest levels. Indeed, these theories are first order perturbation theories and fail under certain conditions leading, without a suitable renormalization, to probabilities above 1.

Unlike the e-V processes described in the previous subsection, the V-V and V-T rates are derived only for single-quantum exchanges. On the one hand, the databases for multi-quanta exchanges are too scarce and there is no available experimental data for comparison; on the other hand, the SSH and SB theories predict a null rate coefficient for these exchanges, while the semiclassical calculations from [58–60] and the Forced Harmonic Oscillator (FHO) calculations from [126] confirm that for the low gas temperatures pertinent to this study multi-quanta transitions in N_2 can be safely disregarded.

V-T relaxation $N_2(v)$-N_2

The V-T energy transfers in nitrogen have been extensively studied. Experimental results are presented in [120, 127–130], while examples of calculations can be found in [50, 54, 55, 57]. Following [50],

in this work we rely on the computations by Billing and Capitelli [52, 121]. Recent experiments from [131] and calculations from [60] confirm the reliability of the results from the semi-classical model of [52, 121]. However, the rates derived in [52, 121] are available only for a few temperatures in the range [200 K ; 8000 K] and a few specific vibration numbers. To generate the missing rate coefficients, we fitted the available data as a function of the gas temperature, T_{gas}. To do so, we fitted the data over two different temperature regimes, according to the exponential form used by Blauer *et al.* [53], $k(v, T_{gas}) = A(v) \exp^{B(v)T_{gas}^{-1/3} + C(v)T_{gas}^{-2/3}}$. The low regime is defined for [200 K ; 1000 K] and the $high$ regime for [1000 K ; 8000 K]. The two fitting functions obtained are then merged using two transition functions, f_{low} and f_{high}. The resulting global fitting function is:

$$\begin{aligned} k(v, T_{gas}) = & f_{low}(T_{gas}) A_{low}(v) \exp^{B_{low}(v)T_{gas}^{-1/3} + C_{low}(v)T_{gas}^{-2/3}} \\ & + f_{high}(T_{gas}) A_{high}(v) \exp^{B_{high}(v)T_{gas}^{-1/3} + C_{high}(v)T_{gas}^{-2/3}} \end{aligned} . \tag{4.3}$$

In this expression, $k(v, T_{gas})$ denotes the V-T rate coefficient associated with the transfer $N_2(v)$ + $N_2 \rightarrow N_2(v-1)$ + N_2 at the corresponding gas temperature; $f_{low}(T_{gas}) = \frac{1}{2}\left(1 - \tanh(\frac{T_{gas}-\alpha}{\beta})\right)$ and $f_{high}(T_{gas}) = \frac{1}{2}\left(1 + \tanh(\frac{T_{gas}-\alpha}{\beta})\right)$ are functions describing the transition from the low temperature regime to the high temperature one; and A, B and C are fitting coefficients depending on the vibrational level v and are given in the Appendix A for $v = 1 - 20$. The limit separating the two temperature regimes is set at $\alpha = 1000$ K, while the 'spread' is defined by $\beta = 150$ K. Compared with the rate coefficients previously used [50, 62] this new fitting function improves the agreement with Billing's calculations [52] and extends the applicability to temperatures in the range [200 K ; 300 K], not captured in [50, 62], as it can be seen in figure 4.1. Figure 4.1 also depicts the FHO calculations by Lino da Silva *et al.* [126], in excellent agreement with Billing's calculations, that can be used for other transitions and higher values of T_{gas}. The collision frequency (or gas kinetic rate) represented in figure 4.1 is estimated *via* a hard sphere model and gives an upper limit for the scaled rate coefficients. Figure 4.2 compares the V-T rate coefficients calculated from (4.3) with those proposed by other authors [54–57]. In the [200 K ; 1000 K] gas temperature range, relevant for DC glow discharges, the quenching of N_2 by itself is underestimated by Capitelli-Kozák's fitting functions [56, 57] as compared with Billing's calculations.

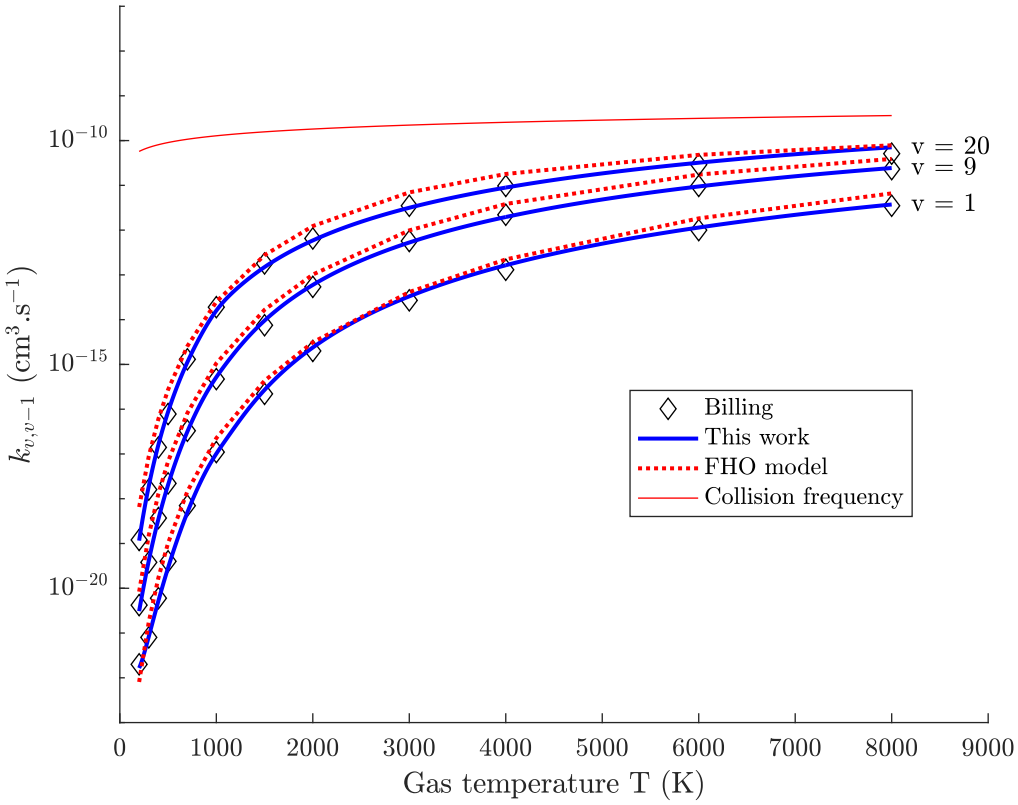

Figure 4.1: Rates coefficients for the reaction $N_2(v)$ + $N_2 \rightarrow N_2(v-1)$ + N_2 used in this work (—), the FHO model by Lino da Silva [126] (···) and calculated by Billing [52] (◇); the collision frequency (—) defines an upper limit for the rate coefficients (see text).

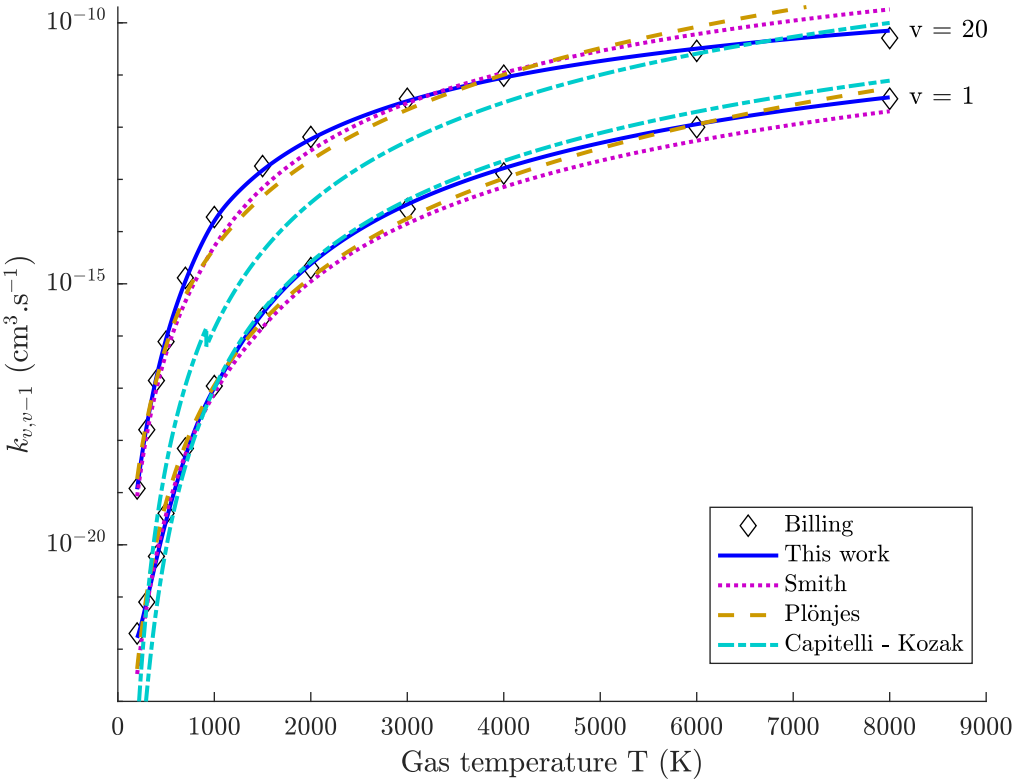

Figure 4.2: Rate coefficients for the reaction $N_2(v)$ + $N_2 \rightarrow N_2(v-1)$ + N_2 according to (· · ·) Smith [54], (– –) Plönjes [55], (– -) Capitelli and Kozák [56, 57] and (⋄) Billing [52]. The present results (—) extend the work of Guerra [50] to the temperature range [200 K ; 300 K].

V-T relaxation $N_2(v)$-CO_2

One possible approach to obtain the $N_2(v)$-CO_2 V-T rate coefficients is to multiply the $N_2(v)$-N_2 coefficients by the constant 'relative efficiency' factor $\Phi = 0.14$ suggested in [53]. However, a more general approach is to scale the rate coefficients according to the theoretical dependences from the SSH theory on the vibrational levels and gas temperature, as it is done in [132] for $N_2(v)$-O_2 energy transfers. Accordingly, the rate coefficient $k_{10}^{CO_2}$ for deactivation of the first vibrational level of nitrogen, corresponding to the process $N_2(1)$+ $CO_2 \rightarrow N_2(0)$ + CO_2, was estimated from the rate coefficient for the relaxation of nitrogen due N_2-N_2 collisions, $k_{10}^{N_2}$, from

$$k_{1,0}^{CO_2}(T_{gas}) = C_{radius} \times C_{mass} \times k_{1,0}^{N_2}(T_{gas}) \ , \tag{4.4}$$

where $C_{radius} = (\frac{r_{N2-CO2}}{r_{N2-N2}})^2$, $r_{i-j} = 0.5(r_i + r_j)$ (*cf.* p. 1111 in [64]), with r_i the diameter of the molecule i in a hard sphere collision model, and $C_{mass} = \sqrt{\frac{\mu_{N_2-CO_2}}{\mu_{N_2-N_2}}}$, where $\mu_{i-j} = \frac{\mu_i \times \mu_j}{\mu_i + \mu_j}$ is the reduced mass of the collision, with μ_i the reduced mass of the molecule i.

The rate coefficients for $v > 1$ are also scaled using the SSH theory,

$$k_{v,v-1}^{CO_2} = k_{1,0}^{CO_2} \times Z_v \times \frac{F(\gamma_v)}{F(\gamma_1)} \ , \tag{4.5}$$

where $Z_v = v \times (1 - x_e)/(1 - v \times x_e)$, x_e being the anharmonicity of the molecules' potential, the adiabaticity function F is given by

$$\begin{aligned} F(\gamma) &= 0.5 \times \exp^{-2\gamma/3} \times (3 - \exp^{-2\gamma/3}), \text{ if } \gamma \leq 21.62 \\ &= 8.1845 \times \gamma^{7/3} \times \exp^{-3\gamma^{2/3}} \text{ , otherwise} \end{aligned} \tag{4.6}$$

and the adiabaticity factor γ is given by

$$\gamma_v(T_{gas}) = 2^{-2/3} \sqrt{c_{ij}/T_{gas}} \mid \Delta E_v \mid \ , \tag{4.7}$$

where c_{ij} are parameters depending on the type of molecules colliding (*cf.* Table 2 in [55]), and ΔE_v is the energy released (or consumed) by the associated reaction.

An equivalent efficiency $\Phi_{eq}(v, T_{gas})$ can be defined as $k_{v,v-1}^{CO_2}(T_{gas}) = \Phi_{eq}(v, T_{gas}) \times k_{v,v-1}^{N_2}(T_{gas})$, to compare with the constant efficiency $\Phi_{Blauer} = 0.14$ suggested in [53]. In the range $T_{gas} \in [200$ K ; 8000 K], $v \in [1; 20]$, the minimum value is $\Phi_{eq}^{min} = \Phi_{eq}(1, 200) = 0.02$ and the maximum is $\Phi_{eq}^{max} = \Phi_{eq}(20, 8000) = 0.98$. In the restricted ranges $v \in [1; 10]$ and $T_{gas} \in [300$ K ; 1000 K], corresponding to the simulations in this work, Φ_{eq} varies between 0.07 and 0.23, hence centered at the suggested value given by Blauer.

The results were fitted for ranges of $T_{gas} \in [200$ K ; 8000 K] and $v \in [1; 20]$ according to the expression 4.3 described above. The coefficients $A_{low}(v)$, $B_{low}(v)$, $C_{low}(v)$, $A_{high}(v)$, $B_{high}(v)$, and $C_{high}(v)$ are given in the Appendix A.

V-T relaxation $CO_2(v)$-N_2

Blauer *et al.* [53] give fitting expressions for the rate coefficients of a large set of V-T CO_2-CO_2 transitions. The corresponding relative efficiencies, Φ, are reported for different quenchers, including N_2. In this case, they correspond to a multiplying factor allowing the calculation of the $CO_2(v)$-N_2 rate coefficients from the knowledge of the ones for CO_2-CO_2 collisions, $k_{CO_2(v)+N2} = \Phi \times k_{CO_2(v)+CO_2}$. These efficiencies vary according to the type of process. For instance, they are different for the V-T mechanisms $CO_2(00^01)$+$N_2 \leftrightharpoons$ $CO_2(10^00)$+N_2 and $CO_2(03^30)$+$N_2 \leftrightharpoons$ $CO_2(10^00)$+N_2. However, they do not depend neither on the gas temperature nor on the excitation levels. Herein the relative efficiencies from [53] are used. This approach will be generalized in the future, as it is done for the $N_2(v)$-CO_2 V-T exchanges described above.

V-V exchanges $N_2(v)$-$N_2(w)$

Different formulae for these rate coefficients are given in [51, 55, 56, 60]. Figure 4.3 shows the comparison between the works from Billing [52], Plönjes [55] Kurnosov [58–60], Lino da Silva *et al.* [126] and Guerra [50, 51, 57, 133]. Considering the semi-classical computations of Billing [52, 121] as a reference, in the ranges of $T_{gas} \in [200\text{ K} ; 3000\text{ K}]$ and $(v, w) \in [1; 20]$ the closest values when the excited state $N_2(1)$ is involved are given by the expressions from Guerra [51, 57, 133] used as well in [50]. These expressions provide a straightforward procedure to obtain accurate rate coefficients for gas temperatures in the domain of interest here. However, they overestimate the rate coefficients for the near-resonant transitions, $N_2(v) + N_2(v) \rightarrow N_2(v-1) + N_2(v+1)$, when T_{gas} increases. In the case of a wider gas temperature range, the FHO model of Lino da Silva [126] may be used. The expressions from Guerra [51, 57, 133] were favored in the present work, due to a slightly better agreement with Billing's data in the range $[200\text{ K} ; 1000\text{ K}]$.

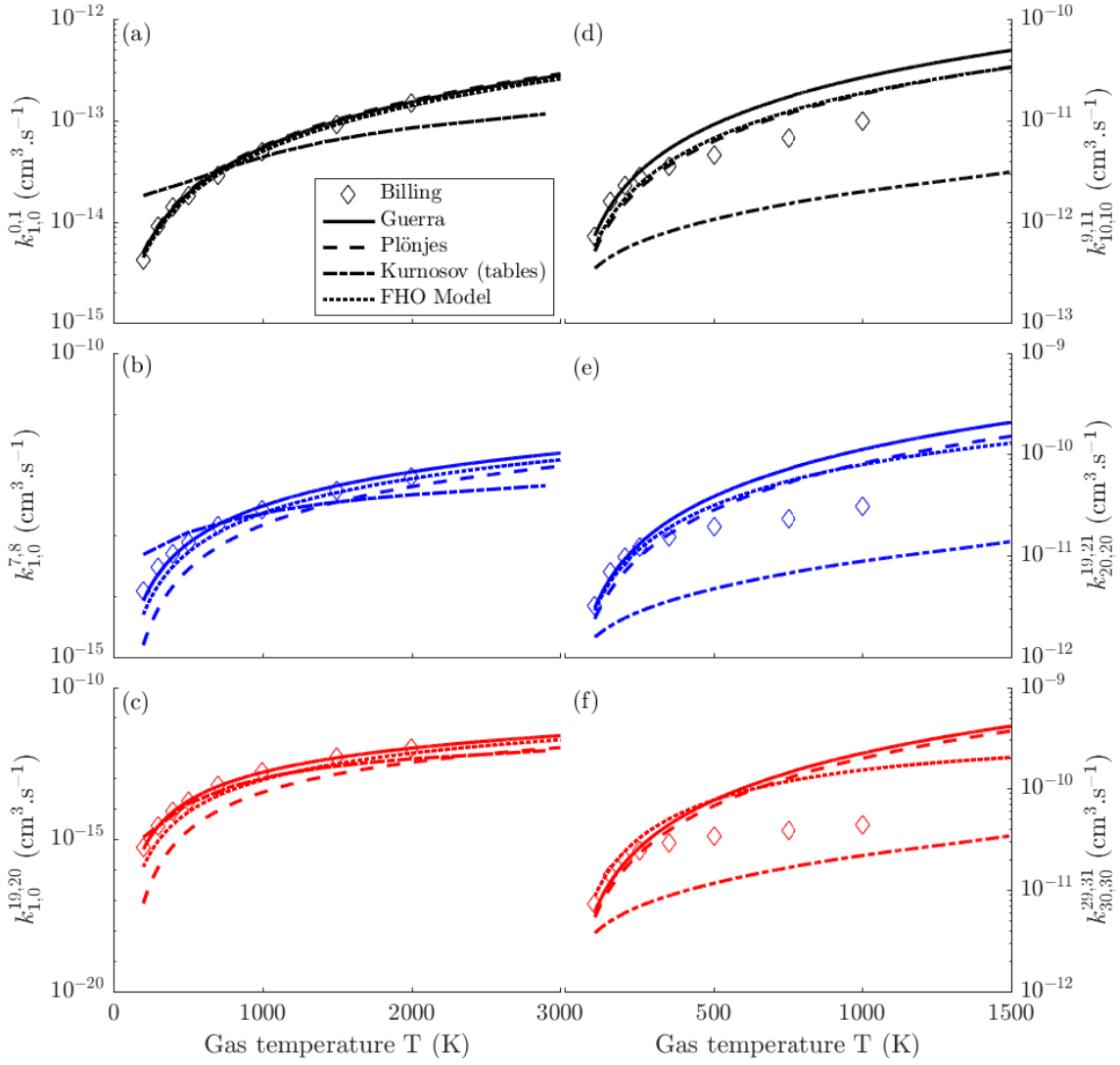

Figure 4.3: Rate coefficients for the reaction $N_2(v)$ + $N_2(w) \rightarrow N_2(v-1)$ + $N_2(w+1)$, $k_{v,v-1}^{w,w+1}$, by different authors against the results from Billing and Capitelli [52, 121] ($\diamond$): (—) Guerra [51, 57], (– –) Plönjes [55] and (– -) Kurnosov [58–60], $(\cdots)$ the FHO model from Lino da Silva *et al.* [126]; (a), (b) and (c) (left side) involve transitions with $v = 1$, (d), (e) and (f) (right side) correspond to near-resonant transitions ($v = w$).

V-V exchanges $N_2(v)$+$CO_2(00^0w)$ $\rightleftharpoons$ $N_2(v-1)$+$CO_2(00^0w+1)$

As pointed out above, the transfers between vibrationally excited nitrogen and the asymmetric stretching mode of CO_2 are very efficient and can promote the ladder climbing mechanism along this CO_2 mode, with a potential positive effect on CO_2 dissociation. The rate coefficient for the

$$N_2(1) + CO_2(00^00) \rightleftharpoons N_2(0) + CO_2(00^01) \tag{4.8}$$

exchange is taken from Blauer [53]. As discussed in section 4.4, the rate coefficients for the upper levels can have a noticeable influence on the results. Here, since only a few vibrational levels of the asymmetric stretching mode are considered in the present model, the rate coefficients for $N_2(v) + CO_2(00^0w) \rightleftharpoons N_2(v-1) + CO_2(00^0w+1)$, with $w \leq 4$, are considered with the same value as for reaction (4.8). The

rate coefficient for process (4.8), in $cm^3.s^{-1}$, is described by:

$$k = \exp^{A+BT_{gas}^{-1/3}+CT_{gas}^{-2/3}} \times \exp^{-\Delta E/T_{gas}} \tag{4.9}$$

where $A = 43.8$, $B = -306$, $C = 1288$, and $\Delta E = E(CO_2(00^01)) - E(N_2(1)) = 43$ K. Note that for the gas temperatures relevant to this work the exchange (4.8) is dominated by long-range interactions [125] and, as such, should not be scaled to higher vibrational levels using the SSH theory.

V-T deactivation by O atoms

The quenching of vibrationally excited CO_2 by O atoms is taken into account following the atmospheric model from Puertas *et al.* [61] (see table 6.2 in p.170 in [61]). Two different mechanisms are considered here,

$$CO_2(00^01) + O \rightleftharpoons CO_2(0v^v0) + O \ , \tag{4.10}$$

with $v \in \{2, 3, 4\}$, and

$$CO_2(0v^v0) + O \rightleftharpoons CO_2(0w^w0) + O \ , \tag{4.11}$$

with $v \in \{1, 2, 3, 4\}$ and $w = v-1$. The rate coefficients of reactions (4.10) and (4.11) are assumed independent of v and given by $k_{v_3-O} = 2 \times 10^{-13}\sqrt{T_{gas}/300}$ $cm^3.s^{-1}$ and $k_{v_2-O} = 2 \times 10^{-12}\sqrt{T_{gas}/300}$ $cm^3.s^{-1}$, respectively [61].

The quenching of vibrationally excited N_2 by O atoms,

$$N_2(v) + O \leftrightharpoons N_2(v-1) + O \ , \tag{4.12}$$

is included as described in [62, 132], namely

$$k_{1,0}^{N_2-O} = 2.3 \times 10^{-13} \exp\left(-\frac{1.280 \times 10^3}{T_{gas}}\right) + 2.7 \times 10^{-11} \exp\left(-\frac{1.084 \times 10^4}{T_{gas}}\right) \ , \tag{4.13}$$

where $k_{1,0}^{N_2-O}$ is the rate in $cm^3.s^{-1}$ associated with the process $N_2(1)$+O $\rightarrow$ $N_2(0)$+O, together with a linear scaling (corresponding to a harmonic oscillator description), such that $k_{v,v-1}^{N_2-O} = v \times k_{1,0}^{N_2-O}$.

Figure 4.4 presents an overview of the V-T reaction rate coefficients responsible for the deactivation of $CO_2(100)$, $CO_2(010)$ and $N_2(1)$. Note that quenching effects moving a quantum from one CO_2 mode to another (*e.g.* $CO_2(001)$ + CO_2 $\rightleftharpoons$ $CO_2(010)$ + CO_2) are not represented in this figure. The quenching from O atoms appears to be dominant as compared with the other reactions. More precisely, O atoms are the only significant quenchers for the deactivation of nitrogen. The reaction rate (see eq. 2.5) calculated is a few times larger than the wall deactivation, detailed in the next sub–section.

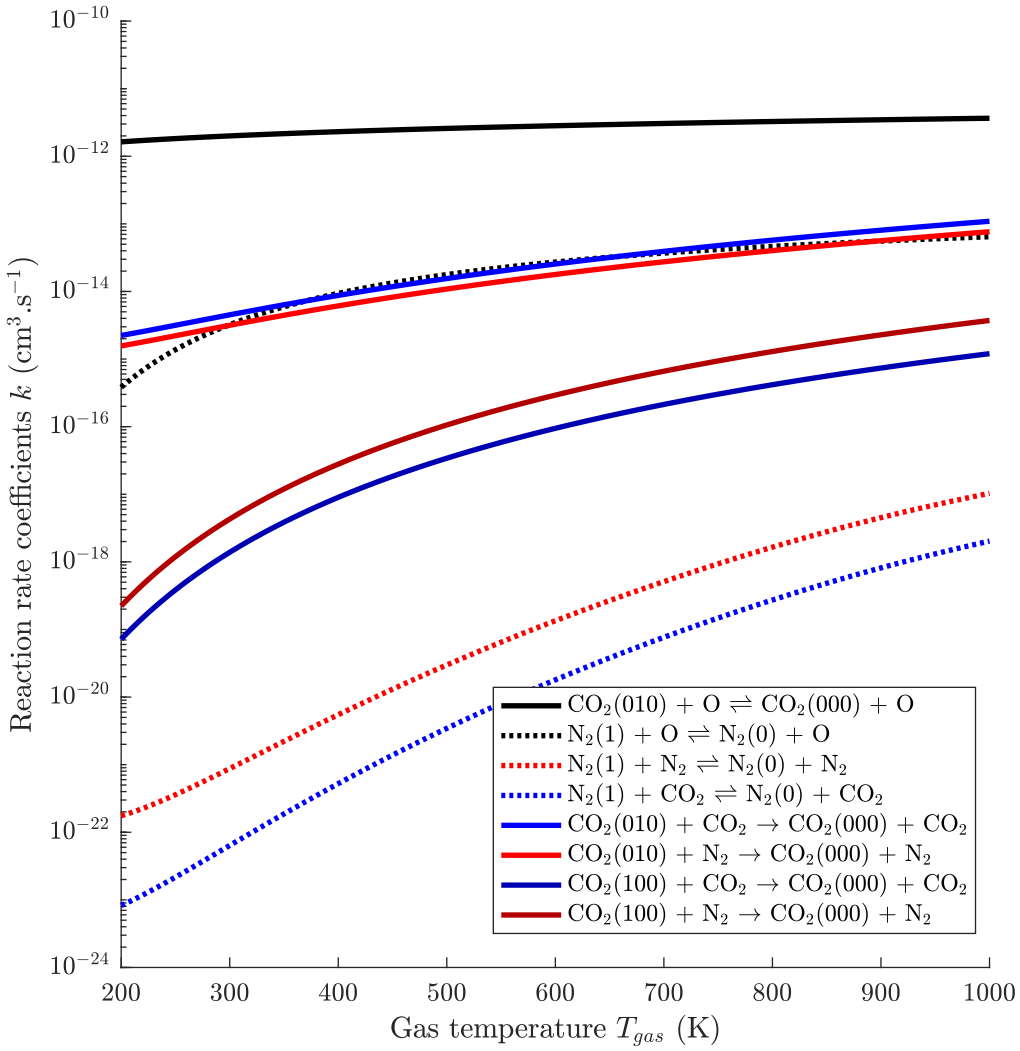

Figure 4.4: Overview of V-T reaction rate coefficients focusing on the deactivation of the 1st excited levels of N_2 and CO_2. Solid lines correspond to the quenching of CO_2, dotted lines correspond to the quenching of N_2. Black lines correspond to the quencher O, red lines to the quencher N_2 and blue lines to the quencher CO_2.

4.2.4 Wall deactivation

The wall deactivation of a molecule excited at a level $v > 0$ to the ground state is an important process to consider in the current simulations, especially at the lower pressures investigated (~ 1 Torr), due to the enhanced diffusion of the neutral species in this case. The frequency of deactivation of vibrational quanta of excited molecules hitting the walls is estimated using the formula given in [62, 63]. Thus, the diffusion coefficient of CO_2 molecules in an excited state $v > 0$ in a mixture of CO_2-N_2 is calculated using Wilke's formula [134],

$$D_{CO_2(v)} = \frac{1 - x_{CO_2(v)}}{\frac{x_{CO_2(w \neq v)}}{D_{CO_2(v) \text{ in } CO_2}} + \frac{x_{N_2}}{D_{CO_2(v) \text{ in } N_2}}} \simeq \frac{1}{\frac{x_{CO_2}}{D_{CO_2(v) \text{ in } CO_2}} + \frac{x_{N_2}}{D_{CO_2(v) \text{ in } N_2}}} \tag{4.14}$$

where $x_{CO_2(v)}$ is the fraction of the excited molecules diffusing towards the walls, and $D_{CO_2(v) \text{ in } CO_2}$, $D_{CO_2(v) \text{ in } N_2}$ are the diffusion coefficients of this excited molecule in pure CO_2 and in pure N_2, respectively.

We use the approximation $x_{CO_2(v)} = 0$ in equation (4.14), so that $x_{CO_2(w\neq v)} = x_{CO_2}$. The differences between the calculations made with this approximation and the exact expression are less than 1%, for all the conditions under study. The equivalent formula for the diffusion of $N_2(v > 0)$ towards the walls is:

$$D_{N_2(v)} = \frac{1 - x_{N_2(v)}}{\frac{x_{CO_2}}{D_{N_2(v)\text{ in }CO_2}} + \frac{x_{N_2(w\neq v)}}{D_{N_2(v)\text{ in }N_2}}} \simeq \frac{1}{\frac{x_{CO_2}}{D_{N_2(v)\text{ in }CO_2}} + \frac{x_{N_2}}{D_{N_2(v)\text{ in }N_2}}} \tag{4.15}$$

where an identical approximation was used, $x_{N_2(v)} = 0$ so $x_{N_2(w\neq v)} = x_{N_2}$.

Moreover, the binary diffusion coefficient of an excited molecule i in a pure gas j is computed following Hirschfelder [64] (p. 539) in cm^2.s^{-1},

$$D_{ij} = \frac{1.929 \times 10^{19} \sqrt{\frac{T_{gas}}{2\mu}}}{N \times \sigma_{12}^2 \times \Omega^{(1,1)*}(T^*)} , \tag{4.16}$$

where N is the total gas density in cm^{-3}, μ is the reduced mass, $T^* = kT_{gas}/\varepsilon_{12}$ is the reduced gas temperature, $\sigma_{12} = (\sigma_1 + \sigma_2)/2$ in Å^2 and $\varepsilon_{12} = \sqrt{\varepsilon_1 \varepsilon_2}$ are parameters of the Lennard-Jones interaction potential, and $\Omega^{(1,1)*}(T^*)$ denotes the collision integral. Their respective values are given p.1111 in [64]. In practice $i = CO_2(v > 0)$ or $N_2(v > 0)$ and j can be CO_2 or N_2.

Once the diffusion coefficient is computed, the characteristic time of the deactivation on the wall of a specific vibrationally excited level, in a cylindrical discharge of radius R, is derived as [62, 63]

$$\tau_i = \frac{1}{D_i} \left(\frac{R}{2.405} \right)^2 + \frac{2R(1 - \gamma_i/2)}{\gamma_i \langle v_i \rangle} , \tag{4.17}$$

where $\langle v_i \rangle$ is the thermal speed and γ_i is the destruction probability at the wall. This latter coefficient depends on the wall material, as well as on the mode being deactivated (see table 1 in [66]). Due to the lack of experimental values, we set the same value of γ_i whatever the mode of CO_2 being deactivated, *i.e.* $\gamma_{CO_2(v>0)} = 0.2$ for a Pyrex surface (average value from table 1 in [66]). As it is assumed for CO_2, we use the same value of the deactivation probability for all levels of N_2, in this case $\gamma_{N_2(v>0)} = 1.1 \times 10^{-3}$ [65]. Typically, the characteristic deactivation time is ~ 0.7 ms for CO_2 and ~ 30 ms for N_2, at 1 Torr. The assumption of constant γ_{CO_2} and γ_{N_2} is acceptable for the purpose of the present investigation and does not modify our conclusions. Nevertheless, it should be noted that some dependence on the vibrational quantum level [135] and on the operating conditions is to be expected. The latter would be the outcome of a possible influence on the deactivation probabilities of pressure, temperature and/or the [CO]/[O] ratio.

4.3 Experiment

The results of the kinetic model are compared against new experimental data obtained in multi-pulse DC discharges (*i.e.*, several on-off cycles occur during the gas residence time, see section 4.2). The experimental setup consists in a plasma reactor made of a cylindrical Pyrex tube of length 23 cm and radius of 1 cm, illustrated in figure 3.4 of chapter 3. The time-resolved measurements of CO_2 vibrational excited state densities were performed at Laboratoire de Physique des Plasmas (LPP), using *in situ*

time-resolved step-scan FTIR schematized in figure 3.1, with a constant total gas flow of 7.4 sccm (cf. sub–section 3.3.3). The discharge takes place under low pressures of 1 and 5 Torr, currents of 20 and 50 mA respectively, with on-off times of 5-10 ms, for pure CO_2 and for mixtures of 75% CO_2 - 25% N_2 and 50% CO_2 - 50% N_2. The DC power supply is triggered using a pulse generator (TTi, TGP110), resulting in square pulses with rise and fall times in the order of a couple μs. The resulting plasma current is monitored and it was verified that there is no ringing. The pressure in the system is measured with a pressure gauge upstream the discharge and is also measured during the plasma pulse from the fitting of the FTIR data (see [109]). The typical gas residence time is of the order of 1 second. The results are analyzed for 4 different conditions, summarized in table 4.1. More details on the experimental setup and diagnostic techniques can be found in chapter 3 and in Klarenaar *et al.* [45, 108, 109], in which the first vibrational states of CO_2 were measured in pure CO_2 plasmas.

Table 4.1: Operating conditions for the 4 experiments under analysis. All experiments are performed in a Pyrex tube of inner radius 1 cm, length 23 cm, total gas flow rate 7.4 sccm and on-off time 5-10 ms

Parameter	**Exp. #1**	**Exp. #2**	**Exp. #3**	**Exp. #4**
Pressure	1 Torr	1 Torr	5 Torr	5 Torr
Mixture	100% CO_2	75% CO_2 - 25% N_2	100% CO_2	50% CO_2 - 50% N_2
Discharge current	20 mA	20 mA	50 mA	50 mA

As detailed in [108, 109], the experimental data provide the time evolution of the different vibrationally excited states, from where it is possible to deduce the characteristic vibrational temperature of the asymmetric stretching mode, T_3, and of the common temperature of the bending and symmetric stretching modes [43], T_{12}. The measurements further give information on the evolution of the gas temperature inside the reactor, T_{gas}, as well as on the vibrational temperature of CO, T_{CO}. Below $T_{CO} = 500$ K however, the peaks in the IR absorption spectra corresponding to vibrationally excited CO are at the noise level, and the fitted T_{CO} becomes then non meaningful [109].

Figures 4.5 and 4.6 show the data recently obtained, exp. #1 and #2 are plotted in figure 4.5 while exp. #3 and #4 are plotted in figure 4.6. The data in pure CO_2 confirm our previous observations: at low pressure and current (1 Torr, 20 mA), T_{CO} and T_3 remain significantly higher than T_{12}, which is on the contrary almost thermalized with T_{gas}. At higher pressure (5 Torr), T_3 and T_{CO} show a very fast increase during the first 1 ms and pass through a maximum, tending to equalize slowly until the end of the pulse. The presence of this maximum at 1 ms is discussed in [41, 43], where it is shown to be due to the increase of some V-T rate coefficients with the gas temperature, which is growing along the discharge pulse. At the end of the plasma pulse, T_3 is almost identical to T_{12} and simply increases again due to the increase in gas temperature.

In the case of CO_2-N_2 mixtures, the measured temperatures are generally higher, in particular T_3, as can be expected from CO_2 laser literature [72]. In spite of higher amplitude, the different temperatures follow similar temporal evolution as in the case of pure CO_2. At 1 Torr, 20 mA and for a mixing ratio 75% CO_2 - 25% N_2, T_{gas} and T_{12} are unchanged compared to the pure CO_2 case, while T_3 and T_{CO} are increased by $\sim$30%. At 5 Torr, 50 mA with a mixture of 50% CO_2 - 50% N_2 all temperatures are higher than in pure CO_2. However, the gas temperature is only slightly increased by $\sim$10% when T_{12} is enhanced by $\sim$25% and T_3 and T_{CO} by $\sim$45%. The maximum reached by T_{CO} and T_3 at 1 ms of the

plasma pulse is still observed in mixtures with N_2, which shows the still great importance of V-T relaxation processes. The stronger effect observed in exp #3 and #4 compared to the effect observed between experiments #1 and #2 could be the result of stronger importance of V-T processes at higher pressure, or due to a larger energy transfer of vibrational energy from N_2 to CO and CO_2 because of a higher N_2 content in experiment #4. This will be discussed in light of the modeling results in the following sections.

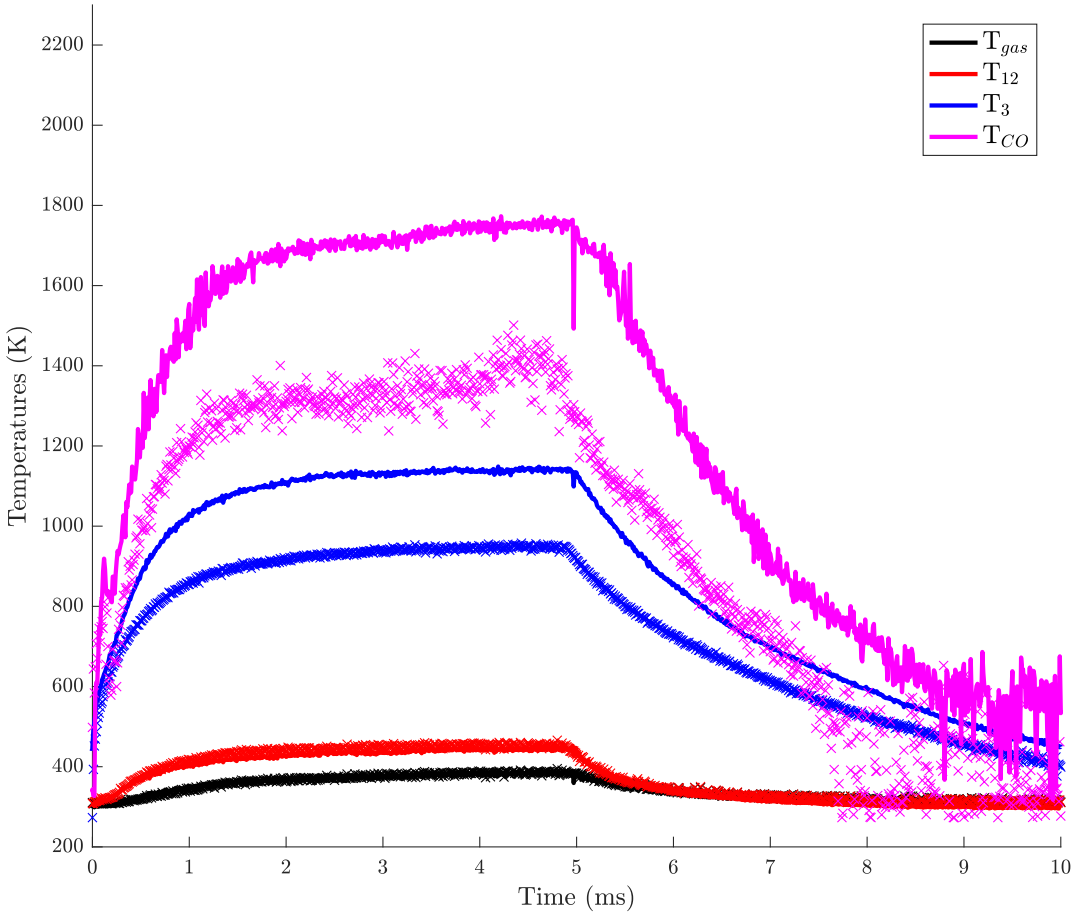

Figure 4.5: Time-resolved temperatures measured at the conditions exp. #1 and #2 in table 4.1 multi-pulse DC discharge, 1 Torr, 20 mA, for a pure CO_2 plasma ($\times$) and 75% CO_2 - 25% N_2 (—). The first 5 ms corresponds to the active part of the discharge.

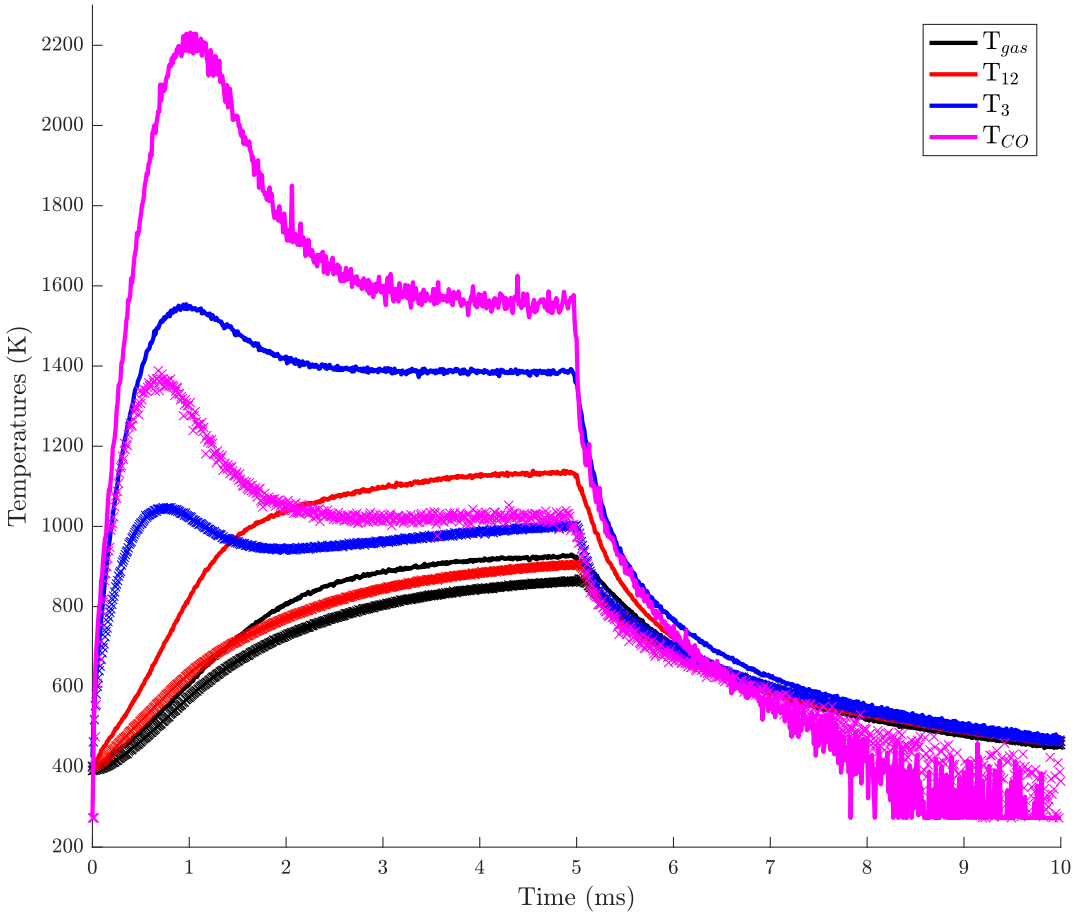

Figure 4.6: Time-resolved temperatures measured at the conditions exp. #3 and #4 in table 4.1 multi-pulse DC discharge, 5 Torr, 50 mA, for a pure CO_2 plasma ($\times$) and 50% CO_2 - 50% N_2 (—). The first 5 ms corresponds to the active part of the discharge.

4.4 Results from simulations

In this section, the time-resolved experimental measurements of the four conditions in table 4.1 and the corresponding simulations are compared. The wall deactivation effect and the influence of the electron density profile are discussed at the end of the section.

Differences between single-pulse and multi-pulse discharges

As pointed out in sections 4.2 and 4.3, in the present conditions CO+O recombination is slower than the off-time of 10 ms and the renewal of the gas is slow, so that a build-up of CO molecules is observed during the first pulses, reaching then a saturation value. The model is reproducing a single-pulse discharge, hence not reproducing the build-up effect. Nevertheless, an off-time of 10 ms is long enough for the gas to almost return to its original temperature in between two pulses, so that the characteristic trends of $CO_2(v_2 = 1)$ and $CO_2(v_3 = 1)$ over time can be discussed. In contrast, the dissociation parameter $\alpha = [CO]/([CO]+[CO_2])$ cannot be compared with the current simulations and will be the object of a future publication. Another consequence of the slow CO+O recombination is that $\alpha(t)$ measured over one pulse is nearly constant, so we chose to refer to the maximum dissociation parameter α_{max} obtained in the

discussion below.

Summary of the 4 conditions: nitrogen increases the dissociation

A prior point worth noting is illustrated in table 4.2, which shows the maximum dissociation parameter, α_{max}, obtained during the experiments. It appears that for the same conditions of current and pressure the addition of nitrogen enhances the dissociation of CO_2, as previously observed for continuous DC discharges from chapter 3 and from [115]. Possible explanations may involve the importance of vibrational excitation of nitrogen and its transfer to the CO_2 asymmetric stretching mode, a role of electronically excited states of nitrogen, the dilution of CO_2 in the mixture and a less efficient conversion of CO back into CO_2 and/or the enhancement of the reduced electric field and the contribution of direct electron impact dissociation, as further discussed below. Table 4.2 also includes the values of the atomic oxygen concentration, relative to the CO_2 density, as obtained or estimated from the experiments presented in [136]. For pure CO_2 cases, the concentrations of O atoms were measured by both actinometry and TALIF in [136]. Assuming that for equivalent pressure and current conditions, the ratios [O]/[CO] are equal in both pure CO_2 plasma and CO_2-N_2 plasma, one can estimate the relative density [O]/[CO_2] in the CO_2-N_2 mixtures using the measured dissociation parameter α.

Table 4.2: Maximum dissociation α_{max} reached during the multi-pulse DC discharges for the 4 experiments. The reduced electric fields are measured in continuous discharges for the same pressures and mixture compositions, at 40 mA (cf. chapter 3). The ratio [O]/[CO_2] is measured from preliminary experiments in pure CO_2 plasmas, and estimated for CO_2-N_2 mixtures.

	α_{max}	**Mixture**	[O]/[CO_2] (estimated)	**Pressure**	**Current**	**E/N**
Exp. #1	0.11	100% CO_2	0.02	1 Torr	20 mA	63 Td
Exp. #2	0.20	75% CO_2 - 25% N_2	0.05	1 Torr	20 mA	80 Td
Exp. #3	0.20	100% CO_2	0.03	5 Torr	50 mA	60 Td
Exp. #4	0.41	50% CO_2 - 50% N_2	0.07	5 Torr	50 mA	72 Td

The asymmetric stretching mode is of special concern in CO_2 plasma reforming. In very general terms, it can be said that typically this mode is populated in the beginning of the discharge pulse (up to ~ 1 ms) by direct electron impact and by V-V transfers from N_2 due to N_2-CO_2 collisions, with an input of vibrational energy into the lowest v_3 levels. Subsequently, V-V transfers involving only the asymmetric stretching mode (so-called V-V_3 exchanges) help to populate higher v_3 levels. As the temperature raises in the discharge pulse, V-T deactivation increases and hinders further excitation. Along the afterglow, the redistribution of vibrational energy due to V-T and V-V processes drives the relaxation to thermal equilibrium.

Collisional channels

Figures 4.7 (a), $(a1)$ and $(a2)$ show some of the collisional channels of transfer of electron power to the heavy species, plotted versus the reduced electric field, E/N. More specifically, they show the fraction η of the power lost by electrons impacting on heavy molecules in the excitation of the first vibrational levels of N_2 and CO_2, as well as the power used in CO_2 electronic excitation described by losses with thresholds

$e_1 = 7$ eV and $e_2 = 10.5$ eV [40]. Note that the cross-sections associated with these electronic excitations e_1 and e_2, recommended by Phelps [137], represent an upper limit of the electron impact dissociation cross-section (see discussion in [40, 88]). The power transferred to the heavy molecules is normalized to the power gained by the electrons from the electric field. Two conditions are compared, corresponding to $p = 5$ Torr and $I = 50$ mA, in a 50% CO_2 - 50% N_2 mixture (exp. #4 in table 4.1 and represented by full lines) and in a pure CO_2 plasma (exp. #3 in table 4.1 and represented by dotted lines). The corresponding EEDFs are plotted in figure 4.7 (b). The calculations are carried out using the measured values of T_{12} and T_3 at the somewhat arbitrary time $t = 2.5$ ms during the active part, while the vibrational temperature of nitrogen is assumed to be equal to T_3. In the case of a mixture with nitrogen, it appears that at 72 Td the vibrational excitation of N_2 is favored compared with the asymmetric and bending modes of CO_2. On the contrary, at 60 Td for a pure CO_2 plasma, the dissociation by electronic excitation e_1 and e_2 is favored, although the excitation of the asymmetric mode is not negligible. The two E/N values used for these calculations were determined from experiment. The EEDF derived for a CO_2-N_2 plasma has a *lower* population of electrons around the dissociation energies, $e_1 = 7$ eV and $e_2 = 10.5$ eV, than a pure CO_2 plasma, which means that the direct electron dissociation rate coefficient is lower with the presence of N_2. However, the measurements show a *larger* conversion of CO_2 when nitrogen is mixed in the plasma. An estimation of the relative importance of the direct electron dissociation as compared to the asymmetric pumping, represented by $r = (\eta_{e1} + \eta_{e2})/\eta_{000\rightarrow001}$, shows that $r_{exp.\ \#4} \simeq 0.83 \times r_{exp.\ \#3}$, calculated for 72 Td and 60 Td respectively. It indicates that $CO_2(00^01)$ excitation is enhanced relatively to direct electron dissociation when N_2 is added in the plasma. Together with the previous statement about a lower direct electron dissociation in a CO_2-N_2 plasma, this suggests that the increase in the CO_2 conversion when N_2 is added into the mixture is not due to an enhancement of the direct electron impact dissociation on ground state molecules but rather to the role of vibrational kinetics. Other possibilities would be the involvement of nitrogen electronically excited states, which are quickly populated in the first instants of the pulsed discharge [138], or the reduction of the role of reactions converting CO back to CO_2. Note also that this analysis still applies if the E/N values used to compute EEDFs are taken equal for both experiments, instead of their respective measured values of 60 Td and 72 Td, as long as $E/N \geq 10$ Td. These simple considerations cannot explain alone the enhanced dissociation reached with the addition of N_2 and a more detailed scheme is required for a thorough clarification of this question. Nevertheless they show that, in the range of $E/N \in$ [1 Td; 100 Td], an important part of electron energy is transferred into the vibrational excitation of both CO_2 and N_2, emphasizing the importance of having an accurate reaction rate for the process $CO_2(00^00)$+$N_2(1) \rightleftharpoons CO_2(00^01)$+$N_2(0)$ and a correct description of vibrational energy transfers between N_2 and CO_2.

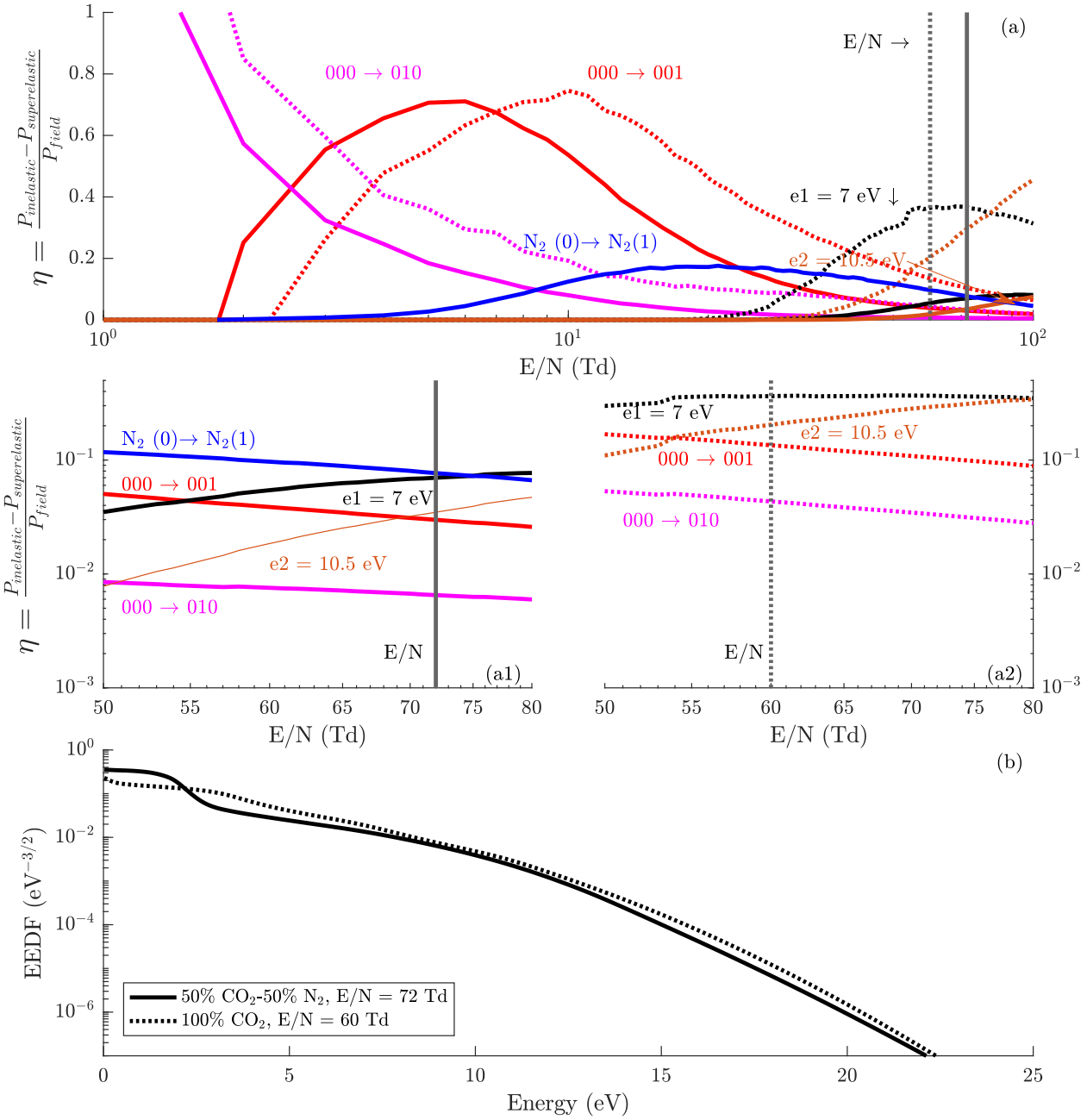

Figure 4.7: Main channeling for the electron energy as a function of the reduced electric field for: (—) 50% CO_2 - 50% N_2 mixture (exp. #4 in table 4.1); $(\cdots)$ pure CO_2 (exp. #3 in table 4.1). The electron power transfer is normalized to the power gained from the field. e_1 and e_2 denote CO_2 dissociation reached by electronic excitation. Results plotted (a) for a wide range of E/N and $(a1)$, $(a2)$ zoomed on the E/N range of interest for this work. Corresponding electron energy distribution functions (b)

Time-resolved densities: afterglow

The relative time-resolved densities of the $CO_2(00^01)$ and $CO_2(01^10)$ levels are plotted in figures 4.8 to 4.11, comparing the simulations with the measurements for both the afterglow and the active discharge. In these four figures, panels (a) to (d) correspond to exp. #1 to exp. #4, respectively. Three simulations are carried out for each experimental condition, corresponding to three different imposed values of the atomic oxygen concentration [O]: [O] $= 0$, [O] $= 0.1\times$[CO_2] and [O] $= 0.2\times$[CO_2]. The relative importance

of the quenching from O atoms is expected to grow as the dissociation parameter α increases (see table 4.2). Figures 4.8 and 4.9 focus on the relaxation of the asymmetric and the bending modes along the afterglow, respectively, whereas figures 4.10 and 4.11 concern the evolution of the asymmetric and the bending mode during the active part, respectively.

Figures 4.8 and 4.9 show that the simulations describe relatively well the measurements in the afterglow for all experimental conditions. The agreement is excellent in a pure CO_2 plasma (see figures 4.8 and 4.9 (a) at [O] $= 0$ cm^{-3} and (c) for any density of O atoms). However, the calculations made for the CO_2-N_2 mixture exhibit some discrepancies. Regarding the (00^{0}1) level, for the 50%CO_2-50%N_2 mixture at $p = 5$ Torr, the calculations in figure 4.8(d) overestimate the density of $CO_2(00^01)$. Note that the O-atom density at exp. #4 is estimated at about $0.07\times$[CO_2] (see table 4.2), so that the results should be compared with the calculations shown in dashed lines. As for the (01^{1}0) level, there is a small deviation for the 75%CO_2-25%N_2 discharge at $p = 1$ Torr (panel (b) in figure 4.9). Note that in the latter case, the O atom density is estimated at [O]=0.05[CO_2] (see table 4.2).

In this work, the higher dissociation case (exp. #4, panel (d)) coincides with the higher discrepancy between simulations and experiment. This suggests that relevant mechanisms between N_2 and the products of CO_2 decomposition may be missing, namely CO and O_2. In fact, additional calculations based on the rates provided by Plönjes *et al.* [55] show that the contributions of the V-V exchange $N_2(1)$ + CO$(0) \rightleftharpoons N_2(0)$ + CO(1) may have an importance roughly equivalent to the V-V exchange $N_2(1)$ + $CO_2(00^00) \rightleftharpoons N_2(0)$ + $CO_2(00^01)$. Work is in progress to clarify this question.

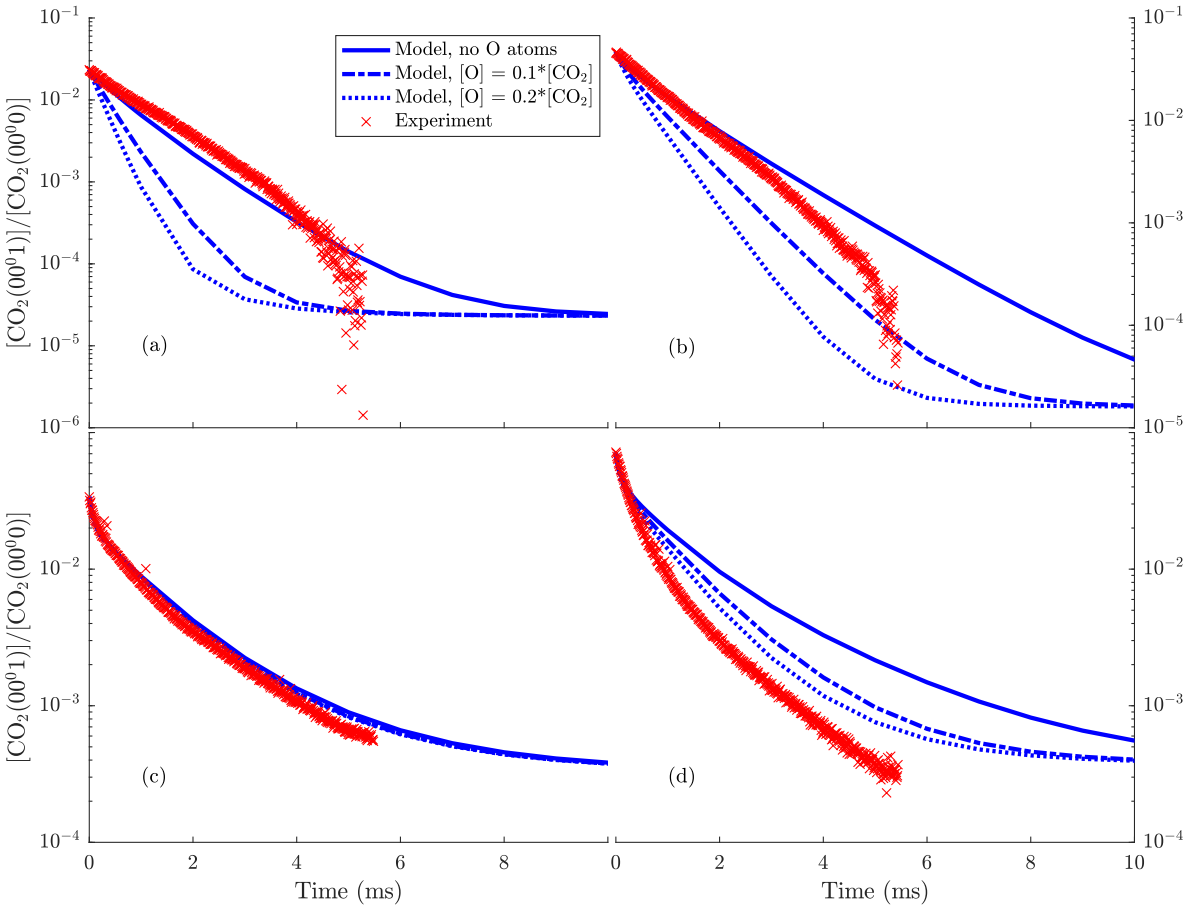

Figure 4.8: Relative densities of the 1^{st} excited asymmetric level $CO_2(00^01)$ during the afterglow. Panels (a) to (d) correspond respectively to the conditions of exp. #1 to #4 from table 4.1.

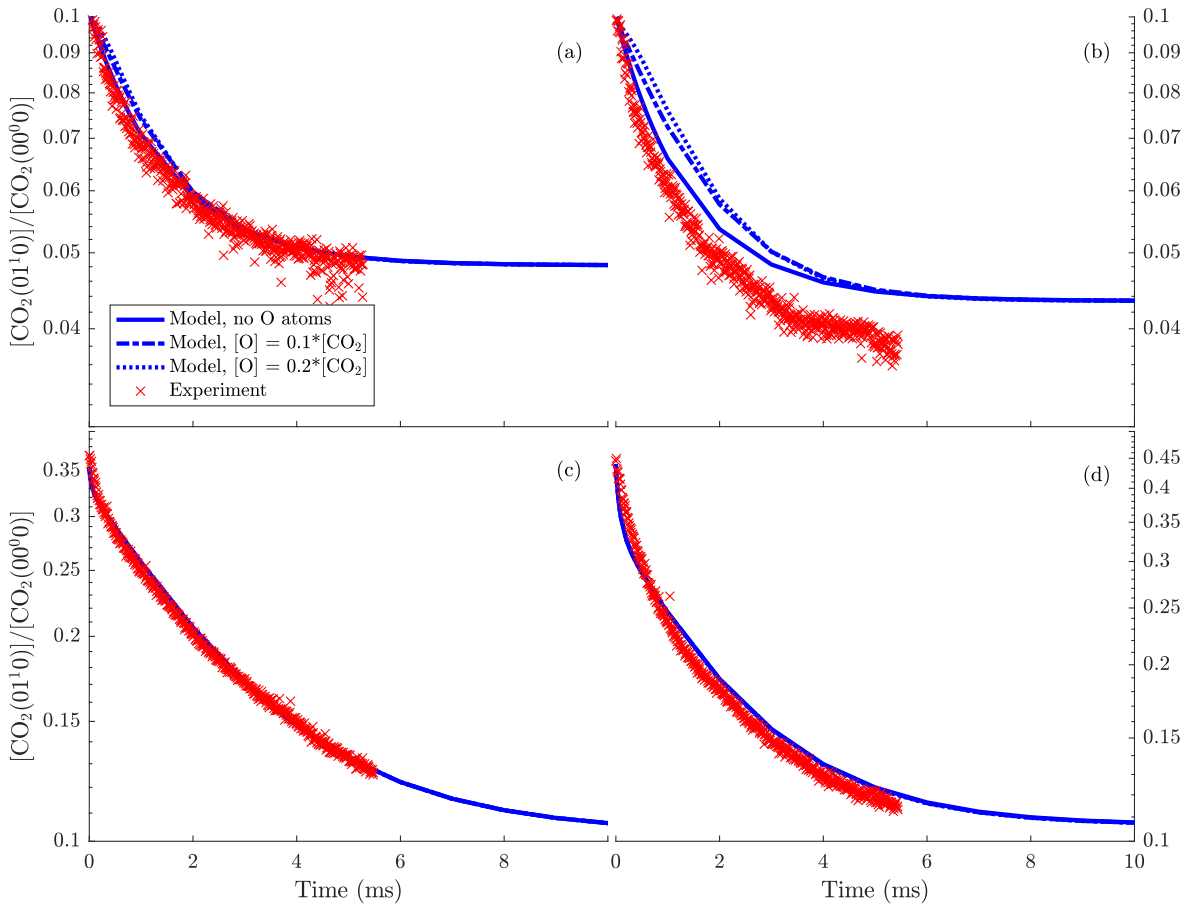

Figure 4.9: Relative densities of the 1st excited bending level $CO_2(01^10)$ during the afterglow. Panels (a) to (d) correspond respectively to the conditions of exp. #1 to #4 from table 4.1.

Time-resolved densities: active part

Figures 4.10 and 4.11 show that the model describes also satisfactorily the main features of the time evolution of the first levels of both the asymmetric stretching and the bending modes during the active phase of the discharge, despite some quantitative disagreements at specific conditions. For instance, the simulations capture the maximum of $CO_2(00^01)$ density ocurring at $t \simeq 1$ ms at 5 Torr, both in pure CO_2 and in the CO_2-N_2 mixture, and inexistent at $p = 1$ Torr. As discussed in [43], this effect in pure CO_2 is connected with several V-T and V-V processes involving this level, and with the temperature dependence of these rate coefficients. For CO_2-N_2 mixtures, the V-V energy transfers in CO_2-N_2 collisions (described in subsection 4.2.3) are also of importance. For example, simulations made with a reduced set of V-V CO_2-N_2 processes led to a flat profile, even at 5 Torr. This reduced set consisted in disabling any VV CO_2-N_2 where the difference of energy ΔE between the left hand side and the right hand side was above 0.0124 eV $= 100$ cm^{-1}, as could be suggested by the Sharma-Brau theory [125].

The global trends shown in figures 4.8 to 4.11 unveil the importance of V-T deactivation of vibrationally excited CO_2 and N_2 by O atoms. These mechanisms can depopulate directly the CO_2 and N_2 vibrational distribution functions (VDFs). The former process has a direct influence on the population of the CO_2 vibrational levels, whereas the latter reduces the importance of the transfer (4.8) pumping the asymmetric stretching mode, by depopulating the N_2 VDF. Interestingly, V-T collisions with O atoms seem to affect more the population of the asymmetric stretching levels (figures 4.8 and 4.10) than the population of the levels in the bending mode (figures 4.9 and 4.11). Although the deactivation of the bending mode in equation (4.11) is one order of magnitude higher than the asymmetric relaxation of equation (4.10), the energy difference between consecutive $CO_2(0v_20)$ levels is smaller than for the other modes (see figure 1.5 in chapter 1), which results in rather important inverse reactions. In this way, the loss of quanta in the bending mode induced by the direct reaction in (4.11) is compensated to a large extent by the inverse reaction in (4.11) plus the direct reaction in (4.10), explaining why the time-resolved density $CO_2(01^10)$ is less affected when [O] increases. The measurements for both pulsed and continuous discharges show that the vibrational temperature T_{12} is thermalized with T_{gas} in most situations, inducing therefore a similar trend as the one of the gas temperature.

Overall, the trends obtained in the model predictions are very reasonable and give some confidence on the cross sections used to describe the e-V processes. Nevertheless, some uncertainties remain, mainly surrounding the electron density profile along the pulse (discussed below, see figures 4.16 and 4.17) and the exact role of energy transfers involving O, O_2 and CO, and should be further investigated in the future.

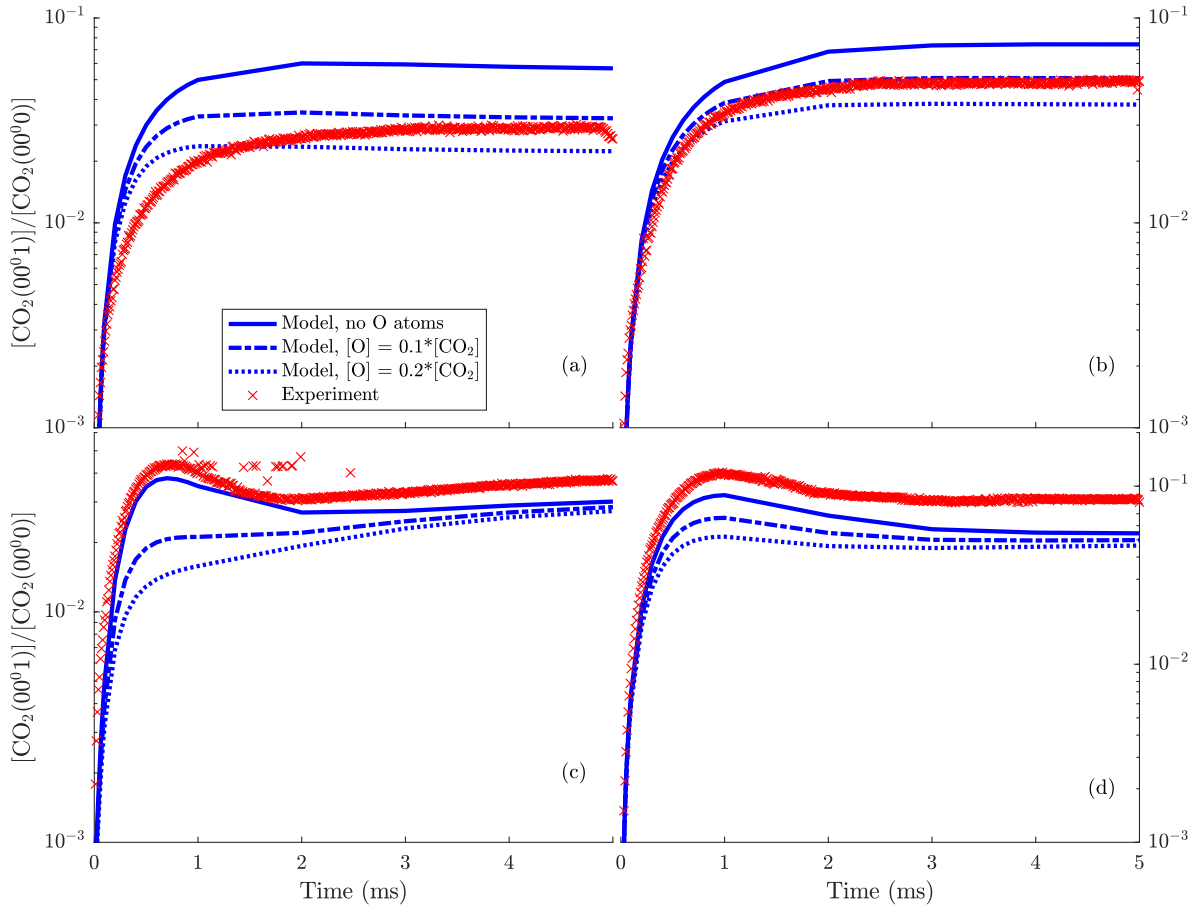

Figure 4.10: Relative densities of the 1st excited asymmetric level $CO_2(00^01)$ during the active part. Panels (a) to (d) correspond respectively to the conditions of exp. #1 to #4 from table 4.1.

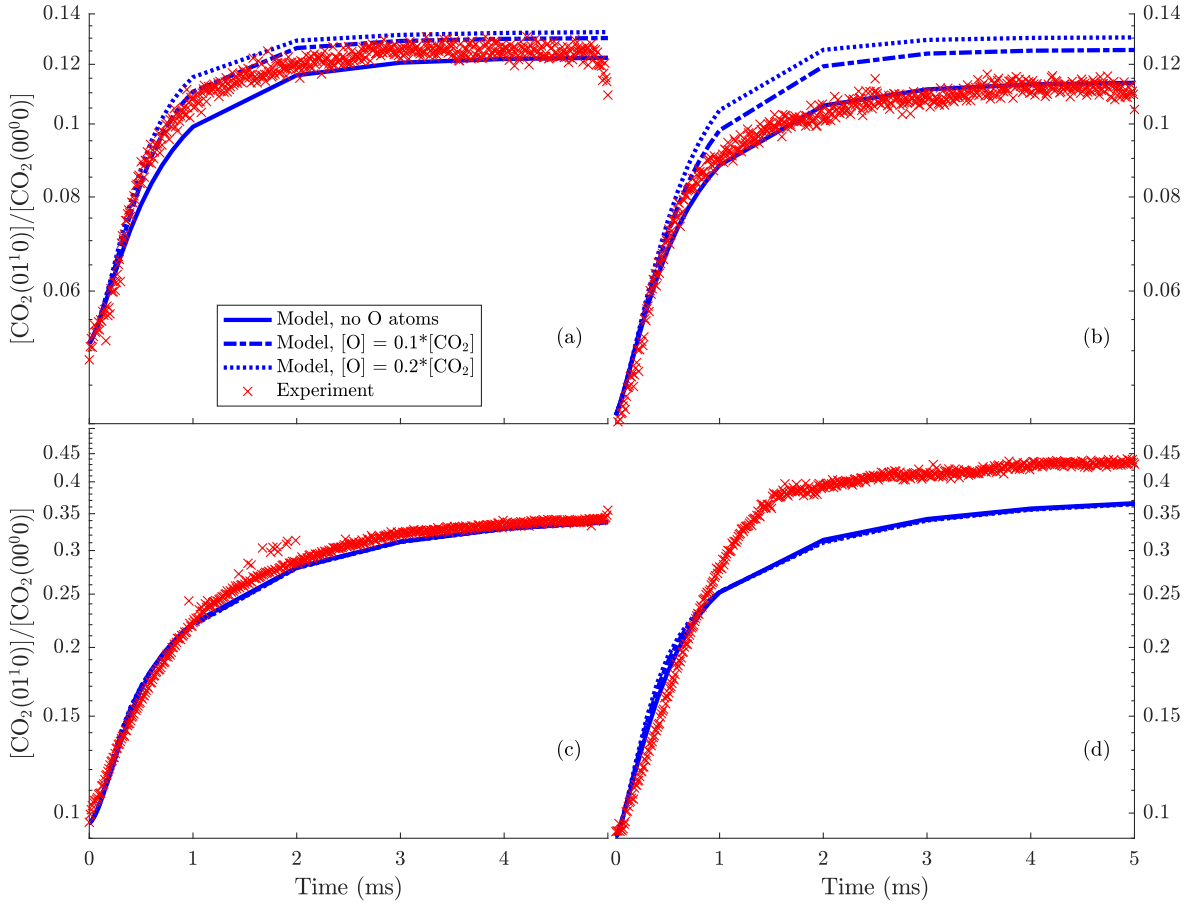

Figure 4.11: Relative densities of the 1st excited bending level $CO_2(01^10)$ during the active part. Panels (a) to (d) correspond respectively to the conditions of exp. #1 to #4 from table 4.1.

Time-resolved vibrational temperatures

Figures 4.12 and 4.13 show the time-evolution of the measured and calculated characteristic vibrational temperatures along the discharge pulse and its afterglow, respectively, for the four conditions under analysis. Note that these 'temperatures' were obtained from a Boltzmann fit to the individual populations calculated from the state-to-state model (cf. chapter 2 for details). A Treanor fit was also tested, but for the present conditions the resulting characteristic vibrational temperatures are nearly the same. These figures confirm the strong non-equilibrium character of the plasma, with T_{12} typically very close to the gas temperature T_{gas}, while T_3 and T_{N_2} raise quickly above T_{gas}. At 5 Torr and 50%CO_2-50%N_2 (exp. #4), the measurements indicate T_{12} departing as well from T_{gas}, a feature not reproduced in the calculations that requires further investigation. Also worth noting the slower decay of T_{N_2} as compared to T_3, which for the present conditions is essentially controlled by deactivation of the N_2 VDF at the wall. This can provide an interesting way to keep pumping the asymmetric stretching mode of CO_2 in the afterglow and allow an optimization of the reactor geometry to this purpose.

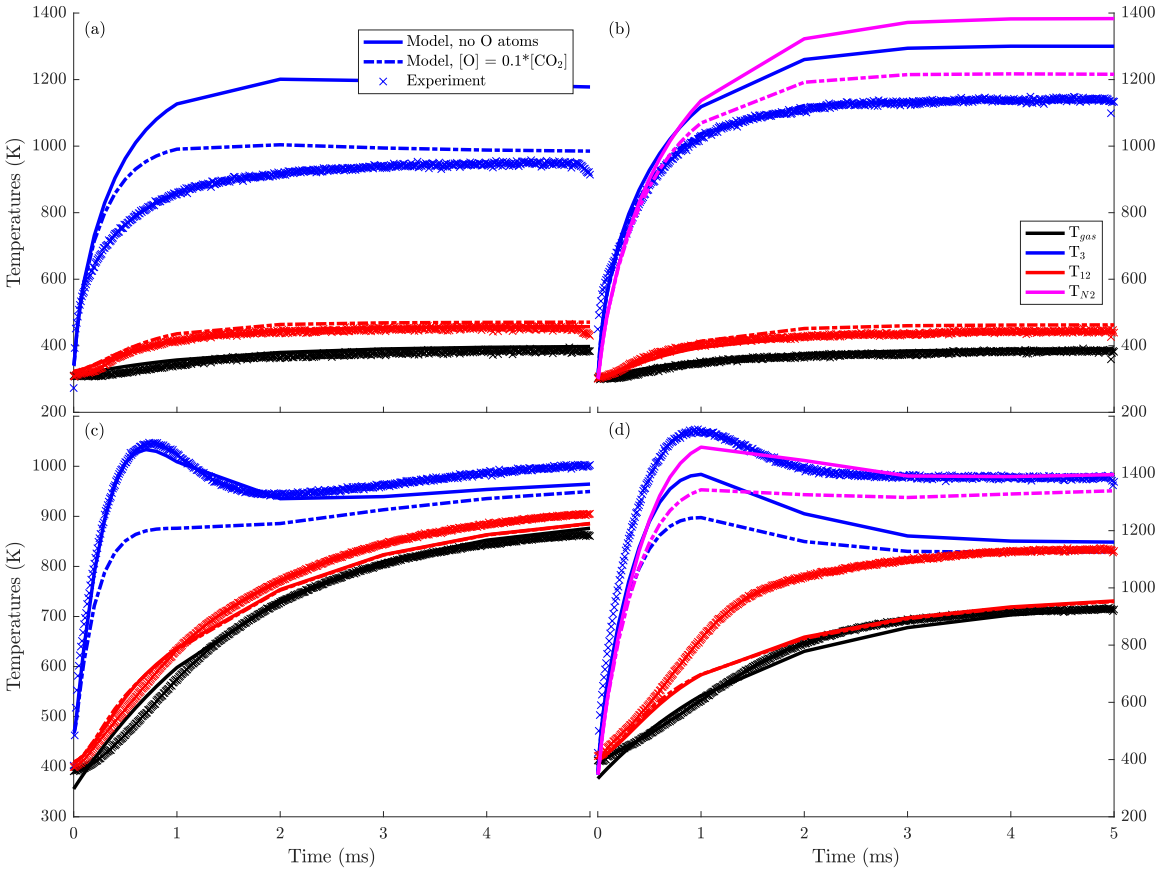

Figure 4.12: Vibrational and gas temperatures from measurements and simulations, during the active part. [O] = 0 and [O] = $0.1\times$[CO_2]. Panels (a) to (d) correspond respectively to the conditions of exp. #1 to #4 from table 4.1.

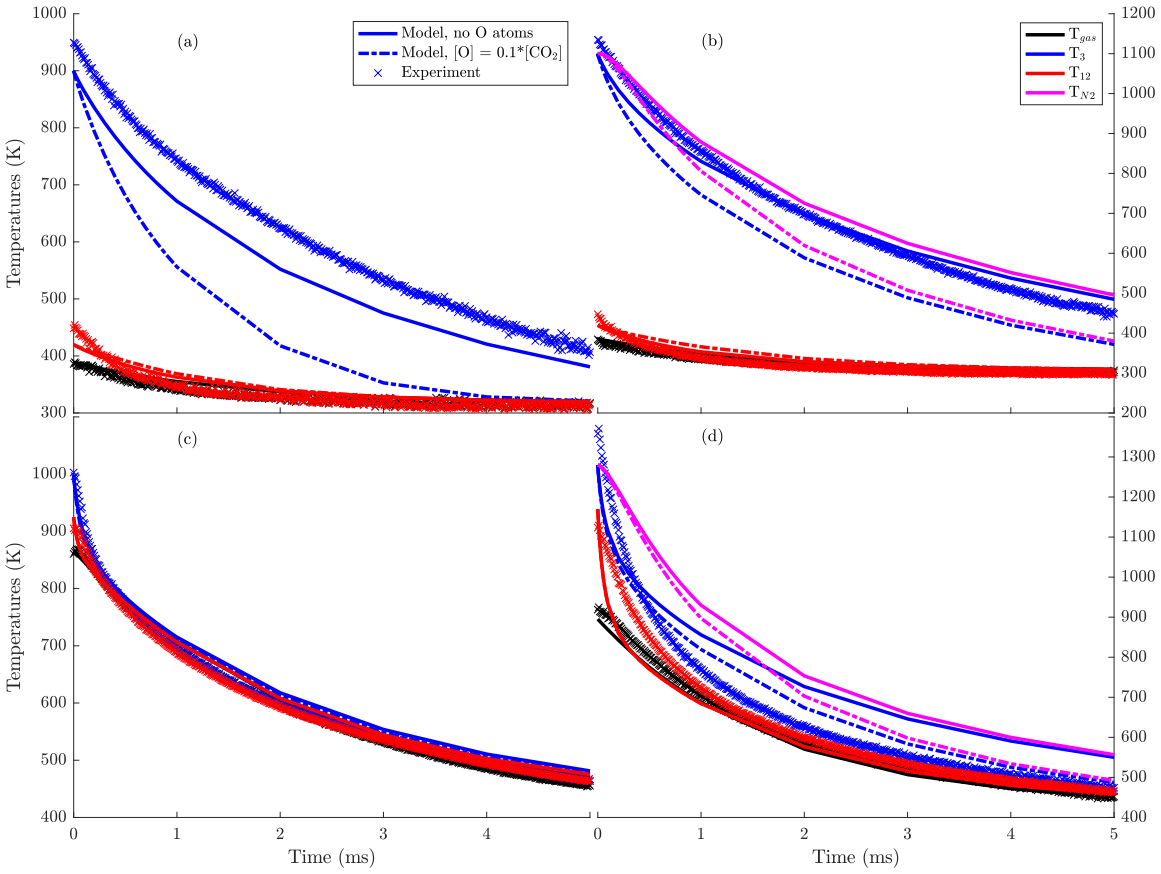

Figure 4.13: Vibrational and gas temperatures from measurements and simulations, during the afterglow. [O] = 0 and [O] = $0.1\times$[CO_2]. Panels (a) to (d) correspond respectively to the conditions of exp. #1 to #4 from table 4.1.

Influence of the wall deactivation

The influence of deactivation of vibrationally excited molecules at the walls, described in section 4.2.4, is illustrated in figures 4.14 and 4.15. Figure 4.14 shows the relative density of the $CO_2(00^01)$ state during the afterglow of a pure CO_2 plasma, for 1 Torr in (a) and 5 Torr in (b) (exp. #1 and exp. #3, respectively). In both cases, the inclusion of the wall deactivation processes of vibrationally excited CO_2 molecules leads to a better agreement with the measurements. The results change drastically in the case of a discharge at 1 Torr, while they do not modify the global trend at 5 Torr. Indeed, with the conditions described in table 4.1, at 1 Torr the vibrational relaxation in collisions on the walls is so important that the normalized density of the first CO_2 asymmetric level is modified by 2 orders of magnitude at 5 ms in the afterglow.

Additional calculations, not shown in this work, confirm the importance of the wall deactivation of both CO_2 and N_2 vibrationally excited states in CO_2-N_2 mixtures at relatively low-pressures. Although the deactivation probability γ_i for nitrogen is typically 2 to 3 orders of magnitude lower than for carbon dioxide in our conditions (see section 4.2.4), it appears that this is the dominant process to reach relaxation of the N_2 VDF in a relevant characteristic time, typically ~ 1 second in pure N_2 cold plasma. In addition, a stronger relaxation of the nitrogen VDF affects the CO_2 vibrational distribution functions, as the V-V energy transfers from N_2 to CO_2 (*cf.* mechanism (4.8)) become less effective.

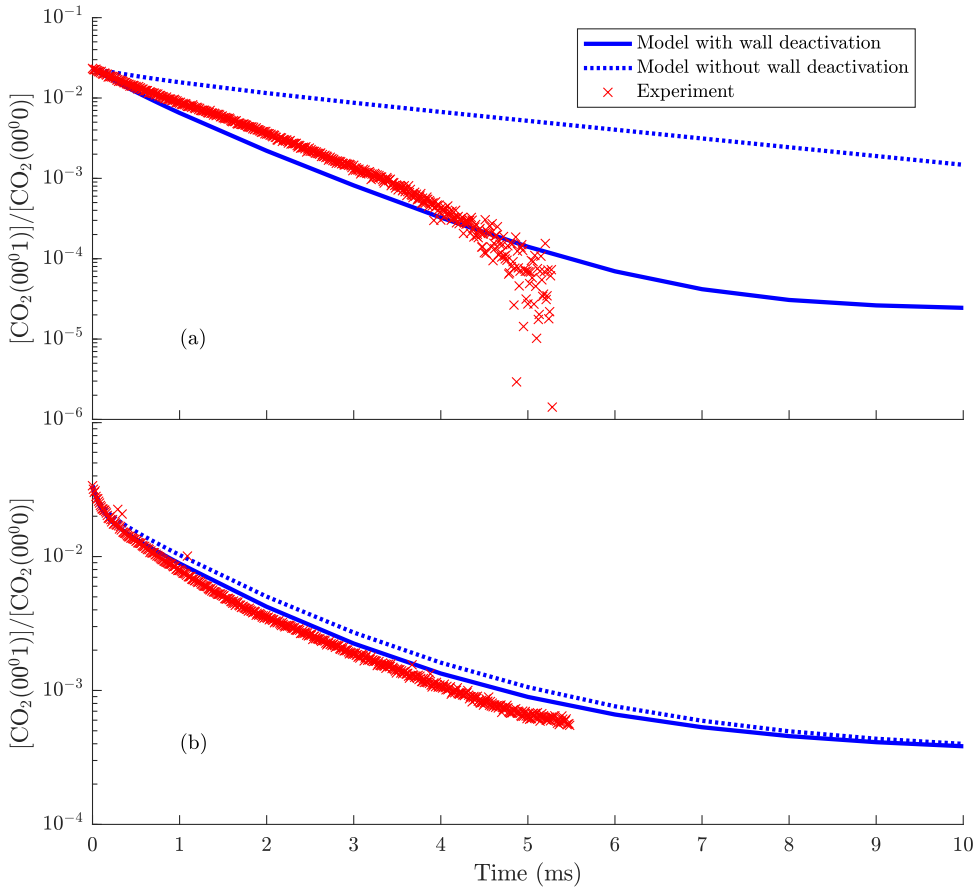

Figure 4.14: Influence of the wall deactivation on the asymmetric mode of CO_2, during the afterglow, for a pure CO_2 plasma. The simulations correspond to the conditions of (a) 1 Torr (exp. #1 in table 4.1) and (b) 5 Torr (exp #3 in table 4.1).

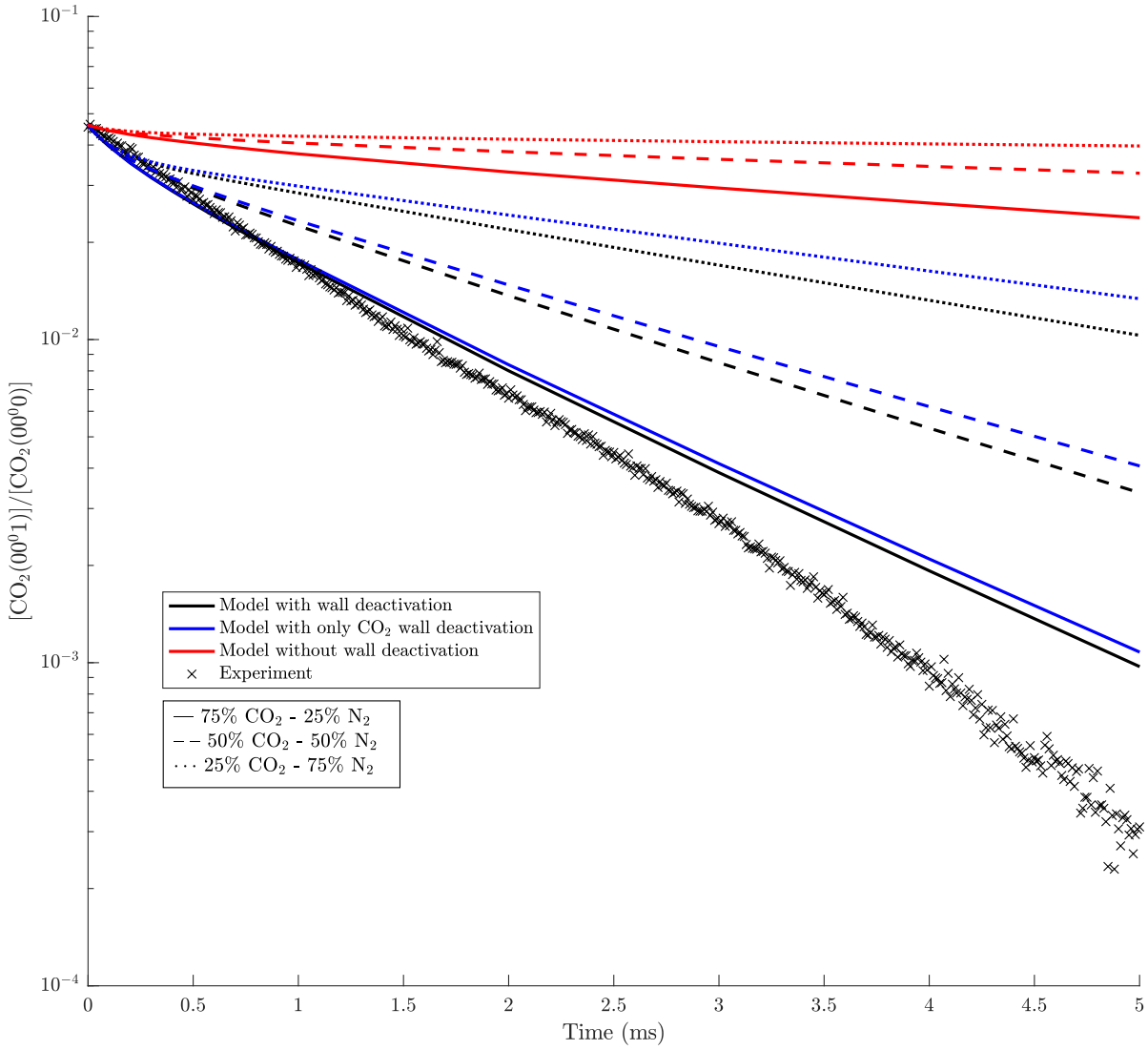

Figure 4.15: Influence of the wall deactivation on the asymmetric mode of CO_2, during the afterglow, for CO_2-N_2 plasmas at $p = 1$ Torr: (—) 75% CO_2-25% N_2 (conditions of exp. #2 in table 4.1); (– –) 50% CO_2-50% N_2; (. . .) 25% CO_2-75% N_2. The colors correspond to: (—) base model, with wall deactivation of vibrationally excited CO_2 and N_2 molecules included; (—) no wall deactivation of N_2; (—) no wall deactivation.

Influence of the electron density profile

In order to estimate the importance of the adopted electron density profile along the pulse, simulations were carried out with 3 different temporal growths for $n_e(t)$, keeping the steady-state values unchanged. Figures 4.16 (a) and 4.17 (a) show the relative density of the first excited CO_2 bending and asymmetric levels, respectively, during the active part of the discharge. The corresponding $n_e(t)$ profiles are plotted in figures 4.16 (b) and 4.17 (b) (see chapter 2 for details on the initial and the steady-state values of n_e). Figures 4.16 and 4.17 correspond to 1 Torr in a 75% CO_2 - 25% N_2 mixture (exp #2) and 5 Torr in a 50% CO_2 - 50% N_2 mixture (exp #4), respectively. In spite of some differences observable in the results, especially at 5 Torr where the maximum around $t = 1$ ms flattens, the global behavior of the calculated concentrations is not modified. Hence, it is unlikely that the existing disagreements between simulations and measurements are due to a significant uncertainty in the general procedure used to estimate the electron density.

Additional simulations, not presented in this work, were performed with different values of the steady-state electron density (see equation (2.14) in chapter 2). The results show a relatively low influence of the steady-state value, not sufficient to explain the discrepancy observable in the figure 4.11 (d).

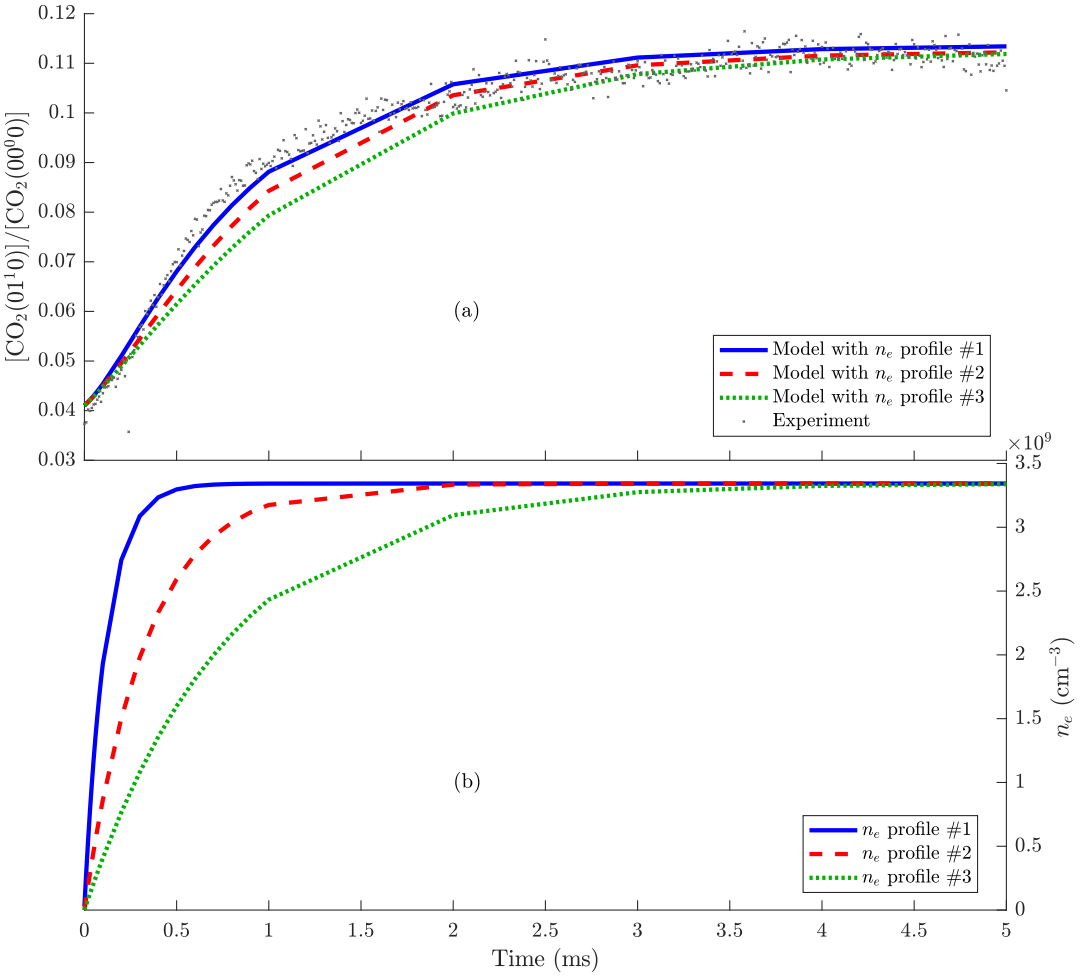

Figure 4.16: (a) Relative density of the first excited bending level $CO_2(01^10)$, during the active part of the discharge, for 3 different electron density profiles. The conditions are for a 75% CO_2 - 25% N_2 mixture, 1 Torr and 20 mA (exp #2 in table 4.1). The electron densities over time are presented in (b). The saturation value is kept constant, and depends only on the current used for the experiment. The best agreement with the measurements is obtained for the faster growth, with profile #1.

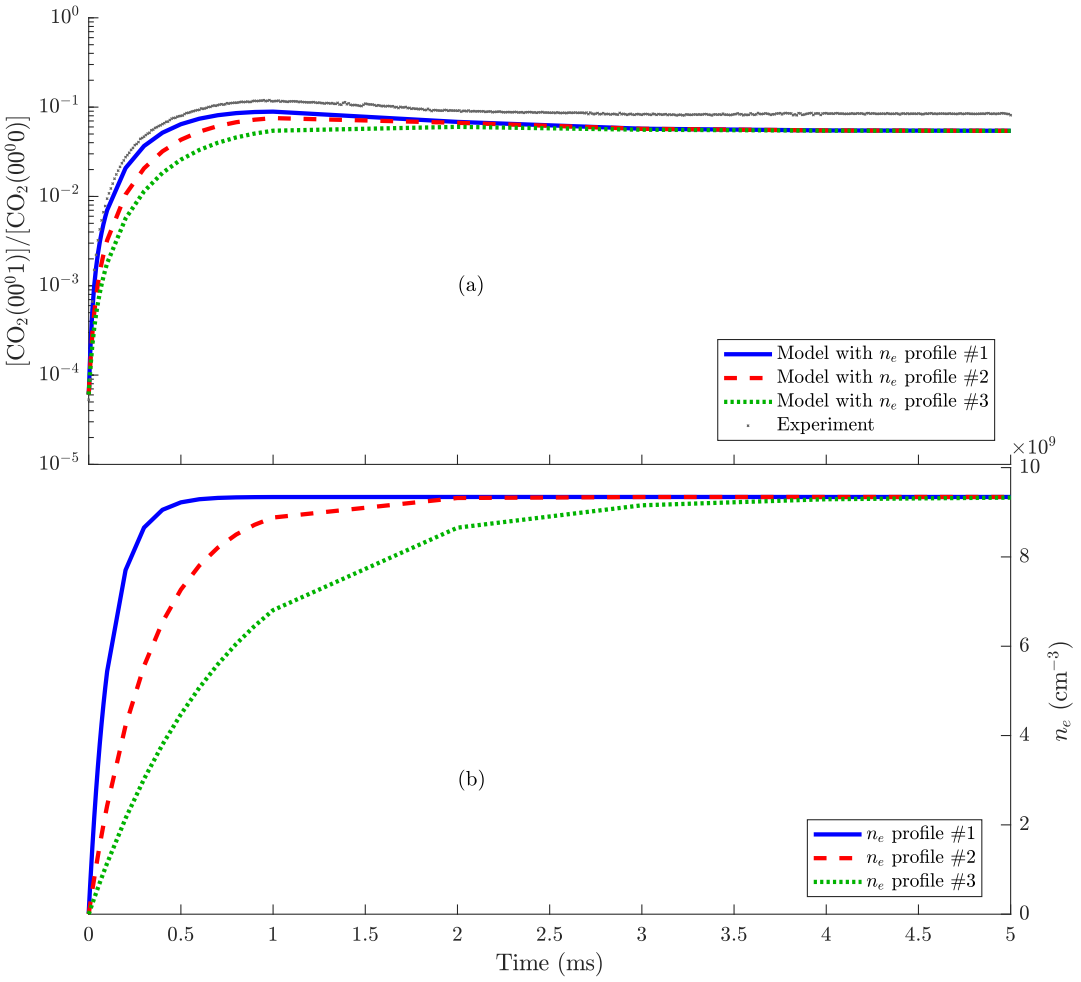

Figure 4.17: (a) Relative density of the first excited asymmetric level $CO_2(00^01)$, during the active part of the discharge, for 3 different electron density profiles. The conditions are for a 50% CO_2 - 50% N_2 mixture, 5 Torr and 50 mA (exp #4 in table 4.1). The electron densities over time are presented in (b). The saturation value is kept constant, and depends only on the current used for the experiment.

4.5 Conclusions

In this work the model from Silva *et al.* [40–43], previously validated for low pressure pulsed DC glow discharge in a CO_2 plasma, was extended to account for the addition of molecular nitrogen. A total of 72 vibrational levels for CO_2 and 10 vibrational levels for N_2 are considered at this stage. New e-V, V-V and V-T reaction rates were included, resulting in about 3000 reactions. The present results for the afterglow confirm the correctness of the set of reactions and rate coefficients previously derived to account for the CO_2 vibrational kinetics [41–43] and validate the new set for CO_2-N_2 vibrational kinetics. The results for the active discharge further validate the electron kinetics and the e-V processes and cross sections considered, since the agreement between the simulations and the experiments is generally very satisfactory: on the one hand, the trends are very well reproduced, notably the presence of a peak for the $CO_2(00^01)$ density in the active part at 5 Torr, that does not appear at 1 Torr, both in the simulations and measurements; on the other hand, the calculated orders of magnitude are also in agreement with the experimental data.

The experimental data show an enhanced conversion of CO_2 when N_2 is added to the plasma. The modelling study strongly suggests that this effect cannot be attributed to dissociation by direct electron impact on ground state $CO_2(00^00)$ molecules. Therefore, it should rather be the outcome of a hindrance of reactions involving CO molecules and giving back CO_2 and/or of other dissociation processes, for instance involving CO_2 vibrationally excited states or nitrogen electronically excited states. Unveiling the exact mechanisms underlying the increase in CO_2 dissociation with nitrogen still requires further investigation.

The current results may be affected by the kinetics of CO, O_2 and O, for instance via the V-V N_2-CO, the V-T N_2-O, and the V-T CO_2-O processes. In fact, although the comparison with repetitive pulsed experiments in pure CO_2 gives a reasonably good agreement considering only the vibrational kinetics of CO_2 [41–43], with the addition of N_2 the discrepancies appear to be larger. The dissociation fraction is higher in the latter case, enhancing the relative importance of V-V processes implying CO, while the energy of the CO vibrational levels is quasi-resonant with those of the asymmetric stretching mode of CO_2 and of N_2. This suggest that vibrationally excited CO could possibly release energy to excite $CO_2(00v_3)$ and N_2 *via* V-V exchange processes, which are not taken into account in the model.

The present study corroborates the importance of the vibrational transfers from $N_2(v = 1)$ to $CO_2(00^01)$, suggesting the possible use of N_2 to help up-pumping the vibrational ladder of the CO_2 asymmetric stretching mode. However, it is also shown that V-T collisions with O atoms can markedly affect the CO_2 Vibrational Distribution Function (VDF), both by direct deactivation of CO_2 vibrationally excited states, and by quenching of the N_2 VDF and subsequent reduction of the V-V transfers from N_2 to the CO_2 asymmetric stretching mode.

The relative importance of the wall deactivation as compared with the V-T and V-V processes is governed by the pressure, due to the larger mean-free path of the heavy particles at lower pressures and the consequent enhanced diffusion. The present results indicate that wall deactivation of vibrationally excited CO_2 and N_2 plays an important role at $p = 1$ Torr and has to be taken into account in plasmas

operating at these (or lower) pressures. *A prori*, wall deactivation should be minimized to reach an efficient CO_2 dissociation, as it reduces the excited population of CO_2. However, increasing the pressure also leads to a higher number of heavy molecule collisions, hence to a faster thermalization of the gas and a decrease of the population highly vibrationally excited. In the end, a compromise between a fast thermalization and an important wall contribution has probably to be found.

This work sets up the basis for the definition of a validated set of reactions and corresponding rate coefficients, often denoted as a 'reaction mechanism', for CO_2-N_2 plasmas. It can be extended along different lines. From the experimental point of view, new 'single pulse' experiments may be attempted, in order to achieve a stricter validation of the proposed kinetic scheme and to remove the possible influence of CO, O and O_2. In addition, dedicated experiments to assess the role of the processes involving these species can be designed. From the modelling point of view, the extension to higher excitation regimes and the investigation of the impact of the energy transfer mechanism between vibrationally excited nitrogen and the asymmetric stretching mode on CO_2 dissociation should be pursued. In case a positive effect of vibrationally excited nitrogen is confirmed, as observed as well in [115], the possibility of adding excited nitrogen into a CO_2 afterglow can also be studied, taking advantage of the efficient vibrational excitation and relatively long relaxation time in pure nitrogen discharges [50].

Chapter 5

Sensitivity Analysis: the Morris method and refinements [1]

5.1 Introduction

As described in chapter 1, cold plasmas are highly reactive environments characterized by a rather low ionization degree (10^{-6} to 10^{-3}), a high electron temperature ($\sim$1 eV) and low to moderate heavy-species temperatures (300 K to 10000 K). Numerous kinetic reactions take place in cold plasmas, like electron-electron collisions, electronic or vibrational excitation of heavy species from electron impact, ionization, dissociation, recombination, etc. While electrons are mainly characterized by their kinetic energy, the heavy-species are more complex to describe: often they are characterized by their rotational temperature, their translational temperature, their electronic state, their vibrational state and their electric charge (neutral, positive or negative). It results in environments with a high degree of complexity, with dozens of species potentially interacting with each other. One advantage of modeling over experimental measurements is that numerical codes can easily handle each state as a distinct species and access some that are difficult/impossible to detect experimentally, as long as the interactions of this species with others are known. This is usually done by implementing reaction rates in the model, which represent the probability for a specific reaction to occur. In this thesis, the main equations of the model under study are described in chapter 2, while chapter 4 presents details about N_2 reaction rates implementation and a comparison of simulations to experiments.

In this chapter we do a Sensitivity Analysis (SA) of an established model of oxygen cold plasmas. Although O_2 NTPs are simpler to model than CO_2 NTPs (fewer species and reactions), the kinetic processes are very similar to those of carbon dioxide. Consequently, a SA of O_2 plasmas constitutes a good first step towards a general SA tool for molecular plasmas. The reaction scheme includes a total of 51 species for 179 reactions. The equations driving the electron kinetics and the chemistry are solved with the LisbOn KInetics (LoKI) simulation tools [67–69]. We followed essentially the Morris approach for the SA, which consists in short in varying only one input per simulation and measuring the variations

[1] Parts of this chapter are based on [23]

in the outputs. As suggested by different authors, we also tested different refinements of the original approach, such as the grouping method or an improved sampling of the input values. The minimum number of simulations required is investigated, as well as the influence of two types of distributions for the input values.

The structure of this chapter is as follows. Section 5.2 summarizes the existing works for similar contexts. Section 5.4 describes the main features of the numerical code, while section 5.3 focuses on the oxygen model. Section 5.5 introduces the Morris method, and how we adapted the suggested refinements to our problematic. The SA parameters were tested in section 5.6, which also presents non-intuitive results obtained for a full set of reactions. Section 5.7 presents a more detailed ranking for the 'heavy collisions' (ions + neutrals), obtained during the testing phase of the SA tool. Finally, the relevancy of the method and of the results is discussed in section 5.8.

5.2 Overview of existing analyzes in combustion and cold plasma communities

There are numerous ways of analyzing how a model responds to a change in its inputs, classified according to the goal of the user and the method implemented. For instance, the plasma community often differentiates *sensitivity analysis*, giving a qualitative evaluation of the inputs' influence, and *uncertainty quantification*, giving a quantitative evaluation of the error bars propagated by the model. Note, however, that some authors include quantitative measures (*e.g.* Sobol indices) in the sensitivity analysis group. Other authors use the term of 'uncertainty analysis', denoting a method typically based on a sensitivity analysis method but focusing on giving an 'envelop' of the output uncertainties. Another distinction is about *local* and *global* methods, the former measuring the effect of small perturbations near the input space of 'reference' while the latter focuses on the influence of the inputs' variance on the output variance. Once again, authors' opinion about the Morris method, described in section 5.5, varies between *local* and *global*. This lack of agreement on the classification illustrates well the recent apparition and use of such tools. In this work, we chose to refer to the Morris method as a *sensitivity analysis* method as the ranking of influence calculated is qualitative.

As mentioned in chapter 1, the interest for sensitivity analysis is relatively recent in the cold plasma community, as compared with the combustion [39, 139–145] or the atmospheric communities. Because they have roughly similar contexts, it is common for researchers to adapt a method from another community. In the combustion field, Zador *et al.* [39] compared 4 different methods for a methane flame model and listed the numerous publications from the atmospheric field they were inspired by. Among the listed authors, Campolongo *et al.* proposed later on [26] some enhancements of the Morris method, which largely inspired the work presented in this chapter. One typical goal of a sensitivity analysis is to identify the most influential inputs, in order to focus experimental or fundamental investigations on their corresponding cross-sections/rate coefficients [29, 71, 146]. Another common situation is the opposite goal, where the users want to identify the most negligible inputs in order to reduce the variables of a

model, typically the number of reactions or species. This is the case for van Oijen *et al.* [38] for the combustion field, with the so-called Flamelet-Generated Manifold method. Reduction of chemical/kinetic sets is also being investigated in the cold plasma community, often in order to reduce a computational time too large to increase the dimensions of a model. Methods such as the *Principal Component Analysis* [33, 147], *Direct Relation Graph* [148] and *Pathway Analysis* [36, 37, 149] use the very different time-scale of the reactions to achieve skeletal reduction. Finally, although debatable, some authors assess the uncertainties of the model thanks to sensitivity analysis methods, approaching the results given by uncertainty quantification methods at a lower computational cost [30, 31, 34, 35].

5.3 The oxygen kinetic scheme

Non-equilibrium oxygen plasmas are widely used in the industry, are very important for atmospheric studies, and as such, were the object of numerous experimental and modeling investigations. In most modeling attempts of plasma chemistry in oxygen, the O_2 vibrational excitation is thought as relatively low. Accordingly, its vibrational states are not discriminated, *i.e.* they were not considered as distinct species in the simulations. However, some recent experimental observations [150, 151] questionned this assumption and, together with the calculation of new cross-sections for electron impact on O_2, derived by Laporta *et al.* [152, 153], they motivated new experimental and numerical investigations of cold pure oxygen plasmas. A representative example is the recent work of Annušová *et al.* [70], whose results are discussed in section 5.6. The species can be molecular oxygen O_2, atomic oxygen O or ozone O_3. The molecular oxygen states are $O_2(a^1\Delta_g)$ and $O_2(b^1\Sigma_g^+)$ hereafter denoted by O_2(a1Dg) and O_2(b1Sg+), the positive ion O_2(+,X) and 42 vibrational states O_2(X,v=0,...,41). The atomic oxygen states are O(3P), O(1D), the positive ion O(+,gnd) and the negative ion O(-,gnd), where 'gnd' stands for 'ground state'. The ozone states are O_3(X) and O_3(exc). In the end, it results in 51 distinct species and 179 reactions.

To avoid confusion in the terms, the word 'model' will be used for the 'physical/mathematical view of NTPs', while the words 'kinetic scheme' will refer more specifically to the sets of implemented reactions. In this work, the SA is applied to a model and a kinetic scheme similar to the one used in [70]. Chronologically, the first study consisted in varying reactions within a restricted set among all implemented reactions. The restricted set is detailed in section 5.7, offering an insight on a few specific reactions after some more general results are presented. The second part of the study dealt with a SA applied to the whole kinetic scheme, *i.e.* all the reaction rate coefficients were modified (otherwise stated). The full list of reactions is presented hereafter. Results were obtained (see section 5.6) for two different operating regimes: a 'low pressure' regime with $p = 40$ mTorr corresponding to the conditions in [70], and a 'moderate pressure' regime at $p = 1$ Torr. The specific conditions are discussed more in detail in section 5.6, where the results are also compared with the conclusions from [70].

The full kinetic scheme

This sub–section details the 175 oxygen reactions which are modified for the **full SA**, plus 4 that are left out because they directly depend on other reactions (cf. group No. G10, reactions with red font).

These reactions are gathered into 16 different groups. Numerous different classifications are possible, *e.g.* sorting the reactions according to the species involved (electrons, atoms, molecules), or separating the 3-body reactions from the 2-body reactions. The choice of how the groups are constituted depends on the aims of the user, as well as numerical limitations like the computational cost.

G1	**electron impact excitation, 4 reactions**
1	e + O_2(X,v=0) $\rightleftharpoons$ e + O_2(a1Dg)
2	e + O_2(X,v=0) $\rightleftharpoons$ e + O_2(b1Sg+)
3	e + O_2(a1Dg) $\rightleftharpoons$ e + O_2(b1Sg+)
4	e + O(3P) $\rightleftharpoons$ e + O(1D)
G2	**electron impact dissociation, 7 reactions**
5	e + O_2(X,v=0) $\rightarrow$ e + 2O(3P)
6	e + O_2(X,v=0) $\rightarrow$ e + O(3P) + O(1D)
7	e + O_2(a1Dg) $\rightarrow$ e + 2O(3P)
8	e + O_2(a1Dg) $\rightarrow$ e + O(3P) + O(1D)
9	e + O_2(b1Sg+) $\rightarrow$ e + 2O(3P)
10	e + O_2(b1Sg+) $\rightarrow$ e + O(3P) + O(1D)
11	e + O_3(X) $\rightarrow$ e + O(3P) + O_2(X,v=0)
G3	**electron impact ionization, 4 reactions**
12	e + O_2(X,v=0) $\rightarrow$ 2e + O_2(+,X)
13	e + O_2(a1Dg) $\rightarrow$ 2e + O_2(+,X)
14	e + O(3P) $\rightarrow$ 2e + O(+,gnd)
15	e + O(-,gnd) $\rightarrow$ 2e + O(3P)
G4	**electron impact dissociative ionization, 2 reactions**
16	e + O_2(X,v=0) $\rightarrow$ 2e + O(3P) + O(+,gnd)
17	e + O_2(a1Dg) $\rightarrow$ 2e + O(3P) + O(+,gnd)
G5	**electron dissociative attachment, 2 reactions**
18	e + O_2(X,v=0) $\rightarrow$ O(-,gnd) + O(3P)
19	e + O_2(a1Dg) $\rightarrow$ O(-,gnd) + O(3P)
G6	**electron dissociative recombination, 2 reactions**
20	e + O_2(+,X) $\rightarrow$ 2O(3P)
21	e + O_2(+,X) $\rightarrow$ O(3P) + O(1D)

G7 heavy neutral collisions, 28 reactions

22 O_2(a1Dg) + O(3P) → O_2(X,v=0) + O(3P)
23 O_2(b1Sg+) + O(3P) → O_2(X,v=0) + O(3P)
24 O_2(b1Sg+) + O(3P) → O_2(a1Dg) + O(3P)
25 O(3P) + O(1D) → O(3P) + O(3P)
26 O(1D) + O_2(X,v=0) → O(3P) + O_2(a1Dg)
27 O_2(b1Sg+) + O_3(X) → 2O_2(X,v=0) + O(3P)
28 O(1D) + O_3(X) → 2O_2(X,v=0)
29 O(1D) + O_3(X) → O_2(X,v=0) + 2O(3P)
30 O_3(exc) + O(3P) → O_3(X) + O(3P)
31 O_3(exc) + O_2(X) → O_3(X) + O_2(X)
32 2O(3P) + O_2(X,v=0) → O_3(X) + O(3P)
33 O_2(a1Dg) + O_3(X) → 2O_2(X,v=0) + O(3P)
34 O(3P) + O_3(X) → 2O_2(X,v=0)
35 O(3P) + O_3(X) → O_2(a1Dg) + O_2(X,v=0)
36 O(3P) + O_3(X) → O_2(b1Sg+) + O_2(X,v=0)
37 O(1D) + O_2(X,v=0) → O(3P) + O_2(b1Sg+)
38 O_2(a1Dg) + O_3(exc) → 2O_2(X,v=0) + O(3P)
39 O(3P) + O_3(exc) → 2O_2(X,v=0)
40 O(3P) + O_2(X,v=0) + O_2(X) → O_3(X) + O_2(X)
41 O(3P) + O_2(X,v=0) + O_2(X) → O_3(exc) + O_2(X)
42 O(1D) + O_2(X) → O(3P) + O_2(X)
43 2O_2(a1Dg) → O_2(b1Sg+) + O_2(X,v=0)
44 2O(3P) + O_2(X) → O_2(X,v=0) + O_2(X)
45 2O(3P) + O_2(X) → O_2(X) + O_2(a1Dg)
46 2O(3P) + O_2(X) → O_2(X) + O_2(b1Sg+)
47 O(3P) + O_2(X,v=0) + O_3(X) → 2O_3(X)
48 3O(3P) → O_2(X,v=0) + O(3P)
49 O_2(a1Dg) + O_2(X) → O_2(X,v=0) + O_2(X)

G8	**ion transport, 2 reactions**
50	O_2(+,X) + wall $\rightarrow$ O_2(X,v=0
51	O(+,gnd) + wall $\rightarrow$ O(3P)
G9	**neutral transport, 5 reactions**
52	O_2(a1Dg) + wall $\rightarrow$ O_2(X,v=0)
53	O_2(b1Sg+) + wall $\rightarrow$ O_2(X,v=0)
54	O(3P) + wall $\rightarrow$ 0.5O_2(X,v=0)
55	O(1D) + wall $\rightarrow$ O(3P)
56	O_3(exc) + wall $\rightarrow$ O_3(X)
G10	**electron impact processes from O_2(X,v>0), 2 reactions**
57	e + O_2(X,v=1:41) $\rightarrow$ 2e + O_2(+,X)
58	e + O_2(X,v=1:41) $\rightarrow$ e + 2O(3P)
59	e + O_2(X,v=1:41) $\rightarrow$ e + O(3P) + O(1D)
60	e + O_2(X,v=1:6) $\rightarrow$ e + O_2(a1Dg)
61	e + O_2(X,v=1:8) $\rightarrow$ e + O_2(b1Sg+)
62	e + O_2(X,v=1:41) $\rightarrow$ O(3P) + O(-,gnd)
G11	**vibrational excitation by electron impact, 41 reactions**
63	e + O_2(X,v=0:40) $\rightleftharpoons$ e + O_2(X,v=41)
64	e + O_2(X,v=0:39) $\rightleftharpoons$ e + O_2(X,v=40)
65	e + O_2(X,v=0:38) $\rightleftharpoons$ e + O_2(X,v=39)
66	e + O_2(X,v=0:37) $\rightleftharpoons$ e + O_2(X,v=38)
67	e + O_2(X,v=0:36) $\rightleftharpoons$ e + O_2(X,v=37)
68	e + O_2(X,v=0:35) $\rightleftharpoons$ e + O_2(X,v=36)
69	e + O_2(X,v=0:34) $\rightleftharpoons$ e + O_2(X,v=35)
70	e + O_2(X,v=0:33) $\rightleftharpoons$ e + O_2(X,v=34)
71	e + O_2(X,v=0:32) $\rightleftharpoons$ e + O_2(X,v=33)
72	e + O_2(X,v=0:31) $\rightleftharpoons$ e + O_2(X,v=32)
73	e + O_2(X,v=0:30) $\rightleftharpoons$ e + O_2(X,v=31)
74	e + O_2(X,v=0:29) $\rightleftharpoons$ e + O_2(X,v=30)
75	e + O_2(X,v=0:28) $\rightleftharpoons$ e + O_2(X,v=29)
76	e + O_2(X,v=0:27) $\rightleftharpoons$ e + O_2(X,v=28)
77	e + O_2(X,v=0:26) $\rightleftharpoons$ e + O_2(X,v=27)
78	e + O_2(X,v=0:25) $\rightleftharpoons$ e + O_2(X,v=26)
79	e + O_2(X,v=0:24) $\rightleftharpoons$ e + O_2(X,v=25)
80	e + O_2(X,v=0:23) $\rightleftharpoons$ e + O_2(X,v=24)
81	e + O_2(X,v=0:22) $\rightleftharpoons$ e + O_2(X,v=23)
82	e + O_2(X,v=0:21) $\rightleftharpoons$ e + O_2(X,v=22)
83	e + O_2(X,v=0:20) $\rightleftharpoons$ e + O_2(X,v=21)
84	e + O_2(X,v=0:19) $\rightleftharpoons$ e + O_2(X,v=20)
85	e + O_2(X,v=0:18) $\rightleftharpoons$ e + O_2(X,v=19)
86	e + O_2(X,v=0:17) $\rightleftharpoons$ e + O_2(X,v=18)
87	e + O_2(X,v=0:16) $\rightleftharpoons$ e + O_2(X,v=17)
88	e + O_2(X,v=0:15) $\rightleftharpoons$ e + O_2(X,v=16)
89	e + O_2(X,v=0:14) $\rightleftharpoons$ e + O_2(X,v=15)
90	e + O_2(X,v=0:13) $\rightleftharpoons$ e + O_2(X,v=14)
91	e + O_2(X,v=0:12) $\rightleftharpoons$ e + O_2(X,v=13)
92	e + O_2(X,v=0:11) $\rightleftharpoons$ e + O_2(X,v=12)

G11	**vibrational excitation by electron impact (cont.)**
93	$e + O_2(X,v=0:10) \rightleftharpoons e + O_2(X,v=11)$
94	$e + O_2(X,v=0:9) \rightleftharpoons e + O_2(X,v=10)$
95	$e + O_2(X,v=0:8) \rightleftharpoons e + O_2(X,v=9)$
96	$e + O_2(X,v=0:7) \rightleftharpoons e + O_2(X,v=8)$
97	$e + O_2(X,v=0:6) \rightleftharpoons e + O_2(X,v=7)$
98	$e + O_2(X,v=0:5) \rightleftharpoons e + O_2(X,v=6)$
99	$e + O_2(X,v=0:4) \rightleftharpoons e + O_2(X,v=5)$
100	$e + O_2(X,v=0:3) \rightleftharpoons e + O_2(X,v=4)$
101	$e + O_2(X,v=0:2) \rightleftharpoons e + O_2(X,v=3)$
102	$e + O_2(X,v=0:1) \rightleftharpoons e + O_2(X,v=2)$
103	$e + O_2(X,v=0) \rightleftharpoons e + O_2(X,v=1)$
G12	**molecular V-T processes, 2 reactions**
104	$O_2(X,v=1:41) + O_2(X) \rightleftharpoons O_2(X,v=v-1) + O_2(X)$
105	$O_2(X,v=41) + O_2(X) \rightarrow 2O(3P) + O_2(X)$
G13	**atomic V-T processes, 62 reactions**
106	$O_2(X,v=1:41) + O(3P) \rightleftharpoons O_2(X,w=v-1) + O(3P)$
107	$O_2(X,v=2:41) + O(3P) \rightleftharpoons O_2(X,w=v-2) + O(3P)$
108	$O_2(X,v=3:41) + O(3P) \rightleftharpoons O_2(X,w=v-3) + O(3P)$
109	$O_2(X,v=4:41) + O(3P) \rightleftharpoons O_2(X,w=v-4) + O(3P)$
110	$O_2(X,v=5:41) + O(3P) \rightleftharpoons O_2(X,w=v-5) + O(3P)$
111	$O_2(X,v=6:41) + O(3P) \rightleftharpoons O_2(X,w=v-6) + O(3P)$
112	$O_2(X,v=7:41) + O(3P) \rightleftharpoons O_2(X,w=v-7) + O(3P)$
113	$O_2(X,v=8:41) + O(3P) \rightleftharpoons O_2(X,w=v-8) + O(3P)$
114	$O_2(X,v=9:41) + O(3P) \rightleftharpoons O_2(X,w=v-9) + O(3P)$
115	$O_2(X,v=10:41) + O(3P) \rightleftharpoons O_2(X,w=v-10) + O(3P)$
116	$O_2(X,v=11:41) + O(3P) \rightleftharpoons O_2(X,w=v-11) + O(3P)$
117	$O_2(X,v=12:41) + O(3P) \rightleftharpoons O_2(X,w=v-12) + O(3P)$
118	$O_2(X,v=13:41) + O(3P) \rightleftharpoons O_2(X,w=v-13) + O(3P)$
119	$O_2(X,v=14:41) + O(3P) \rightleftharpoons O_2(X,w=v-14) + O(3P)$
120	$O_2(X,v=15:41) + O(3P) \rightleftharpoons O_2(X,w=v-15) + O(3P)$
121	$O_2(X,v=16:41) + O(3P) \rightleftharpoons O_2(X,w=v-16) + O(3P)$
122	$O_2(X,v=17:41) + O(3P) \rightleftharpoons O_2(X,w=v-17) + O(3P)$
123	$O_2(X,v=18:41) + O(3P) \rightleftharpoons O_2(X,w=v-18) + O(3P)$
124	$O_2(X,v=19:41) + O(3P) \rightleftharpoons O_2(X,w=v-19) + O(3P)$
125	$O_2(X,v=20:41) + O(3P) \rightleftharpoons O_2(X,w=v-20) + O(3P)$
126	$O_2(X,v=21:41) + O(3P) \rightleftharpoons O_2(X,w=v-21) + O(3P)$
127	$O_2(X,v=22:41) + O(3P) \rightleftharpoons O_2(X,w=v-22) + O(3P)$
128	$O_2(X,v=23:41) + O(3P) \rightleftharpoons O_2(X,w=v-23) + O(3P)$
129	$O_2(X,v=24:41) + O(3P) \rightleftharpoons O_2(X,w=v-24) + O(3P)$
130	$O_2(X,v=25:41) + O(3P) \rightleftharpoons O_2(X,w=v-25) + O(3P)$
131	$O_2(X,v=26:41) + O(3P) \rightleftharpoons O_2(X,w=v-26) + O(3P)$
132	$O_2(X,v=27:41) + O(3P) \rightleftharpoons O_2(X,w=v-27) + O(3P)$
133	$O_2(X,v=28:41) + O(3P) \rightleftharpoons O_2(X,w=v-28) + O(3P)$
134	$O_2(X,v=29:41) + O(3P) \rightleftharpoons O_2(X,w=v-29) + O(3P)$
135	$O_2(X,v=30:41) + O(3P) \rightleftharpoons O_2(X,w=v-30) + O(3P)$
136	$O_2(X,v=1:41) + O(1D) \rightleftharpoons O_2(X,w=v-1) + O(1D)$

G13 atomic V-T processes (cont.)

137 O_2(X,v=2:41) + O(1D) $\rightleftharpoons$ O_2(X,w=v-2) + O(1D)
138 O_2(X,v=3:41) + O(1D) $\rightleftharpoons$ O_2(X,w=v-3) + O(1D)
139 O_2(X,v=4:41) + O(1D) $\rightleftharpoons$ O_2(X,w=v-4) + O(1D)
140 O_2(X,v=5:41) + O(1D) $\rightleftharpoons$ O_2(X,w=v-5) + O(1D)
141 O_2(X,v=6:41) + O(1D) $\rightleftharpoons$ O_2(X,w=v-6) + O(1D)
142 O_2(X,v=7:41) + O(1D) $\rightleftharpoons$ O_2(X,w=v-7) + O(1D)
143 O_2(X,v=8:41) + O(1D) $\rightleftharpoons$ O_2(X,w=v-8) + O(1D)
144 O_2(X,v=9:41) + O(1D) $\rightleftharpoons$ O_2(X,w=v-9) + O(1D)
145 O_2(X,v=10:41) + O(1D) $\rightleftharpoons$ O_2(X,w=v-10) + O(1D)
146 O_2(X,v=11:41) + O(1D) $\rightleftharpoons$ O_2(X,w=v-11) + O(1D)
147 O_2(X,v=12:41) + O(1D) $\rightleftharpoons$ O_2(X,w=v-12) + O(1D)
148 O_2(X,v=13:41) + O(1D) $\rightleftharpoons$ O_2(X,w=v-13) + O(1D)
149 O_2(X,v=14:41) + O(1D) $\rightleftharpoons$ O_2(X,w=v-14) + O(1D)
150 O_2(X,v=15:41) + O(1D) $\rightleftharpoons$ O_2(X,w=v-15) + O(1D)
151 O_2(X,v=16:41) + O(1D) $\rightleftharpoons$ O_2(X,w=v-16) + O(1D)
152 O_2(X,v=17:41) + O(1D) $\rightleftharpoons$ O_2(X,w=v-17) + O(1D)
153 O_2(X,v=18:41) + O(1D) $\rightleftharpoons$ O_2(X,w=v-18) + O(1D)
154 O_2(X,v=19:41) + O(1D) $\rightleftharpoons$ O_2(X,w=v-19) + O(1D)
155 O_2(X,v=20:41) + O(1D) $\rightleftharpoons$ O_2(X,w=v-20) + O(1D)
156 O_2(X,v=21:41) + O(1D) $\rightleftharpoons$ O_2(X,w=v-21) + O(1D)
157 O_2(X,v=22:41) + O(1D) $\rightleftharpoons$ O_2(X,w=v-22) + O(1D)
158 O_2(X,v=23:41) + O(1D) $\rightleftharpoons$ O_2(X,w=v-23) + O(1D)
159 O_2(X,v=24:41) + O(1D) $\rightleftharpoons$ O_2(X,w=v-24) + O(1D)
160 O_2(X,v=25:41) + O(1D) $\rightleftharpoons$ O_2(X,w=v-25) + O(1D)
161 O_2(X,v=26:41) + O(1D) $\rightleftharpoons$ O_2(X,w=v-26) + O(1D)
162 O_2(X,v=27:41) + O(1D) $\rightleftharpoons$ O_2(X,w=v-27) + O(1D)
163 O_2(X,v=28:41) + O(1D) $\rightleftharpoons$ O_2(X,w=v-28) + O(1D)
164 O_2(X,v=29:41) + O(1D) $\rightleftharpoons$ O_2(X,w=v-29) + O(1D)
165 O_2(X,v=30:41) + O(1D) $\rightleftharpoons$ O_2(X,w=v-30) + O(1D)
166 O_2(X,v=12:41) + O(3P) $\rightarrow$ 3O(3P)
167 O_2(X,v=12:41) + O(1D) $\rightarrow$ O(1D) + 2O(3P)

G14 molecular V-Vprocesses, 2 reactions

168 O_2(X,v=1:40) + O_2(X,w=v:40) $\rightleftharpoons$ O_2(X,v=v-1) + O_2(X,v=w+1)
169 O_2(X,v=1:40) + O_2(X,w=41) $\rightarrow$ O_2(X,v=v-1) + 2O(3P)

G15 wall vibrational de-excitation, 1 reaction

170 O_2(X,v=1:41) + wall $\rightarrow$ O_2(X,v=v-1)

G16 heavy ion collisions, 9 reactions

171 O(-,gnd) + O_2(a1Dg) $\rightarrow$ O_3(X) + e
172 O(-,gnd) + O(3P) $\rightarrow$ O_2(X,v=0) + e
173 O(-,gnd) + O_2(X,v=0) $\rightarrow$ O_3(X) + e
174 O(-,gnd) + O_2(b1Sg+) $\rightarrow$ O(3P) + O_2(X,v=0) + e
175 O(+,gnd) + O(-,gnd) $\rightarrow$ 2O(3P)
176 O(+,gnd) + O_3(X) $\rightarrow$ O_2(+,X) + O_2(X,v=0)
177 O(+,gnd) + O_2(X,v=0) $\rightarrow$ O_2(+,X) + O(3P)
178 O(+,gnd) + O_2(a1Dg) $\rightarrow$ O_2(+,X) + O(3P)
179 O_2(+,X) + O(-,gnd) $\rightarrow$ O_2(X,v=0) + O(3P)

5.4 Numerical code: the Lisbon KInetics tool suite

The LisbOn KInetics (LoKI) tool suite [67, 69], implemented on MATLAB, couples two modules: (1) an open-source Boltzmann solver LoKI-B [49, 68], (2) a chemistry solver LoKI-C.

5.4.1 LoKI-B

LoKI-B solves the stationary electron Boltzmann equation (EBE) for non-magnetized non-equilibrium low-temperature plasmas excited by Direct-Current (DC)[2]or High-Frequency (HF) electric fields:

$$\overrightarrow{\nabla_r} \cdot (\vec{v}f) + \frac{\partial}{\partial \vec{v}} \cdot \left(\frac{e\vec{E}}{m_e} f \right) = \left(\frac{\partial f}{\partial t} \right)_{\text{coll}} \tag{5.1}$$

where $\vec{v}$ is the velocity vector of the electrons, f is the Electron Distribution Function (EDF) normalized in the velocity space to the electron density, m_e is the electron mass, $\vec{E}$ is the total electric field and $\left(\frac{\partial f}{\partial t}\right)_{\text{coll}}$ is the variation of the EDF due to electron collisions. The modeled plasma being in non-equilibrium it is impossible to assume a given shape of the EDF. Therefore, some assumptions [68, 154] are required to simplify the calculation of the EBE: steady-state ($\vec{E(t)} \equiv \vec{E}$ in DC case), plasma homogeneity, small anisotropies coming from $\vec{E}$, etc. The quasi-neutrality and flux conservation assumptions are required to extend the transport theory from [155] to the low-pressure plasmas, accounting for several positive ions and at least one negative ion. In the DC case, it is possible to expand the EDF in spherical harmonics in the velocity space and simplify it to:

$$f(\vec{v}) = \sum_l \sum_p f_l^p(v) P_l(\cos(\theta)) \approx \left[f^0(v) + \frac{\vec{v}}{v} f^1(v) \right] \times n_e \tag{5.2}$$

where P_l are Legendre polynomials and n_e is the electron density. The last term on the right corresponds to the so-called 'two-terms' approximation, with f^0 the isotropic part of the EDF (the so-called Electron Energy Distribution Function, or EEDF) and f^1 the anisotropic part. More details can be found in [156].

Typical outputs of LoKI-B are the EEDF, reaction rate coefficients and swarm parameters computed for the reduced electric fields set as inputs by the user. It can deal with any type of gas mixture, as long as the pertinent cross-sections are provided.

5.4.2 LoKI-C

LoKI-C solves the 0D (volume average) rate balance equations (cf. eq 2.12) for the heavy species, neutrals or ions. The model is the same as the one described in section 2.3, in the sense that:

- The vibrational/electronic states are discriminated into individual species.
- The electron-electron collisions are neglected in this work.
- The same types of reactions are considered.

[2]Only the DC case is used in this work

- The same principles apply to the calculation of the reaction rate coefficients.

However, concerning the numerical implementation, LoKI-C differs from the code of Silva *et al.*:

- LoKI-C solves the rate balance equations in steady-state only, hence there are no time-resolved outputs.
- Creation/destruction of heavy species may modify the initial pressure set by the user. At each loop, LoKI-C iterates the mixture/pressure until the initial pressure matches the final one. It provides a self-consistent calculation of the resulting gas mixture at the steady-state conditions defined by the user.
- LoKI-C benefits from its companion module LoKI-B to access easily accurate collisional rates between electrons and heavy species, as they are updated for each modification of the reduced electric field and the mixture.
- The organization of the database and the object-oriented implementation allows a greater flexibility .

Typical outputs are the densities of the heavy species, *i.e.* neutrals and ions.

5.4.3 LoKI workflow

In this work both modules are used to solve cold oxygen-plasma chemistry and electron kinetics. The workflow of LoKI is schematized in figure 5.1, illustrating the coupling between LoKI-B (in blue) and LoKI-C (in yellow), plus the required inputs (in red). The 3 represented loops ensure self-consistent calculations of the final electron and heavy species densities.

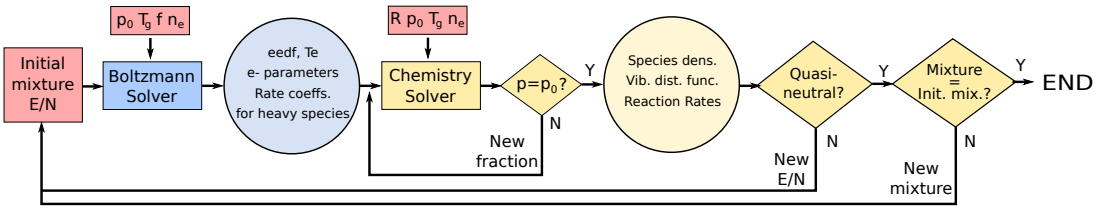

Figure 5.1: Figure extracted from [157]. The workflow of both LoKI modules is represented: (i) LoKI-B in the 'Boltzmann Solver' blue rectangle and (ii) LoKI-C in the 'Chemistry Solver' yellow rectangle. p_0 is the initial pressure, T_g is the gas temperature, E/N is the reduced electric field.

5.5 The original Morris method and its enhancements

Deterministic models are widely spread in many areas of interest and have in common the production of outputs from an initial set of inputs. When the number k of inputs is big (typically from a few dozens to thousands) and/or the equations to solve are complicated, it can be difficult to identify the most important inputs or the most negligible ones in terms of their influence on the results. Determining the influence of the inputs is interesting for the global understanding of any complex modeling (*e.g.* plasma chemistry

with many species involved), reducing the running cost of the simulations by removing non-important processes.

Assuming that one defines a range of variation for all the k-inputs, each of them divided into p discrete values, then an intuitive method to quantify input influence is the One-At-a-Time (OAT) procedure, where only one input is modified between each simulation. When applied in the most simple way, this procedure requires only k simulations (one for each input varying) to obtain results. Any modification observed in the outputs is then a direct consequence of the concerned varying input, which leads to a relatively easy interpretation. However, although it is still widely used in the cold plasma community, this method has been proved to fail in identifying strong interactions between inputs. The opposite 'brute force' procedure would be to evaluate variations in the outputs for all the possible input configurations, hence requiring p^k simulations to cover the whole space of values. Considering as an example a model whose running time is ~ 100 s, with $k = 100$ inputs to vary over a rather poor vector of $p = 4$ possible values, it would result then in a total running time of $T = 100 \times 4^{100} = 1.6 \times 10^{62}$ seconds, hence not feasible in practice.

The aim of the so-called Morris method [25] is to provide a preliminary approach for input influence identification, with a relatively low computational cost. It does not provide a full quantification of the output variation relative to a specific input modification but rather a *ranking* of input influence. This approach also allows to check the kind of influence (linear/non-linear) of a specific input on the output. It was specifically designed for models with a high number of inputs and moderate running times, such as the oxygen plasma model using LoKI, described in section 5.4. In this work, we chose to rely on the Morris method enhanced by some more recent improvements, described in detail in the next sub–sections.

5.5.1 The Morris Method: Elementary Effects

We consider a deterministic computational model with k input factors, denoting $\mathbf{X} = (X_1, X_2, ..., X_k)$ the vector of all the input factors, and $y(\mathbf{X})$ a specific scalar output computed by the code. It is desirable to have scalar outputs, but not always mandatory [71]. In the case of LoKI, the outputs can be the density of a species, the maintenance reduced electric field, the drift velocity, etc. For the sake of simplicity, we will describe the Morris method in this sub–section as if the model had only one scalar output. The input factors are real numbers such as constant coefficients used to compute a reaction rate, physics quantities such as electron density, gas temperature, pressure, etc. or geometrical dimensions. We assume the input factors X_i to take values in $[0; 1]$, hence the *region of interest* Ω is a k-dimensional unit hypercube. Each input can take p discrete values in the *region of experimentation* $\omega = \{0, 1/(p-1), 2/(p-1), ..., (p-2)/(p-1), 1\}$. To obtain physical values one has to transform the uniform distribution in $[0; 1]$ to the actual distribution of the input.

The key quantity is the so-called *elementary effect* d_i, a measure of the variation of an output when the i-th input value varies of an increment Δ. It is defined as:

$$d_i(\mathbf{X}) = \frac{y(\mathbf{X} + \Delta \cdot \mathbf{e_i}) - y(\mathbf{X})}{\Delta} \tag{5.3}$$

where $\mathbf{e_i}$ is a unit vector for the i-th coordinate (positive or negative) and Δ is a multiple of $1/(p-1)$, with

$0 < \Delta < 1$. A common practice for the Elementary Effects method is to take p even (typically $4 \leq p \leq 10$) and Δ equal to the smallest multiple of $1/(p-1)$ greater than 0.5, that is $\Delta = p/(2(p-1))$ (cf. [25, 26]). This choice ensures that for any initial value of X_i in ω, there is one and only one value $X_i \pm \Delta$ in ω.

A *trajectory* is built by generating one random value in ω for each X_i, representing a starting 'node' in the unit hypercube. It corresponds to the generation of points A and N in figure 5.2), which schematizes two Morris trajectories for $k = 3$ and $p = 6$. Then, the second 'node' is reached by moving one X_i of $\pm\Delta$, corresponding to points B and O in figure 5.2. The choice of the varied input is random with the condition that all inputs can be moved only once. This process is repeated until all the inputs X_i have been moved of Δ, hence a full trajectory consists in a collection of $k+1$ sets of inputs. **Each trajectory will require $k+1$ runs** (one run for each point) **and will provide k elementary effects d_i.** Morris uses the term *economy*, e, to define the quantity of elementary effects obtained divided by the number of effective runs: $e = k/(k+1)$. Some more economical designs were studied [27] but are beyond the scope of this work.

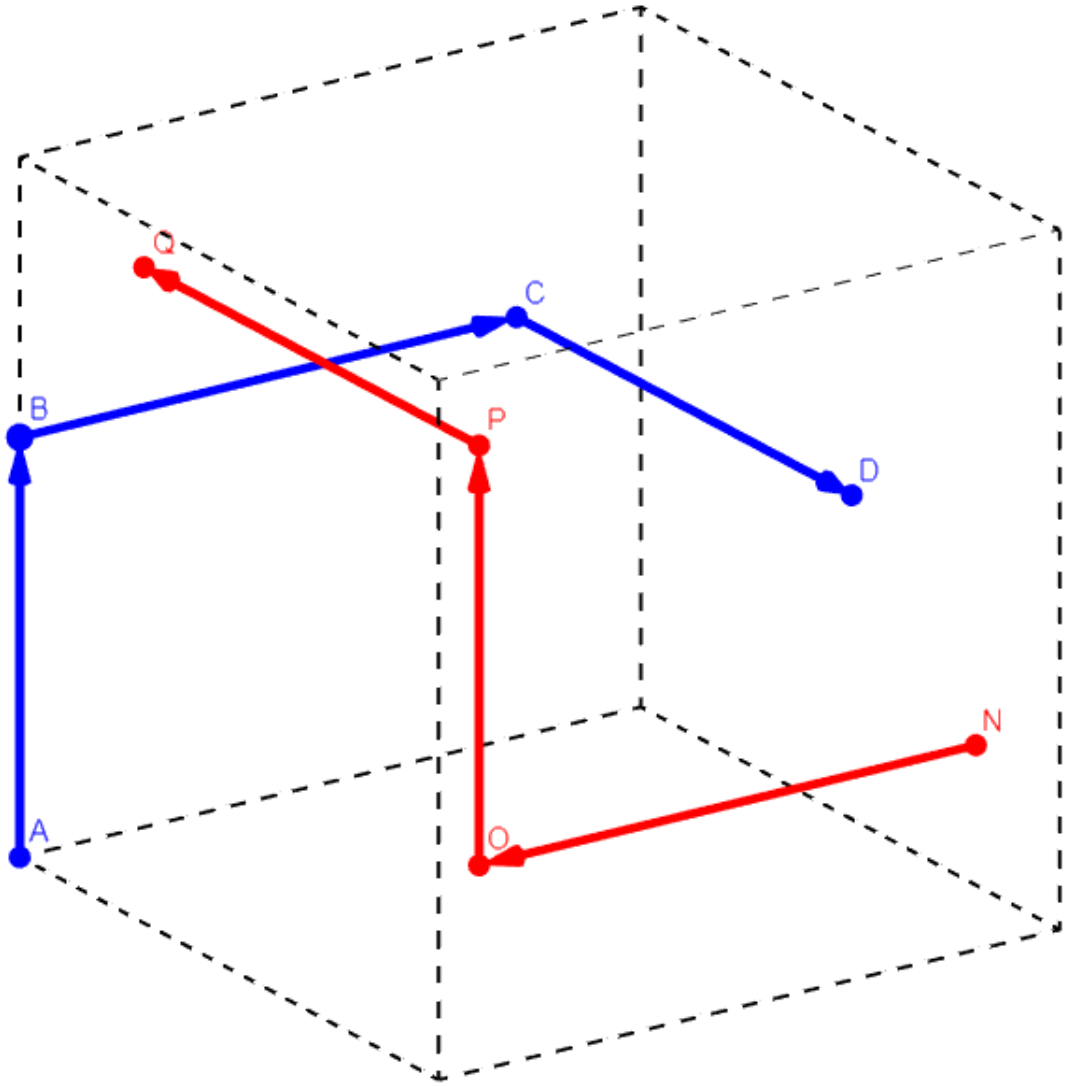

Figure 5.2: Scheme of two Morris trajectories: (A,B,C,D) and (N,O,P,Q), each of them requiring 4 simulations, one per node. In this example $k = 3$ and $p = 6$.

A certain number r of Morris trajectories are generated to reduce the statistical error. The choice of

this number depends on the user but several authors choose values typically between 10 and 50 [26, 31, 71]. Naturally, the set of generated trajectories should be clean of duplicates. The elementary effects are then averaged over the r values obtained, defining the mean value μ_i,

$$\mu_i = \frac{1}{r}\sum_{j=1}^{r} d_i^j, \tag{5.4}$$

where d_i^j is the elementary effect of the i-th input from the j-th Morris trajectory. The standard deviation σ_i is defined as:

$$\sigma_i = \sqrt{\frac{1}{r}\sum_{j=1}^{r}(d_i^j - \mu_i)^2}. \tag{5.5}$$

A large value of μ_i indicates a strong influence of the i-th input on the model output. If $\sigma_i \ll \mid \mu_i \mid$, then the influence is linear ; otherwise, it indicates a non-linearity, a strong dependence on another input, or both [25, 26, 31, 71]. The μ_i and σ_i can be normalized to factor c_0, in order to compare dimensionless quantities for example when the outputs have different units. In the literature, c_0 can be the average output value over the $r(k+1)$ runs [31] or the quantity $c_0 = \max_{i=\{1,\ldots,k\}} \sqrt{\mu_i^2 + \sigma_i^2}$ [71]. The latter is suited to define an absolute threshold of influence, for instance only the inputs meeting the criteria $c_i/c_0 = \sqrt{\mu_i^2 + \sigma_i^2}/c_0 \geq 0.1$ are identified as influential. Otherwise specified, all the results in this work were normalized to another measure, the so-called 'reference value', *i.e.* the output value obtained when all the inputs have their default value.

5.5.2 Enhancements

The method described by Morris is a good basis for generic SA applied to complex codes ; however, a pure random sampling of the inputs might not cover the whole region of interest Ω, or lead to large statistical errors. In the case of a code with multiple outputs, such as LoKI, it may also be difficult to analyze all μ_i and σ_i for each different output. Different authors applied the Morris method to complex codes and proposed some enhancements [26–28].

The Measure μ^* instead of μ and σ

Campolongo *et al.* [26] proposed to use another parameter, μ_i^*, defined as the mean of the absolute elementary effects $\mid d_i \mid$, instead of the classic mean μ_i. The advantage lies in having only one measure to provide an efficient ranking of the input influence, rather than considering both μ_i and σ_i at the same time. The classic mean μ_i cannot be used alone as strong positive and negative d_i might cancel each other when computing the mean value, resulting in a low μ_i although the influence of some i-th inputs is big. This effect is removed when computing the mean of the absolute elementary effects. It is also easier to compute than the measures provided by variance-based methods [158, 159]. Comparisons between the rankings provided by both types of methods were made in [26] for two test cases, showing that μ^* provides an excellent ranking at low cost, especially when the Morris trajectories are carefully chosen.

Improving the Sampling Method

Campolongo *et al.* [26] also revised the generation of random Morris trajectories to improve the coverage of the region of interest Ω. Their method requires to generate a high number of trajectories, $M \sim 500 - 1000$, and then to select the r ones maximizing the 'spread' using the Euclidean distance d_{ml}:

$$d_{ml} = \sum_{u=1}^{k+1} \sum_{v=1}^{k+1} \sqrt{\sum_{i=1}^{k} \left[X_i^m(u) - X_i^l(v) \right]^2} \tag{5.6}$$

where m and l are two trajectories among the M ones, u and v are the corresponding 'nodes' within the trajectories, and i is the input index among k. Note that for consistency d_{ml} is set to 0 if $m = l$. In their work [26], Campolongo *et al.* showed empirically that the distribution of the inputs was more uniform while using their selection process rather than a pure random one. However, this was questioned by Norton [28] who showed that such selection tends to maximize the distribution on the edges of the region ω. This is not a problem by itself, as one may prefer to maximize the spread between trajectories rather than having a uniform distribution. On the other hand, the selection method from Campolongo requires $M!/((M-r)!r!)$ comparisons, which is not applicable in practice. To circumvent this difficulty, Norton proposed a faster ranking procedure, pre-selecting m trajectories out of M, with $m \ll M$ and $m \geq r$, and then applies the Campolongo selection method on the m pre-selected trajectories. The subset of m trajectories is chosen using the Manhattan distance rather than the Euclidean one, because it is faster to compute as there is no squaring in its formulation. We found out that for $r \geq 20$, the number m has to be so close to r to be computationally affordable that it loses interest; in practice we set $m = r$, and $M = 1000$. Other possibilities are mentioned in Norton [28], such as defining a maximum of points in common with any previously accepted trajectories as a criteria to accept a new one. This selection method was not tested in this work.

Grouping the Inputs

Another feature described in Campolongo *et al.* [26] is the possibility to work with groups of inputs, rather than varying them one-by-one. This is very interesting to compare the influence of a 'type' of reaction versus another, for instance comparing the group *neutral transport* against the group *ion transport*, each of them constituted of a few different reactions. It is also possible to discriminate the reactions by species involved, or assess *a priori* for example grouping all the supposedly negligible ones together. Gathering inputs into s_G groups allows to drastically reduce the running cost of the SA, as a Morris trajectory will consist in $s_G + 1$ runs rather than $k + 1$. From a procedure point of view, all inputs within a group are moved at the same time by an increment $\pm\Delta$ *in the unit hypercube space*, the sign depending on their initial value in ω. Indeed, only one of the two values $X_i + \Delta$ and $X_i - \Delta$ is in $[0; 1]$ for each input i within the same group. Note that although the variation in constant in the unit hypercube space it does not imply an equal variation for all the rates i within the same group. Finally, because the increment can be both positive and negative within a group, the measure μ becomes less meaningful: it is not possible anymore to relate its sign to an increase or a decrease of an input. Hence, it is recommended in [26] to work with

μ^* only.

5.5.3 Adapting the SA Method to the LoKI Tool Suite

In this work, the guiding philosophy is to create a numerical tool to run a Morris-like sensitivity analysis, with the enhancements described previously. The SA is restricted to the code LoKI, described in section 5.4 and appendices C and D, with only one species involved in the initial gas mixture, namely molecular oxygen O_2. The goal of the investigation is twofold: to obtain a deeper understanding of the influence of the inputs from a physics point of view, and also to verify how robust and consistent this SA procedure is. Once this is verified the approach can be extended to more complex gas mixtures and generalized to other schemes.

The inputs corresponding to the operating conditions of the discharge (gas temperature, electron density, pressure, etc.) were fixed, in order to allow ranking comparison with other similar works. Learning more about their respective influence is also of importance, but beyond the scope of this work.

Defining the values to sample from for the rate coefficients

The ranking obtained from the SA may depend on the assumptions made, such as the distribution of the input factors. As shown in appendices C and D, the input factors consist in constant coefficients used by different mathematical laws, for example the coefficients A, B, C provided by the user for an Arrhenius-type law: $k = AT^B \exp^{C/T}$, where k is a rate coefficient in $cm^3.s^{-1}$ for a 2-body reaction (see e.g. reaction No. 39 in section 5.3), and T is either an electron temperature or a gas temperature. These laws vary from one reaction to another (see details in appendix C) so an efficiency factor Φ was applied to all of them, allowing a **scalar multiplication directly on the calculated rate coefficient**. An alternative approach, not used here, would be to modify the constant coefficients directly. We chose to study two types of region of experimentation ω_Φ, representing the p possible values of the efficiency factor Φ before normalization to $[0; 1]$:

- A *linear* ω_Φ^{lin}, built from a linear spacing of Φ between the limits 0.5 and 1.5. In other words, the inputs, *i.e.* the calculated rate coefficients, are sampled uniformly between 50% and 150% of their reference values.

- A *log* ω_Φ^{log}, built from a logarithmic spacing of Φ between the limits 0.1 and 10. In other words, the inputs, *i.e.* the calculated rate coefficients, are sampled between a factor of 10 smaller and a factor of 10 higher than their reference values. The distribution on this vector is also uniform, but the use of a logarithmic scale allows half the sampled efficiencies to be lower than 1.

For all the results from the full-varying kinetic scheme shown in this work (cf. section 5.6), we set $p = 8$. Hence, the **efficiency factor** Φ multiplied to the rate coefficients takes values in $\omega_\Phi^{lin} = \{0.50$ $; 0.64; 0.79; 0.93; 1.07; 1.21; 1.36; 1.50\}$ or in $\omega_\Phi^{log} = \{0.10; 0.19; 0.37; 0.72; 1.39; 2.68; 5.18; 10.00\}$, according to the user's choice. Defining such regions of experimentation prevents the modified inputs to take any non-physical value, like negative or extremely large values.

Discussion about the sampling regions

We define k^{ini} as the initial sampled value of a rate coefficient, k^{new} as its incremented value, k^{ref} as its reference value and δ_Φ the *efficiency increment* which depends on the spacing adopted. The quantities Φ^{ini} and Φ^{new} are equivalent to k^{ini} and k^{new} but for the efficiency values instead of the rate coefficient values. The absolute variation of the rate coefficients, *i.e.* $\epsilon_{abs} = k^{new} - k^{ini}$, is equal to $\epsilon_{abs} = \pm\delta_\Phi \times k^{ref}$, which is roughly $\pm 0.57 \times k_{ref}$ for the linear spacing and $p = 8$ but varies according to the initial value for the logarithmic spacing. In both cases, the absolute variation of a rate coefficient depends on its reference value. The relative variation of the rate coefficients, defined as $\epsilon_{rel} = k^{new}/k^{ini}$, is equal to $\epsilon_{rel} = 1 \pm \delta_\Phi/\Phi^{ini}$. It does not depend on the reference value, but on the initial value sampled. Note that, for the logarithmic spacing, $\epsilon_{rel} = 13.895$ if $k^{new} > k^{ini}$ and $\epsilon_{rel} = 0.072$ otherwise. Therefore, one must consider the SA results with caution. Typically, the elementary effect d_i is not a partial derivative, although it has a similar definition. Its measure may overestimate the sensitivity of the largest rate coefficients, as their absolute variations are likely to be the largest ones as well. For the sake of simplicity we decided to adopt a common practice [31] and take the constant $\Delta \sim 0.57$ from the unit hypercube as the denominator of the elementary effects.

The different studies conducted

The scripts written for the SA were first tested on a restricted set of reactions, presented in sub–section 5.7.1. This preliminary step allowed a computationally cheap validation of the implementation of the SA tool and gave results, shown in 5.7, about the most influential/negligible inputs within the heavy collisions group. These results put the stress on two specific groups over the 16 discussed in section 5.6. For this 'restricted' study, a total of $k = 37$ reactions were assigned an efficiency Φ. For the full-varying kinetic scheme, two different sets of conditions are compared: a 'low pressure' one at 40 mTorr and a 'moderate pressure' one at 1 Torr. Further details are given in table 5.1 in section 5.6. In the end, a total of $k = 175$ reaction rate coefficients were assigned an efficiency Φ. To evaluate if the use of groups provides a reliable ranking, the results obtained from a full-varying SA are compared with group-varying SA with $s_G = 16$, as shown in section 5.6. Additional information about the groups can be found in section 5.3.

5.6 Results for: complete oxygen set

Results obtained from SA consist in a collection of averaged elementary effects, specific to both each input and each output considered, as described in section 5.5. In the case of a SA applied to the code LoKI, it deals with many data that are not trivial to analyze nor display. This section presents some characteristic results in a non-exhaustive way. The **oxygen kinetic scheme** is the **full one**, presented in section 5.3. The section is organized as follows:

- Sub–section 5.6.1: ranking obtained for different numbers r of trajectories, all conditions fixed.
- Sub–section 5.6.2: ranking obtained for the 2 different regions of experimentation (linear and logarithmic) at fixed conditions.

- Sub–section 5.6.3: averaged ranking for the group study vs the full-varying study.
- Sub–section 5.6.4: ranking comparison between the results of A. Annušová [70] and this work, at low pressure.

Table 5.1: Discharge conditions for the two reference cases chosen. Only the ion transport follows a different law, which concerns 2 reactions out of 175.

Parameters	**Low pressure**	**Moderate pressure**
Pressure (Pa)	5.33	133.33
Gas temperature (K)	780	384
Electron density (m^{-3})	3.25×10^{16}	4.42×10^{15}
Electron temperature (eV)	3	2.55
Chamber length (m)	0.10	0.56
Chamber radius (m)	0.275	0.010
Initial gas mixture	100% O_2	100% O_2
Electron-electron collisions	Not considered	Not considered
Ion transport law	Lieberman diffusion [70]	Classical Ambipolar diffusion [62]

The two reference cases chosen for this work have different discharge parameters, summarized in the table 5.1. For analysis' purpose, a total of 12 outputs were considered, listed below.

1. Molecular oxygen O_2:
   - O_2(X): total density of molecular oxygen at electronic ground state but any vibrational state from $v = 0$ to $v = 41$.
   - O_2(a1Dg): density of the first electronically excited state.
   - O_2(b1Sg+): density of the second electronically excited state.
   - O_2(+,X): density of positive molecular oxygen ions.
2. Atomic oxygen O:
   - O(3P): density of the ground electronic state.
   - O(1D): density of the first electronically excited state.
   - O(+,gnd): density of positive atomic oxygen ions at ground state.
   - O(-,gnd): density of negative atomic oxygen ions at ground state.
3. Ozone O_3:
   - O_3(X): density of ground state ozone.
   - O_3(exc): density of vibrationally excited ozone.
4. Swarm parameters:
   - E/N: reduced electric field.
   - v_d: electron drift velocity.

Except otherwise noted, the Morris trajectories were generated considering $s_G = 16$ different groups of inputs, detailed in section 5.3. The means $\mu_i^*(j)$ of the absolute elementary effects are computed for each input/group i and each output j listed above. More global measures were also defined as the mean of the $\mu_i^*(Q)$ where Q denotes outputs with the same species or the swarm parameters: the 4 new measures are $\mu_i^*(\mathrm{O}_2)$, $\mu_i^*(\mathrm{O})$, $\mu_i^*(\mathrm{O}_3)$ and $\mu_i^*(\mathrm{swarm})$. The average over the 12 outputs is denoted $\mu_i^*(\mathrm{tot})$, and measures the 'total' influence of the input i on the model outputs. Otherwise specified, all rankings given were made with the measure $\mu_i^*(\mathrm{tot})$ for the sake of simplicity. All the results were normalized to the corresponding reference value (obtained for all efficiencies Φ set to 1) in order to compare dimensionless quantities.

5.6.1 Evolution with r

The number r of Morris trajectories generated is a crucial parameter of a SA: indeed, while working with $s_G = 16$, doubling r from $r = 20$ to $r = 40$ results in $20(s_G + 1) = 340$ new simulations to run. While working with the full-varying inputs, it results in $20(k + 1) = 3600$ new simulations, each of them taking between 180 s and 500 s to be completed. It is then advantageous to minimize r as much as possible, but keeping it high enough to get a consistent ranking.

Figures 5.3, 5.4 and 5.5 show the evolution of $\mu_i^*(j)$ with the increase of r for the 12 considered outputs and $s_G = 15$ groups of inputs (the 'ion transport' group was not considered in this sub–section). Results were iterated from the same initial set of trajectories, and as such the $r = 20$ set is also included in the $r = 40$ and $r = 60$ sets of trajectories. The 'spread' of trajectories in the unit hypercube space was maximized using the Manhattan distance (see sub–section 5.5.2). It can be seen from the figures that the group ranking is almost identical in the 3 situations. It means that: (1) the simpler selection criteria (as compared to Campolongo [26]) of Morris trajectories *via* the Manhattan distance is good enough, (2) one can save running time by limiting the SA to $r = 20$. For any other figure shown in this article, r was set to 40 when the inputs are grouped and to 20 when all the inputs vary independently.

5.6.2 Two Regions of Experimentation ω

The region of experimentation $\omega = \{0, 1/(p-1), ..., 1\}$ is also an important variable of the SA. A too restricted region may fail to provide consistent results for physics analysis, especially in the case of reaction rates with great uncertainties attached. On the other hand, a too large region of experimentation would require a number p sufficiently high to have a proper spacing of the region. Any input i takes only 2 values per trajectory (the initial value X_i and the incremented one $X_i + \Delta$), hence $2r$ different values over the whole SA. If $p \geq r$ then the region of experimentation would not be covered properly by the random sampling. It is worth mentioning that in the case of an uncertainty analysis the user would attach a range/distribution of values specific to each input, while for a sensitivity analysis (like this work) this is not mandatory nor desirable. Hence we chose to fix $p = 8$ with r typically a few times greater, and we study the changes in the global ranking for two different input distributions ω^{lin} and ω^{log} (see sub–section 5.5.3), identical for each X_i.

Tables 5.2 and 5.3 show the ranks obtained from $\mu_i^*(\text{tot})$ for the low pressure conditions and the moderate pressure conditions, respectively. An additional column shows the relative values $\mu_i^{\text{rel}} = \mu_i^* / \sum_{j=1}^{16} \mu_j^*$. The Morris trajectories were generated considering all $s_G = 16$ groups. In the tables, the group labels were sorted according to results obtained using the ω^{log} region of experimentation. The red background cells highlight the differences of ranking between ω^{lin} and ω^{log}. As expected, the value of $\mu_i^*(\text{tot})$ is greater for ω^{log} results, because the outputs vary more from their reference value (obtained for all $\Phi_i = 1$) when the inputs can take values in a larger range.

In the low pressure case (table 5.2), there are some differences in the identification of the relative influence of the different groups, although the relative means μ_i^{rel} are always comparable. The groups 'neutral transport', 'heavy neutral collisions' and 'electron impact dissociation' appear as very influential, on the top 4 in both cases, with high μ_i^{rel} values. On the other hand, the groups 'ion transport' and 'electron impact ionization' are in the top 5 for the linear distribution, whereas they are ranked 6$^{\text{th}}$ and 8$^{\text{th}}$, respectively, with the logarithmic distribution. The 5 last groups are recognized as negligible by both rankings. For the moderate pressure case, shown in table 5.3, the top 3 of most influential groups is identical for the two distributions. The main difference lies in the respective ranks of the groups 'heavy ion collisions' and 'electron impact ionization', which are interchanged with the linear distribution. The relatively high difference of rank for the group 'wall vibrational de-excitation' is not meaningful here, as its relative mean μ_i^{rel} is negligible with both distributions. Overall, the differences in the rankings are small and may be due to the design of the Morris method itself which does not intend to provide an absolute ranking, but rather to cluster the inputs into influential and non-influential ones. Despite small discrepancies in the ranks, there is no situation where inputs jump from a very influential group to a negligible group. If it were the case, non-trivial additional work would be required to properly assess the inputs ranges, as for an uncertainty analysis. As the measures μ_i^{rel} and the rankings do not drastically change from one distribution to the other, it means that valuable information can be acquired without requiring very accurate input distributions.

Table 5.2: Mean and relative mean of the absolute elementary effects, averaged over the 12 considered outputs, for two types of input distributions, at low pressure. The colored cells highlight groups that are ranked differently for the two input distributions.

Low pressure	ω^{lin}			ω^{log}		
Group	μ_i^*(tot)	μ_i^{rel}(tot)	**rank**	μ_i^*(tot)	μ_i^{rel}(tot)	**rank**
G9: neutral transport	5.11E-01	0.249	1	2.18E+00	0.199	1
G7: heavy neutral collisions	2.55E-01	0.124	4	1.56E+00	0.142	2
G2: e^- impact dissociation	2.97E-01	0.145	2	1.45E+00	0.132	3
G16: heavy ion collisions	1.78E-01	0.087	6	1.25E+00	0.115	4
G5: e^- dissociative attachment	8.70E-02	0.042	8	1.05E+00	0.096	5
G8: ion transport	2.89E-01	0.141	3	1.03E+00	0.094	6
G1: e^- impact excitation	1.38E-01	0.067	7	9.23E-01	0.084	7
G3: e^- impact ionization	2.28E-01	0.111	5	8.77E-01	0.080	8
G10: e^- proc. from O_2(X,v>0)	2.28E-02	0.011	9	2.26E-01	0.021	9
G13: atomic V-T processes	1.64E-02	0.008	11	1.50E-01	0.014	10
G11: vib. exc. by e^- impact	1.66E-02	0.008	10	1.17E-01	0.011	11
G6: e^- dissoc. recombination	9.57E-03	0.005	12	8.42E-02	0.008	12
G14: molecular V-V processes	9.03E-04	0.000	14	2.62E-02	0.002	13
G4: e^- impact dissoc. ioni.	1.38E-03	0.001	13	2.50E-02	0.002	14
G15: wall vib. de-excitation	7.00E-05	0.000	15	9.87E-04	0.000	15
G12: molecular V-T processes	4.13E-05	0.000	16	4.96E-04	0.000	16

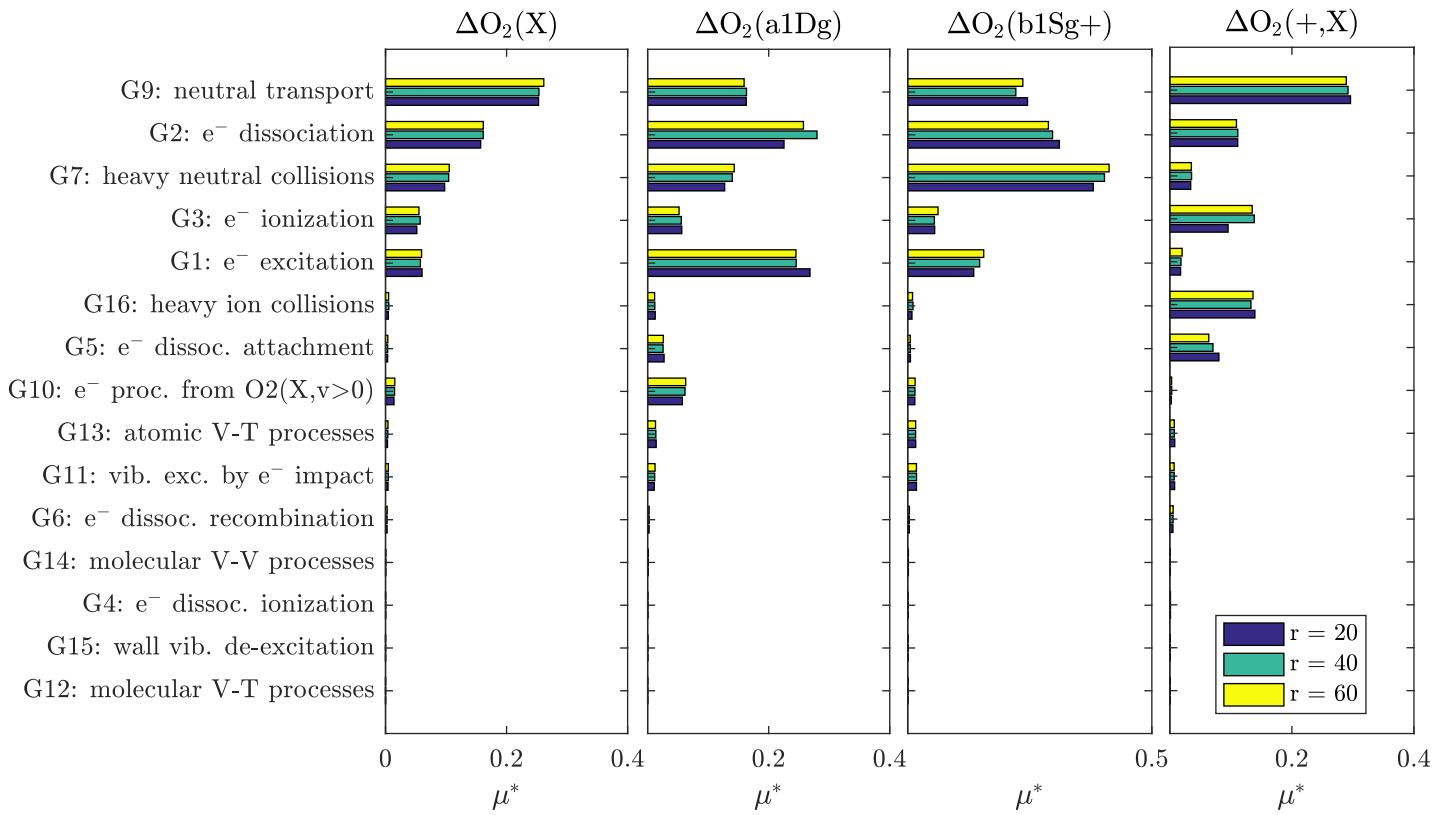

Figure 5.3: Mean $\mu_i^*(j)$ of the absolute elementary effects for molecular oxygen. The results were obtained with $s_G = 15$ groups of inputs and a linear region of experimentation.

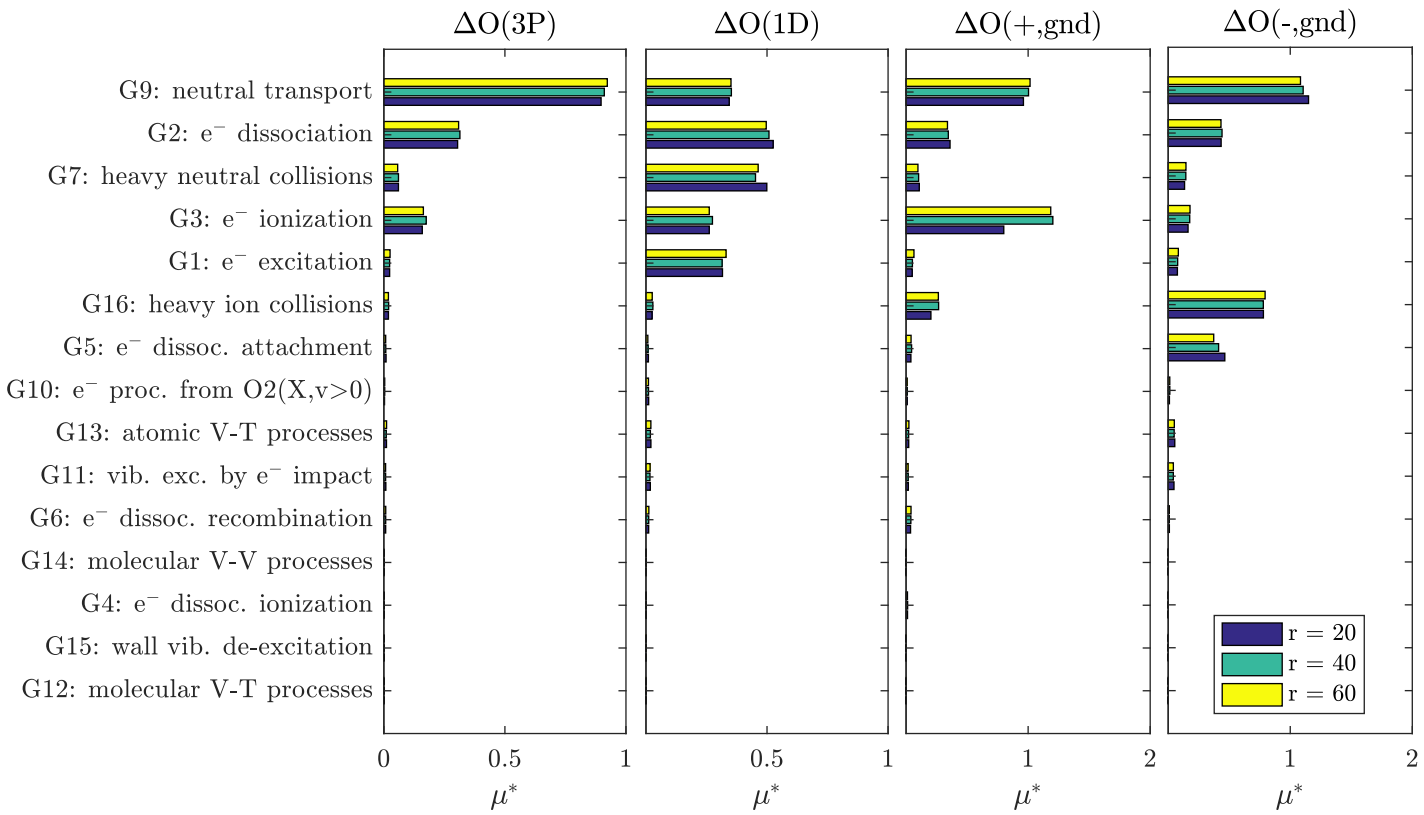

Figure 5.4: Mean $\mu_i^*(j)$ of the absolute elementary effects for atomic oxygen. The results were obtained with $s_G = 15$ groups of inputs and a linear region of experimentation.

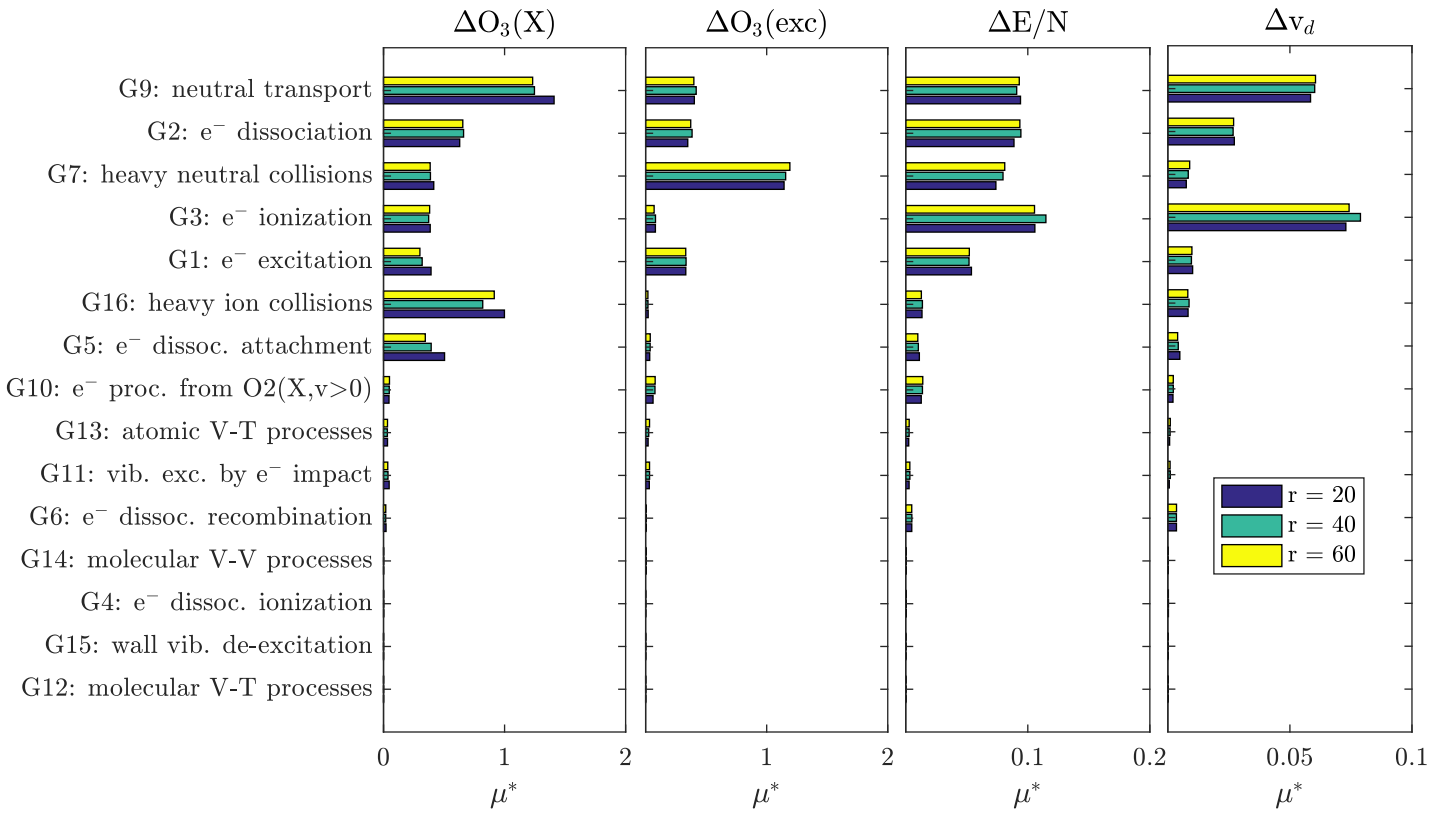

Figure 5.5: Mean $\mu_i^*(j)$ of the absolute elementary effects for ozone and swarm parameters. The results were obtained with $s_G = 15$ groups of inputs and a linear region of experimentation.

Table 5.3: Mean and relative mean of the absolute elementary effects, averaged over the 12 considered outputs, for two types of input distributions, at moderate pressure. The colored cells highlight groups that are ranked differently for the two input distributions.

Moderate pressure	ω^{lin}			ω^{log}		
Group	μ_i^*(tot)	μ_i^{rel}(tot)	**rank**	μ_i^*(tot)	μ_i^{rel}(tot)	**rank**
G9: neutral transport	4.66E-01	0.232	1	5.54E+00	0.207	1
G7: heavy neutral collisions	3.27E-01	0.163	2	4.54E+00	0.170	2
G8: ion transport	2.63E-01	0.131	3	3.96E+00	0.148	3
G16: heavy ion collisions	1.79E-01	0.089	7	3.42E+00	0.128	4
G3: e^- impact ionization	1.90E-01	0.095	6	2.90E+00	0.109	5
G2: e^- impact dissociation	2.37E-01	0.118	5	2.83E+00	0.106	6
G1: e^- impact excitation	2.52E-01	0.126	4	2.48E+00	0.093	7
G5: e^- dissociative attachment	8.83E-02	0.044	8	9.15E-01	0.034	8
G15: wall vib. de-excitation	8.27E-07	0.000	14	5.87E-02	0.002	9
G13: atomic V-T processes	5.53E-05	0.000	12	3.62E-02	0.001	10
G10: e^- proc. from O_2(X,v>0)	4.58E-04	0.000	9	2.55E-02	0.001	11
G14: molecular V-V processes	7.21E-07	0.000	15	9.22E-03	0.000	12
G4: e^- impact dissoc. ioni.	2.45E-04	0.000	11	6.36E-03	0.000	13
G11: vib. exc. by e^- impact	3.70E-05	0.000	13	5.69E-03	0.000	14
G6: e^- dissoc. recombination	2.55E-04	0.000	10	5.63E-03	0.000	15
G12: molecular V-T processes	1.50E-07	0.000	16	3.07E-05	0.000	16

5.6.3 Influence of the Method of Groups

As stated in section 5.5, the grouping method introduced by Campolongo [26] can help to reduce drastically the number of runs needed per Morris trajectory. It can be used as a preliminary step to identify the most influential inputs. However, it goes together with a loss of information and could fail to identify negligible inputs. For the sake of clarity, we denote 'Error Type I' a group identified as very influential although most of its components are negligible, and 'Error Type II' a group identified as negligible although some of its components are very influential. Without any "statistical weights" associated to the measures μ_i^*, there is a risk of having an Error Type I when working with groups, as shown in the following example.

Let us consider a testing case of 5 input factors $\{X_1, X_2, X_3, X_4, X_5\}$, and assume that only X_1 and X_2 are very influential, the other being negligible. We define $s_G = 2$ groups constituted as $g_1 = X_1$ and $g_2 = \{X_2, X_3, X_4, X_5\}$. Then, the SA would rank equally the groups g_1 and g_2 as $\mu^*_{g_1} \sim \mu^*_{g_2}$, failing to identify X_3, X_4 and X_5 as negligible. Although a full-varying SA (*i.e.* no grouping) would correctly discriminate the influential inputs from the negligible ones, we want to avoid using it as it is computationally more expensive. To do so, we suggest to divide the measures μ_i^* by the number of inputs within a group, in other words we apply "statistical weights" in order to get a different ranking. Denoting $\mu^*_{g_1,\,\text{weighted}}$ and $\mu^*_{g_2,\,\text{weighted}}$ the new measures obtained, we have $\mu^*_{g_1,\,\text{weighted}} = \mu^*_{g_1}$ and $\mu^*_{g_2,\,\text{weighted}} = \mu^*_{g_2}/4 < \mu^*_{g_2}$, hence a ranking without the Error Type I mentioned above. However, using the $\mu^*_{i,\,\text{weighted}}$ alone may lead to an Error Type II if a group is very large with only a few influential reactions within. A suggestion to overcome this issue would be to use both weighted and non-weighted measures at the same time, and compare the rankings obtained.

Table 5.4 shows a ranking comparison for the output O(3P) density. This output was chosen because the dissociation of O_2 into O is a typical crucial variable of cold plasma modeling. The region of

experimentation is the logarithmic ω^{log}. In order to study the consistency of the method described above, a full-varying SA is also performed for reference. The measures μ_i^* obtained for the individual 175 inputs are clustered into groups and averaged to give comparable results with the group SA. The ranking obtained doing so is labeled 'Full varying-SA' in table 5.4, and compared with the weighted group ranking, labeled 'Groups with weights', and the classic group ranking, labeled 'Groups without weights'.

An Error Type I is visible in table 5.4 for the group 'heavy neutral collisions' (group G7). Its influence is overestimated in the ranking obtained without weights. This group consists in 28 reactions, *i.e.* it is the 3rd largest groups in this study. The detailed ranking for the 175 varying-inputs reveals that 2 reactions (No. 37 and 42 in section 5.3) are among the 20 most influential ones, while 12 reactions (No. 30, 31, 32, 38, 39, 40, 41, 44, 45, 46, 47 and 48) are among the 20 least influential. In this case, the ranking provided by the weighted measures is more accurate, as it allows to overcome the Error Type I.

On the other hand, an Error Type II occurs for the group 'vibrational excitation by electron impact' (group G11). Its influence is slightly underestimated by the ranking obtained with weights. This group is the 2nd largest of the study, and despite the fact that a few reactions with low excitation level v are not negligible, the weight applied is so big that it lowers μ_{G11}^* too much to get the same ranking as the one provided by the full-varying SA.

Overall, the ranking provided by the groups with weights is more accurate than the one without weights, especially to get an accurate *group ranking*. However, a group SA can also be used as a low computational cost preliminary step, in order to identify which groups contain the most influential reactions. Using the ranking provided without weights is then more recommended, as the results depend more on the number of very influential reactions within a group than the number of negligible reactions. In this case, the next step would be to perform a detailed SA, restricted only to the groups previously identified, rather than the whole system of reactions.

Table 5.4: Comparison of ranking from the full-varying SA vs the group SA, with and without statistical weights applied to the groups. Low-pressure case.

Rank for O(3P) density variation	**Full-varying SA**	**Groups with weights**	**Groups without weights**
G9: neutral transport	1	1	1
G8: ion transport	2	2	3
G2: e^- impact dissociation	3	3	2
G3: e^- impact ionization	4	4	4
G5: e^- dissociative attachment	5	6	8
G1: e^- impact excitation	6	5	5
G16: heavy ion collisions	7	8	7
G6: e^- dissociative recombination	8	7	9
G7: heavy neutral collisions	9	9	6
G10: e^- proc. from O_2(X,v>0)	10	10	12
G11: vib. exc. by e^- impact	11	13	11
G4: e^- impact dissoc. ioni.	12	11	13
G13: atomic V-T processes	13	14	10
G12: molecular V-V processes	14	12	14
G15: wall vib. de-excitation	15	15	15
G12: molecular V-T processes	16	16	16

5.6.4 Comparison with the Ranking Provided by Annušová *et al.*

In this sub–section, we compare the ranking obtained from the SA with the main mechanisms identified by Annušová in [70], relative to creation and destruction of O_2(a1Dg) and O(+,gnd). These 2 outputs were chosen among the 7 available in [70] because they are representative of the interest of the SA: one ranking is very similar to the one provided by Annušová *et al*, while the other differs from their results. The ranking shown for the full-varying SA corresponds to the low pressure case (40 mTorr) and is derived from a logarithmic region of experimentation ω^{log}.

In her work, Annušová differentiated the creation processes from the destruction ones, so the direction of the arrow in the reaction matters. It is not the case for the ranking provided by the full-varying SA because the modification of an input will alter both the forward and the backward reaction rates. When considering the main reactions involved in O_2(a1Dg) variations, tables 5.5 and 5.6 show that the 7 reactions identified by Annušová are all among the 7th most important reactions identified by the SA. Note that reaction "e + O_2(a1Dg) $\leftarrow$ e + O_2(b1Sg+)" and reaction "e + O_2(X,v=0) $\rightarrow$ e + O_2(a1Dg)" are repeated, as their forward/backward counterpart is also in the top of the ranking. However, as opposed to the work in [70], the ranking from the SA is not limited to the reactions directly involving the concerned species. As such, we identified two new reactions as very influential: "O(3P) + wall $\rightarrow$ 0.5O_2(X,v=0)" and "O(1D) + O_2(X,v=0) $\rightarrow$ O(3P) + O_2(b1Sg+)", denoted R1 and R2 respectively. An increased rate of R1 means that more O_2(X,v=0) is produced, enhancing the probability of the reaction "e + O_2(X,v=0) $\rightarrow$ e + O_2(a1Dg)", ranked 3rd by the SA, to occur. An increased rate of R2 produces more O_2(b1Sg+), which is the main reactant leading to O_2(a1Dg) creation through the reaction "e + O_2(a1Dg) $\leftarrow$ e + O_2(b1Sg+)", with a contribution of 51% according to [70]. Note that such straightforward explanations should be considered with care, as some reactions can also increase the number of reactants destroying the considered species. Overall, for the case of O_2(a1Dg), the agreement between the ranking from Annušová and the one from the SA is very good.

Table 5.5: Main creation (top part) / destruction (bottom part) reactions identified by Annušová *et al.* for O_2(a1Dg).

Creation/Destruction of O_2(a1Dg) in [70]	**Rank**
e + O_2(a1Dg) $\leftarrow$ e + O_2(b1Sg+)	1
e + O_2(X,v=0) $\rightarrow$ e + O_2(a1Dg)	2
e + O_2(X,v=1:6) $\rightarrow$ e + O_2(a1Dg)	3
e + O_2(a1Dg) $\rightarrow$ e + O(3P) + O(1D)	1
e + O_2(a1Dg) $\rightarrow$ e + O_2(b1Sg+)	2
e + O_2(a1Dg) $\rightarrow$ e + 2O(3P)	3
e + O_2(X,v=0) $\leftarrow$ e + O_2(a1Dg)	4

Table 5.6: Ranking of the 7 most important processes for $O_2(a1Dg)$ variations, provided by a full-varying SA.

Variations of O_2(a1Dg), from the SA	**Rank**	**In [70]**
e + O_2(a1Dg) $\rightarrow$ e + O(3P) + O(1D)	1	Yes
O(3P) + wall $\rightarrow$ 0.5O_2(X,v=0)	2	No
e + O_2(X,v=0) $\rightleftharpoons$ e + O_2(a1Dg)	3	Yes
e + O_2(a1Dg) $\rightarrow$ e + 2O(3P)	4	Yes
e + O_2(X,v=1:6) $\rightarrow$ e + O_2(a1Dg)	5	Yes
O(1D) + O_2(X,v=0) $\rightarrow$ O(3P) + O_2(b1Sg+)	6	No
e + O_2(a1Dg) $\rightleftharpoons$ e + O_2(b1Sg+)	7	Yes

On the other hand, this is not the case for the variations of O(+,gnd), as illustrated in tables 5.7 and 5.8. Only two reactions, namely "e + O(3P) $\rightarrow$ 2e + O(+,gnd)" (R3) and "O(+,gnd) + O_2(X,v=0) $\rightarrow$ O_2(+,X) + O(3P)" (R4), are common to both rankings. This is an expected result for the reaction R3, as its contribution to O(+,gnd) creation is evaluated at 98% by Annušová. However, the main destruction reaction, responsible for 64% of O(+,gnd) loss in [70] is ranked 10th by the SA, hence not appearing in the SA ranking of table 5.8. From these results it appears that the neutralization of *molecular* positive ions at the walls has more effect on the final O(+,gnd) quantity than the neutralization of positive *atomic* ions at the walls. Such non-intuitive results illustrate well the interest of applying a detailed sensitivity analysis to complex systems.

The two examples studied evince the difference between identifying the *main reactions* of creation/destruction of a certain species and the *most influential* ones. The latter identification gives the key information required to optimize a specific plasma-based process.

Table 5.7: Main creation (top part) / destruction (bottom part) reactions identified by Annušová *et al.* for O(+,gnd).

Creation/Destruction of O(+,gnd) in [70]	**Rank**
e + O(3P) $\rightarrow$ 2e + O(+,gnd)	1
e + O_2(X,v=0) $\rightarrow$ 2e + O(3P) + O(+,gnd)	2
O(+,gnd) + wall $\rightarrow$ O(3P)	1
O(+,gnd) + O_2(X,v=0) $\rightarrow$ O_2+ + O(3P)	2
O(+,gnd) + O(-,gnd) $\rightarrow$ 2O(3P)	3
O(+,gnd) + O_2(a) $\rightarrow$ O_2+ + O(3P)	4

Table 5.8: Ranking of the 6 most important processes for O(+,gnd) variations, provided by a full-varying SA.

Variations of O(+,gnd), from the SA	**Rank**	**In [70]**
O_2(+,X) + wall $\rightarrow$ O_2(X,v=0)	1	No
O(3P) + wall $\rightarrow$ 0.5O_2(X,v=0)	2	No
e + O_2(X,v=0) $\rightarrow$ 2e + O_2(+,X)	3	No
e + O(3P) $\rightarrow$ 2e + O(+,gnd)	4	Yes
O(-,gnd) + O(3P) $\rightarrow$ O_2(X,v=0) + e	5	No
O(+,gnd) + O_2(X,v=0) $\rightarrow$ O_2(+,X) + O(3P)	6	Yes

5.7 Results for: restricted oxygen set

To test the procedure and the implementation in a realistic but simpler kinetic scheme, the vibrationally excited states were removed from the set, as shown in sub–section 5.7.1. Only $k = 37$ reactions, corresponding to groups 7 and 16, were assigned an efficiency coefficient Φ. The other reactions were left untouched, *i.e.* at their reference value. The 'heavy neutral collisions' and 'heavy ion collisions' are large groups with numerous reactions within. These types of reactions constitute a well-defined subset, as compared to electronic reactions and pure vibrational processes. Investigating their respective influence is of interest in many contexts, like in natural plasmas, atmospheric chemistry, atmospheric pressure jets, etc. The analysis of the SA with the complete kinetic scheme reveals that the group 7 (heavy neutral collisions) has a large influence on the variations of O_2(a1Dg), while the group 16 (heavy ion collisions) is especially important for the variations of O(+,gnd). This section presents the restricted kinetic scheme and the corresponding varying reaction rate coefficients, along with the rankings obtained from the 37-varying SA for the two outputs O_2(a1Dg) and O(+,gnd). It is worth mentioning that, as a direct consequence of a SA performed on a restricted set, the results may fail to identify potential interactions between the reactions.

5.7.1 The restricted kinetic scheme

Species

Being simplified, the restricted kinetic scheme does not discriminate the 41 vibrationally excited levels included in the full scheme. Hence, the total number of species is reduced from 51 to 10.

Reactions and varying reaction rate coefficients

The restricted kinetic scheme does not take any vibrational process into account. Consequently, the groups no. 10, 11, 12, 13, 14 and 15, detailed in section 5.3, are not part of the LoKI's inputs in this study. Overall, the number of reactions was reduced from 179 to 65. The varying reaction rate coefficients for the **restricted SA** correspond to the $k = 37$ reactions listed hereafter. These reactions are **not** split into groups, **all of them vary independently** from the other during the study. The varying restricted set consists in the heavy collisions: (i) for neutrals and (ii) for ions, corresponding to the group numbers 7 and 16, respectively, in section 5.3. The other $j = 65 - 37 = 28$ reaction rate coefficients (*i.e.* groups no. 1–6, 8 and 9) were not modified during the study.

G7	**heavy neutral collisions, 28 reactions**
22	O_2(a1Dg) + O(3P) $\rightarrow$ O_2(X,v=0) + O(3P)
23	O_2(b1Sg+) + O(3P) $\rightarrow$ O_2(X,v=0) + O(3P)
24	O_2(b1Sg+) + O(3P) $\rightarrow$ O_2(a1Dg) + O(3P)
25	O(3P) + O(1D) $\rightarrow$ O(3P) + O(3P)
26	O(1D) + O_2(X,v=0) $\rightarrow$ O(3P) + O_2(a1Dg)
27	O_2(b1Sg+) + O_3(X) $\rightarrow$ 2O_2(X,v=0) + O(3P)
28	O(1D) + O_3(X) $\rightarrow$ 2O_2(X,v=0)
29	O(1D) + O_3(X) $\rightarrow$ O_2(X,v=0) + 2O(3P)
30	O_3(exc) + O(3P) $\rightarrow$ O_3(X) + O(3P)
31	O_3(exc) + O_2(X) $\rightarrow$ O_3(X) + O_2(X)
32	2O(3P) + O_2(X,v=0) $\rightarrow$ O_3(X) + O(3P)
33	O_2(a1Dg) + O_3(X) $\rightarrow$ 2O_2(X,v=0) + O(3P)
34	O(3P) + O_3(X) $\rightarrow$ 2O_2(X,v=0)
35	O(3P) + O_3(X) $\rightarrow$ O_2(a1Dg) + O_2(X,v=0)
36	O(3P) + O_3(X) $\rightarrow$ O_2(b1Sg+) + O_2(X,v=0)
37	O(1D) + O_2(X,v=0) $\rightarrow$ O(3P) + O_2(b1Sg+)
38	O_2(a1Dg) + O_3(exc) $\rightarrow$ 2O_2(X,v=0) + O(3P)
39	O(3P) + O_3(exc) $\rightarrow$ 2O_2(X,v=0)
40	O(3P) + O_2(X,v=0) + O_2(X) $\rightarrow$ O_3(X) + O_2(X)
41	O(3P) + O_2(X,v=0) + O_2(X) $\rightarrow$ O_3(exc) + O_2(X)
42	O(1D) + O_2(X) $\rightarrow$ O(3P) + O_2(X)
43	2O_2(a1Dg) $\rightarrow$ O_2(b1Sg+) + O_2(X,v=0)
44	2O(3P) + O_2(X) $\rightarrow$ O_2(X,v=0) + O_2(X)
45	2O(3P) + O_2(X) $\rightarrow$ O_2(X) + O_2(a1Dg)
46	2O(3P) + O_2(X) $\rightarrow$ O_2(X) + O_2(b1Sg+)
47	O(3P) + O_2(X,v=0) + O_3(X) $\rightarrow$ 2O_3(X)
48	3O(3P) $\rightarrow$ O_2(X,v=0) + O(3P)
49	O_2(a1Dg) + O_2(X) $\rightarrow$ O_2(X,v=0) + O_2(X)

G16	**heavy ion collisions, 9 reactions**
171	O(-,gnd) + O_2(a1Dg) $\rightarrow$ O_3(X) + e
172	O(-,gnd) + O(3P) $\rightarrow$ O_2(X,v=0) + e
173	O(-,gnd) + O_2(X,v=0) $\rightarrow$ O_3(X) + e
174	O(-,gnd) + O_2(b1Sg+) $\rightarrow$ O(3P) + O_2(X,v=0) + e
175	O(+,gnd) + O(-,gnd) $\rightarrow$ 2O(3P)
176	O(+,gnd) + O_3(X) $\rightarrow$ O_2(+,X) + O_2(X,v=0)
177	O(+,gnd) + O_2(X,v=0) $\rightarrow$ O_2(+,X) + O(3P)
178	O(+,gnd) + O_2(a1Dg) $\rightarrow$ O_2(+,X) + O(3P)
179	O_2(+,X) + O(-,gnd) $\rightarrow$ O_2(X,v=0) + O(3P)

SA parameters

As for the full kinetic scheme, we set $p = 8$. Only the linear spacing of Φ was tested for the restricted kinetic scheme, with variations of the reaction rate coefficients between 0.5 and 1.5 their reference value. Consequently, the *region of experimentation* ω is equal to: $\omega_{\Phi}^{lin} = \{0.50; 0.64; 0.79; 0.93; 1.07; 1.21; 1.36 ; 1.50\}$. Initially, a set of $M = 400$ Morris trajectories was generated, *i.e.* 400 matrices of size 37×38. Among this set, only $r = 40$ Morris trajectories maximizing the 'distance' between each other were chosen to run the SA.

The option $p = 4$ was tested with minimal discrepancies in the results: most of the ranks are equal with both values of p. Note that reducing the number p does not allow to reduce the computational cost, hence it seems more interesting to detail the *region of experimentation* as long as the suggested criterion $r \geq 2p$ is observed. Finally, it is worth mentioning that two types of grouping were also tested, although

not presented here: **(i)** a 'clever' grouping, where the 37 inputs are sorted and separated into 4 groups of increasing influence and **(ii)** an 'uncertain' grouping, where the 37 inputs are separated into 4 groups of roughly equal importance. Evidently, doing so required the results from the 37-varying inputs study as a preliminary step. The results are not shown in this work but the conclusions were somewhat expected: the results from **(i)** allowed to identify properly the respective influence of the 4 groups, while the measures μ^* from **(ii)** were too close to give a reliable ranking of the groups.

Discharge conditions

Table 5.9 summarizes the discharge conditions for the SA on a restricted kinetic scheme. The discharge conditions for the 175-varying SA at 1 Torr are also written for a comparison purpose. The pressure from the restricted scheme is equal to the *Moderate pressure case* from the full kinetic scheme study. Other parameters are roughly equal, with the exception of the chamber length and the coefficients γ for the de-excitation of neutrals at the walls. Changes in the chamber length does not induce any large discrepancy in the results, as compared with the *Moderate pressure case*. However, the model is very sensitive to the wall deactivation probabilities, as shown in section 5.6 where the group No. 9 (neutral transport) is ranked 1^{st} for most of the outputs variations. Consequently, ranking comparisons between the 37-varying SA and the 175-varying SA are limited to qualitative assertions, the two discharge setups being too different to allow quantitative analysis.

Table 5.9: Discharge conditions for the restricted kinetic scheme.

Parameters	**Restricted case**	**Moderate pressure case**
Pressure (Pa)	133.33	133.33
Gas temperature (K)	300	384
Electron density (m^{-3})	3.67×10^{15}	4.42×10^{15}
Electron temperature (eV)	2.51	2.55
Chamber length (m)	0	0.56
Chamber radius (m)	0.01	0.01
Initial gas mixture	95% O_2 – 5% O	100% O_2
Electron-electron collisions	Not considered	Not considered
Ion transport law	Effective Ambipolar diffusion [154]	Classical Ambipolar Diffusion [62]
Neutral transport γ inputs: reactions No. 52–56	$5 \times 10^{-5}, 2 \times 10^{-2}, 8 \times 10^{-3}, 1, 1 \times 10^{-2}$	$2 \times 10^{-5}, 2 \times 10^{-2}, 4.6 \times 10^{-4}, 1, 1 \times 10^{-1}$

5.7.2 Results

Tables 5.10 and 5.11 present the ranking obtained from the 37-varying SA (column **Rank/37**), with the former results from the 175-varying SA at 1 Torr (column **Rank/175**), for comparison purposes. The blue background cells corresponds to the 'heavy neutral collisions' (group No. 7) reactions while the yellow back ground cells correspond to the 'heavy ion collisions' reactions (group No. 16). The outputs considered, O_2(a1Dg) and O(+,gnd), correspond to the densities for which groups No. 7 and 16 have the most influence, respectively. The reactions are sorted in decreasing order of influence relatively to the 37-varying inputs results. The ranking was obtained by considering μ^* rather than μ plus σ, at the

cost of the sign of μ. Note, however, that values of μ^* are close to those of σ, while some values of μ do not reflect the influence of the reaction, as positive and negative contributions cancel each other. This is well illustrated in figures 5.6 and 5.7 where the computed μ and σ are displayed for each of the 37 reactions. Except for a few cases, and due to large σ values 'hiding' the smaller μ values, it may be difficult to rank properly the reactions. Large values of σ, as compared to μ, indicate non-linearity or strong dependence on other inputs, or both. A strong dependency of the reactions on each other is an expected result in a kinetic scheme with 65 reactions for only 10 species. As already illustrated in section 5.6, such interdependence, common in complex systems, is one of the reasons justifying the use of a SA tool. Indeed, the analysis of the results allows to identify a reaction as very influential regarding a specific species creation/destruction, although this species does not appear in the reaction itself. This is the case, for instance, of reactions No. 42, 23 and 37, respectively ranked 2nd, 4th and 6th, for the variations of O_2(a1Dg) density (see table 5.10). These 3 reactions are among the most important for the creation/destruction of O_2(a1Dg) although this state is not part of them.

Albeit having different discharge conditions, a qualitative comparison of the rankings from the 37-varying SA and the 175-varying SA is of interest to understand the driving mechanisms of these systems. Both SA identify the 'heavy ion collisions' group has very influential for O(+,gnd) variations, as shown in table 5.11. Some discrepancies appear in the respective rankings, such as for reactions No. 26 and 44 in table 5.10. They may be due to some interdependence effects: indeed, while the 175-varying inputs SA is likely to capture the dependency of heavy collision reactions with other types of reactions, it is not the case for the 37-varying inputs SA. However, other large discrepancies (see ranks of reactions No. 50, 52, 53 and 58 in table 5.11) may be attributed, instead, to the differences in the discharge conditions, as they all involve the negative ion O(-,gnd). A comparison of the outputs shows that, at steady-state, the density of O atom is about 3.8% of the total mixture density for the reduced kinetic scheme case, while it is at least 10 times larger for the full kinetic scheme case. Nevertheless, the absolute density of the negative ion O(-,gnd) is larger in the first case. Mixtures are then different enough to justify the observed differences of rank, as O(-,gnd) is clearly playing a major role in the present kinetics. These rather large discrepancies are likely to be caused by the differences in the wall deactivation probabilities γ, summarized in table 5.9, which were proved in section 5.6 to be extremely influential on the results. More figures about the 37-varying SA are available in Appendix B.

The 37-varying SA, initially developed to test at low computational cost the implementation of the SA tool, proved to give consistent results with the general conclusions of section 5.6. The largest discrepancies observed by comparing the ranking with a 'relatively close' case, namely the *Moderate pressure case*, are explained by the difference in wall deactivation and recombination probabilities (see table 5.9). It is also likely that, considering the large values of σ, the SA on the restricted kinetic scheme may fail to fully identify the strong interdependence of the reactions on each other. Overall, it is shown here that, under these conditions, a few reactions only are influential enough to drive the kinetics. Some of them do not include the concerned output species, highlighting the interest of running such analysis. A large part of them can also be considered as negligible, which is interesting in the perspective of a kinetic scheme reduction.

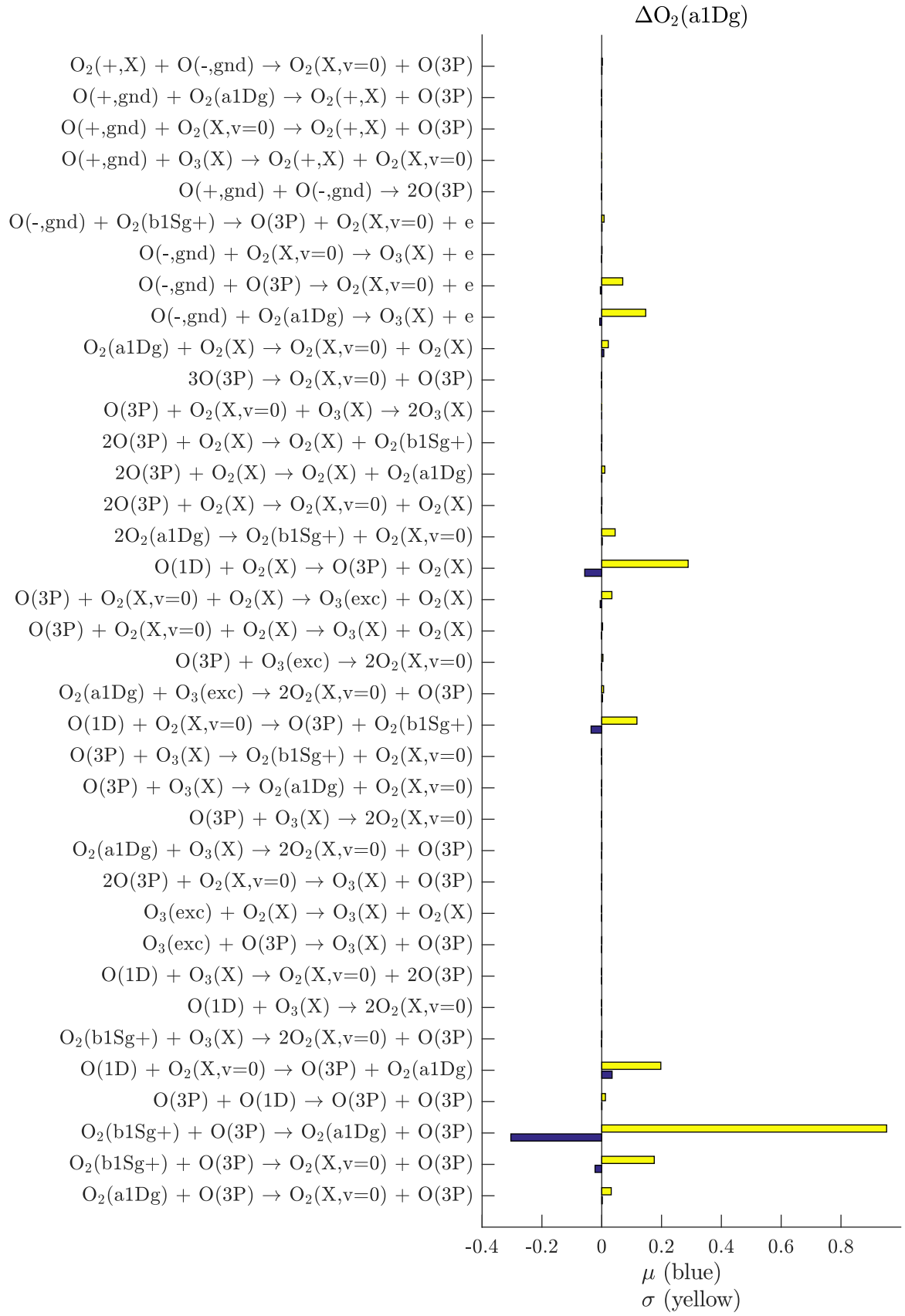

Figure 5.6: Mean μ and standard deviation σ for the 37 reactions varying in the restricted scheme, regarding O_2(a1Dg) variations.

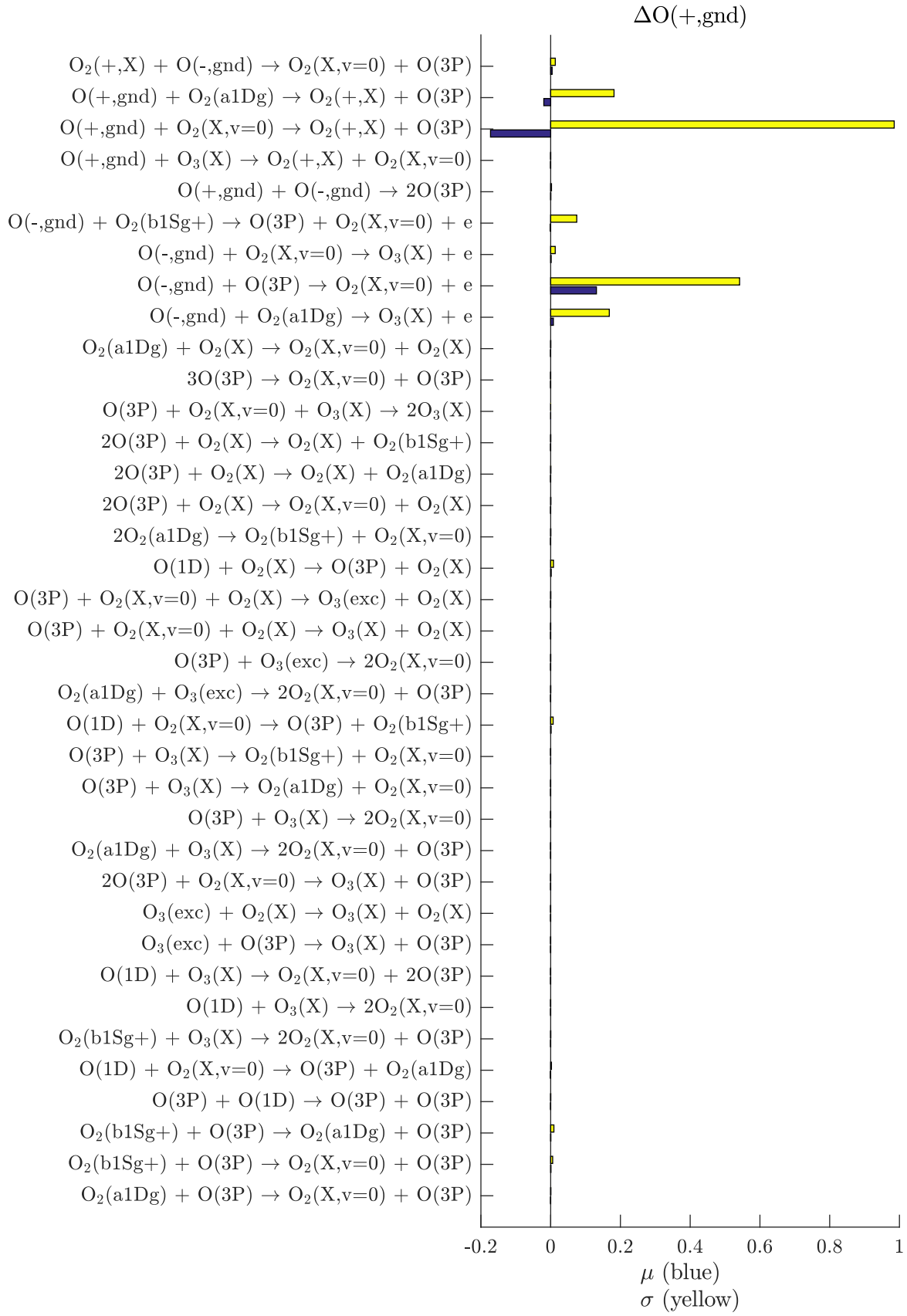

Figure 5.7: Mean μ and standard deviation σ for the 37 reactions varying in the restricted scheme, regarding O(+,gnd) variations.

Table 5.10: Rank comparison for O_2(a1Dg) variations, obtained with the measure μ^*, between: (i) results from the 37-varying inputs, with the restricted kinetic scheme (column Rank/37), (ii) results from the *Moderate pressure case*, with 175-varying inputs and the full kinetic scheme (column Rank/175). Blue background corresponds to group No. 7 (heavy neutral collisions) and yellow background to group No. 16 (heavy ion collisions).

Variations of O_2(a1Dg)			
No.	**Reactions**	**Rank/37**	**Rank/175**
24	O_2(b1Sg+) + O(3P) → O_2(a1Dg) + O(3P)	1	1
42	O(1D) + O_2(X) → O(3P) + O_2(X)	2	12
26	O(1D) + O_2(X,v=0) → O(3P) + O_2(a1Dg)	3	16
23	O_2(b1Sg+) + O(3P) → O_2(X,v=0) + O(3P)	4	7
171	O(-,gnd) + O_2(a1Dg) → O_3(X) + e	5	31
37	O(1D) + O_2(X,v=0) → O(3P) + O_2(b1Sg+)	6	9
172	O(-,gnd) + O(3P) → O_2(X,v=0) + e	7	28
43	2O_2(a1Dg) → O_2(b1Sg+) + O_2(X,v=0)	8	25
41	O(3P) + O_2(X,v=0) + O_2(X) → O_3(exc) + O_2(X)	9	30
22	O_2(a1Dg) + O(3P) → O_2(X,v=0) + O(3P)	10	21
49	O_2(a1Dg) + O_2(X) → O_2(X,v=0) + O_2(X)	11	35
25	O(3P) + O(1D) → O(3P) + O(3P)	12	13
45	2O(3P) + O_2(X) → O_2(X) + O_2(a1Dg)	13	20
38	O_2(a1Dg) + O_3(exc) → 2O_2(X,v=0) + O(3P)	14	38
39	O(3P) + O_3(exc) → 2O_2(X,v=0)	15	39
174	O(-,gnd) + O_2(b1Sg+) → O(3P) + O_2(X,v=0) + e	16	51
40	O(3P) + O_2(X,v=0) + O_2(X) → O_3(X) + O_2(X)	17	46
179	O_2(+,X) + O(-,gnd) → O_2(X,v=0) + O(3P)	18	53
173	O(-,gnd) + O_2(X,v=0) → O_3(X) + e	19	63
33	O_2(a1Dg) + O_3(X) → 2O_2(X,v=0) + O(3P)	20	45
46	2O(3P) + O_2(X) → O_2(X) + O_2(b1Sg+)	21	27
44	2O(3P) + O_2(X) → O_2(X,v=0) + O_2(X)	22	26
30	O_3(exc) + O(3P) → O_3(X) + O(3P)	23	52
32	2O(3P) + O_2(X,v=0) → O_3(X) + O(3P)	24	37
27	O_2(b1Sg+) + O_3(X) → 2O_2(X,v=0) + O(3P)	25	41
35	O(3P) + O_3(X) → O_2(a1Dg) + O_2(X,v=0)	26	40
31	O_3(exc) + O_2(X) → O_3(X) + O_2(X)	27	78
177	O(+,gnd) + O_2(X,v=0) → O_2(+,X) + O(3P)	28	44
178	O(+,gnd) + O_2(a1Dg) → O_2(+,X) + O(3P)	29	49
34	O(3P) + O_3(X) → 2O_2(X,v=0)	30	47
36	O(3P) + O_3(X) → O_2(b1Sg+) + O_2(X,v=0)	31	48
28	O(1D) + O_3(X) → 2O_2(X,v=0)	32	61
29	O(1D) + O_3(X) → O_2(X,v=0) + 2O(3P)	33	60
48	3O(3P) → O_2(X,v=0) + O(3P)	34	43
175	O(+,gnd) + O(-,gnd) → 2O(3P)	35	73
47	O(3P) + O_2(X,v=0) + O_3(X) → 2O_3(X)	36	132
176	O(+,gnd) + O_3(X) → O_2(+,X) + O_2(X,v=0)	37	125

Table 5.11: Rank comparison for O(+,gnd) variations, obtained with the measure μ^*, between: (i) results from the 37-varying inputs, with the restricted kinetic scheme (column Rank/37), (ii) results from the *Moderate pressure case*, with 175-varying inputs and the full kinetic scheme (column Rank/175). Blue background corresponds to group No. 7 (heavy neutral collisions) and yellow background to group No. 16 (heavy ion collisions).

Variations of O(+,gnd)			
No.	**Reactions**	**Rank/37**	**Rank/175**
177	O(+,gnd) + O_2(X,v=0) → O_2(+,X) + O(3P)	1	4
172	O(-,gnd) + O(3P) → O_2(X,v=0) + e	2	12
171	O(-,gnd) + O_2(a1Dg) → O_3(X) + e	3	35
178	O(+,gnd) + O_2(a1Dg) → O_2(+,X) + O(3P)	4	9
174	O(-,gnd) + O_2(b1Sg+) → O(3P) + O_2(X,v=0) + e	5	48
179	O_2(+,X) + O(-,gnd) → O_2(X,v=0) + O(3P)	6	41
173	O(-,gnd) + O_2(X,v=0) → O_3(X) + e	7	58
42	O(1D) + O_2(X) → O(3P) + O_2(X)	8	25
24	O_2(b1Sg+) + O(3P) → O_2(a1Dg) + O(3P)	9	13
37	O(1D) + O_2(X,v=0) → O(3P) + O_2(b1Sg+)	10	22
23	O_2(b1Sg+) + O(3P) → O_2(X,v=0) + O(3P)	11	21
175	O(+,gnd) + O(-,gnd) → 2O(3P)	12	55
26	O(1D) + O_2(X,v=0) → O(3P) + O_2(a1Dg)	13	33
44	2O(3P) + O_2(X) → O_2(X,v=0) + O_2(X)	14	20
43	2O_2(a1Dg) → O_2(b1Sg+) + O_2(X,v=0)	15	40
45	2O(3P) + O_2(X) → O_2(X) + O_2(a1Dg)	16	24
22	O_2(a1Dg) + O(3P) → O_2(X,v=0) + O(3P)	17	32
39	O(3P) + O_3(exc) → 2O_2(X,v=0)	18	45
41	O(3P) + O_2(X,v=0) + O_2(X) → O_3(exc) + O_2(X)	19	42
46	2O(3P) + O_2(X) → O_2(X) + O_2(b1Sg+)	20	27
38	O_2(a1Dg) + O_3(exc) → 2O_2(X,v=0) + O(3P)	21	43
25	O(3P) + O(1D) → O(3P) + O(3P)	22	26
49	O_2(a1Dg) + O_2(X) → O_2(X,v=0) + O_2(X)	23	51
27	O_2(b1Sg+) + O_3(X) → 2O_2(X,v=0) + O(3P)	24	37
176	O(+,gnd) + O_3(X) → O_2(+,X) + O_2(X,v=0)	25	56
40	O(3P) + O_2(X,v=0) + O_2(X) → O_3(X) + O_2(X)	26	47
28	O(1D) + O_3(X) → 2O_2(X,v=0)	27	59
34	O(3P) + O_3(X) → 2O_2(X,v=0)	28	46
35	O(3P) + O_3(X) → O_2(a1Dg) + O_2(X,v=0)	29	49
32	2O(3P) + O_2(X,v=0) → O_3(X) + O(3P)	30	36
33	O_2(a1Dg) + O_3(X) → 2O_2(X,v=0) + O(3P)	31	57
48	3O(3P) → O_2(X,v=0) + O(3P)	32	29
36	O(3P) + O_3(X) → O_2(b1Sg+) + O_2(X,v=0)	33	52
30	O_3(exc) + O(3P) → O_3(X) + O(3P)	34	67
31	O_3(exc) + O_2(X) → O_3(X) + O_2(X)	35	131
29	O(1D) + O_3(X) → O_2(X,v=0) + 2O(3P)	36	62
47	O(3P) + O_2(X,v=0) + O_3(X) → 2O_3(X)	37	141

5.8 Conclusions

Physical models solved *via* numerical simulations are becoming ever more important in society, with an inherent growing in complexity. This complexity can be a source of opacity for the user, as it is often difficult to relate precisely a change in the results with the variations of the inputs. However, such knowledge is often required for a deep understanding/optimization of the model. Various systemic approaches exist to answer this problematic, such as the one used as a baseline in this work, the so-called Morris method [25]. Originally designed in 1991, it belongs to the sensitivity analysis methods and was later refined by

other authors. It provides a ranking of the inputs' influence at a relatively low computational cost.

We applied the Morris method and its enhancements to a rather complex kinetic model for cold oxygen plasmas, including 51 species and 179 reactions. Some typical parameters of this method can have an important influence on the results and the total running time. Among them, the number r of Morris trajectories has an important influence on the accuracy of the ranking and on the computational cost. We found that $r = 20$ was enough to have a reliable ranking at a low cost, as already suggested by different authors. Considering the complexity of the system and the relatively large number of inputs to the model, this number may seem surprisingly low. Still, it can be even reduced, but we suggest to keep at least $r \geq 2p$ for a proper sampling of the input values, where p denotes the number of possible values an input can take.

Other important parameters are the possible input values, named region of experimentation ω, and their distribution within this interval. Different regions of experimentation exist in the literature, from the uniform distribution on a vector of equally spaced values [71], to log-normal distributions over a half infinite interval [31]. We chose to assign the same regions of experimentation to any varying reaction per SA performed. We compared the influence of ω by sampling uniformly input values on two different vectors. The first has a linear spacing from 50% to 150% of the reference value, while the second has a logarithmic spacing from 10% to 1000% of the reference value. We found that although the rankings differ in each case, they roughly identify the same very influential groups and the same negligible groups. This is a very interesting result as it avoids the user dedicating too many effort in knowing the precise distributions of each input, which sometimes is not even feasible.

The possibility of working with groups of inputs, introduced by Campolongo [26], allows to drastically reduce the computational time at the cost of a loss of information on the precise role of each reaction within a group. We tested this grouping approach and compared the ranking, weighted or not, to a full-varying SA performed for the same conditions. The weighted ranking from the group SA was found to be very similar to the one obtained from the full-varying SA. On the other hand, the non-weighted ranking brings useful information to detect the most influential reactions whichever group they belong to. A group SA can also be used to compare the influence of different reaction types, for example 'electron impact reactions' vs 'heavy neutral reactions'. The use of both weighted and non-weighted rankings should be enough to avoid typical errors, where a group is identified as very influential although most of its components are negligible or a group is identified as negligible although some of its components are very influential.

Finally, we compared the rankings obtained at low pressure from the SA and proposed in [70], adopting a very similar model. The ranking in [70] relative to a species density [X] is applied only to reactions involving the species X, while it is not the case for the ranking issued from the SA. For species highly present in the plasma, like the O_2 low-lying excited states, we found that our ranking is in very good agreement with the one from [70]. However, for rarer species like the positive ion O(+,gnd), our analysis brings a very different and deeper insight on the most influential reactions. This is one advantage of performing a sensitivity analysis rather than a direct creation/destruction analysis: the former directly identifies the most influential reactions among all the existing ones, not being restricted to the reactions

where the output is directly involved. Such non-intuitive results are of high importance for the plasma kinetics and are not limited to a single model or type of mixture.

It is worth mentioning two possible extensions of the SA, not explored in this work, which are based on the output of the Morris method, *i.e.* the identification of very influential and negligible inputs. The first one is uncertainty analysis, where a well-defined uncertainty range is associated to each different input, to assess the uncertainty ranges in the outputs. In general, the accuracy of the results depends on the total number of simulations, which can correspond to substantial computation costs. However, it is possible to mitigate this burden by articulating the analysis with the output of the Morris method, applying the uncertainty ranges only to those inputs identified as most influential in the results [31, 32]. The second extension is model reduction, especially important for passing from a 0D model to a 2D or 3D geometry. Typical models used in the cold plasma community are usually very complex, dealing with dozens of species and hundreds to thousands of reactions. At the same time, depending on the conditions, the outputs of interest may depend only on a few species/reactions. The Morris method can be used to identify such restricted set, and then reduce considerably the computational time by removing all negligible processes. In the particular case of our model and for the conditions under study, SA shows that almost all species appear in influential reactions, the only exception being the highly vibrationally excited O_2(v$>$12), which eventually could be removed from the kinetic scheme. Note that the removal of reactions should take over the removal of species, the latter being acceptable only in cases where the species does not intervene in any SA-relevant reaction.

Future investigation will address the application of the current SA analysis to other complex plasma-chemistry systems and its extension to uncertainty analysis and model reduction.

Chapter 6

Conclusions

The work presented along this thesis is focused on vibrational kinetics in Non-Thermal Plasmas (NTPs), with the underlying goal of optimizing CO_2 dissociation. The influence of nitrogen on the kinetics is explored in the first half of the work, while a sensitivity analysis tool is investigated in the second half. This chapter summarizes the main achievements of the PhD project and gives possible axis for future work.

6.1 Achievements

The first steps of the PhD project were dedicated to the investigation of the nitrogen kinetics, more specifically the vibrational processes in N_2-N_2 and N_2-CO_2 mixtures. Partially based on the data from Plonjes *et al.* [55], Blauer *et al.* [53] and Guerra *et al.* [50, 62], the reaction rate coefficients were fitted on larger gas temperature range and corrected to better fit the calculations from Billing *et al.* [52], taken as a reference here. For format reasons, most of the fitting functions have the same mathematical formula, except when it was impossible to obtain accurate-enough values on the full gas temperature range. Together with the electron reaction rate coefficients computed by the Lisbon KInetics (LoKI) tool [49, 67–69], this preliminary work led to the creation of a complete and consistent kinetic scheme for N_2-CO_2 cold plasmas, including ~ 3000 reactions.

The next steps consisted in the implementation of the new kinetic scheme in a physical model, in order to investigate the driving mechanism in CO_2-N_2 NTPs. To do so, the model previously developed and validated by Silva *et al.* [42, 43] for pure CO_2 DC glow discharges was further completed to take into account the set of nitrogen-related reactions. The new model obtained needed to be validated, which was done by comparing the results from the simulations to the measurements of vibrationally excited species in DC pulsed discharges, newly acquired by Morillo-Candas *et al.* [45]. The model complexity was kept fairly low in order to identify the origin of potential discrepancies, following a step-by-step validation of the kinetic rates for the lowest vibrational levels. The type of discharge chosen is suitable for such study, as the DC pulsed discharges correspond to a low-excitation regime. Therefore, the excitation level v of nitrogen was kept at $v \leq 10$ and those of CO_2 were kept at $v_1 \leq 2$, $v_2 \leq 5$ and $v_3 \leq 5$, resulting in 72 distinct CO_2 levels. The CO_2 level limitations correspond to the measurable populations from the

experiments and, although the complexity is reasonable, the maximum levels are nevertheless higher than in former models from the CO_2-N_2 laser community. The agreement obtained was considered as good enough for the validation of the model. The largest discrepancies concerned situations where the dissociation parameter α was at its maximum, hence they are likely to be due to missing kinetics implying CO molecules and/or O atoms. This assumption was further confirmed by including a simple quenching effect from O atoms, improving the agreement between experiments and simulations.

Both the measurements and the simulations confirmed the important influence of nitrogen on CO_2 kinetics. As a matter of fact, the dissociation parameter α always increased with the fraction of N_2, *i.e.* the *conversion efficiency* was larger, which is very interesting for CO_2 dissociation investigations. It is worth mentioning that similar behaviors were observed in plasmas at atmospheric pressure by Gans *et al.* [160]: the maximum CO_2 dissociation was obtained for a ratio 1:1 of CO_2-N_2 mixture, in an argon background. In some cases, like the DC pulsed discharge at 1 Torr and 20 mA, even the **absolute** quantity of CO produced was larger with the addition of nitrogen. However, increasing the N_2 fractions usually goes together with a loss of *energy efficiency* since a larger voltage is required to sustain the discharge at constant current. The reasons behind an enhanced dissociation were investigated during the PhD but remain uncertain. Under such low-excitation regimes, it is likely that dissociation from pure vibrational ladder-climbing processes represents a negligible part of the total dissociation mechanisms. However, α and T_3 or T_{CO} follow similar trends when plotted vs the fraction of N_2, reaching important values when N_2 is maximized. This observation, together with an electron power channeling analysis (cf. chapter 4), tend to indicate that vibrational processes do have an influence on the dissociation. Therefore, we can conclude that, in such discharges, CO_2 may undergo step-wise dissociation by electron impact on already excited vibrational levels. Overall, taking advantage of the favored energy transfers between vibrationally excited N_2 and the asymmetric stretching mode of CO_2 seem to be a promising way to reach an efficient CO_2 dissociation. However, as it requires to take fully advantage of the vibrational processes, it is preferable to inject an already-excited nitrogen in the plasma or to tune the discharge to reach populations with high-tail VDFs.

After the model was validated for DC glow discharges, some time was dedicated to investigate the main mechanisms at each time step of the active part and the afterglow. Regarding the complexity of analyzing such systems, it was decided to create a Sensitivity Analysis (SA) tool, in order to identify the most/least influential reactions and parameters in a more systematic way. Based on the Morris method [25], the SA tool was further enhanced with recent improvements suggested by Campolongo *et al.* [26] and J. P. Norton [28]. It was successfully tested on a physical model for oxygen cold plasmas, including 179 reactions for 51 species. Working with oxygen has the advantage of a lower complexity than CO_2 systems while keeping a somewhat similar kinetics. Different SA parameters and methods were tested in order to check the robustness of this approach. In particular, the possibility of working with groups rather than varying each input independently allows a low computational cost analysis on rather complex kinetic schemes. The results were then benchmarked against the ranking provided by Annušová *et al.* [70] with a similar model. Not only the SA gave consistent results regarding the well-known influential reactions, but it was also possible to rank indirect reactions whose influence is much more difficult to assess. Typically,

considering a specific density output [X], the analysis performed by Annušová *et al.* [70] only allowed to rank reactions where the species X was involved, while the SA could identify very influential reactions where this species does not appear. Such a numerical tool is relatively easy to generalize to any type of mixtures, including CO_2-N_2 plasmas, and does not require any maintenance while running to gather data. For the system studied in this work, 15 days were necessary to obtain a full SA where all inputs were varied independently from each other, and such a task can be run in the background of a remote server. The applications are numerous: it is of great interest to determine the driving mechanisms in complex dynamic systems, but also to identify negligible parameters in order to simplify the scheme. It may also constitute a preliminary step for more quantified analysis like Uncertainty Quantification (UQ) analysis.

Overall, the work realized during this PhD project showed the importance of N_2 in non-equilibrium CO_2 plasmas and opens the doors to new investigations in higher excitation regimes. Fundamental research and new experiments are still required to fully understand the underlying kinetics, but the enhanced dissociation seems promising to reach an efficient CO_2 dissociation. Analyzing the driving mechanisms of such systems is anything but trivial, hence an efficient systematic screening method was developed to answer this issue. To conclude, the work realized set solid basis for future investigations of the potential ladder-climbing effect in CO_2-N_2 plasmas.

List of publications

- As first author:
  - Terraz, L.; Silva, T.; Morillo-Candas, A.-S.; Guaitella, O.; Tejero-del-Caz, A.; Alves, L. L.; Guerra, V. Influence of N_2 on the CO_2 vibrational distribution function and dissociation yield in non-equilibrium plasmas. *J. Phys. D* **2019**, DOI: 10.1088/1361-6463/ab55fb.
  - Terraz, L.; Silva, T.; Tejero-del-Caz, A.; Alves, L. L.; Guerra, V. Sensitivity analysis in plasma chemistry: application to oxygen cold plasmas and the LoKI simulation tool. *J. Phys. Chem. A* **2020**, DOI: 10.1021/acs.jpca.0c01932.
- As co-author:
  - Guerra, V.; Silva, T.; Ogloblina, P.; Grofulović, M.; Terraz, L.; da Silva, M. L.;Pintassilgo, C. D.; Alves, L. L.; Guaitella, O. The case for *in situ* resource utilisation for oxygen production on Mars by nonequilibrium plasmas. *Plasma Sources Sci. Technol.* **2017**, DOI: 10.1088/1361-6595/aa8dcc.
  - Silva, T.; Gofulović, M.; Terraz, L.; Pintassilgo, C.; Guerra, V. Modelling the input and relaxation of vibrational energy in CO_2 plasmas. *J. Phys. D* **2018**, DOI: 10.1088/1361-6463/aadbd7.
  - Silva, T.; Grofulović, M.; Terraz, L.; Pintassilgo, C.; Guerra, V. Dynamics of gas heating in the afterglow of pulsed CO_2 and CO_2-N_2 glow discharges at low pressure. *Plasma Chem. Plasma Process.* **2020**, DOI: 10.1007/s11090-020-10061-7.

6.2 Future Work

This section gives possible axis for future research towards an optimal CO_2 dissociation. The energy transfer between vibrationally excited N_2 and the asymmetric stretching mode of CO_2 is a well-known mechanism which was widely used in CO_2 lasers. However, fundamental research is still scarce and the interest for nitrogen regarding CO_2 dissociation is relatively recent. Consequently, it would be very interesting to obtain new experimental data on the time-resolved densities of excited populations in CO_2-N_2 cold plasmas. In parallel, efforts on physical models should be pursued as well to validate reaction rate coefficients databases and develop the kinetic scheme complexity. More specifically, the code developed by Silva *et al.* [42, 43] and the Lisbon KInetics tool suite [49, 67–69] should be adapted to new types of plasma discharges, in order to be able to simulate high-excitation regimes. Especially, taking advantage of the high excitation resulting from Radio-Frequency (RF) or Micro-Wave (MW) discharges seems promising to increase CO_2 dissociation. Another possible direction for experiments would be the creation of a setup allowing to inject highly excited nitrogen, which is easier to do than pumping up specifically the $CO_2(00v_3)$ density. Such an operation would be possible thanks to the very long relaxation time characterizing the nitrogen molecule.

The full process of CO_2 dissociation and utilization also requires efficient capture and separation techniques, which were not investigated in the present work. While CO_2 capture technologies are being improved lastly, the separation methods remain uncertain. The use of a specific membrane to capture either O atoms or CO molecules seems promising but still requires further development. Equivalently, a lot of efforts have been recently dedicated to plasma surface interactions, as the influence of the reactor walls may overcome the chemistry within the plasma.

Finally, systematic analyses allowed by screening methods like the Morris method should definitely be stressed out, due to their adaptability and their efficiency in complex systems. Such procedures are still rare in the cold plasma community, while already well developed in the combustion community. Their generalization would be of great interest to better understand complex kinetics, to focus on the most important reaction rate coefficients which often vary greatly depending on the database considered, to reduce a kinetic scheme in order to increase the spatial dimensions of a model, etc. An immediate future step of the SA tool developed at Lisbon will be its generalization to different mixtures, as well as to develop a simplified interface to allow any user to perform such analysis in an easy way.

Bibliography

(1) Allen, M.; Dube, O.; Solecki, W.; Aragón-Durand, F.; Cramer, W.; Humphreys, S.; Kainuma, M.; Kala, J.; Mahowald, N.; Mulugetta, Y.; Perez, R.; Wairiu, M.; Zickfeld, K. *2018: Global Warming of 1.5 ° C. An IPCC Special Report on the impacts of global warming of 1.5 ° C above pre-industrial levels and related global greenhouse gas emission pathways, in the context of strengthening the global response to the threat of climate change, sustainable development, and efforts to eradicate poverty*; tech. rep.; IPCC, 2018.

(2) Tsutsumi, Y.; Mori, K.; Hirahara, T.; Ikegami, M.; Conway, T. *Technical Report of Global Analysis Method for Major Greenhouse Gases by the World Data Centre for Greenhouse Gases*; tech. rep.; WMO, 2009.

(3) Pachauri, R.; Meyer, L. *Climate Change 2014: Synthesis Report. Contribution of Working Groups I, II and III to the Fifth Assessment Report of the Intergovernmental Panel on Climate Change*; tech. rep.; IPCC, 2014.

(4) Futura CO_2 dans l'atmosphère : une concentration record `https://www.futura-sciences.com/planete/actualites/climatologie-co2-atmosphere-concentration-record-58177/`.

(5) Secretary-General, U. *Report of the Secretary-General on the 2019 Climate Action Summit the way forward in 2020*; tech. rep.; Climate Action Summit, 2019.

(6) IEA World energy balances `https://www.iea.org/reports/world-energy-balances-2019`.

(7) Schlömer, S.; Bruckner, T.; Fulton, L.; Hertwich, E.; McKinnon, A.; Perczyk, D.; Roy, J.; Schaeffer, R.; Sims, R.; Smith, P.; Wiser, R. *2014: Annex III: Technology-specific cost and performance parameters. In: Climate Change 2014: Mitigation of Climate Change. Contribution of Working Group III to the Fifth Assessment Report of the Intergovernmental Panel on Climate Change, Cambridge University*; tech. rep.; IPCC, 2014.

(8) Goede, A.; van de Sanden, R. CO_2-Neutral fuels. *Europhys. News* **2016**, *47*, 22–26, DOI: `10.1051/epn/2016304`.

(9) Silva, T. CO_2 decomposition and related processes in microwave discharges studied by optical diagnostic methods, English, Ph.D. Thesis, Université de Mons, 2015.

(10) Herzberg, G.; Crawford, B. L. Infrared and Raman Spectra of Polyatomic Molecules. *J. Phys. Chem. A* **1946**, *50*, 288–288, DOI: `10.1021/j150447a021`.

(11) Fermi, E. Über den Ramaneffekt des Kohlendioxyds. *Z. Physik* **1931**, *71*, 250–259, DOI: https://doi.org/10.1007/BF01341712.

(12) Grofulović, M. Energy storage and transfer in non-equilibrium CO_2 plasmas, Ph.D. Thesis, Universidade Técnica de Lisboa, Portugal and Eindhoven University of Technology, the Netherlands, 2019.

(13) College, C. Classical Normal Mode Analysis: Harmonic Approximation http://www.colby.edu/chemistry/PChem/notes/NormalModesText.pdf.

(14) Terraz, L.; Silva, T.; Morillo-Candas, A.-S.; Guaitella, O.; Tejero-del-Caz, A.; Alves, L. L.; Guerra, V. Influence of N_2 on the CO_2 vibrational distribution function and dissociation yield in non-equilibrium plasmas. *J. Phys. D.* **2019**, *53*, DOI: 10.1088/1361-6463/ab55fb.

(15) Fridman, A., *Plasma chemistry*; Cambridge University Press: 2008.

(16) Legasov, V. A.; Givotov, V. K.; Krasheninnikov, E. G.; Rusanov, V. D.; Fridman, A. *Sov. Phys., Doklady (Proceedings of USSR Academy of Sciences)* **1978**, *238*, 66.

(17) Asisov, R. I.; Givotov, V. K.; Krasheninnikov, E. G.; Potapkin, B. V.; Rusanov, V. D.; Fridman, A. *Sov. Phys., Doklady (Proceedings of the USSR Academy of Sciences)* **1983**, *271*, 94.

(18) Van Rooij, G. J.; van den Bekerom, D. C. M.; den Harder, N.; Minea, T.; Berden, G.; Bongers, W. A.; Engeln, R.; Graswinckel, M. F.; Zoethout, E.; van de Sanden, M. C. M. Taming microwave plasma to beat thermodynamics in CO_2 dissociation. *Farad. Disc.* **2015**, *183*, 233–248, DOI: 10.1039/C5FD00045A.

(19) Lino da Silva, M.; Vargas, J.; Loureiro, J. STELLAR CO_2 version 2: A database for vibrationally-specific excitation and dissociation rates for Carbon Dioxide http://esther.ist.utl.pt/stellar/STELLAR-CO2.pdf.

(20) Taylor, R. L.; Bitterman, S. Survey of Vibrational Relaxation Data for Processes Important in the CO_2-N_2 Laser System. *Rev. Mod. Phys.* **1969**, *41*, 26–47, DOI: 10.1103/RevModPhys.41.26.

(21) Britun, N.; Silva, T.; Chen, G.; Godfroid, T.; van der Mullen, J.; Snyders, R. Plasma-assisted CO_2 conversion: optimizing performance via microwave power modulation. *J. Phys. D* **2018**, *51*, 144002.

(22) Treanor, C. E.; Rich, J. W.; Rehm, R. G. Vibrational Relaxation of Anharmonic Oscillators with Exchange-Dominated Collisions. *J. Chem. Phys.* **1968**, *48*, 1798–1807, DOI: 10.1063/1.1668914.

(23) Terraz, L.; Silva, T.; Tejero-del-Caz, A.; Alves, L. L.; Guerra, V. Sensitivity analysis in plasma chemistry: application to oxygen cold plasmas and the LoKI simulation tool. *J. Phys. Chem. A* **2020**, DOI: 10.1021/acs.jpca.0c01932.

(24) Turányi, T. Sensitivity analysis of complex kinetic systems. Tools and applications. *J. Math. Chem.* **1990**, *5*, 203–248, DOI: 10.1007/BF01166355.

(25) Morris, M. D. Morris Factorial Sampling Plans for Preliminary Computational Experiments. *Technometrics* **1991**, *33*, 161, DOI: 10.2307/1269043.

(26) Campolongo, F.; Cariboni, J.; Saltelli, A. An effective screening design for sensitivity analysis of large models. *Environ. Model. Softw.* **2007**, *22*, 1509–1518, DOI: https://doi.org/10.1016/j.envsoft.2006.10.004.

(27) Campolongo, F.; Saltelli, A.; Cariboni, J. From screening to quantitative sensitivity analysis. A unified approach. *Comput. Phys. Commun.* **2011**, *182*, 978–988, DOI: 10.1016/j.cpc.2010.12.039.

(28) Norton, J. Selection of Morris Trajectories for Initial Sensitivity Analysis. *IFAC Proceedings Volumes* **2009**, *15*, 670–674, DOI: 10.3182/20090706-3-FR-2004.00111.

(29) Ayilaran, A.; Hanicinec, M.; Mohr, S.; Tennyson, J. Reduced chemistries with the Quantemol database (QDB). *Plasma Sci. Technol.* **2019**, *21*, 064006, DOI: 10.1088/2058-6272/ab00a1.

(30) Turner, M. Uncertainty and error in complex plasma chemistry models. *Plasma Sources Sci. Technol.* **2015**, *24*, 035027, DOI: 10.1088/0963-0252/24/3/035027.

(31) Turner, M. Uncertainty and Sensitivity Analysis in Complex Plasma Chemistry Models. *Plasma Sources Sci. Technol.* **2015**, *25*, 015003, DOI: 10.1088/0963-0252/25/1/015003.

(32) Turner, M. M. Computer Simulation in Low-Temperature Plasma Physics: Future Challenges. *Plasma Process. Polym.* **2017**, *14*, 1600121, DOI: 10.1002/ppap.201600121.

(33) Bellemans, A.; Magin, T.; Coussement, A.; Parente, A. Reduced-order kinetic plasma models using principal component analysis: Model formulation and manifold sensitivity. *Phys. Rev. Fluids* **2017**, *2*, 073201, DOI: 10.1103/PhysRevFluids.2.073201.

(34) Berthelot, A.; Bogaerts, A. Modeling of CO_2 plasma: effect of uncertainties in the plasma chemistry. *Plasma Sources Sci. Technol.* **2017**, *26*, 115002, DOI: 10.1088/1361-6595/aa8ffb.

(35) Wang, W.; Berthelot, A.; Zhang, Q.; Bogaerts, A. Modelling of plasma-based dry reforming: how do uncertainties in the input data affect the calculation results? *J. Journal of Physics D* **2018**, *51*, 204003, DOI: 10.1088/1361-6463/aab97a.

(36) Koelman, P.; Yordanova, D.; Graef, W.; Tadayon Mousavi, S.; van Dijk, J. Uncertainty analysis with a reduced set of input uncertainties selected using pathway analysis. *Plasma Sources Sci. Technol.* **2019**, *28*, 075009, DOI: 10.1088/1361-6595/ab0738.

(37) Koelman, P. Chemical aspects of CO_2 plasma modelling, English, Proefschrift., Ph.D. Thesis, Department of Applied Physics, 2019.

(38) Oijen, J. A. v.; Goey, L. P. H. d. Modelling of premixed counterflow flames using the flamelet-generated manifold method. *Combust. Theor. Model.* **2002**, *6*, 463–478, DOI: 10.1088/1364-7830/6/3/305.

(39) Zádor, J.; Zsély, I. G.; Turányi, T.; Ratto, M.; Tarantola, S.; Saltelli, A. Local and global uncertainty analyses of a methane flame model. *J. Phys. Chem. A* **2005**, *109*, 9795–9807, DOI: 10.1021/jp053270i.

(40) Grofulović, M.; Alves, L.; Guerra, V. Electron-neutral scattering cross sections for CO_2: A complete and consistent set and an assessment of dissociation. *J. Phys. D* **2016**, *49*, 395207, DOI: 10.1088/0022-3727/49/39/395207.

(41) Grofulović, M.; Silva, T.; Klarenaar, B. L. M.; Morillo-Candas, A. S.; Guaitella, O.; Engeln, R.; Pintassilgo, C. D.; Guerra, V. Kinetic study of CO2 plasmas under non-equilibrium conditions. II. Input of vibrational energy. *Plasma Sources Sci. Technol.* **2018**, *27*, 115009, DOI: 10.1088/1361-6595/aadb60.

(42) Silva, T.; Grofulović, M.; Klarenaar, B. L. M.; Morillo-Candas, A. S.; Guaitella, O.; Engeln, R.; Pintassilgo, C. D.; Guerra, V. Kinetic study of low-temperature CO_2 plasmas under non-equilibrium conditions. I. Relaxation of vibrational energy. *Plasma Sources Sci. Technol.* **2018**, *27*, 015019, DOI: 10.1088/1361-6595/aaa56a.

(43) Silva, T.; Grofulović, M.; Terraz, L.; Pintassilgo, C. D.; Guerra, V. Modelling the input and relaxation of vibrational energy in CO_2 plasmas. *J. Phys. D* **2018**, *51*, 464001, DOI: 10.1088/1361-6463/aadbd7.

(44) Terraz, L. In *ICPIG Proceedings*, ed. by Alves, L. L.; Tejero-del-Caz, A., 2017.

(45) Morillo-Candás, A. S. Investigation of fundamental mechanisms of CO_2 plasmas, English, Ph.D. Thesis, Ecole Polytechnique-Université Paris-Saclay, 2020.

(46) Terraz, L. In *ESCAMPIG Proceedings*, ed. by Pintassilgo, C. D., 2018.

(47) Terraz, L. In *PREMiERE workshop Proceedings*, ed. by Guerra, V., 2018.

(48) Terraz, L. In *CESPC Proceedings*, ed. by Mozetič, M., 2019.

(49) Alves, L. L. The LisbOn KInetics - LoKI https://nprime.tecnico.ulisboa.pt/loki.

(50) Guerra, V.; Loureiro, J. Electron and heavy particle kinetics in a low-pressure nitrogen glow discharge. *Plasma Sources Sci. Technol.* **1997**, *6*, 361–372.

(51) Guerra, V. Kinetic study of glow discharges in molecular gases: application to the N_2-O_2 mixture (in Portuguese) Aplicação a Mistura N_2-O_2, Ph.D. Thesis, Universidade Técnica de Lisboa, Portugal, 1998.

(52) Billing, G. D.; Fisher, E. R. VV and VT rate coefficients in N_2 by a quantum-classical model. *J. Chem. Phys.* **1979**, *43*, 395–401, DOI: https://doi.org/10.1016/0301-0104(79)85207-6.

(53) Blauer, J. A.; Nickerson, G. R. A survey of vibrational ralaxation rate data for processes important to CO_2-N_2-H_2O infrared plume radiation. *Ultrasystems, incorporated* **1973**, DOI: 10.2514/6.1974-536.

(54) Smith, N. S.; Hassan, H. A. Power calculations for high-flow CO electric discharge laser systems. *AIAA J.* **1976**, *14*, 374–386, DOI: 10.2514/3.61373.

(55) Plönjes, E.; Palm, P.; Lee, W.; Chidley, M. D.; Adamovich, I. V.; Lempert, W. R.; W Rich, J. W. Vibrational energy storage in high pressure mixtures of diatomic molecules. *J. Chem. Phys.* **2000**, *260*, 353–366, DOI: 10.1016/S0301-0104(00)00257-3.

(56) Kozák, T.; Bogaerts, A. Splitting of CO_2 by vibrational excitation in non-equilibrium plasmas: a reaction kinetics model. *Plasma Sources Sci. Technol.* **2014**, *23*, 045004, DOI: 10.1088/0963-0252/23/4/045004.

(57) Capitelli, M.; Ferreira, C. M.; Gordiets, B. F.; Osipov, A. I., *Plasma Kinetics in Atmospheric Gases*; Springer Series on Atomic, Optical, and Plasma Physics, Vol. 31; Springer Berlin Heidelberg: Berlin, Heidelberg, 2000, DOI: 10.1007/978-3-662-04158-1.

(58) Cacciatore, M.; Kurnosov, A.; Napartovich, A. Vibrational energy transfer in N(2)-N(2) collisions: A new semiclassical study. *J. Chem. Phys.* **2005**, *123*, 174315, DOI: 10.1063/1.2101445.

(59) Kurnosov, A.; Napartovich, A.; Shnyrev, S.; Cacciatore, M. Vibrational Energy Exchanges in Nitrogen: Application of New Rate Constants for Kinetic Modeling. *J. Phys. Chem. A* **2007**, *111*, 7057–65, DOI: 10.1021/jp071657a.

(60) Kurnosov, A.; Napartovich, A.; Shnyrev, S.; Cacciatore, M. A database for V–V state-to-state rate constants in N_2–N_2 and N_2–CO_2 collisions in a wide temperature range: dynamical calculations and analytical approximations. *Plasma Sources Sci. Technol.* **2010**, *19*, 045015, DOI: 10.1088/0963-0252/19/4/045015.

(61) Lopez-Puertas, M.; Taylor, F. W., *Non-LTE radiative transfer in the atmosphere*; World Scientific: 2001; Vol. 3.

(62) Guerra, V.; Tejero-del-Caz, A.; Pintassilgo, C. D.; Alves, L. L. Modelling N_2-O_2 plasmas: volume and surface kinetics. *Plasma Sources Sci. Technol.* **2019**, *28*, 073001, DOI: 10.1088/1361-6595/ab252c.

(63) Kutasi, K.; Guerra, V.; Sá, P. Theoretical insight into Ar–O_2 surface-wave microwave discharges. *J. Phys. D* **2010**, *43*, 175201, DOI: 10.1088/0022-3727/43/17/175201.

(64) Hirschfelder, J. O.; Curtiss, C. F.; Bird, R. B. Molecular Theory of Gases and Liquids. *Science* **1954**, *120*, 1097–1097, DOI: 10.1126/science.120.3131.1097.

(65) Marinov, D.; Lopatik, D.; Guaitella, O.; Hübner, M.; Ionikh, Y.; Röpcke, J.; Rousseau, A. Surface vibrational relaxation of N_2 studied by CO_2 titration with time-resolved quantum cascade laser absorption spectroscopy. *J. Phys. D* **2012**, *45*, 175201, DOI: 10.1088/0022-3727/45/17/175201.

(66) Black, G.; Wise, H.; Schechter, S.; Sharpless, R. L. Measurements of vibrationally excited molecules by Raman scattering.II. Surface deactivation of vibrationally excited N_2. *J. Chem. Phys.* **1974**, *60*, 3526–3536, DOI: 10.1063/1.1681570.

(67) Guerra, V.; Loureiro, J. Kinetic model of a low-pressure microwave discharge in O_2-H_2 including the effects of O^- ions on the characteristics for plasma maintenance. *Plasma Sources Scie. Technol.* **1999**, *8*, 110–124, DOI: 10.1088/0963-0252/8/1/014.

(68) Tejero-del-Caz, A.; Guerra, V.; Gonçalves, D.; Lino da Silva, M.; Marques, L.; Pinhão, N.; Pintassilgo, C.; Alves, L. The LisbOn KInetics Boltzmann solver. *Plasma Sources Sci. Technol.* **2019**, *28*, 043001, DOI: 10.1088/1361-6595/ab0537.

(69) Tejero-Del-Caz, A.; Alves, L.; Guerra, V.; Goncalves, D.; Lino da Silva, M.; Pinhao, N.; Marques, L.; Pintassilgo, C. D. In *APS Annual Gaseous Electronics Meeting Abstracts*, 2018, GT1.071.

(70) Annušová, A.; Marinov, D.; Booth, J.-P.; Sirse, N.; da Silva, M. L.; Lopez, B.; Guerra, V. Kinetics of highly vibrationally excited O_2(X) molecules in inductively-coupled oxygen plasmas. *Plasma Sources Sci. Technol.* **2018**, *27*, 045006, DOI: 10.1088/1361-6595/aab47d.

(71) Obrusník, A.; Bílek, P.; Hoder, T.; Šimek, M.; Bonaventura, Z. Electric field determination in air plasmas from intensity ratio of nitrogen spectral bands: I. Sensitivity analysis and uncertainty quantification of dominant processes. *Plasma Sources Sci. Technol.* **2018**, *27*, 085013, DOI: 10.1088/1361-6595/aad663.

(72) Offenberger, A. A.; Rose, D. J. Roles of Helium and Nitrogen in CO_2 Laser Excitation. *J. Appl. Phys.* **1970**, *41*, 3908–3909, DOI: 10.1063/1.1659530.

(73) Cenian, A.; Chernukho, A.; Borodin, V.; Śliwiński, G. Modeling of Plasma-Chemical Reactions in Gas Mixture of CO_2 Lasers I. Gas Decomposition in Pure CO_2 Glow Discharge. *CoPP* **1994**, *34*, 25–37, DOI: 10.1002/ctpp.2150340105.

(74) Cenian, A.; Chernukho, A.; Borodin, V. Modeling of Plasma-Chemical Reactions in Gas Mixture of CO_2 lasers. II. Theoretical Model and its Verification. *CoPP* **1995**, *35*, 273–296, DOI: 10.1002/ctpp.2150350309.

(75) Heijkers, S.; Snoeckx, R.; Kozák, T.; Silva, T.; Godfroid, T.; Britun, N.; Snyders, R.; Bogaerts, A. CO_2 Conversion in a Microwave Plasma Reactor in the Presence of N_2: Elucidating the Role of Vibrational Levels. *J. Phys. Chem. C* **2015**, *119*, 12815–12828, DOI: 10.1021/acs.jpcc.5b01466.

(76) Snoeckx, R.; Heijkers, S.; Van Wesenbeeck, K.; Lenaerts, S.; Bogaerts, A. CO_2 conversion in a dielectric barrier discharge plasma: N_2 in the mix as a helping hand or problematic impurity? *Energy Environ. Sci.* **2016**, *9*, 999–1011, DOI: 10.1039/C5EE03304G.

(77) Ogloblina, P.; Tejero-del-Caz, A.; Guerra, V.; Alves, L. L. Electron impact cross sections for carbon monoxide and their importance in the electron kinetics of CO_2-CO mixtures. *Plasma Sources Sci. Technol* **2020**, *29*, 015002, DOI: 10.1088/1361-6595/ab4e72.

(78) Berthelot, A.; Bogaerts, A. Modeling of plasma-based CO_2 conversion: lumping of the vibrational levels. *Plasma Sources Sci. Technol* **2016**, *25*, 045022, DOI: 10.1088/0963-0252/25/4/045022.

(79) Diomede, P.; van de Sanden, M. C. M.; Longo, S. Vibrational Kinetics in Plasma as a Functional Problem: A Flux-Matching Approach. *J. Phys. Chem. A* **2018**, *22*, 7918–1923, DOI: 10.1021/acs.jpca.8b05623.

(80) Viegas, P.; van de Sanden, M. C. M.; Longo, S.; Dioemede, P. Validation of the Fokker-Planck approach to vibrational kinetics in CO_2 plasma. *J. Phys. Chem. C* **2019**, *123*, 22823–22831, DOI: 10.1021/acs.jpcc.9b06576.

(81) Levko, D.; Pachuilo, M.; Raja, L. L. Particle-in-cell modeling of streamer branching in CO_2 gas. *J. Phys. D* **2017**, *50*, 354004, DOI: 10.1088/1361-6463/aa7e6c.

(82) Armenise, I.; Kustova, E. V. State-to-state models for CO_2 molecules: From the theory to an application to hypersonic boundary layers. *Chem. Phys.* **2013**, *415*, 269–281, DOI: 10.1016/j.chemphys.2013.01.034.

(83) Armenise, I.; Kustova, E. V. Mechanisms of Coupled Vibrational Relaxation and Dissociation in Carbon Dioxide. *J. Phys. Chem. A* **2018**, *122*, 5107–5120, DOI: 10.1021/acs.jpca.8b03266.

(84) Annaloro, J.; Bultel, A. Vibrational and electronic collisional-radiative model in CO_2-N_2-Ar mixtures for Mars entry problems. *Phys. Plasmas.* **2019**, *26*, 103505, DOI: 10.1063/1.5114792.

(85) Aerts, R.; Martens, T.; Bogaerts, A. Influence of Vibrational States on CO_2 Splitting by Dielectric Barrier Discharges. *J. Phys. Chem. C* **2012**, *116*, 23257–23273, DOI: 10.1021/jp307525t.

(86) Ponduri, S.; Becker, M. M.; Welzel, S.; van de Sanden, M. C. M.; Loffhagen, D.; Engeln, R. Fluid modelling of CO_2 dissociation in a dielectric barrier discharge. *J. Appl. Phys* **2016**, *119*, 093301, DOI: 10.1063/1.4941530.

(87) Mei, D.; He, Y.-L.; Liu, S.; Yan, J.; Tu, X. Optimization of CO_2 Conversion in a Cylindrical Dielectric Barrier Discharge Reactor Using Design of Experiments. *Plasma Processes and Polymers* **2016**, *13*, 544–556, DOI: 10.1002/ppap.201500159.

(88) Bogaerts, A.; Wang, W.; Berthelot, A.; Guerra, V. Modeling plasma-based CO_2 conversion: crucial role of the dissociation cross section. *Plasma Sources Sci. Technol.* **2016**, *25*, 055016, DOI: 10.1088/0963-0252/25/5/055016.

(89) Capitelli, M.; Colonna, G.; D'Ammando, G.; Pietanza, L. D. Self-consistent time dependent vibrational and free electron kinetics for CO_2 dissociation and ionization in cold plasmas. *Plasma Sources Sci. Technol* **2017**, *26*, 055009, DOI: 10.1088/1361-6595/aa6427.

(90) Koelman, P.; Heijkers, S.; Tadayon Mousavi, S.; Graef, W.; Mihailova, D.; Kozak, T.; Bogaerts, A.; van Dijk, J. A Comprehensive Chemical Model for the Splitting of CO_2 in Non-Equilibrium Plasmas. *Plasma Process. Polym.* **2017**, *14*, 1600155, DOI: 10.1002/ppap.201600155.

(91) Kozák, T.; Bogaerts, A. Evaluation of the energy efficiency of CO_2 conversion in microwave discharges using a reaction kinetics model. *Plasma Sources Sci. Technol* **2014**, *24*, 015024, DOI: 10.1088/0963-0252/24/1/015024.

(92) De la Fuente, J. F.; Moreno, S. H.; Stankiewicz, A. I.; Stefanidis, G. D. A new methodology for the reduction of vibrational kinetics in non-equilibrium microwave plasma: application to CO_2 dissociation. *React. Chem. Eng.* **2016**, *1*, 540–554, DOI: 10.1039/C6RE00044D.

(93) Berthelot, A.; Bogaerts, A. Modeling of CO_2 Splitting in a Microwave Plasma: How to Improve the Conversion and Energy Efficiency. *J. Phys. Chem. C* **2017**, *121*, 8236–8251, DOI: 10.1021/acs.jpcc.6b12840.

(94) Chen, G.; Britun, N.; Godfroid, T.; Georgieva, V.; Snyders, R.; Delplancke-Ogletree, M.-P. An overview of CO_2 conversion in a microwave discharge: the role of plasma-catalysis. *J. Phys. D* **2017**, *50*, 084001, DOI: 10.1088/1361-6463/aa5616.

(95) Cheng, J.-L.; Wang, H.-X.; Sun, S.-R. Analysis of Dissociation Mechanism of CO_2 in a Micro-Hollow Cathode Discharge. *Chin. Phys. Lett* **2016**, *33*, 108201, DOI: 10.1088/0256-307x/33/10/108201.

(96) Wang, W.; Mei, D.; Tu, X.; Bogaerts, A. Gliding arc plasma for CO_2 conversion: Better insights by a combined experimental and modelling approach. *Chem. Eng. Sci.* **2017**, *330*, 11–25, DOI: 10.1016/j.cej.2017.07.133.

(97) Moss, M. S.; Yanallah, K.; Allen, R. W. K.; Pontiga, F. An investigation of CO_2 splitting using nanosecond pulsed corona discharge: effect of argon addition on CO_2 conversion and energy efficiency. *Plasma Sources Sci. Technol* **2017**, *26*, 035009, DOI: 10.1088/1361-6595/aa5b1d.

(98) Pietanza, L. D.; Colonna, G.; D'Ammando, G.; Laricchiuta, A.; Capitelli, M. Vibrational excitation and dissociation mechanisms of CO_2 under non-equilibrium discharge and post-discharge conditions. *Plasma Sources Sci. Technol* **2015**, *24*, 042002, DOI: 10.1088/0963-0252/24/4/042002.

(99) Pietanza, L. D.; Colonna, G.; D'Ammando, G.; Laricchiuta, A.; Capitelli, M. Electron energy distribution functions and fractional power transfer in "cold" and excited CO_2 discharge and post discharge conditions. *Phys. Plasmas* **2016**, *23*, 013515, DOI: 10.1063/1.4940782.

(100) Pietanza, L.; Colonna, G.; D'Ammando, G.; Laricchiuta, A.; Capitelli, M. Non equilibrium vibrational assisted dissociation and ionization mechanisms in cold CO_2 plasmas. *Chem. Phys.* **2016**, *468*, 44–52, DOI: 10.1016/j.chemphys.2016.01.007.

(101) Boffard, J. B.; Jung, R. O.; Lin, C. C.; Wendt, A. E. Optical emission measurements of electron energy distributions in low-pressure argon inductively coupled plasmas. *Plasma Sources Sci. Technol.* **2010**, *19*, 065001, DOI: 10.1088/0963-0252/19/6/065001.

(102) Sugai, H.; Ghanashev, I.; Hosokawa, M.; Mizuno, K.; Nakamura, K.; Toyoda, H.; Yamauchi, K. Electron energy distribution functions and the influence on fluorocarbon plasma chemistry. *Plasma Sources Sci. Technol.* **2001**, *10*, 378–385, DOI: 10.1088/0963-0252/10/2/327.

(103) Colonna, G.; Laporta, V.; Celiberto, R.; Capitelli, M.; Tennyson, J. Non-equilibrium vibrational and electron energy distributions functions in atmospheric nitrogen ns pulsed discharges and μs post-discharges: the role of electron molecule vibrational excitation scaling-laws. *Plasma Sources Sci. Technol.* **2015**, *24*, 035004, DOI: 10.1088/0963-0252/24/3/035004.

(104) Silva, T.; Grofulović, M.; Terraz, L.; Pintassilgo, C.; Guerra, V. Dynamics of gas heating in the afterglow of pulsed CO_2 and CO_2–N_2 glow discharges at low pressure. *Plasma Chem. Plasma Process.* **2020**, DOI: 10.1007/s11090-020-10061-7.

(105) Lee, C.; Lieberman, M. A. Global model of Ar, O_2, Cl_2, and Ar/O_2 high-density plasma discharges. *J. Vac. Sci. Technol. 1* **1995**, *13*, 368–380, DOI: https://doi.org/10.1116/1.579366.

(106) Chabert, P. An expression for the h_l factor in low-pressure electronegative plasma discharges. *Plasma Sources Sci. Technol* **2016**, *25*, 025010, DOI: 10.1088/0963-0252/25/2/025010.

(107) Griffiths, P.; Haseth, J. Fourier Transform Infrared Spectrometry, Second Edition. **2006**, DOI: 10.1002/9780470106310.ch9.

(108) Klarenaar, B. L. M.; Brehmer, F.; Welzel, S.; van der Meiden, H. J.; van de Sanden, M. C. M.; Engeln, R. Note: Rotational Raman scattering on CO2 plasma using a volume Bragg grating as a notch filter. *Rev. Sci. Instrum* **2015**, *86*, 046106, DOI: 10.1063/1.4918730.

(109) Klarenaar, B. L. M.; Grofulović, M.; Morillo-Candas, A. S.; van den Bekerom, D. C. M.; Damen, M. A.; van de Sanden, M. C. M.; Guaitella, O.; Engeln, R. A rotational Raman study under non-thermal conditions in a pulsed CO_2 glow discharge. *Plasma Sources Sci. and Technol.* **2018**, *27*, 045009, DOI: 10.1088/1361-6595/aabab6.

(110) Klarenaar, B.; Morillo-Candas, A.; Grofulović, M.; Sanden, M.; Engeln, R.; Guaitella, O. Excitation and relaxation of the asymmetric stretch mode of CO_2 in a pulsed glow discharge. *Plasma Sources Sci. Technol.* **2019**, *28*, 035011, DOI: 10.1088/1361-6595/aada5e.

(111) Röpcke, J.; Davies, P. B.; Lang, N.; Rousseau, A.; Welzel, S. Applications of quantum cascade lasers in plasma diagnostics: a review. *J. Phys. D.* **2012**, *45*, 423001, DOI: 10.1088/0022-3727/45/42/423001.

(112) Klarenaar, B. L. M.; Engeln, R.; van den Bekerom, D. C. M.; van de Sanden, M. C. M.; Morillo-Candas, A. S.; Guaitella, O. Time evolution of vibrational temperatures in a CO_2 glow discharge measured with infrared absorption spectroscopy Experimental methods. *Plasma Sources Sci. Technol.* **2017**, *26*, 1–11.

(113) Gordon, I. et al. The HITRAN2016 molecular spectroscopic database. *J. Quant. Spectrosc. Radiat. Transf.* **2017**, *203*, 3–69, DOI: https://doi.org/10.1016/j.jqsrt.2017.06.038.

(114) Rothman, L.; Gordon, I.; Barber, R.; Dothe, H.; Gamache, R.; Goldman, A.; Perevalov, V.; Tashkun, S.; Tennyson, J. HITEMP, the high-temperature molecular spectroscopic database. *Journal of Quantitative Spectroscopy and Radiative Transfer* **2010**, *111*, XVIth Symposium on High Resolution Molecular Spectroscopy (HighRus-2009), 2139–2150, DOI: https://doi.org/10.1016/j.jqsrt.2010.05.001.

(115) Grofulović, M.; Klarenaar, B. L. M.; Guaitella, O.; Guerra, V.; Engeln, R. A rotational Raman study under non-thermal conditions in pulsed CO_2-N_2 and CO_2-O_2 glow discharges. *Plasma Sources Sci. Technol.* **2019**, *28*, 045014, DOI: 10.1088/1361-6595/ab1240.

(116) Silva, A. F. S.; Morillo-Candas, A. S.; van de Steeg, A.; Guaitella, O.; Guerra, V.; van Rooij, G. In *ISPC24 (24th International Symposium on Plasma Chemistry)*, ed. by Colombo, V.; Favia, P.; Gherardi, M., 2019.

(117) Sierra, R. A.; Brooks, H. L.; Nygaard, K. J. Electron drift velocity in N_2, CO_2, and (N_2+CO_2) laser mixtures. *Appl. Phys. Lett.* **1979**, *35*, 764–765, DOI: 10.1063/1.90962.

(118) The LXCat team LXCat https://fr.lxcat.net/home/.

(119) Loureiro, J.; Ferreira, C. M. Coupled electron energy and vibrational distribution functions in stationary N_2 discharges. *J. Phys. D* **1986**, *19*, 17–35, DOI: 10.1088/0022-3727/19/1/007.

(120) Millikan, R. C.; White, D. R. Vibrational Energy Exchange between N_2 and CO. The Vibrational Relaxation of Nitrogen. *J. Chem. Phys.* **1963**, *39*, 98–101, DOI: 10.1063/1.1734039.

(121) Capitelli, M.; Gorse, C.; Billing, G. D. V-V pumping up in non-equilibrium nitrogen: effects on the dissociation rate. *J. Chem. Phys.* **1980**, *52*, 299–304, DOI: https://doi.org/10.1016/0301-0104(80)85233-5.

(122) Schwartz, R. N.; Slawsky, Z. I.; Herzfeld, K. F. Calculation of Vibrational Relaxation Times in Gases. *J. Chem. Phys.* **1952**, *20*, 1591–1599, DOI: 10.1063/1.1700221.

(123) Schwartz, R. N.; Herzfeld, K. F. Vibrational Relaxation Times in Gases (Three-Dimensional Treatment). *J. Chem. Phys.* **1954**, *22*, 767–773, DOI: 10.1063/1.1740190.

(124) Gordiets, B. F.; Ferreira, C. M.; Guerra, V. L.; Loureiro, J. M. A. H.; Nahorny, J.; Pagnon, D.; Touzeau, M.; Vialle, M. Kinetic model of a low-pressure N_2-O_2 flowing glow discharge. *IEEE Trans. Plasma Sci.* **1995**, *23*, 750–768, DOI: 10.1109/27.467998.

(125) Sharma, R. D.; Brau, C. A. Energy Transfer in Near-Resonant Molecular Collisions due to Long-Range Forces with Application to Transfer of Vibrational Energy from v_3 Mode of CO_2 to N_2. *J. Chem. Phys.* **1969**, *50*, 924–930, DOI: 10.1063/1.1671145.

(126) Lino da Silva, M.; Guerra, V.; Loureiro, J. State-resolved dissociation rates for extremely nonequilibrium atmospheric entries. *J. Thermophys. Heat Tr.* **2007**, *21*, 40–49.

(127) Huber, P. W.; Kantrowitz, A. Heat-Capacity Lag Measurements in Various Gases. *J. Chem. Phys.* **1947**, *15*, 275–284, DOI: 10.1063/1.1746496.

(128) Lukasik, S. J.; Young, J. E. Vibrational Relaxation Times in Nitrogen. *J. Chem. Phys.* **1957**, *27*, 1149–1155, DOI: 10.1063/1.1743947.

(129) Henderson, M. C. Vibrational Relaxation in Nitrogen and Other Gases. *J. Acoust. Soc. Am.* **1962**, *34*, 349–350, DOI: 10.1121/1.1928125.

(130) Parker, J. G. Comparison of Experimental and Theoretical Vibrational Relaxation Times for Diatomic Gases. *J. Chem. Phys.* **1964**, *41*, 1600–1609, DOI: 10.1063/1.1726130.

(131) Ahn, T.; Adamovich, I. V.; Lempert, W. R. Determination of nitrogen V-V transfer rates by stimulated Raman pumping. *J. Chem. Phys.* **2004**, *298*, 233–240.

(132) Guerra, V.; Loureiro, J. Non-equilibrium coupled kinetics in stationary N_2-O_2 discharges. *J. Phys. D.* **1995**, *27*, 1903–1918.

(133) Alves, L. L.; Marques, L.; Pintassilgo, C. D.; Wattieaux, G.; Es-sebbar, E.; Berndt, J.; Kovacević, E.; Carrasco, N.; Boufendi, L.; Cernogora, G. Capacitively coupled radio-frequency discharges in nitrogen at low pressures. *Plasma Sources Sci. Technol.* **2012**, *21*, 045008, DOI: 10.1088/0963-0252/21/4/045008.

(134) Cheng, T. S.; Wu, C. Y.; Chen, C. P.; Li, Y. H.; Chao, Y. C.; Yuan, T.; Leu, T. S. Detailed measurement and assessment of laminar hydrogen jet diffusion flames. *Combust. Flame* **2006**, *146*, 268–282, DOI: https://doi.org/10.1016/j.combustflame.2006.03.005.

(135) Yaney, P.; W. Parish, J. Studies of Surface Deactivation of Vibrationally-Excited Homonuclear Molecules in Gaseous Discharge Media Using Coherent Anti-Stokes Raman Spectroscopy (CARS). *Technical report, Dayton Univ. Oh.* **1999**, *30*, 61.

(136) Morillo-Candas, A.; Drag, C.; Booth, J.-P.; Dias, T. C.; Guerra, V.; Guaitella, O. Oxygen atom kinetics in CO_2 plasmas ignited in a DC glow discharge. *Plasma Sources Sci. Technol.* **2019**, *28*, 075010, DOI: 10.1088/1361-6595/ab2b84.

(137) Lowke, J. J.; Phelps, A. V.; Irwin, B. W. Predicted electron transport coefficients and operating characteristics of CO_2-N_2-He laser mixtures. *J. Appl. Phys* **1973**, *44*, 4664–4671, DOI: 10.1063/1.1662017.

(138) Pintassilgo, C. D.; Guerra, V.; Guaitella, O.; Rousseau, A. Study of gas heating mechanisms in millisecond pulsed discharges and afterglows in air at low pressures. *Plasma Sources Sci. Technol.* **2014**, *23*, 025006, DOI: 10.1088/0963-0252/23/2/025006.

(139) Togai, K.; Tsolas, N.; Yetter, R. A. Kinetic modeling and sensitivity analysis of plasma-assisted oxidation in a H_2/O_2/Ar mixture. *Combust. Flame* **2016**, *164*, 239–249, DOI: 10.1016/j.combustflame.2015.11.020.

(140) Phenix, B. D.; Dinaro, J. L.; Tatang, M. A.; Tester, J. W.; Howard, J. B.; McRae, G. J. Incorporation of parametric uncertainty into complex kinetic mechanisms: Application to hydrogen oxidation in supercritical water. *Combus. Flame* **1998**, *112*, 132–146, DOI: 10.1016/S0010-2180(97)81762-2.

(141) Reagan, M. T.; Najm, H. N.; Ghanem, R. G.; Knio, O. M. Uncertainty quantification in reacting-flow simulations through non-intrusive spectral projection. *Combust. Flame* **2003**, *132*, 545–555, DOI: 10.1016/S0010-2180(02)00503-5.

(142) Zsély, I.; Zádor, J.; Turányi, T. Uncertainty analysis of updated hydrogen and carbon monoxide oxidation mechanisms. *Proc. Combust. Inst.* **2005**, *30*, 1273–1281, DOI: 10.1016/j.proci.2004.08.172.

(143) Warnatz, J. Resolution of gas phase and surface combustion chemistry into elementary reactions. *Proc. Combust. Inst.* **1992**, *24*, 553–579, DOI: 10.1016/S0082-0784(06)80070-6.

(144) Bromly, J. H.; Barnes, F. J.; Muris, S.; You, X.; Haynes, B. S. Kinetic and Thermodynamic Sensitivity Analysis of the NO-Sensitised Oxydation of Methane. *Combust. Sci. Technol* **1996**, 159–296, DOI: 10.1090/001022090608935532.

(145) Brown, M.; Smith, D.; Taylor, S. Influence of uncertainties in rate constants on computed burning velocities. *Combust. Flame* **1999**, *117*, DOI: 10.1016/S0010-2180(98)00117-5.

(146) Shin, H. H.; Yoon, W. S. Hydrocarbon Effects on the Promotion of Non-Thermal Plasma NO–NO_2 Conversion. *Plasma Chem. Plasma Process.* **2003**, *23*, 681–704, DOI: 10.1023/A:1025595318945.

(147) Peerenboom, K.; Parente, A.; Kozák, T.; Bogaerts, A.; Degrez, G. Dimension reduction of non-equilibrium plasma kinetic models using principal component analysis. *Plasma Sources Sci. Technol* **2015**, *24*, 025004, DOI: 10.1088/0963-0252/24/2/025004.

(148) Sun, S. R.; Wang, H. X.; Bogaerts, A. Chemistry reduction of complex CO_2 chemical kinetics: application to a gliding arc plasma. *Plasma Sources Sci. Technol* **2020**, *29*, 025012, DOI: 10.1088/1361-6595/ab540f.

(149) Markosyan, A.; Luque, A.; Gordillo-Vázquez, F.; Ebert, U. PumpKin: A tool to find principal pathways in plasma chemical models. *Comput. Phys. Commun.* **2014**, *185*, 2697–2702, DOI: 10.1016/j.cpc.2014.05.019.

(150) Foucher, M.; Marinov, D.; Carbone, E.; Chabert, P.; Booth, J.-P. Highly vibrationally excited O_2 molecules in low-pressure inductively-coupled plasmas detected by high sensitivity ultra-broad-band optical absorption spectroscopy. *Plasma Sources Sci. Technol.* **2015**, *24*, 042001, DOI: 10.1088/0963-0252/24/4/042001.

(151) Marinov, D.; Foucher, M.; Campbell, E.; Brouard, M.; Chabert, P.; Booth, J.-P. High sensitivity ultra-broad-band absorption spectroscopy of inductively coupled chlorine plasma. *Plasma Sources Sci. Technol.* **2016**, *25*, 035019, DOI: 10.1088/0963-0252/25/3/035019.

(152) Laporta, V.; Celiberto, R.; Tennyson, J. Resonant vibrational-excitation cross sections and rate constants for low-energy electron scattering by molecular oxygen. *Plasma Sources Sci. Technol.* **2013**, *22*, 025001, DOI: 10.1088/0963-0252/22/2/025001.

(153) Laporta, V.; Celiberto, R.; Tennyson, J. Dissociative electron attachment and electron-impact resonant dissociation of vibrationally excited O_2 molecules. *Phys. Rev. A* **2015**, *91*, 012701, DOI: 10.1103/PhysRevA.91.012701.

(154) Coche, P.; Guerra, V.; Alves, L. L. Microwave air plasmas in capillaries at low pressure I. Self-consistent modeling. *J. Phys. D* **2016**, *49* 235207, 235207, DOI: 10.1088/0022-3727/49/23/235207.

(155) Self, S. A.; Ewald, H. N. Static Theory of a Discharge Column at Intermediate Pressures. *Phys. Fluids.* **1966**, *9*, 2486–2492, DOI: 10.1063/1.1761642.

(156) Alves, L. L.; Bogaerts, A.; Guerra, V.; Turner, M. M. Foundations of modelling of nonequilibrium low-temperature plasmas. *Plasma Sources Science and Technology* **2018**, *27*, 023002, DOI: 10.1088/1361-6595/aaa86d.

(157) Silva, A. F. S. The role of Argon in CO_2 dissociation, Master thesis, Instituto Superior Técnico, 2018.

(158) Saltelli, A.; Sobol, I. M. About the use of rank transformation in sensitivity analysis of model output. *Reliability Engineering and System Safety* **1995**, *50*, 225–239, DOI: https://doi.org/10.1016/0951-8320(95)00099-2.

(159) Saltelli, A.; Tarantola, S.; Chan, K. P.-S. A Quantitative Model-Independent Method for Global Sensitivity Analysis of Model Output. *Technometrics* **1999**, *41*, 39–56, DOI: 10.1080/00401706.1999.10485594.

(160) Gans, T. In *PREMiERE Workshop, Ericeira, Portugal*, ed. by Guerra, V., 2018.

(161) Alves, L. L.; Coche, P.; Ridenti, M. A.; Guerra, V. Electron scattering cross sections for the modelling of oxygen-containing plasmas. **2016**, *70*, DOI: https://doi.org/10.1140/epjd/e2016-70102-1.

(162) Esposito, F.; Armenise, I.; Capitta, G.; Capitelli, M. O–O_2 state-to-state vibrational relaxation and dissociation rates based on quasiclassical calculations. *Chem. Phys.* **2008**, *351*, 91–98, DOI: https://doi.org/10.1016/j.chemphys.2008.04.004.

Appendix A

Reaction rate coefficients for CO_2-N_2 DC glow discharge modeling

The coefficients used to fit Vibration-Translation (V-T) and Vibration-Vibration (V-V) rate coefficients versus the gas temperature T_g (in K) are given as tables. Together with the information from chapters 2 and 4, it constitutes an exhaustive database of the reaction rate coefficients used in the simulations described in chapter 4. The rate units are in $cm^3.s^{-1}$.

A.1 Vibration-Translation (V-T) rate coefficients

A.1.1 V-T relaxation $N_2(v)$ + N_2

Expressions:

$$k(v,T_g) = f_{low}(T_g)A_{low}(v)\exp^{B_{low}(v)T_g^{-1/3}+C_{low}(v)T_g^{-2/3}} + f_{high}(T_g)A_{high}(v)\exp^{B_{high}(v)T_g^{-1/3}+C_{high}(v)T_g^{-2/3}}$$

$$f_{low}(T_g) = \frac{1}{2}\left(1-\tanh(\frac{T_g-1000}{150})\right)$$

$$f_{high}(T_g) = \frac{1}{2}\left(1+\tanh(\frac{T_g-1000}{150})\right)$$

Table A.1 for A_{low}, B_{low}, C_{low}, A_{high}, B_{high} and C_{high}:

Reaction	A_{low}	B_{low}	C_{low}	A_{high}	B_{high}	C_{high}
$N_2(1)+N_2 \rightarrow N_2(0)+N_2$	4.22E+02	-6.19E+02	1.70E+03	9.24E-08	-1.72E+02	-6.06E+02
$N_2(2)+N_2 \rightarrow N_2(1)+N_2$	1.96E+02	-5.91E+02	1.58E+03	1.08E-07	-1.61E+02	-6.36E+02
$N_2(3)+N_2 \rightarrow N_2(2)+N_2$	7.09E+01	-5.64E+02	1.47E+03	1.01E-07	-1.52E+02	-6.58E+02
$N_2(4)+N_2 \rightarrow N_2(3)+N_2$	2.68E+01	-5.39E+02	1.37E+03	8.89E-08	-1.44E+02	-6.73E+02
$N_2(5)+N_2 \rightarrow N_2(4)+N_2$	1.13E+01	-5.18E+02	1.29E+03	7.69E-08	-1.37E+02	-6.82E+02
$N_2(6)+N_2 \rightarrow N_2(5)+N_2$	5.29E+00	-4.99E+02	1.22E+03	6.69E-08	-1.31E+02	-6.86E+02
$N_2(7)+N_2 \rightarrow N_2(6)+N_2$	2.72E+00	-4.82E+02	1.15E+03	5.91E-08	-1.26E+02	-6.83E+02
$N_2(8)+N_2 \rightarrow N_2(7)+N_2$	1.51E+00	-4.67E+02	1.09E+03	5.34E-08	-1.22E+02	-6.75E+02
$N_2(9)+N_2 \rightarrow N_2(8)+N_2$	9.03E-01	-4.54E+02	1.04E+03	4.96E-08	-1.19E+02	-6.61E+02
$N_2(10)+N_2 \rightarrow N_2(9)+N_2$	5.69E-01	-4.41E+02	9.95E+02	4.74E-08	-1.17E+02	-6.41E+02
$N_2(11)+N_2 \rightarrow N_2(10)+N_2$	3.76E-01	-4.30E+02	9.53E+02	4.68E-08	-1.16E+02	-6.14E+02
$N_2(12)+N_2 \rightarrow N_2(11)+N_2$	2.59E-01	-4.19E+02	9.14E+02	4.78E-08	-1.16E+02	-5.82E+02
$N_2(13)+N_2 \rightarrow N_2(12)+N_2$	1.85E-01	-4.09E+02	8.79E+02	5.08E-08	-1.18E+02	-5.42E+02
$N_2(14)+N_2 \rightarrow N_2(13)+N_2$	1.41E-01	-4.01E+02	8.48E+02	5.50E-08	-1.19E+02	-5.00E+02
$N_2(15)+N_2 \rightarrow N_2(14)+N_2$	1.15E-01	-3.93E+02	8.22E+02	6.00E-08	-1.21E+02	-4.56E+02
$N_2(16)+N_2 \rightarrow N_2(15)+N_2$	9.96E-02	-3.86E+02	8.00E+02	6.58E-08	-1.24E+02	-4.12E+02
$N_2(17)+N_2 \rightarrow N_2(16)+N_2$	9.09E-02	-3.81E+02	7.82E+02	7.25E-08	-1.26E+02	-3.66E+02
$N_2(18)+N_2 \rightarrow N_2(17)+N_2$	8.67E-02	-3.76E+02	7.66E+02	8.04E-08	-1.28E+02	-3.20E+02
$N_2(19)+N_2 \rightarrow N_2(18)+N_2$	8.55E-02	-3.71E+02	7.53E+02	8.96E-08	-1.31E+02	-2.74E+02
$N_2(20)+N_2 \rightarrow N_2(19)+N_2$	8.67E-02	-3.68E+02	7.42E+02	1.00E-07	-1.34E+02	-2.26E+02

Table A.1: N_2 quenched by N_2

A.1.2 V-T relaxation $N_2(v)$ + CO_2

Expressions:

$$k(v,T_g) = f_{low}(T_g)A_{low}(v)\exp^{B_{low}(v)T_g^{-1/3}+C_{low}(v)T_g^{-2/3}} + f_{high}(T_g)A_{high}(v)\exp^{B_{high}(v)T_g^{-1/3}+C_{high}(v)T_g^{-2/3}}$$

$$f_{low}(T_g) = \frac{1}{2}\left(1-\tanh(\frac{T_g-1000}{150})\right)$$

$$f_{high}(T_g) = \frac{1}{2}\left(1+\tanh(\frac{T_g-1000}{150})\right)$$

Table A.2 for A_{low}, B_{low}, C_{low}, A_{high}, B_{high} and C_{high}:

Reaction	A_{low}	B_{low}	C_{low}	A_{high}	B_{high}	C_{high}
$N_2(1)+CO_2 \rightarrow N_2(0)+CO_2$	4.87E+02	-6.36E+02	1.69E+03	3.04E-07	-2.15E+02	-4.53E+02
$N_2(2)+CO_2 \rightarrow N_2(1)+CO_2$	2.37E+02	-6.08E+02	1.57E+03	3.49E-07	-2.03E+02	-4.88E+02
$N_2(3)+CO_2 \rightarrow N_2(2)+CO_2$	9.05E+01	-5.81E+02	1.47E+03	3.18E-07	-1.93E+02	-5.17E+02
$N_2(4)+CO_2 \rightarrow N_2(3)+CO_2$	3.62E+01	-5.58E+02	1.37E+03	2.72E-07	-1.84E+02	-5.40E+02
$N_2(5)+CO_2 \rightarrow N_2(4)+CO_2$	1.62E+01	-5.37E+02	1.29E+03	2.28E-07	-1.76E+02	-5.57E+02
$N_2(6)+CO_2 \rightarrow N_2(5)+CO_2$	8.06E+00	-5.19E+02	1.22E+03	1.92E-07	-1.69E+02	-5.69E+02
$N_2(7)+CO_2 \rightarrow N_2(6)+CO_2$	4.43E+00	-5.03E+02	1.16E+03	1.64E-07	-1.62E+02	-5.75E+02
$N_2(8)+CO_2 \rightarrow N_2(7)+CO_2$	2.65E+00	-4.89E+02	1.10E+03	1.42E-07	-1.57E+02	-5.77E+02
$N_2(9)+CO_2 \rightarrow N_2(8)+CO_2$	1.71E+00	-4.76E+02	1.05E+03	1.26E-07	-1.52E+02	-5.73E+02
$N_2(10)+CO_2 \rightarrow N_2(9)+CO_2$	1.16E+00	-4.65E+02	1.01E+03	1.15E-07	-1.49E+02	-5.64E+02
$N_2(11)+CO_2 \rightarrow N_2(10)+CO_2$	8.37E-01	-4.54E+02	9.75E+02	1.09E-07	-1.46E+02	-5.50E+02
$N_2(12)+CO_2 \rightarrow N_2(11)+CO_2$	6.28E-01	-4.45E+02	9.41E+02	1.05E-07	-1.44E+02	-5.29E+02
$N_2(13)+CO_2 \rightarrow N_2(12)+CO_2$	4.90E-01	-4.36E+02	9.10E+02	1.06E-07	-1.44E+02	-5.03E+02
$N_2(14)+CO_2 \rightarrow N_2(13)+CO_2$	4.08E-01	-4.28E+02	8.84E+02	1.08E-07	-1.43E+02	-4.74E+02
$N_2(15)+CO_2 \rightarrow N_2(14)+CO_2$	3.62E-01	-4.22E+02	8.63E+02	1.11E-07	-1.43E+02	-4.44E+02
$N_2(16)+CO_2 \rightarrow N_2(15)+CO_2$	3.37E-01	-4.16E+02	8.44E+02	1.15E-07	-1.43E+02	-4.13E+02
$N_2(17)+CO_2 \rightarrow N_2(16)+CO_2$	3.25E-01	-4.11E+02	8.29E+02	1.19E-07	-1.44E+02	-3.82E+02
$N_2(18)+CO_2 \rightarrow N_2(17)+CO_2$	3.19E-01	-4.06E+02	8.15E+02	1.25E-07	-1.44E+02	-3.49E+02
$N_2(19)+CO_2 \rightarrow N_2(18)+CO_2$	3.13E-01	-4.02E+02	8.01E+02	1.31E-07	-1.45E+02	-3.15E+02
$N_2(20)+CO_2 \rightarrow N_2(19)+CO_2$	3.02E-01	-3.97E+02	7.87E+02	1.39E-07	-1.46E+02	-2.79E+02

Table A.2: N_2 quenched by CO_2

A.1.3 V-T relaxation $CO_2(v_1, v_2^{l2}, v_3)$ + N_2

Note: in table A.3 the vibration states of $CO_2(v_1, v_2, l_2, v_3, N)$ are written following Herzberg's notation, the last number N denoting the number of states grouped as one on our model. For example: $CO_2(1,0,0,0,2) = CO_2(1,0,0,0) + CO_2(0,2,0,0)$, while $CO_2(0,2,2,0)$ belongs to another group of only 1 state in this case.

Expression:

$$k(v, T_g) = \Phi \times 1.66 \times 10^{-24} \exp^{A(v)+B(v)T_g^{-1/3}+C(v)T_g^{-2/3}}$$

Table A.3 for A, B, C and Φ:

Reaction	A	B	C	Φ
$CO_2(0,0,0,1,1)+N_2 \rightarrow CO_2(0,1,1,0,1)+N_2$	5.39E+01	-4.07E+02	8.24E+02	3.00E-01
$CO_2(0,0,0,1,1)+N_2 \rightarrow CO_2(1,0,0,0,2)+N_2$	5.46E+01	-4.04E+02	1.10E+03	3.00E-01
$CO_2(0,0,0,1,1)+N_2 \rightarrow CO_2(1,1,1,0,2)+N_2$	4.36E+01	-2.52E+02	6.85E+02	3.00E-01
$CO_2(0,0,0,2,1)+N_2 \rightarrow CO_2(0,1,1,1,1)+N_2$	5.46E+01	-4.06E+02	8.29E+02	3.00E-01
$CO_2(0,0,0,2,1)+N_2 \rightarrow CO_2(1,0,0,1,2)+N_2$	5.53E+01	-4.04E+02	1.10E+03	3.00E-01
$CO_2(0,0,0,2,1)+N_2 \rightarrow CO_2(1,1,1,1,2)+N_2$	4.43E+01	-2.53E+02	6.83E+02	3.00E-01
$CO_2(0,0,0,3,1)+N_2 \rightarrow CO_2(0,1,1,2,1)+N_2$	5.50E+01	-4.05E+02	8.33E+02	3.00E-01
$CO_2(0,0,0,3,1)+N_2 \rightarrow CO_2(1,0,0,2,2)+N_2$	5.57E+01	-4.03E+02	1.10E+03	3.00E-01
$CO_2(0,0,0,3,1)+N_2 \rightarrow CO_2(1,1,1,2,2)+N_2$	4.47E+01	-2.53E+02	6.81E+02	3.00E-01
$CO_2(0,0,0,4,1)+N_2 \rightarrow CO_2(0,1,1,3,1)+N_2$	5.52E+01	-4.04E+02	8.38E+02	3.00E-01
$CO_2(0,0,0,4,1)+N_2 \rightarrow CO_2(1,0,0,3,2)+N_2$	5.60E+01	-4.03E+02	1.10E+03	3.00E-01

CO_2(0,0,0,4,1)+N_2 → CO_2(1,1,1,3,2)+N_2	4.50E+01	-2.54E+02	6.79E+02	3.00E-01
CO_2(0,0,0,5,1)+N_2 → CO_2(0,1,1,4,1)+N_2	5.55E+01	-4.03E+02	8.43E+02	3.00E-01
CO_2(0,0,0,5,1)+N_2 → CO_2(1,0,0,4,2)+N_2	5.62E+01	-4.02E+02	1.10E+03	3.00E-01
CO_2(0,0,0,5,1)+N_2 → CO_2(1,1,1,4,2)+N_2	4.52E+01	-2.54E+02	6.77E+02	3.00E-01
CO_2(0,1,1,0,1)+N_2 → CO_2(0,0,0,0,1)+N_2	3.83E+01	-1.77E+02	4.51E+02	7.00E-01
CO_2(0,1,1,1,1)+N_2 → CO_2(0,0,0,1,1)+N_2	3.83E+01	-1.77E+02	4.51E+02	7.00E-01
CO_2(0,1,1,1,1)+N_2 → CO_2(0,2,2,0,1)+N_2	5.39E+01	-4.07E+02	8.24E+02	3.00E-01
CO_2(0,1,1,1,1)+N_2 → CO_2(1,1,1,0,2)+N_2	5.46E+01	-4.04E+02	1.10E+03	3.00E-01
CO_2(0,1,1,1,1)+N_2 → CO_2(1,2,2,0,2)+N_2	4.36E+01	-2.52E+02	6.85E+02	3.00E-01
CO_2(0,1,1,1,1)+N_2 → CO_2(2,0,0,0,3)+N_2	4.36E+01	-2.52E+02	6.85E+02	3.00E-01
CO_2(0,1,1,2,1)+N_2 → CO_2(0,0,0,2,1)+N_2	3.83E+01	-1.77E+02	4.51E+02	7.00E-01
CO_2(0,1,1,2,1)+N_2 → CO_2(0,2,2,1,1)+N_2	5.46E+01	-4.06E+02	8.29E+02	3.00E-01
CO_2(0,1,1,2,1)+N_2 → CO_2(1,1,1,1,2)+N_2	5.53E+01	-4.04E+02	1.10E+03	3.00E-01
CO_2(0,1,1,2,1)+N_2 → CO_2(1,2,2,1,2)+N_2	4.43E+01	-2.53E+02	6.83E+02	3.00E-01
CO_2(0,1,1,2,1)+N_2 → CO_2(2,0,0,1,3)+N_2	4.43E+01	-2.53E+02	6.83E+02	3.00E-01
CO_2(0,1,1,3,1)+N_2 → CO_2(0,0,0,3,1)+N_2	3.83E+01	-1.77E+02	4.51E+02	7.00E-01
CO_2(0,1,1,3,1)+N_2 → CO_2(0,2,2,2,1)+N_2	5.50E+01	-4.05E+02	8.33E+02	3.00E-01
CO_2(0,1,1,3,1)+N_2 → CO_2(1,1,1,2,2)+N_2	5.57E+01	-4.03E+02	1.10E+03	3.00E-01
CO_2(0,1,1,3,1)+N_2 → CO_2(1,2,2,2,2)+N_2	4.47E+01	-2.53E+02	6.81E+02	3.00E-01
CO_2(0,1,1,3,1)+N_2 → CO_2(2,0,0,2,3)+N_2	4.47E+01	-2.53E+02	6.81E+02	3.00E-01
CO_2(0,1,1,4,1)+N_2 → CO_2(0,0,0,4,1)+N_2	3.83E+01	-1.77E+02	4.51E+02	7.00E-01
CO_2(0,1,1,4,1)+N_2 → CO_2(0,2,2,3,1)+N_2	5.52E+01	-4.04E+02	8.38E+02	3.00E-01
CO_2(0,1,1,4,1)+N_2 → CO_2(1,1,1,3,2)+N_2	5.60E+01	-4.03E+02	1.10E+03	3.00E-01
CO_2(0,1,1,4,1)+N_2 → CO_2(1,2,2,3,2)+N_2	4.50E+01	-2.54E+02	6.79E+02	3.00E-01
CO_2(0,1,1,4,1)+N_2 → CO_2(2,0,0,3,3)+N_2	4.50E+01	-2.54E+02	6.79E+02	3.00E-01
CO_2(0,1,1,5,1)+N_2 → CO_2(0,0,0,5,1)+N_2	3.83E+01	-1.77E+02	4.51E+02	7.00E-01
CO_2(0,1,1,5,1)+N_2 → CO_2(0,2,2,4,1)+N_2	5.55E+01	-4.03E+02	8.43E+02	3.00E-01
CO_2(0,1,1,5,1)+N_2 → CO_2(1,1,1,4,2)+N_2	5.62E+01	-4.02E+02	1.10E+03	3.00E-01
CO_2(0,1,1,5,1)+N_2 → CO_2(1,2,2,4,2)+N_2	4.52E+01	-2.54E+02	6.77E+02	3.00E-01
CO_2(0,1,1,5,1)+N_2 → CO_2(2,0,0,4,3)+N_2	4.52E+01	-2.54E+02	6.77E+02	3.00E-01
CO_2(0,2,2,0,1)+N_2 → CO_2(0,1,1,0,1)+N_2	3.90E+01	-1.77E+02	4.51E+02	7.00E-01
CO_2(0,2,2,1,1)+N_2 → CO_2(0,1,1,1,1)+N_2	3.90E+01	-1.77E+02	4.51E+02	7.00E-01
CO_2(0,2,2,1,1)+N_2 → CO_2(0,3,3,0,1)+N_2	5.39E+01	-4.07E+02	8.24E+02	3.00E-01
CO_2(0,2,2,1,1)+N_2 → CO_2(1,2,2,0,2)+N_2	5.46E+01	-4.04E+02	1.10E+03	3.00E-01
CO_2(0,2,2,1,1)+N_2 → CO_2(1,3,3,0,2)+N_2	4.36E+01	-2.52E+02	6.85E+02	3.00E-01
CO_2(0,2,2,1,1)+N_2 → CO_2(2,0,0,0,3)+N_2	5.46E+01	-4.04E+02	1.10E+03	3.00E-01
CO_2(0,2,2,1,1)+N_2 → CO_2(2,1,1,0,3)+N_2	4.36E+01	-2.52E+02	6.85E+02	3.00E-01

$CO_2(0,2,2,2,1)+N_2 \rightarrow CO_2(0,1,1,2,1)+N_2$	3.90E+01	-1.77E+02	4.51E+02	7.00E-01
$CO_2(0,2,2,2,1)+N_2 \rightarrow CO_2(0,3,3,1,1)+N_2$	5.46E+01	-4.06E+02	8.29E+02	3.00E-01
$CO_2(0,2,2,2,1)+N_2 \rightarrow CO_2(1,2,2,1,2)+N_2$	5.53E+01	-4.04E+02	1.10E+03	3.00E-01
$CO_2(0,2,2,2,1)+N_2 \rightarrow CO_2(1,3,3,1,2)+N_2$	4.43E+01	-2.53E+02	6.83E+02	3.00E-01
$CO_2(0,2,2,2,1)+N_2 \rightarrow CO_2(2,0,0,1,3)+N_2$	5.53E+01	-4.04E+02	1.10E+03	3.00E-01
$CO_2(0,2,2,2,1)+N_2 \rightarrow CO_2(2,1,1,1,3)+N_2$	4.43E+01	-2.53E+02	6.83E+02	3.00E-01
$CO_2(0,2,2,3,1)+N_2 \rightarrow CO_2(0,1,1,3,1)+N_2$	3.90E+01	-1.77E+02	4.51E+02	7.00E-01
$CO_2(0,2,2,3,1)+N_2 \rightarrow CO_2(0,3,3,2,1)+N_2$	5.50E+01	-4.05E+02	8.33E+02	3.00E-01
$CO_2(0,2,2,3,1)+N_2 \rightarrow CO_2(1,2,2,2,2)+N_2$	5.57E+01	-4.03E+02	1.10E+03	3.00E-01
$CO_2(0,2,2,3,1)+N_2 \rightarrow CO_2(1,3,3,2,2)+N_2$	4.47E+01	-2.53E+02	6.81E+02	3.00E-01
$CO_2(0,2,2,3,1)+N_2 \rightarrow CO_2(2,0,0,2,3)+N_2$	5.57E+01	-4.03E+02	1.10E+03	3.00E-01
$CO_2(0,2,2,3,1)+N_2 \rightarrow CO_2(2,1,1,2,3)+N_2$	4.47E+01	-2.53E+02	6.81E+02	3.00E-01
$CO_2(0,2,2,4,1)+N_2 \rightarrow CO_2(0,1,1,4,1)+N_2$	3.90E+01	-1.77E+02	4.51E+02	7.00E-01
$CO_2(0,2,2,4,1)+N_2 \rightarrow CO_2(0,3,3,3,1)+N_2$	5.52E+01	-4.04E+02	8.38E+02	3.00E-01
$CO_2(0,2,2,4,1)+N_2 \rightarrow CO_2(1,2,2,3,2)+N_2$	5.60E+01	-4.03E+02	1.10E+03	3.00E-01
$CO_2(0,2,2,4,1)+N_2 \rightarrow CO_2(1,3,3,3,2)+N_2$	4.50E+01	-2.54E+02	6.79E+02	3.00E-01
$CO_2(0,2,2,4,1)+N_2 \rightarrow CO_2(2,0,0,3,3)+N_2$	5.60E+01	-4.03E+02	1.10E+03	3.00E-01
$CO_2(0,2,2,4,1)+N_2 \rightarrow CO_2(2,1,1,3,3)+N_2$	4.50E+01	-2.54E+02	6.79E+02	3.00E-01
$CO_2(0,2,2,5,1)+N_2 \rightarrow CO_2(0,1,1,5,1)+N_2$	3.90E+01	-1.77E+02	4.51E+02	7.00E-01
$CO_2(0,2,2,5,1)+N_2 \rightarrow CO_2(0,3,3,4,1)+N_2$	5.55E+01	-4.03E+02	8.43E+02	3.00E-01
$CO_2(0,2,2,5,1)+N_2 \rightarrow CO_2(1,2,2,4,2)+N_2$	5.62E+01	-4.02E+02	1.10E+03	3.00E-01
$CO_2(0,2,2,5,1)+N_2 \rightarrow CO_2(1,3,3,4,2)+N_2$	4.52E+01	-2.54E+02	6.77E+02	3.00E-01
$CO_2(0,2,2,5,1)+N_2 \rightarrow CO_2(2,0,0,4,3)+N_2$	5.62E+01	-4.02E+02	1.10E+03	3.00E-01
$CO_2(0,2,2,5,1)+N_2 \rightarrow CO_2(2,1,1,4,3)+N_2$	4.52E+01	-2.54E+02	6.77E+02	3.00E-01
$CO_2(0,3,3,0,1)+N_2 \rightarrow CO_2(0,2,2,0,1)+N_2$	3.94E+01	-1.77E+02	4.51E+02	7.00E-01
$CO_2(0,3,3,0,1)+N_2 \rightarrow CO_2(1,0,0,0,2)+N_2$	3.15E+01	-1.71E+02	2.64E+02	1.80E+00
$CO_2(0,3,3,1,1)+N_2 \rightarrow CO_2(0,2,2,1,1)+N_2$	3.94E+01	-1.77E+02	4.51E+02	7.00E-01
$CO_2(0,3,3,1,1)+N_2 \rightarrow CO_2(0,4,4,0,1)+N_2$	5.39E+01	-4.07E+02	8.24E+02	3.00E-01
$CO_2(0,3,3,1,1)+N_2 \rightarrow CO_2(1,0,0,1,2)+N_2$	3.15E+01	-1.71E+02	2.64E+02	1.80E+00
$CO_2(0,3,3,1,1)+N_2 \rightarrow CO_2(1,3,3,0,2)+N_2$	5.46E+01	-4.04E+02	1.10E+03	3.00E-01
$CO_2(0,3,3,1,1)+N_2 \rightarrow CO_2(2,1,1,0,3)+N_2$	5.46E+01	-4.04E+02	1.10E+03	3.00E-01
$CO_2(0,3,3,2,1)+N_2 \rightarrow CO_2(0,2,2,2,1)+N_2$	3.94E+01	-1.77E+02	4.51E+02	7.00E-01
$CO_2(0,3,3,2,1)+N_2 \rightarrow CO_2(0,4,4,1,1)+N_2$	5.46E+01	-4.06E+02	8.29E+02	3.00E-01
$CO_2(0,3,3,2,1)+N_2 \rightarrow CO_2(1,0,0,2,2)+N_2$	3.15E+01	-1.71E+02	2.64E+02	1.80E+00
$CO_2(0,3,3,2,1)+N_2 \rightarrow CO_2(1,3,3,1,2)+N_2$	5.53E+01	-4.04E+02	1.10E+03	3.00E-01
$CO_2(0,3,3,2,1)+N_2 \rightarrow CO_2(2,1,1,1,3)+N_2$	5.53E+01	-4.04E+02	1.10E+03	3.00E-01
$CO_2(0,3,3,3,1)+N_2 \rightarrow CO_2(0,2,2,3,1)+N_2$	3.94E+01	-1.77E+02	4.51E+02	7.00E-01

CO_2(0,3,3,3,1)+N_2 → CO_2(0,4,4,2,1)+N_2	5.50E+01	-4.05E+02	8.33E+02	3.00E-01
CO_2(0,3,3,3,1)+N_2 → CO_2(1,0,0,3,2)+N_2	3.15E+01	-1.71E+02	2.64E+02	1.80E+00
CO_2(0,3,3,3,1)+N_2 → CO_2(1,3,3,2,2)+N_2	5.57E+01	-4.03E+02	1.10E+03	3.00E-01
CO_2(0,3,3,3,1)+N_2 → CO_2(2,1,1,2,3)+N_2	5.57E+01	-4.03E+02	1.10E+03	3.00E-01
CO_2(0,3,3,4,1)+N_2 → CO_2(0,2,2,4,1)+N_2	3.94E+01	-1.77E+02	4.51E+02	7.00E-01
CO_2(0,3,3,4,1)+N_2 → CO_2(0,4,4,3,1)+N_2	5.52E+01	-4.04E+02	8.38E+02	3.00E-01
CO_2(0,3,3,4,1)+N_2 → CO_2(1,0,0,4,2)+N_2	3.15E+01	-1.71E+02	2.64E+02	1.80E+00
CO_2(0,3,3,4,1)+N_2 → CO_2(1,3,3,3,2)+N_2	5.60E+01	-4.03E+02	1.10E+03	3.00E-01
CO_2(0,3,3,4,1)+N_2 → CO_2(2,1,1,3,3)+N_2	5.60E+01	-4.03E+02	1.10E+03	3.00E-01
CO_2(0,3,3,5,1)+N_2 → CO_2(0,2,2,5,1)+N_2	3.94E+01	-1.77E+02	4.51E+02	7.00E-01
CO_2(0,3,3,5,1)+N_2 → CO_2(0,4,4,4,1)+N_2	5.55E+01	-4.03E+02	8.43E+02	3.00E-01
CO_2(0,3,3,5,1)+N_2 → CO_2(1,0,0,5,2)+N_2	3.15E+01	-1.71E+02	2.64E+02	1.80E+00
CO_2(0,3,3,5,1)+N_2 → CO_2(1,3,3,4,2)+N_2	5.62E+01	-4.02E+02	1.10E+03	3.00E-01
CO_2(0,3,3,5,1)+N_2 → CO_2(2,1,1,4,3)+N_2	5.62E+01	-4.02E+02	1.10E+03	3.00E-01
CO_2(0,4,4,0,1)+N_2 → CO_2(0,3,3,0,1)+N_2	3.97E+01	-1.77E+02	4.51E+02	7.00E-01
CO_2(0,4,4,0,1)+N_2 → CO_2(1,1,1,0,2)+N_2	3.01E+01	-1.71E+02	2.64E+02	1.60E+00
CO_2(0,4,4,1,1)+N_2 → CO_2(0,3,3,1,1)+N_2	3.97E+01	-1.77E+02	4.51E+02	7.00E-01
CO_2(0,4,4,1,1)+N_2 → CO_2(0,5,5,0,1)+N_2	5.39E+01	-4.07E+02	8.24E+02	3.00E-01
CO_2(0,4,4,1,1)+N_2 → CO_2(1,1,1,1,2)+N_2	3.01E+01	-1.71E+02	2.64E+02	1.60E+00
CO_2(0,4,4,2,1)+N_2 → CO_2(0,3,3,2,1)+N_2	3.97E+01	-1.77E+02	4.51E+02	7.00E-01
CO_2(0,4,4,2,1)+N_2 → CO_2(0,5,5,1,1)+N_2	5.46E+01	-4.06E+02	8.29E+02	3.00E-01
CO_2(0,4,4,2,1)+N_2 → CO_2(1,1,1,2,2)+N_2	3.01E+01	-1.71E+02	2.64E+02	1.60E+00
CO_2(0,4,4,3,1)+N_2 → CO_2(0,3,3,3,1)+N_2	3.97E+01	-1.77E+02	4.51E+02	7.00E-01
CO_2(0,4,4,3,1)+N_2 → CO_2(0,5,5,2,1)+N_2	5.50E+01	-4.05E+02	8.33E+02	3.00E-01
CO_2(0,4,4,3,1)+N_2 → CO_2(1,1,1,3,2)+N_2	3.01E+01	-1.71E+02	2.64E+02	1.60E+00
CO_2(0,4,4,4,1)+N_2 → CO_2(0,3,3,4,1)+N_2	3.97E+01	-1.77E+02	4.51E+02	7.00E-01
CO_2(0,4,4,4,1)+N_2 → CO_2(0,5,5,3,1)+N_2	5.52E+01	-4.04E+02	8.38E+02	3.00E-01
CO_2(0,4,4,4,1)+N_2 → CO_2(1,1,1,4,2)+N_2	3.01E+01	-1.71E+02	2.64E+02	1.60E+00
CO_2(0,4,4,5,1)+N_2 → CO_2(0,3,3,5,1)+N_2	3.97E+01	-1.77E+02	4.51E+02	7.00E-01
CO_2(0,4,4,5,1)+N_2 → CO_2(0,5,5,4,1)+N_2	5.55E+01	-4.03E+02	8.43E+02	3.00E-01
CO_2(0,4,4,5,1)+N_2 → CO_2(1,1,1,5,2)+N_2	3.01E+01	-1.71E+02	2.64E+02	1.60E+00
CO_2(0,5,5,0,1)+N_2 → CO_2(0,4,4,0,1)+N_2	3.99E+01	-1.77E+02	4.51E+02	7.00E-01
CO_2(0,5,5,1,1)+N_2 → CO_2(0,4,4,1,1)+N_2	3.99E+01	-1.77E+02	4.51E+02	7.00E-01
CO_2(0,5,5,2,1)+N_2 → CO_2(0,4,4,2,1)+N_2	3.99E+01	-1.77E+02	4.51E+02	7.00E-01
CO_2(0,5,5,3,1)+N_2 → CO_2(0,4,4,3,1)+N_2	3.99E+01	-1.77E+02	4.51E+02	7.00E-01
CO_2(0,5,5,4,1)+N_2 → CO_2(0,4,4,4,1)+N_2	3.99E+01	-1.77E+02	4.51E+02	7.00E-01
CO_2(0,5,5,5,1)+N_2 → CO_2(0,4,4,5,1)+N_2	3.99E+01	-1.77E+02	4.51E+02	7.00E-01

CO_2(1,0,0,0,2)+N_2 → CO_2(0,0,0,0,1)+N_2	3.41E+01	-1.37E+02	0.00E+00	3.10E+00
CO_2(1,0,0,0,2)+N_2 → CO_2(0,1,1,0,1)+N_2	3.93E+01	-1.77E+02	4.51E+02	7.00E-01
CO_2(1,0,0,0,2)+N_2 → CO_2(0,2,2,0,1)+N_2	3.65E+01	-8.89E+01	2.26E+02	9.00E-01
CO_2(1,0,0,1,2)+N_2 → CO_2(0,0,0,1,1)+N_2	3.41E+01	-1.37E+02	0.00E+00	3.10E+00
CO_2(1,0,0,1,2)+N_2 → CO_2(0,1,1,1,1)+N_2	3.93E+01	-1.77E+02	4.51E+02	7.00E-01
CO_2(1,0,0,1,2)+N_2 → CO_2(0,2,2,1,1)+N_2	3.65E+01	-8.89E+01	2.26E+02	9.00E-01
CO_2(1,0,0,2,2)+N_2 → CO_2(0,0,0,2,1)+N_2	3.41E+01	-1.37E+02	0.00E+00	3.10E+00
CO_2(1,0,0,2,2)+N_2 → CO_2(0,1,1,2,1)+N_2	3.93E+01	-1.77E+02	4.51E+02	7.00E-01
CO_2(1,0,0,2,2)+N_2 → CO_2(0,2,2,2,1)+N_2	3.65E+01	-8.89E+01	2.26E+02	9.00E-01
CO_2(1,0,0,3,2)+N_2 → CO_2(0,0,0,3,1)+N_2	3.41E+01	-1.37E+02	0.00E+00	3.10E+00
CO_2(1,0,0,3,2)+N_2 → CO_2(0,1,1,3,1)+N_2	3.93E+01	-1.77E+02	4.51E+02	7.00E-01
CO_2(1,0,0,3,2)+N_2 → CO_2(0,2,2,3,1)+N_2	3.65E+01	-8.89E+01	2.26E+02	9.00E-01
CO_2(1,0,0,4,2)+N_2 → CO_2(0,0,0,4,1)+N_2	3.41E+01	-1.37E+02	0.00E+00	3.10E+00
CO_2(1,0,0,4,2)+N_2 → CO_2(0,1,1,4,1)+N_2	3.93E+01	-1.77E+02	4.51E+02	7.00E-01
CO_2(1,0,0,4,2)+N_2 → CO_2(0,2,2,4,1)+N_2	3.65E+01	-8.89E+01	2.26E+02	9.00E-01
CO_2(1,0,0,5,2)+N_2 → CO_2(0,0,0,5,1)+N_2	3.41E+01	-1.37E+02	0.00E+00	3.10E+00
CO_2(1,0,0,5,2)+N_2 → CO_2(0,1,1,5,1)+N_2	3.93E+01	-1.77E+02	4.51E+02	7.00E-01
CO_2(1,0,0,5,2)+N_2 → CO_2(0,2,2,5,1)+N_2	3.65E+01	-8.89E+01	2.26E+02	9.00E-01
CO_2(1,1,1,0,2)+N_2 → CO_2(0,1,1,0,1)+N_2	3.41E+01	-1.37E+02	0.00E+00	3.10E+00
CO_2(1,1,1,0,2)+N_2 → CO_2(0,2,2,0,1)+N_2	3.94E+01	-1.77E+02	4.51E+02	7.00E-01
CO_2(1,1,1,0,2)+N_2 → CO_2(0,3,3,0,1)+N_2	3.72E+01	-8.93E+01	2.27E+02	9.00E-01
CO_2(1,1,1,0,2)+N_2 → CO_2(1,0,0,0,2)+N_2	3.97E+01	-1.77E+02	4.51E+02	7.00E-01
CO_2(1,1,1,1,2)+N_2 → CO_2(0,1,1,1,1)+N_2	3.41E+01	-1.37E+02	0.00E+00	3.10E+00
CO_2(1,1,1,1,2)+N_2 → CO_2(0,2,2,1,1)+N_2	3.94E+01	-1.77E+02	4.51E+02	7.00E-01
CO_2(1,1,1,1,2)+N_2 → CO_2(0,3,3,1,1)+N_2	3.72E+01	-8.93E+01	2.27E+02	9.00E-01
CO_2(1,1,1,1,2)+N_2 → CO_2(1,0,0,1,2)+N_2	3.97E+01	-1.77E+02	4.51E+02	7.00E-01
CO_2(1,1,1,2,2)+N_2 → CO_2(0,1,1,2,1)+N_2	3.41E+01	-1.37E+02	0.00E+00	3.10E+00
CO_2(1,1,1,2,2)+N_2 → CO_2(0,2,2,2,1)+N_2	3.94E+01	-1.77E+02	4.51E+02	7.00E-01
CO_2(1,1,1,2,2)+N_2 → CO_2(0,3,3,2,1)+N_2	3.72E+01	-8.93E+01	2.27E+02	9.00E-01
CO_2(1,1,1,2,2)+N_2 → CO_2(1,0,0,2,2)+N_2	3.97E+01	-1.77E+02	4.51E+02	7.00E-01
CO_2(1,1,1,3,2)+N_2 → CO_2(0,1,1,3,1)+N_2	3.41E+01	-1.37E+02	0.00E+00	3.10E+00
CO_2(1,1,1,3,2)+N_2 → CO_2(0,2,2,3,1)+N_2	3.94E+01	-1.77E+02	4.51E+02	7.00E-01
CO_2(1,1,1,3,2)+N_2 → CO_2(0,3,3,3,1)+N_2	3.72E+01	-8.93E+01	2.27E+02	9.00E-01
CO_2(1,1,1,3,2)+N_2 → CO_2(1,0,0,3,2)+N_2	3.97E+01	-1.77E+02	4.51E+02	7.00E-01
CO_2(1,1,1,4,2)+N_2 → CO_2(0,1,1,4,1)+N_2	3.41E+01	-1.37E+02	0.00E+00	3.10E+00
CO_2(1,1,1,4,2)+N_2 → CO_2(0,2,2,4,1)+N_2	3.94E+01	-1.77E+02	4.51E+02	7.00E-01
CO_2(1,1,1,4,2)+N_2 → CO_2(0,3,3,4,1)+N_2	3.72E+01	-8.93E+01	2.27E+02	9.00E-01

CO_2(1,1,1,4,2)+N_2 → CO_2(1,0,0,4,2)+N_2	3.97E+01	-1.77E+02	4.51E+02	7.00E-01
CO_2(1,1,1,5,2)+N_2 → CO_2(0,1,1,5,1)+N_2	3.41E+01	-1.37E+02	0.00E+00	3.10E+00
CO_2(1,1,1,5,2)+N_2 → CO_2(0,2,2,5,1)+N_2	3.94E+01	-1.77E+02	4.51E+02	7.00E-01
CO_2(1,1,1,5,2)+N_2 → CO_2(0,3,3,5,1)+N_2	3.72E+01	-8.93E+01	2.27E+02	9.00E-01
CO_2(1,1,1,5,2)+N_2 → CO_2(1,0,0,5,2)+N_2	3.97E+01	-1.77E+02	4.51E+02	7.00E-01
CO_2(1,2,2,0,2)+N_2 → CO_2(0,3,3,0,1)+N_2	3.97E+01	-1.77E+02	4.51E+02	7.00E-01
CO_2(1,2,2,0,2)+N_2 → CO_2(0,4,4,0,1)+N_2	3.78E+01	-9.04E+01	2.30E+02	9.00E-01
CO_2(1,2,2,0,2)+N_2 → CO_2(1,1,1,0,2)+N_2	4.01E+01	-1.77E+02	4.51E+02	7.00E-01
CO_2(1,2,2,0,2)+N_2 → CO_2(2,0,0,0,3)+N_2	3.81E+01	-9.04E+01	2.30E+02	9.00E-01
CO_2(1,2,2,1,2)+N_2 → CO_2(0,3,3,1,1)+N_2	3.97E+01	-1.77E+02	4.51E+02	7.00E-01
CO_2(1,2,2,1,2)+N_2 → CO_2(0,4,4,1,1)+N_2	3.78E+01	-9.04E+01	2.30E+02	9.00E-01
CO_2(1,2,2,1,2)+N_2 → CO_2(1,1,1,1,2)+N_2	4.01E+01	-1.77E+02	4.51E+02	7.00E-01
CO_2(1,2,2,1,2)+N_2 → CO_2(2,0,0,1,3)+N_2	3.81E+01	-9.04E+01	2.30E+02	9.00E-01
CO_2(1,2,2,2,2)+N_2 → CO_2(0,3,3,2,1)+N_2	3.97E+01	-1.77E+02	4.51E+02	7.00E-01
CO_2(1,2,2,2,2)+N_2 → CO_2(0,4,4,2,1)+N_2	3.78E+01	-9.04E+01	2.30E+02	9.00E-01
CO_2(1,2,2,2,2)+N_2 → CO_2(1,1,1,2,2)+N_2	4.01E+01	-1.77E+02	4.51E+02	7.00E-01
CO_2(1,2,2,2,2)+N_2 → CO_2(2,0,0,2,3)+N_2	3.81E+01	-9.04E+01	2.30E+02	9.00E-01
CO_2(1,2,2,3,2)+N_2 → CO_2(0,3,3,3,1)+N_2	3.97E+01	-1.77E+02	4.51E+02	7.00E-01
CO_2(1,2,2,3,2)+N_2 → CO_2(0,4,4,3,1)+N_2	3.78E+01	-9.04E+01	2.30E+02	9.00E-01
CO_2(1,2,2,3,2)+N_2 → CO_2(1,1,1,3,2)+N_2	4.01E+01	-1.77E+02	4.51E+02	7.00E-01
CO_2(1,2,2,3,2)+N_2 → CO_2(2,0,0,3,3)+N_2	3.81E+01	-9.04E+01	2.30E+02	9.00E-01
CO_2(1,2,2,4,2)+N_2 → CO_2(0,3,3,4,1)+N_2	3.97E+01	-1.77E+02	4.51E+02	7.00E-01
CO_2(1,2,2,4,2)+N_2 → CO_2(0,4,4,4,1)+N_2	3.78E+01	-9.04E+01	2.30E+02	9.00E-01
CO_2(1,2,2,4,2)+N_2 → CO_2(1,1,1,4,2)+N_2	4.01E+01	-1.77E+02	4.51E+02	7.00E-01
CO_2(1,2,2,4,2)+N_2 → CO_2(2,0,0,4,3)+N_2	3.81E+01	-9.04E+01	2.30E+02	9.00E-01
CO_2(1,2,2,5,2)+N_2 → CO_2(0,3,3,5,1)+N_2	3.97E+01	-1.77E+02	4.51E+02	7.00E-01
CO_2(1,2,2,5,2)+N_2 → CO_2(0,4,4,5,1)+N_2	3.78E+01	-9.04E+01	2.30E+02	9.00E-01
CO_2(1,2,2,5,2)+N_2 → CO_2(1,1,1,5,2)+N_2	4.01E+01	-1.77E+02	4.51E+02	7.00E-01
CO_2(1,2,2,5,2)+N_2 → CO_2(2,0,0,5,3)+N_2	3.81E+01	-9.04E+01	2.30E+02	9.00E-01
CO_2(1,3,3,0,2)+N_2 → CO_2(0,3,3,0,1)+N_2	3.41E+01	-1.37E+02	0.00E+00	3.10E+00
CO_2(1,3,3,0,2)+N_2 → CO_2(0,4,4,0,1)+N_2	3.99E+01	-1.77E+02	4.51E+02	7.00E-01
CO_2(1,3,3,0,2)+N_2 → CO_2(0,5,5,0,1)+N_2	3.80E+01	-8.89E+01	2.26E+02	9.00E-01
CO_2(1,3,3,0,2)+N_2 → CO_2(1,2,2,0,2)+N_2	4.04E+01	-1.77E+02	4.51E+02	7.00E-01
CO_2(1,3,3,1,2)+N_2 → CO_2(0,3,3,1,1)+N_2	3.41E+01	-1.37E+02	0.00E+00	3.10E+00
CO_2(1,3,3,1,2)+N_2 → CO_2(0,4,4,1,1)+N_2	3.99E+01	-1.77E+02	4.51E+02	7.00E-01
CO_2(1,3,3,1,2)+N_2 → CO_2(0,5,5,1,1)+N_2	3.80E+01	-8.89E+01	2.26E+02	9.00E-01
CO_2(1,3,3,1,2)+N_2 → CO_2(1,2,2,1,2)+N_2	4.04E+01	-1.77E+02	4.51E+02	7.00E-01

$CO_2(1,3,3,2,2)+N_2 \rightarrow CO_2(0,3,3,2,1)+N_2$	3.41E+01	-1.37E+02	0.00E+00	3.10E+00
$CO_2(1,3,3,2,2)+N_2 \rightarrow CO_2(0,4,4,2,1)+N_2$	3.99E+01	-1.77E+02	4.51E+02	7.00E-01
$CO_2(1,3,3,2,2)+N_2 \rightarrow CO_2(0,5,5,2,1)+N_2$	3.80E+01	-8.89E+01	2.26E+02	9.00E-01
$CO_2(1,3,3,2,2)+N_2 \rightarrow CO_2(1,2,2,2,2)+N_2$	4.04E+01	-1.77E+02	4.51E+02	7.00E-01
$CO_2(1,3,3,3,2)+N_2 \rightarrow CO_2(0,3,3,3,1)+N_2$	3.41E+01	-1.37E+02	0.00E+00	3.10E+00
$CO_2(1,3,3,3,2)+N_2 \rightarrow CO_2(0,4,4,3,1)+N_2$	3.99E+01	-1.77E+02	4.51E+02	7.00E-01
$CO_2(1,3,3,3,2)+N_2 \rightarrow CO_2(0,5,5,3,1)+N_2$	3.80E+01	-8.89E+01	2.26E+02	9.00E-01
$CO_2(1,3,3,3,2)+N_2 \rightarrow CO_2(1,2,2,3,2)+N_2$	4.04E+01	-1.77E+02	4.51E+02	7.00E-01
$CO_2(1,3,3,4,2)+N_2 \rightarrow CO_2(0,3,3,4,1)+N_2$	3.41E+01	-1.37E+02	0.00E+00	3.10E+00
$CO_2(1,3,3,4,2)+N_2 \rightarrow CO_2(0,4,4,4,1)+N_2$	3.99E+01	-1.77E+02	4.51E+02	7.00E-01
$CO_2(1,3,3,4,2)+N_2 \rightarrow CO_2(0,5,5,4,1)+N_2$	3.80E+01	-8.89E+01	2.26E+02	9.00E-01
$CO_2(1,3,3,4,2)+N_2 \rightarrow CO_2(1,2,2,4,2)+N_2$	4.04E+01	-1.77E+02	4.51E+02	7.00E-01
$CO_2(1,3,3,5,2)+N_2 \rightarrow CO_2(0,3,3,5,1)+N_2$	3.41E+01	-1.37E+02	0.00E+00	3.10E+00
$CO_2(1,3,3,5,2)+N_2 \rightarrow CO_2(0,4,4,5,1)+N_2$	3.99E+01	-1.77E+02	4.51E+02	7.00E-01
$CO_2(1,3,3,5,2)+N_2 \rightarrow CO_2(0,5,5,5,1)+N_2$	3.80E+01	-8.89E+01	2.26E+02	9.00E-01
$CO_2(1,3,3,5,2)+N_2 \rightarrow CO_2(1,2,2,5,2)+N_2$	4.04E+01	-1.77E+02	4.51E+02	7.00E-01
$CO_2(2,0,0,0,3)+N_2 \rightarrow CO_2(0,0,0,1,1)+N_2$	3.00E+01	-1.08E+02	1.65E+02	1.20E+00
$CO_2(2,0,0,0,3)+N_2 \rightarrow CO_2(0,2,2,0,1)+N_2$	3.92E+01	-2.71E+02	4.38E+02	3.10E+00
$CO_2(2,0,0,0,3)+N_2 \rightarrow CO_2(0,3,3,0,1)+N_2$	3.02E+01	-1.71E+02	2.64E+02	1.80E+00
$CO_2(2,0,0,0,3)+N_2 \rightarrow CO_2(1,0,0,0,2)+N_2$	4.37E+01	-2.72E+02	4.37E+02	3.00E+00
$CO_2(2,0,0,0,3)+N_2 \rightarrow CO_2(1,1,1,0,2)+N_2$	4.01E+01	-1.77E+02	4.51E+02	7.00E-01
$CO_2(2,0,0,1,3)+N_2 \rightarrow CO_2(0,0,0,2,1)+N_2$	3.00E+01	-1.08E+02	1.65E+02	1.20E+00
$CO_2(2,0,0,1,3)+N_2 \rightarrow CO_2(0,2,2,1,1)+N_2$	3.92E+01	-2.71E+02	4.38E+02	3.10E+00
$CO_2(2,0,0,1,3)+N_2 \rightarrow CO_2(0,3,3,1,1)+N_2$	3.02E+01	-1.71E+02	2.64E+02	1.80E+00
$CO_2(2,0,0,1,3)+N_2 \rightarrow CO_2(1,0,0,1,2)+N_2$	4.37E+01	-2.72E+02	4.37E+02	3.00E+00
$CO_2(2,0,0,1,3)+N_2 \rightarrow CO_2(1,1,1,1,2)+N_2$	4.01E+01	-1.77E+02	4.51E+02	7.00E-01
$CO_2(2,0,0,2,3)+N_2 \rightarrow CO_2(0,0,0,3,1)+N_2$	3.00E+01	-1.08E+02	1.65E+02	1.20E+00
$CO_2(2,0,0,2,3)+N_2 \rightarrow CO_2(0,2,2,2,1)+N_2$	3.92E+01	-2.71E+02	4.38E+02	3.10E+00
$CO_2(2,0,0,2,3)+N_2 \rightarrow CO_2(0,3,3,2,1)+N_2$	3.02E+01	-1.71E+02	2.64E+02	1.80E+00
$CO_2(2,0,0,2,3)+N_2 \rightarrow CO_2(1,0,0,2,2)+N_2$	4.37E+01	-2.72E+02	4.37E+02	3.00E+00
$CO_2(2,0,0,2,3)+N_2 \rightarrow CO_2(1,1,1,2,2)+N_2$	4.01E+01	-1.77E+02	4.51E+02	7.00E-01
$CO_2(2,0,0,3,3)+N_2 \rightarrow CO_2(0,0,0,4,1)+N_2$	3.00E+01	-1.08E+02	1.65E+02	1.20E+00
$CO_2(2,0,0,3,3)+N_2 \rightarrow CO_2(0,2,2,3,1)+N_2$	3.92E+01	-2.71E+02	4.38E+02	3.10E+00
$CO_2(2,0,0,3,3)+N_2 \rightarrow CO_2(0,3,3,3,1)+N_2$	3.02E+01	-1.71E+02	2.64E+02	1.80E+00
$CO_2(2,0,0,3,3)+N_2 \rightarrow CO_2(1,0,0,3,2)+N_2$	4.37E+01	-2.72E+02	4.37E+02	3.00E+00
$CO_2(2,0,0,3,3)+N_2 \rightarrow CO_2(1,1,1,3,2)+N_2$	4.01E+01	-1.77E+02	4.51E+02	7.00E-01
$CO_2(2,0,0,4,3)+N_2 \rightarrow CO_2(0,0,0,5,1)+N_2$	3.00E+01	-1.08E+02	1.65E+02	1.20E+00

CO_2(2,0,0,4,3)+N_2 → CO_2(0,2,2,4,1)+N_2	3.92E+01	-2.71E+02	4.38E+02	3.10E+00
CO_2(2,0,0,4,3)+N_2 → CO_2(0,3,3,4,1)+N_2	3.02E+01	-1.71E+02	2.64E+02	1.80E+00
CO_2(2,0,0,4,3)+N_2 → CO_2(1,0,0,4,2)+N_2	4.37E+01	-2.72E+02	4.37E+02	3.00E+00
CO_2(2,0,0,4,3)+N_2 → CO_2(1,1,1,4,2)+N_2	4.01E+01	-1.77E+02	4.51E+02	7.00E-01
CO_2(2,0,0,5,3)+N_2 → CO_2(0,2,2,5,1)+N_2	3.92E+01	-2.71E+02	4.38E+02	3.10E+00
CO_2(2,0,0,5,3)+N_2 → CO_2(0,3,3,5,1)+N_2	3.02E+01	-1.71E+02	2.64E+02	1.80E+00
CO_2(2,0,0,5,3)+N_2 → CO_2(1,0,0,5,2)+N_2	4.37E+01	-2.72E+02	4.37E+02	3.00E+00
CO_2(2,0,0,5,3)+N_2 → CO_2(1,1,1,5,2)+N_2	4.01E+01	-1.77E+02	4.51E+02	7.00E-01
CO_2(2,1,1,0,3)+N_2 → CO_2(1,1,1,0,2)+N_2	3.52E+01	-1.37E+02	0.00E+00	3.10E+00
CO_2(2,1,1,0,3)+N_2 → CO_2(1,2,2,0,2)+N_2	4.04E+01	-1.77E+02	4.51E+02	7.00E-01
CO_2(2,1,1,0,3)+N_2 → CO_2(1,3,3,0,2)+N_2	3.84E+01	-8.89E+01	2.26E+02	9.00E-01
CO_2(2,1,1,0,3)+N_2 → CO_2(2,0,0,0,3)+N_2	4.05E+01	-1.77E+02	4.51E+02	7.00E-01
CO_2(2,1,1,1,3)+N_2 → CO_2(1,1,1,1,2)+N_2	3.52E+01	-1.37E+02	0.00E+00	3.10E+00
CO_2(2,1,1,1,3)+N_2 → CO_2(1,2,2,1,2)+N_2	4.04E+01	-1.77E+02	4.51E+02	7.00E-01
CO_2(2,1,1,1,3)+N_2 → CO_2(1,3,3,1,2)+N_2	3.84E+01	-8.89E+01	2.26E+02	9.00E-01
CO_2(2,1,1,1,3)+N_2 → CO_2(2,0,0,1,3)+N_2	4.05E+01	-1.77E+02	4.51E+02	7.00E-01
CO_2(2,1,1,2,3)+N_2 → CO_2(1,1,1,2,2)+N_2	3.52E+01	-1.37E+02	0.00E+00	3.10E+00
CO_2(2,1,1,2,3)+N_2 → CO_2(1,2,2,2,2)+N_2	4.04E+01	-1.77E+02	4.51E+02	7.00E-01
CO_2(2,1,1,2,3)+N_2 → CO_2(1,3,3,2,2)+N_2	3.84E+01	-8.89E+01	2.26E+02	9.00E-01
CO_2(2,1,1,2,3)+N_2 → CO_2(2,0,0,2,3)+N_2	4.05E+01	-1.77E+02	4.51E+02	7.00E-01
CO_2(2,1,1,3,3)+N_2 → CO_2(1,1,1,3,2)+N_2	3.52E+01	-1.37E+02	0.00E+00	3.10E+00
CO_2(2,1,1,3,3)+N_2 → CO_2(1,2,2,3,2)+N_2	4.04E+01	-1.77E+02	4.51E+02	7.00E-01
CO_2(2,1,1,3,3)+N_2 → CO_2(1,3,3,3,2)+N_2	3.84E+01	-8.89E+01	2.26E+02	9.00E-01
CO_2(2,1,1,3,3)+N_2 → CO_2(2,0,0,3,3)+N_2	4.05E+01	-1.77E+02	4.51E+02	7.00E-01
CO_2(2,1,1,4,3)+N_2 → CO_2(1,1,1,4,2)+N_2	3.52E+01	-1.37E+02	0.00E+00	3.10E+00
CO_2(2,1,1,4,3)+N_2 → CO_2(1,2,2,4,2)+N_2	4.04E+01	-1.77E+02	4.51E+02	7.00E-01
CO_2(2,1,1,4,3)+N_2 → CO_2(1,3,3,4,2)+N_2	3.84E+01	-8.89E+01	2.26E+02	9.00E-01
CO_2(2,1,1,4,3)+N_2 → CO_2(2,0,0,4,3)+N_2	4.05E+01	-1.77E+02	4.51E+02	7.00E-01
CO_2(2,1,1,5,3)+N_2 → CO_2(1,1,1,5,2)+N_2	3.52E+01	-1.37E+02	0.00E+00	3.10E+00
CO_2(2,1,1,5,3)+N_2 → CO_2(1,2,2,5,2)+N_2	4.04E+01	-1.77E+02	4.51E+02	7.00E-01
CO_2(2,1,1,5,3)+N_2 → CO_2(1,3,3,5,2)+N_2	3.84E+01	-8.89E+01	2.26E+02	9.00E-01
CO_2(2,1,1,5,3)+N_2 → CO_2(2,0,0,5,3)+N_2	4.05E+01	-1.77E+02	4.51E+02	7.00E-01

Table A.3: N_2 quenched by CO_2

A.1.4 V-T relaxation $CO_2(v_1, v_2^{l2}, v_3)$ + CO_2

Expression:

$$k(v, T_g) = 1.66 \times 10^{-24} \exp^{A(v)+B(v)T_g^{-1/3}+C(v)T_g^{-2/3}}$$

Table A.4 A, B and C:

Reaction	A	B	C
CO_2(0,0,0,1,1)+CO_2 → CO_2(0,1,1,0,1)+CO_2	5.39E+01	-4.07E+02	8.24E+02
CO_2(0,0,0,1,1)+CO_2 → CO_2(1,0,0,0,2)+CO_2	5.46E+01	-4.04E+02	1.10E+03
CO_2(0,0,0,1,1)+CO_2 → CO_2(1,1,1,0,2)+CO_2	4.36E+01	-2.52E+02	6.85E+02
CO_2(0,0,0,2,1)+CO_2 → CO_2(0,1,1,1,1)+CO_2	5.46E+01	-4.06E+02	8.29E+02
CO_2(0,0,0,2,1)+CO_2 → CO_2(1,0,0,1,2)+CO_2	5.53E+01	-4.04E+02	1.10E+03
CO_2(0,0,0,2,1)+CO_2 → CO_2(1,1,1,1,2)+CO_2	4.43E+01	-2.53E+02	6.83E+02
CO_2(0,0,0,3,1)+CO_2 → CO_2(0,1,1,2,1)+CO_2	5.50E+01	-4.05E+02	8.33E+02
CO_2(0,0,0,3,1)+CO_2 → CO_2(1,0,0,2,2)+CO_2	5.57E+01	-4.03E+02	1.10E+03
CO_2(0,0,0,3,1)+CO_2 → CO_2(1,1,1,2,2)+CO_2	4.47E+01	-2.53E+02	6.80E+02
CO_2(0,0,0,4,1)+CO_2 → CO_2(0,1,1,3,1)+CO_2	5.52E+01	-4.04E+02	8.38E+02
CO_2(0,0,0,4,1)+CO_2 → CO_2(1,0,0,3,2)+CO_2	5.60E+01	-4.03E+02	1.10E+03
CO_2(0,0,0,4,1)+CO_2 → CO_2(1,1,1,3,2)+CO_2	4.50E+01	-2.54E+02	6.78E+02
CO_2(0,0,0,5,1)+CO_2 → CO_2(0,1,1,4,1)+CO_2	5.55E+01	-4.03E+02	8.43E+02
CO_2(0,0,0,5,1)+CO_2 → CO_2(1,0,0,4,2)+CO_2	5.62E+01	-4.02E+02	1.10E+03
CO_2(0,0,0,5,1)+CO_2 → CO_2(1,1,1,4,2)+CO_2	4.52E+01	-2.55E+02	6.76E+02
CO_2(0,1,1,0,1)+CO_2 → CO_2(0,0,0,0,1)+CO_2	3.83E+01	-1.77E+02	4.51E+02
CO_2(0,1,1,1,1)+CO_2 → CO_2(0,0,0,1,1)+CO_2	3.83E+01	-1.77E+02	4.51E+02
CO_2(0,1,1,1,1)+CO_2 → CO_2(0,2,2,0,1)+CO_2	5.39E+01	-4.07E+02	8.24E+02
CO_2(0,1,1,1,1)+CO_2 → CO_2(1,1,1,0,2)+CO_2	5.46E+01	-4.04E+02	1.10E+03
CO_2(0,1,1,1,1)+CO_2 → CO_2(1,2,2,0,2)+CO_2	4.36E+01	-2.52E+02	6.85E+02
CO_2(0,1,1,1,1)+CO_2 → CO_2(2,0,0,0,3)+CO_2	4.36E+01	-2.52E+02	6.85E+02
CO_2(0,1,1,2,1)+CO_2 → CO_2(0,0,0,2,1)+CO_2	3.83E+01	-1.77E+02	4.51E+02
CO_2(0,1,1,2,1)+CO_2 → CO_2(0,2,2,1,1)+CO_2	5.46E+01	-4.06E+02	8.29E+02
CO_2(0,1,1,2,1)+CO_2 → CO_2(1,1,1,1,2)+CO_2	5.53E+01	-4.04E+02	1.10E+03
CO_2(0,1,1,2,1)+CO_2 → CO_2(1,2,2,1,2)+CO_2	4.43E+01	-2.53E+02	6.83E+02
CO_2(0,1,1,2,1)+CO_2 → CO_2(2,0,0,1,3)+CO_2	4.43E+01	-2.53E+02	6.83E+02
CO_2(0,1,1,3,1)+CO_2 → CO_2(0,0,0,3,1)+CO_2	3.83E+01	-1.77E+02	4.51E+02
CO_2(0,1,1,3,1)+CO_2 → CO_2(0,2,2,2,1)+CO_2	5.50E+01	-4.05E+02	8.33E+02
CO_2(0,1,1,3,1)+CO_2 → CO_2(1,1,1,2,2)+CO_2	5.57E+01	-4.03E+02	1.10E+03
CO_2(0,1,1,3,1)+CO_2 → CO_2(1,2,2,2,2)+CO_2	4.47E+01	-2.53E+02	6.80E+02
CO_2(0,1,1,3,1)+CO_2 → CO_2(2,0,0,2,3)+CO_2	4.47E+01	-2.53E+02	6.80E+02
CO_2(0,1,1,4,1)+CO_2 → CO_2(0,0,0,4,1)+CO_2	3.83E+01	-1.77E+02	4.51E+02

CO_2(0,1,1,4,1)+CO_2 → CO_2(0,2,2,3,1)+CO_2	5.52E+01	-4.04E+02	8.38E+02
CO_2(0,1,1,4,1)+CO_2 → CO_2(1,1,1,3,2)+CO_2	5.60E+01	-4.03E+02	1.10E+03
CO_2(0,1,1,4,1)+CO_2 → CO_2(1,2,2,3,2)+CO_2	4.50E+01	-2.54E+02	6.78E+02
CO_2(0,1,1,4,1)+CO_2 → CO_2(2,0,0,3,3)+CO_2	4.50E+01	-2.54E+02	6.78E+02
CO_2(0,1,1,5,1)+CO_2 → CO_2(0,0,0,5,1)+CO_2	3.83E+01	-1.77E+02	4.51E+02
CO_2(0,1,1,5,1)+CO_2 → CO_2(0,2,2,4,1)+CO_2	5.55E+01	-4.03E+02	8.43E+02
CO_2(0,1,1,5,1)+CO_2 → CO_2(1,1,1,4,2)+CO_2	5.62E+01	-4.02E+02	1.10E+03
CO_2(0,1,1,5,1)+CO_2 → CO_2(1,2,2,4,2)+CO_2	4.52E+01	-2.55E+02	6.76E+02
CO_2(0,1,1,5,1)+CO_2 → CO_2(2,0,0,4,3)+CO_2	4.52E+01	-2.55E+02	6.76E+02
CO_2(0,2,2,0,1)+CO_2 → CO_2(0,1,1,0,1)+CO_2	3.90E+01	-1.77E+02	4.51E+02
CO_2(0,2,2,1,1)+CO_2 → CO_2(0,1,1,1,1)+CO_2	3.90E+01	-1.77E+02	4.51E+02
CO_2(0,2,2,1,1)+CO_2 → CO_2(0,3,3,0,1)+CO_2	5.39E+01	-4.07E+02	8.24E+02
CO_2(0,2,2,1,1)+CO_2 → CO_2(1,2,2,0,2)+CO_2	5.46E+01	-4.04E+02	1.10E+03
CO_2(0,2,2,1,1)+CO_2 → CO_2(1,3,3,0,2)+CO_2	4.36E+01	-2.52E+02	6.85E+02
CO_2(0,2,2,1,1)+CO_2 → CO_2(2,0,0,0,3)+CO_2	5.46E+01	-4.04E+02	1.10E+03
CO_2(0,2,2,1,1)+CO_2 → CO_2(2,1,1,0,3)+CO_2	4.36E+01	-2.52E+02	6.85E+02
CO_2(0,2,2,2,1)+CO_2 → CO_2(0,1,1,2,1)+CO_2	3.90E+01	-1.77E+02	4.51E+02
CO_2(0,2,2,2,1)+CO_2 → CO_2(0,3,3,1,1)+CO_2	5.46E+01	-4.06E+02	8.29E+02
CO_2(0,2,2,2,1)+CO_2 → CO_2(1,2,2,1,2)+CO_2	5.53E+01	-4.04E+02	1.10E+03
CO_2(0,2,2,2,1)+CO_2 → CO_2(1,3,3,1,2)+CO_2	4.43E+01	-2.53E+02	6.83E+02
CO_2(0,2,2,2,1)+CO_2 → CO_2(2,0,0,1,3)+CO_2	5.53E+01	-4.04E+02	1.10E+03
CO_2(0,2,2,2,1)+CO_2 → CO_2(2,1,1,1,3)+CO_2	4.43E+01	-2.53E+02	6.83E+02
CO_2(0,2,2,3,1)+CO_2 → CO_2(0,1,1,3,1)+CO_2	3.90E+01	-1.77E+02	4.51E+02
CO_2(0,2,2,3,1)+CO_2 → CO_2(0,3,3,2,1)+CO_2	5.50E+01	-4.05E+02	8.33E+02
CO_2(0,2,2,3,1)+CO_2 → CO_2(1,2,2,2,2)+CO_2	5.57E+01	-4.03E+02	1.10E+03
CO_2(0,2,2,3,1)+CO_2 → CO_2(1,3,3,2,2)+CO_2	4.47E+01	-2.53E+02	6.80E+02
CO_2(0,2,2,3,1)+CO_2 → CO_2(2,0,0,2,3)+CO_2	5.57E+01	-4.03E+02	1.10E+03
CO_2(0,2,2,3,1)+CO_2 → CO_2(2,1,1,2,3)+CO_2	4.47E+01	-2.53E+02	6.80E+02
CO_2(0,2,2,4,1)+CO_2 → CO_2(0,1,1,4,1)+CO_2	3.90E+01	-1.77E+02	4.51E+02
CO_2(0,2,2,4,1)+CO_2 → CO_2(0,3,3,3,1)+CO_2	5.52E+01	-4.04E+02	8.38E+02
CO_2(0,2,2,4,1)+CO_2 → CO_2(1,2,2,3,2)+CO_2	5.60E+01	-4.03E+02	1.10E+03
CO_2(0,2,2,4,1)+CO_2 → CO_2(1,3,3,3,2)+CO_2	4.50E+01	-2.54E+02	6.78E+02
CO_2(0,2,2,4,1)+CO_2 → CO_2(2,0,0,3,3)+CO_2	5.60E+01	-4.03E+02	1.10E+03
CO_2(0,2,2,4,1)+CO_2 → CO_2(2,1,1,3,3)+CO_2	4.50E+01	-2.54E+02	6.78E+02
CO_2(0,2,2,5,1)+CO_2 → CO_2(0,1,1,5,1)+CO_2	3.90E+01	-1.77E+02	4.51E+02
CO_2(0,2,2,5,1)+CO_2 → CO_2(0,3,3,4,1)+CO_2	5.55E+01	-4.03E+02	8.43E+02
CO_2(0,2,2,5,1)+CO_2 → CO_2(1,2,2,4,2)+CO_2	5.62E+01	-4.02E+02	1.10E+03

CO_2(0,2,2,5,1)+CO_2 → CO_2(1,3,3,4,2)+CO_2	4.52E+01	-2.55E+02	6.76E+02
CO_2(0,2,2,5,1)+CO_2 → CO_2(2,0,0,4,3)+CO_2	5.62E+01	-4.02E+02	1.10E+03
CO_2(0,2,2,5,1)+CO_2 → CO_2(2,1,1,4,3)+CO_2	4.52E+01	-2.55E+02	6.76E+02
CO_2(0,3,3,0,1)+CO_2 → CO_2(0,2,2,0,1)+CO_2	3.94E+01	-1.77E+02	4.51E+02
CO_2(0,3,3,0,1)+CO_2 → CO_2(1,0,0,0,2)+CO_2	3.15E+01	-1.71E+02	2.64E+02
CO_2(0,3,3,1,1)+CO_2 → CO_2(0,2,2,1,1)+CO_2	3.94E+01	-1.77E+02	4.51E+02
CO_2(0,3,3,1,1)+CO_2 → CO_2(0,4,4,0,1)+CO_2	5.39E+01	-4.07E+02	8.24E+02
CO_2(0,3,3,1,1)+CO_2 → CO_2(1,0,0,1,2)+CO_2	3.15E+01	-1.71E+02	2.64E+02
CO_2(0,3,3,1,1)+CO_2 → CO_2(1,3,3,0,2)+CO_2	5.46E+01	-4.04E+02	1.10E+03
CO_2(0,3,3,1,1)+CO_2 → CO_2(2,1,1,0,3)+CO_2	5.46E+01	-4.04E+02	1.10E+03
CO_2(0,3,3,2,1)+CO_2 → CO_2(0,2,2,2,1)+CO_2	3.94E+01	-1.77E+02	4.51E+02
CO_2(0,3,3,2,1)+CO_2 → CO_2(0,4,4,1,1)+CO_2	5.46E+01	-4.06E+02	8.29E+02
CO_2(0,3,3,2,1)+CO_2 → CO_2(1,0,0,2,2)+CO_2	3.15E+01	-1.71E+02	2.64E+02
CO_2(0,3,3,2,1)+CO_2 → CO_2(1,3,3,1,2)+CO_2	5.53E+01	-4.04E+02	1.10E+03
CO_2(0,3,3,2,1)+CO_2 → CO_2(2,1,1,1,3)+CO_2	5.53E+01	-4.04E+02	1.10E+03
CO_2(0,3,3,3,1)+CO_2 → CO_2(0,2,2,3,1)+CO_2	3.94E+01	-1.77E+02	4.51E+02
CO_2(0,3,3,3,1)+CO_2 → CO_2(0,4,4,2,1)+CO_2	5.50E+01	-4.05E+02	8.33E+02
CO_2(0,3,3,3,1)+CO_2 → CO_2(1,0,0,3,2)+CO_2	3.15E+01	-1.71E+02	2.64E+02
CO_2(0,3,3,3,1)+CO_2 → CO_2(1,3,3,2,2)+CO_2	5.57E+01	-4.03E+02	1.10E+03
CO_2(0,3,3,3,1)+CO_2 → CO_2(2,1,1,2,3)+CO_2	5.57E+01	-4.03E+02	1.10E+03
CO_2(0,3,3,4,1)+CO_2 → CO_2(0,2,2,4,1)+CO_2	3.94E+01	-1.77E+02	4.51E+02
CO_2(0,3,3,4,1)+CO_2 → CO_2(0,4,4,3,1)+CO_2	5.52E+01	-4.04E+02	8.38E+02
CO_2(0,3,3,4,1)+CO_2 → CO_2(1,0,0,4,2)+CO_2	3.15E+01	-1.71E+02	2.64E+02
CO_2(0,3,3,4,1)+CO_2 → CO_2(1,3,3,3,2)+CO_2	5.60E+01	-4.03E+02	1.10E+03
CO_2(0,3,3,4,1)+CO_2 → CO_2(2,1,1,3,3)+CO_2	5.60E+01	-4.03E+02	1.10E+03
CO_2(0,3,3,5,1)+CO_2 → CO_2(0,2,2,5,1)+CO_2	3.94E+01	-1.77E+02	4.51E+02
CO_2(0,3,3,5,1)+CO_2 → CO_2(0,4,4,4,1)+CO_2	5.55E+01	-4.03E+02	8.43E+02
CO_2(0,3,3,5,1)+CO_2 → CO_2(1,0,0,5,2)+CO_2	3.15E+01	-1.71E+02	2.64E+02
CO_2(0,3,3,5,1)+CO_2 → CO_2(1,3,3,4,2)+CO_2	5.62E+01	-4.02E+02	1.10E+03
CO_2(0,3,3,5,1)+CO_2 → CO_2(2,1,1,4,3)+CO_2	5.62E+01	-4.02E+02	1.10E+03
CO_2(0,4,4,0,1)+CO_2 → CO_2(0,3,3,0,1)+CO_2	3.97E+01	-1.77E+02	4.51E+02
CO_2(0,4,4,0,1)+CO_2 → CO_2(1,1,1,0,2)+CO_2	3.01E+01	-1.71E+02	2.64E+02
CO_2(0,4,4,1,1)+CO_2 → CO_2(0,3,3,1,1)+CO_2	3.97E+01	-1.77E+02	4.51E+02
CO_2(0,4,4,1,1)+CO_2 → CO_2(0,5,5,0,1)+CO_2	5.39E+01	-4.07E+02	8.24E+02
CO_2(0,4,4,1,1)+CO_2 → CO_2(1,1,1,1,2)+CO_2	3.01E+01	-1.71E+02	2.64E+02
CO_2(0,4,4,2,1)+CO_2 → CO_2(0,3,3,2,1)+CO_2	3.97E+01	-1.77E+02	4.51E+02
CO_2(0,4,4,2,1)+CO_2 → CO_2(0,5,5,1,1)+CO_2	5.46E+01	-4.06E+02	8.29E+02

CO_2(0,4,4,2,1)+CO_2 → CO_2(1,1,1,2,2)+CO_2	3.01E+01	-1.71E+02	2.64E+02
CO_2(0,4,4,3,1)+CO_2 → CO_2(0,3,3,3,1)+CO_2	3.97E+01	-1.77E+02	4.51E+02
CO_2(0,4,4,3,1)+CO_2 → CO_2(0,5,5,2,1)+CO_2	5.50E+01	-4.05E+02	8.33E+02
CO_2(0,4,4,3,1)+CO_2 → CO_2(1,1,1,3,2)+CO_2	3.01E+01	-1.71E+02	2.64E+02
CO_2(0,4,4,4,1)+CO_2 → CO_2(0,3,3,4,1)+CO_2	3.97E+01	-1.77E+02	4.51E+02
CO_2(0,4,4,4,1)+CO_2 → CO_2(0,5,5,3,1)+CO_2	5.52E+01	-4.04E+02	8.38E+02
CO_2(0,4,4,4,1)+CO_2 → CO_2(1,1,1,4,2)+CO_2	3.01E+01	-1.71E+02	2.64E+02
CO_2(0,4,4,5,1)+CO_2 → CO_2(0,3,3,5,1)+CO_2	3.97E+01	-1.77E+02	4.51E+02
CO_2(0,4,4,5,1)+CO_2 → CO_2(0,5,5,4,1)+CO_2	5.55E+01	-4.03E+02	8.43E+02
CO_2(0,4,4,5,1)+CO_2 → CO_2(1,1,1,5,2)+CO_2	3.01E+01	-1.71E+02	2.64E+02
CO_2(0,5,5,0,1)+CO_2 → CO_2(0,4,4,0,1)+CO_2	3.99E+01	-1.77E+02	4.51E+02
CO_2(0,5,5,1,1)+CO_2 → CO_2(0,4,4,1,1)+CO_2	3.99E+01	-1.77E+02	4.51E+02
CO_2(0,5,5,2,1)+CO_2 → CO_2(0,4,4,2,1)+CO_2	3.99E+01	-1.77E+02	4.51E+02
CO_2(0,5,5,3,1)+CO_2 → CO_2(0,4,4,3,1)+CO_2	3.99E+01	-1.77E+02	4.51E+02
CO_2(0,5,5,4,1)+CO_2 → CO_2(0,4,4,4,1)+CO_2	3.99E+01	-1.77E+02	4.51E+02
CO_2(0,5,5,5,1)+CO_2 → CO_2(0,4,4,5,1)+CO_2	3.99E+01	-1.77E+02	4.51E+02
CO_2(1,0,0,0,2)+CO_2 → CO_2(0,0,0,0,1)+CO_2	3.41E+01	-1.37E+02	0.00E+00
CO_2(1,0,0,0,2)+CO_2 → CO_2(0,1,1,0,1)+CO_2	3.93E+01	-1.77E+02	4.51E+02
CO_2(1,0,0,0,2)+CO_2 → CO_2(0,2,2,0,1)+CO_2	3.65E+01	-8.89E+01	2.26E+02
CO_2(1,0,0,1,2)+CO_2 → CO_2(0,0,0,1,1)+CO_2	3.41E+01	-1.37E+02	0.00E+00
CO_2(1,0,0,1,2)+CO_2 → CO_2(0,1,1,1,1)+CO_2	3.93E+01	-1.77E+02	4.51E+02
CO_2(1,0,0,1,2)+CO_2 → CO_2(0,2,2,1,1)+CO_2	3.65E+01	-8.89E+01	2.26E+02
CO_2(1,0,0,2,2)+CO_2 → CO_2(0,0,0,2,1)+CO_2	3.41E+01	-1.37E+02	0.00E+00
CO_2(1,0,0,2,2)+CO_2 → CO_2(0,1,1,2,1)+CO_2	3.93E+01	-1.77E+02	4.51E+02
CO_2(1,0,0,2,2)+CO_2 → CO_2(0,2,2,2,1)+CO_2	3.65E+01	-8.89E+01	2.26E+02
CO_2(1,0,0,3,2)+CO_2 → CO_2(0,0,0,3,1)+CO_2	3.41E+01	-1.37E+02	0.00E+00
CO_2(1,0,0,3,2)+CO_2 → CO_2(0,1,1,3,1)+CO_2	3.93E+01	-1.77E+02	4.51E+02
CO_2(1,0,0,3,2)+CO_2 → CO_2(0,2,2,3,1)+CO_2	3.65E+01	-8.89E+01	2.26E+02
CO_2(1,0,0,4,2)+CO_2 → CO_2(0,0,0,4,1)+CO_2	3.41E+01	-1.37E+02	0.00E+00
CO_2(1,0,0,4,2)+CO_2 → CO_2(0,1,1,4,1)+CO_2	3.93E+01	-1.77E+02	4.51E+02
CO_2(1,0,0,4,2)+CO_2 → CO_2(0,2,2,4,1)+CO_2	3.65E+01	-8.89E+01	2.26E+02
CO_2(1,0,0,5,2)+CO_2 → CO_2(0,0,0,5,1)+CO_2	3.41E+01	-1.37E+02	0.00E+00
CO_2(1,0,0,5,2)+CO_2 → CO_2(0,1,1,5,1)+CO_2	3.93E+01	-1.77E+02	4.51E+02
CO_2(1,0,0,5,2)+CO_2 → CO_2(0,2,2,5,1)+CO_2	3.65E+01	-8.89E+01	2.26E+02
CO_2(1,1,1,0,2)+CO_2 → CO_2(0,1,1,0,1)+CO_2	3.41E+01	-1.37E+02	0.00E+00
CO_2(1,1,1,0,2)+CO_2 → CO_2(0,2,2,0,1)+CO_2	3.94E+01	-1.77E+02	4.51E+02
CO_2(1,1,1,0,2)+CO_2 → CO_2(0,3,3,0,1)+CO_2	3.72E+01	-8.93E+01	2.27E+02

CO_2(1,1,1,0,2)+CO_2 → CO_2(1,0,0,0,2)+CO_2	3.97E+01	-1.77E+02	4.51E+02
CO_2(1,1,1,1,2)+CO_2 → CO_2(0,1,1,1,1)+CO_2	3.41E+01	-1.37E+02	0.00E+00
CO_2(1,1,1,1,2)+CO_2 → CO_2(0,2,2,1,1)+CO_2	3.94E+01	-1.77E+02	4.51E+02
CO_2(1,1,1,1,2)+CO_2 → CO_2(0,3,3,1,1)+CO_2	3.72E+01	-8.93E+01	2.27E+02
CO_2(1,1,1,1,2)+CO_2 → CO_2(1,0,0,1,2)+CO_2	3.97E+01	-1.77E+02	4.51E+02
CO_2(1,1,1,2,2)+CO_2 → CO_2(0,1,1,2,1)+CO_2	3.41E+01	-1.37E+02	0.00E+00
CO_2(1,1,1,2,2)+CO_2 → CO_2(0,2,2,2,1)+CO_2	3.94E+01	-1.77E+02	4.51E+02
CO_2(1,1,1,2,2)+CO_2 → CO_2(0,3,3,2,1)+CO_2	3.72E+01	-8.93E+01	2.27E+02
CO_2(1,1,1,2,2)+CO_2 → CO_2(1,0,0,2,2)+CO_2	3.97E+01	-1.77E+02	4.51E+02
CO_2(1,1,1,3,2)+CO_2 → CO_2(0,1,1,3,1)+CO_2	3.41E+01	-1.37E+02	0.00E+00
CO_2(1,1,1,3,2)+CO_2 → CO_2(0,2,2,3,1)+CO_2	3.94E+01	-1.77E+02	4.51E+02
CO_2(1,1,1,3,2)+CO_2 → CO_2(0,3,3,3,1)+CO_2	3.72E+01	-8.93E+01	2.27E+02
CO_2(1,1,1,3,2)+CO_2 → CO_2(1,0,0,3,2)+CO_2	3.97E+01	-1.77E+02	4.51E+02
CO_2(1,1,1,4,2)+CO_2 → CO_2(0,1,1,4,1)+CO_2	3.41E+01	-1.37E+02	0.00E+00
CO_2(1,1,1,4,2)+CO_2 → CO_2(0,2,2,4,1)+CO_2	3.94E+01	-1.77E+02	4.51E+02
CO_2(1,1,1,4,2)+CO_2 → CO_2(0,3,3,4,1)+CO_2	3.72E+01	-8.93E+01	2.27E+02
CO_2(1,1,1,4,2)+CO_2 → CO_2(1,0,0,4,2)+CO_2	3.97E+01	-1.77E+02	4.51E+02
CO_2(1,1,1,5,2)+CO_2 → CO_2(0,1,1,5,1)+CO_2	3.41E+01	-1.37E+02	0.00E+00
CO_2(1,1,1,5,2)+CO_2 → CO_2(0,2,2,5,1)+CO_2	3.94E+01	-1.77E+02	4.51E+02
CO_2(1,1,1,5,2)+CO_2 → CO_2(0,3,3,5,1)+CO_2	3.72E+01	-8.93E+01	2.27E+02
CO_2(1,1,1,5,2)+CO_2 → CO_2(1,0,0,5,2)+CO_2	3.97E+01	-1.77E+02	4.51E+02
CO_2(1,2,2,0,2)+CO_2 → CO_2(0,3,3,0,1)+CO_2	3.97E+01	-1.77E+02	4.51E+02
CO_2(1,2,2,0,2)+CO_2 → CO_2(0,4,4,0,1)+CO_2	3.78E+01	-9.04E+01	2.30E+02
CO_2(1,2,2,0,2)+CO_2 → CO_2(1,1,1,0,2)+CO_2	4.01E+01	-1.77E+02	4.51E+02
CO_2(1,2,2,0,2)+CO_2 → CO_2(2,0,0,0,3)+CO_2	3.81E+01	-9.04E+01	2.30E+02
CO_2(1,2,2,1,2)+CO_2 → CO_2(0,3,3,1,1)+CO_2	3.97E+01	-1.77E+02	4.51E+02
CO_2(1,2,2,1,2)+CO_2 → CO_2(0,4,4,1,1)+CO_2	3.78E+01	-9.04E+01	2.30E+02
CO_2(1,2,2,1,2)+CO_2 → CO_2(1,1,1,1,2)+CO_2	4.01E+01	-1.77E+02	4.51E+02
CO_2(1,2,2,1,2)+CO_2 → CO_2(2,0,0,1,3)+CO_2	3.81E+01	-9.04E+01	2.30E+02
CO_2(1,2,2,2,2)+CO_2 → CO_2(0,3,3,2,1)+CO_2	3.97E+01	-1.77E+02	4.51E+02
CO_2(1,2,2,2,2)+CO_2 → CO_2(0,4,4,2,1)+CO_2	3.78E+01	-9.04E+01	2.30E+02
CO_2(1,2,2,2,2)+CO_2 → CO_2(1,1,1,2,2)+CO_2	4.01E+01	-1.77E+02	4.51E+02
CO_2(1,2,2,2,2)+CO_2 → CO_2(2,0,0,2,3)+CO_2	3.81E+01	-9.04E+01	2.30E+02
CO_2(1,2,2,3,2)+CO_2 → CO_2(0,3,3,3,1)+CO_2	3.97E+01	-1.77E+02	4.51E+02
CO_2(1,2,2,3,2)+CO_2 → CO_2(0,4,4,3,1)+CO_2	3.78E+01	-9.04E+01	2.30E+02
CO_2(1,2,2,3,2)+CO_2 → CO_2(1,1,1,3,2)+CO_2	4.01E+01	-1.77E+02	4.51E+02
CO_2(1,2,2,3,2)+CO_2 → CO_2(2,0,0,3,3)+CO_2	3.81E+01	-9.04E+01	2.30E+02

CO_2(1,2,2,4,2)+CO_2 → CO_2(0,3,3,4,1)+CO_2	3.97E+01	-1.77E+02	4.51E+02
CO_2(1,2,2,4,2)+CO_2 → CO_2(0,4,4,4,1)+CO_2	3.78E+01	-9.04E+01	2.30E+02
CO_2(1,2,2,4,2)+CO_2 → CO_2(1,1,1,4,2)+CO_2	4.01E+01	-1.77E+02	4.51E+02
CO_2(1,2,2,4,2)+CO_2 → CO_2(2,0,0,4,3)+CO_2	3.81E+01	-9.04E+01	2.30E+02
CO_2(1,2,2,5,2)+CO_2 → CO_2(0,3,3,5,1)+CO_2	3.97E+01	-1.77E+02	4.51E+02
CO_2(1,2,2,5,2)+CO_2 → CO_2(0,4,4,5,1)+CO_2	3.78E+01	-9.04E+01	2.30E+02
CO_2(1,2,2,5,2)+CO_2 → CO_2(1,1,1,5,2)+CO_2	4.01E+01	-1.77E+02	4.51E+02
CO_2(1,2,2,5,2)+CO_2 → CO_2(2,0,0,5,3)+CO_2	3.81E+01	-9.04E+01	2.30E+02
CO_2(1,3,3,0,2)+CO_2 → CO_2(0,3,3,0,1)+CO_2	3.41E+01	-1.37E+02	0.00E+00
CO_2(1,3,3,0,2)+CO_2 → CO_2(0,4,4,0,1)+CO_2	3.99E+01	-1.77E+02	4.51E+02
CO_2(1,3,3,0,2)+CO_2 → CO_2(0,5,5,0,1)+CO_2	3.80E+01	-8.89E+01	2.26E+02
CO_2(1,3,3,0,2)+CO_2 → CO_2(1,2,2,0,2)+CO_2	4.04E+01	-1.77E+02	4.51E+02
CO_2(1,3,3,1,2)+CO_2 → CO_2(0,3,3,1,1)+CO_2	3.41E+01	-1.37E+02	0.00E+00
CO_2(1,3,3,1,2)+CO_2 → CO_2(0,4,4,1,1)+CO_2	3.99E+01	-1.77E+02	4.51E+02
CO_2(1,3,3,1,2)+CO_2 → CO_2(0,5,5,1,1)+CO_2	3.80E+01	-8.89E+01	2.26E+02
CO_2(1,3,3,1,2)+CO_2 → CO_2(1,2,2,1,2)+CO_2	4.04E+01	-1.77E+02	4.51E+02
CO_2(1,3,3,2,2)+CO_2 → CO_2(0,3,3,2,1)+CO_2	3.41E+01	-1.37E+02	0.00E+00
CO_2(1,3,3,2,2)+CO_2 → CO_2(0,4,4,2,1)+CO_2	3.99E+01	-1.77E+02	4.51E+02
CO_2(1,3,3,2,2)+CO_2 → CO_2(0,5,5,2,1)+CO_2	3.80E+01	-8.89E+01	2.26E+02
CO_2(1,3,3,2,2)+CO_2 → CO_2(1,2,2,2,2)+CO_2	4.04E+01	-1.77E+02	4.51E+02
CO_2(1,3,3,3,2)+CO_2 → CO_2(0,3,3,3,1)+CO_2	3.41E+01	-1.37E+02	0.00E+00
CO_2(1,3,3,3,2)+CO_2 → CO_2(0,4,4,3,1)+CO_2	3.99E+01	-1.77E+02	4.51E+02
CO_2(1,3,3,3,2)+CO_2 → CO_2(0,5,5,3,1)+CO_2	3.80E+01	-8.89E+01	2.26E+02
CO_2(1,3,3,3,2)+CO_2 → CO_2(1,2,2,3,2)+CO_2	4.04E+01	-1.77E+02	4.51E+02
CO_2(1,3,3,4,2)+CO_2 → CO_2(0,3,3,4,1)+CO_2	3.41E+01	-1.37E+02	0.00E+00
CO_2(1,3,3,4,2)+CO_2 → CO_2(0,4,4,4,1)+CO_2	3.99E+01	-1.77E+02	4.51E+02
CO_2(1,3,3,4,2)+CO_2 → CO_2(0,5,5,4,1)+CO_2	3.80E+01	-8.89E+01	2.26E+02
CO_2(1,3,3,4,2)+CO_2 → CO_2(1,2,2,4,2)+CO_2	4.04E+01	-1.77E+02	4.51E+02
CO_2(1,3,3,5,2)+CO_2 → CO_2(0,3,3,5,1)+CO_2	3.41E+01	-1.37E+02	0.00E+00
CO_2(1,3,3,5,2)+CO_2 → CO_2(0,4,4,5,1)+CO_2	3.99E+01	-1.77E+02	4.51E+02
CO_2(1,3,3,5,2)+CO_2 → CO_2(0,5,5,5,1)+CO_2	3.80E+01	-8.89E+01	2.26E+02
CO_2(1,3,3,5,2)+CO_2 → CO_2(1,2,2,5,2)+CO_2	4.04E+01	-1.77E+02	4.51E+02
CO_2(2,0,0,0,3)+CO_2 → CO_2(0,0,0,1,1)+CO_2	3.00E+01	-1.08E+02	1.65E+02
CO_2(2,0,0,0,3)+CO_2 → CO_2(0,2,2,0,1)+CO_2	3.92E+01	-2.71E+02	4.38E+02
CO_2(2,0,0,0,3)+CO_2 → CO_2(0,3,3,0,1)+CO_2	3.02E+01	-1.71E+02	2.64E+02
CO_2(2,0,0,0,3)+CO_2 → CO_2(1,0,0,0,2)+CO_2	4.37E+01	-2.72E+02	4.37E+02
CO_2(2,0,0,0,3)+CO_2 → CO_2(1,1,1,0,2)+CO_2	4.01E+01	-1.77E+02	4.51E+02

$CO_2(2,0,0,1,3)+CO_2 \rightarrow CO_2(0,0,0,2,1)+CO_2$	3.00E+01	-1.08E+02	1.65E+02
$CO_2(2,0,0,1,3)+CO_2 \rightarrow CO_2(0,2,2,1,1)+CO_2$	3.92E+01	-2.71E+02	4.38E+02
$CO_2(2,0,0,1,3)+CO_2 \rightarrow CO_2(0,3,3,1,1)+CO_2$	3.02E+01	-1.71E+02	2.64E+02
$CO_2(2,0,0,1,3)+CO_2 \rightarrow CO_2(1,0,0,1,2)+CO_2$	4.37E+01	-2.72E+02	4.37E+02
$CO_2(2,0,0,1,3)+CO_2 \rightarrow CO_2(1,1,1,1,2)+CO_2$	4.01E+01	-1.77E+02	4.51E+02
$CO_2(2,0,0,2,3)+CO_2 \rightarrow CO_2(0,0,0,3,1)+CO_2$	3.00E+01	-1.08E+02	1.65E+02
$CO_2(2,0,0,2,3)+CO_2 \rightarrow CO_2(0,2,2,2,1)+CO_2$	3.92E+01	-2.71E+02	4.38E+02
$CO_2(2,0,0,2,3)+CO_2 \rightarrow CO_2(0,3,3,2,1)+CO_2$	3.02E+01	-1.71E+02	2.64E+02
$CO_2(2,0,0,2,3)+CO_2 \rightarrow CO_2(1,0,0,2,2)+CO_2$	4.37E+01	-2.72E+02	4.37E+02
$CO_2(2,0,0,2,3)+CO_2 \rightarrow CO_2(1,1,1,2,2)+CO_2$	4.01E+01	-1.77E+02	4.51E+02
$CO_2(2,0,0,3,3)+CO_2 \rightarrow CO_2(0,0,0,4,1)+CO_2$	3.00E+01	-1.08E+02	1.65E+02
$CO_2(2,0,0,3,3)+CO_2 \rightarrow CO_2(0,2,2,3,1)+CO_2$	3.92E+01	-2.71E+02	4.38E+02
$CO_2(2,0,0,3,3)+CO_2 \rightarrow CO_2(0,3,3,3,1)+CO_2$	3.02E+01	-1.71E+02	2.64E+02
$CO_2(2,0,0,3,3)+CO_2 \rightarrow CO_2(1,0,0,3,2)+CO_2$	4.37E+01	-2.72E+02	4.37E+02
$CO_2(2,0,0,3,3)+CO_2 \rightarrow CO_2(1,1,1,3,2)+CO_2$	4.01E+01	-1.77E+02	4.51E+02
$CO_2(2,0,0,4,3)+CO_2 \rightarrow CO_2(0,0,0,5,1)+CO_2$	3.00E+01	-1.08E+02	1.65E+02
$CO_2(2,0,0,4,3)+CO_2 \rightarrow CO_2(0,2,2,4,1)+CO_2$	3.92E+01	-2.71E+02	4.38E+02
$CO_2(2,0,0,4,3)+CO_2 \rightarrow CO_2(0,3,3,4,1)+CO_2$	3.02E+01	-1.71E+02	2.64E+02
$CO_2(2,0,0,4,3)+CO_2 \rightarrow CO_2(1,0,0,4,2)+CO_2$	4.37E+01	-2.72E+02	4.37E+02
$CO_2(2,0,0,4,3)+CO_2 \rightarrow CO_2(1,1,1,4,2)+CO_2$	4.01E+01	-1.77E+02	4.51E+02
$CO_2(2,0,0,5,3)+CO_2 \rightarrow CO_2(0,2,2,5,1)+CO_2$	3.92E+01	-2.71E+02	4.38E+02
$CO_2(2,0,0,5,3)+CO_2 \rightarrow CO_2(0,3,3,5,1)+CO_2$	3.02E+01	-1.71E+02	2.64E+02
$CO_2(2,0,0,5,3)+CO_2 \rightarrow CO_2(1,0,0,5,2)+CO_2$	4.37E+01	-2.72E+02	4.37E+02
$CO_2(2,0,0,5,3)+CO_2 \rightarrow CO_2(1,1,1,5,2)+CO_2$	4.01E+01	-1.77E+02	4.51E+02
$CO_2(2,1,1,0,3)+CO_2 \rightarrow CO_2(1,1,1,0,2)+CO_2$	3.52E+01	-1.37E+02	0.00E+00
$CO_2(2,1,1,0,3)+CO_2 \rightarrow CO_2(1,2,2,0,2)+CO_2$	4.04E+01	-1.77E+02	4.51E+02
$CO_2(2,1,1,0,3)+CO_2 \rightarrow CO_2(1,3,3,0,2)+CO_2$	3.84E+01	-8.89E+01	2.26E+02
$CO_2(2,1,1,0,3)+CO_2 \rightarrow CO_2(2,0,0,0,3)+CO_2$	4.05E+01	-1.77E+02	4.51E+02
$CO_2(2,1,1,1,3)+CO_2 \rightarrow CO_2(1,1,1,1,2)+CO_2$	3.52E+01	-1.37E+02	0.00E+00
$CO_2(2,1,1,1,3)+CO_2 \rightarrow CO_2(1,2,2,1,2)+CO_2$	4.04E+01	-1.77E+02	4.51E+02
$CO_2(2,1,1,1,3)+CO_2 \rightarrow CO_2(1,3,3,1,2)+CO_2$	3.84E+01	-8.89E+01	2.26E+02
$CO_2(2,1,1,1,3)+CO_2 \rightarrow CO_2(2,0,0,1,3)+CO_2$	4.05E+01	-1.77E+02	4.51E+02
$CO_2(2,1,1,2,3)+CO_2 \rightarrow CO_2(1,1,1,2,2)+CO_2$	3.52E+01	-1.37E+02	0.00E+00
$CO_2(2,1,1,2,3)+CO_2 \rightarrow CO_2(1,2,2,2,2)+CO_2$	4.04E+01	-1.77E+02	4.51E+02
$CO_2(2,1,1,2,3)+CO_2 \rightarrow CO_2(1,3,3,2,2)+CO_2$	3.84E+01	-8.89E+01	2.26E+02
$CO_2(2,1,1,2,3)+CO_2 \rightarrow CO_2(2,0,0,2,3)+CO_2$	4.05E+01	-1.77E+02	4.51E+02
$CO_2(2,1,1,3,3)+CO_2 \rightarrow CO_2(1,1,1,3,2)+CO_2$	3.52E+01	-1.37E+02	0.00E+00

CO_2(2,1,1,3,3)+CO_2 → CO_2(1,2,2,3,2)+CO_2	4.04E+01	-1.77E+02	4.51E+02
CO_2(2,1,1,3,3)+CO_2 → CO_2(1,3,3,3,2)+CO_2	3.84E+01	-8.89E+01	2.26E+02
CO_2(2,1,1,3,3)+CO_2 → CO_2(2,0,0,3,3)+CO_2	4.05E+01	-1.77E+02	4.51E+02
CO_2(2,1,1,4,3)+CO_2 → CO_2(1,1,1,4,2)+CO_2	3.52E+01	-1.37E+02	0.00E+00
CO_2(2,1,1,4,3)+CO_2 → CO_2(1,2,2,4,2)+CO_2	4.04E+01	-1.77E+02	4.51E+02
CO_2(2,1,1,4,3)+CO_2 → CO_2(1,3,3,4,2)+CO_2	3.84E+01	-8.89E+01	2.26E+02
CO_2(2,1,1,4,3)+CO_2 → CO_2(2,0,0,4,3)+CO_2	4.05E+01	-1.77E+02	4.51E+02
CO_2(2,1,1,5,3)+CO_2 → CO_2(1,1,1,5,2)+CO_2	3.52E+01	-1.37E+02	0.00E+00
CO_2(2,1,1,5,3)+CO_2 → CO_2(1,2,2,5,2)+CO_2	4.04E+01	-1.77E+02	4.51E+02
CO_2(2,1,1,5,3)+CO_2 → CO_2(1,3,3,5,2)+CO_2	3.84E+01	-8.89E+01	2.26E+02
CO_2(2,1,1,5,3)+CO_2 → CO_2(2,0,0,5,3)+CO_2	4.05E+01	-1.77E+02	4.51E+02

Table A.4: CO_2 quenched by CO_2

A.2 Vibration-Vibration (V-V) rate coefficients

A.2.1 V-V exchanges $N_2(v)$ + $N_2(w) \rightleftharpoons N_2(v-1)$ + $N_2(w+1)$

Expression:

$$k(v, T_g) = A(v) \exp^{B(v)T_g^{-1/3} + C(v)T_g^{-2/3}}$$

Table A.5 for A, B and C:

Reaction	A	B	C
N_2(0) + N_2(1) → N_2(1) + N_2(0)	3.93E-11	-8.53E+01	1.94E+02
N_2(1) + N_2(1) → N_2(2) + N_2(0)	8.29E-11	-8.57E+01	1.89E+02
N_2(2) + N_2(1) → N_2(3) + N_2(0)	1.31E-10	-8.60E+01	1.83E+02
N_2(3) + N_2(1) → N_2(4) + N_2(0)	1.85E-10	-8.63E+01	1.75E+02
N_2(4) + N_2(1) → N_2(5) + N_2(0)	2.47E-10	-8.67E+01	1.67E+02
N_2(5) + N_2(1) → N_2(6) + N_2(0)	3.20E-10	-8.73E+01	1.60E+02
N_2(6) + N_2(1) → N_2(7) + N_2(0)	4.05E-10	-8.80E+01	1.52E+02
N_2(7) + N_2(1) → N_2(8) + N_2(0)	5.07E-10	-8.88E+01	1.46E+02
N_2(8) + N_2(1) → N_2(9) + N_2(0)	6.29E-10	-8.98E+01	1.39E+02
N_2(9) + N_2(1) → N_2(10) + N_2(0)	7.21E-10	-9.08E+01	1.33E+02
N_2(10) + N_2(1) → N_2(11) + N_2(0)	8.27E-10	-9.19E+01	1.27E+02
N_2(11) + N_2(1) → N_2(12) + N_2(0)	9.42E-10	-9.31E+01	1.21E+02
N_2(12) + N_2(1) → N_2(13) + N_2(0)	1.07E-09	-9.43E+01	1.16E+02
N_2(13) + N_2(1) → N_2(14) + N_2(0)	1.20E-09	-9.55E+01	1.11E+02
N_2(14) + N_2(1) → N_2(15) + N_2(0)	1.34E-09	-9.68E+01	1.06E+02

$N_2(15) + N_2(1) \rightarrow N_2(16) + N_2(0)$	1.49E-09	-9.81E+01	1.01E+02
$N_2(16) + N_2(1) \rightarrow N_2(17) + N_2(0)$	1.65E-09	-9.94E+01	9.59E+01
$N_2(17) + N_2(1) \rightarrow N_2(18) + N_2(0)$	1.82E-09	-1.01E+02	9.11E+01
$N_2(18) + N_2(1) \rightarrow N_2(19) + N_2(0)$	2.00E-09	-1.02E+02	8.64E+01
$N_2(19) + N_2(1) \rightarrow N_2(20) + N_2(0)$	2.18E-09	-1.03E+02	8.18E+01
$N_2(1) + N_2(2) \rightarrow N_2(2) + N_2(1)$	1.66E-10	-8.53E+01	1.94E+02
$N_2(2) + N_2(2) \rightarrow N_2(3) + N_2(1)$	2.63E-10	-8.57E+01	1.89E+02
$N_2(3) + N_2(2) \rightarrow N_2(4) + N_2(1)$	3.71E-10	-8.60E+01	1.83E+02
$N_2(4) + N_2(2) \rightarrow N_2(5) + N_2(1)$	4.92E-10	-8.63E+01	1.75E+02
$N_2(5) + N_2(2) \rightarrow N_2(6) + N_2(1)$	6.33E-10	-8.67E+01	1.67E+02
$N_2(6) + N_2(2) \rightarrow N_2(7) + N_2(1)$	7.98E-10	-8.73E+01	1.60E+02
$N_2(7) + N_2(2) \rightarrow N_2(8) + N_2(1)$	9.93E-10	-8.80E+01	1.52E+02
$N_2(8) + N_2(2) \rightarrow N_2(9) + N_2(1)$	1.23E-09	-8.88E+01	1.46E+02
$N_2(9) + N_2(2) \rightarrow N_2(10) + N_2(1)$	1.40E-09	-8.98E+01	1.39E+02
$N_2(10) + N_2(2) \rightarrow N_2(11) + N_2(1)$	1.61E-09	-9.08E+01	1.33E+02
$N_2(11) + N_2(2) \rightarrow N_2(12) + N_2(1)$	1.83E-09	-9.19E+01	1.27E+02
$N_2(12) + N_2(2) \rightarrow N_2(13) + N_2(1)$	2.07E-09	-9.31E+01	1.21E+02
$N_2(13) + N_2(2) \rightarrow N_2(14) + N_2(1)$	2.32E-09	-9.43E+01	1.16E+02
$N_2(14) + N_2(2) \rightarrow N_2(15) + N_2(1)$	2.60E-09	-9.55E+01	1.11E+02
$N_2(15) + N_2(2) \rightarrow N_2(16) + N_2(1)$	2.89E-09	-9.68E+01	1.06E+02
$N_2(16) + N_2(2) \rightarrow N_2(17) + N_2(1)$	3.20E-09	-9.81E+01	1.01E+02
$N_2(17) + N_2(2) \rightarrow N_2(18) + N_2(1)$	3.53E-09	-9.94E+01	9.59E+01
$N_2(18) + N_2(2) \rightarrow N_2(19) + N_2(1)$	3.87E-09	-1.01E+02	9.11E+01
$N_2(19) + N_2(2) \rightarrow N_2(20) + N_2(1)$	4.22E-09	-1.02E+02	8.64E+01
$N_2(2) + N_2(3) \rightarrow N_2(3) + N_2(2)$	3.96E-10	-8.53E+01	1.94E+02
$N_2(3) + N_2(3) \rightarrow N_2(4) + N_2(2)$	5.58E-10	-8.57E+01	1.89E+02
$N_2(4) + N_2(3) \rightarrow N_2(5) + N_2(2)$	7.39E-10	-8.60E+01	1.83E+02
$N_2(5) + N_2(3) \rightarrow N_2(6) + N_2(2)$	9.44E-10	-8.63E+01	1.75E+02
$N_2(6) + N_2(3) \rightarrow N_2(7) + N_2(2)$	1.18E-09	-8.67E+01	1.67E+02
$N_2(7) + N_2(3) \rightarrow N_2(8) + N_2(2)$	1.47E-09	-8.73E+01	1.60E+02
$N_2(8) + N_2(3) \rightarrow N_2(9) + N_2(2)$	1.80E-09	-8.80E+01	1.52E+02
$N_2(9) + N_2(3) \rightarrow N_2(10) + N_2(2)$	2.06E-09	-8.88E+01	1.46E+02
$N_2(10) + N_2(3) \rightarrow N_2(11) + N_2(2)$	2.35E-09	-8.98E+01	1.39E+02
$N_2(11) + N_2(3) \rightarrow N_2(12) + N_2(2)$	2.66E-09	-9.08E+01	1.33E+02
$N_2(12) + N_2(3) \rightarrow N_2(13) + N_2(2)$	3.00E-09	-9.19E+01	1.27E+02
$N_2(13) + N_2(3) \rightarrow N_2(14) + N_2(2)$	3.37E-09	-9.31E+01	1.21E+02
$N_2(14) + N_2(3) \rightarrow N_2(15) + N_2(2)$	3.77E-09	-9.43E+01	1.16E+02

$N_2(15) + N_2(3) \rightarrow N_2(16) + N_2(2)$	4.20E-09	-9.55E+01	1.11E+02
$N_2(16) + N_2(3) \rightarrow N_2(17) + N_2(2)$	4.65E-09	-9.68E+01	1.06E+02
$N_2(17) + N_2(3) \rightarrow N_2(18) + N_2(2)$	5.12E-09	-9.81E+01	1.01E+02
$N_2(18) + N_2(3) \rightarrow N_2(19) + N_2(2)$	5.61E-09	-9.94E+01	9.59E+01
$N_2(19) + N_2(3) \rightarrow N_2(20) + N_2(2)$	6.13E-09	-1.01E+02	9.11E+01
$N_2(3) + N_2(4) \rightarrow N_2(4) + N_2(3)$	7.46E-10	-8.53E+01	1.94E+02
$N_2(4) + N_2(4) \rightarrow N_2(5) + N_2(3)$	9.90E-10	-8.57E+01	1.89E+02
$N_2(5) + N_2(4) \rightarrow N_2(6) + N_2(3)$	1.26E-09	-8.60E+01	1.83E+02
$N_2(6) + N_2(4) \rightarrow N_2(7) + N_2(3)$	1.57E-09	-8.63E+01	1.75E+02
$N_2(7) + N_2(4) \rightarrow N_2(8) + N_2(3)$	1.93E-09	-8.67E+01	1.67E+02
$N_2(8) + N_2(4) \rightarrow N_2(9) + N_2(3)$	2.37E-09	-8.73E+01	1.60E+02
$N_2(9) + N_2(4) \rightarrow N_2(10) + N_2(3)$	2.68E-09	-8.80E+01	1.52E+02
$N_2(10) + N_2(4) \rightarrow N_2(11) + N_2(3)$	3.05E-09	-8.88E+01	1.46E+02
$N_2(11) + N_2(4) \rightarrow N_2(12) + N_2(3)$	3.45E-09	-8.98E+01	1.39E+02
$N_2(12) + N_2(4) \rightarrow N_2(13) + N_2(3)$	3.89E-09	-9.08E+01	1.33E+02
$N_2(13) + N_2(4) \rightarrow N_2(14) + N_2(3)$	4.36E-09	-9.19E+01	1.27E+02
$N_2(14) + N_2(4) \rightarrow N_2(15) + N_2(3)$	4.87E-09	-9.31E+01	1.21E+02
$N_2(15) + N_2(4) \rightarrow N_2(16) + N_2(3)$	5.42E-09	-9.43E+01	1.16E+02
$N_2(16) + N_2(4) \rightarrow N_2(17) + N_2(3)$	6.00E-09	-9.55E+01	1.11E+02
$N_2(17) + N_2(4) \rightarrow N_2(18) + N_2(3)$	6.61E-09	-9.68E+01	1.06E+02
$N_2(18) + N_2(4) \rightarrow N_2(19) + N_2(3)$	7.25E-09	-9.81E+01	1.01E+02
$N_2(19) + N_2(4) \rightarrow N_2(20) + N_2(3)$	7.91E-09	-9.94E+01	9.59E+01
$N_2(4) + N_2(5) \rightarrow N_2(5) + N_2(4)$	1.24E-09	-8.53E+01	1.94E+02
$N_2(5) + N_2(5) \rightarrow N_2(6) + N_2(4)$	1.58E-09	-8.57E+01	1.89E+02
$N_2(6) + N_2(5) \rightarrow N_2(7) + N_2(4)$	1.96E-09	-8.60E+01	1.83E+02
$N_2(7) + N_2(5) \rightarrow N_2(8) + N_2(4)$	2.40E-09	-8.63E+01	1.75E+02
$N_2(8) + N_2(5) \rightarrow N_2(9) + N_2(4)$	2.93E-09	-8.67E+01	1.67E+02
$N_2(9) + N_2(5) \rightarrow N_2(10) + N_2(4)$	3.30E-09	-8.73E+01	1.60E+02
$N_2(10) + N_2(5) \rightarrow N_2(11) + N_2(4)$	3.74E-09	-8.80E+01	1.52E+02
$N_2(11) + N_2(5) \rightarrow N_2(12) + N_2(4)$	4.22E-09	-8.88E+01	1.46E+02
$N_2(12) + N_2(5) \rightarrow N_2(13) + N_2(4)$	4.74E-09	-8.98E+01	1.39E+02
$N_2(13) + N_2(5) \rightarrow N_2(14) + N_2(4)$	5.30E-09	-9.08E+01	1.33E+02
$N_2(14) + N_2(5) \rightarrow N_2(15) + N_2(4)$	5.91E-09	-9.19E+01	1.27E+02
$N_2(15) + N_2(5) \rightarrow N_2(16) + N_2(4)$	6.56E-09	-9.31E+01	1.21E+02
$N_2(16) + N_2(5) \rightarrow N_2(17) + N_2(4)$	7.26E-09	-9.43E+01	1.16E+02
$N_2(17) + N_2(5) \rightarrow N_2(18) + N_2(4)$	7.99E-09	-9.55E+01	1.11E+02
$N_2(18) + N_2(5) \rightarrow N_2(19) + N_2(4)$	8.77E-09	-9.68E+01	1.06E+02

$N_2(19) + N_2(5) \rightarrow N_2(20) + N_2(4)$	9.57E-09	-9.81E+01	1.01E+02
$N_2(5) + N_2(6) \rightarrow N_2(6) + N_2(5)$	1.90E-09	-8.53E+01	1.94E+02
$N_2(6) + N_2(6) \rightarrow N_2(7) + N_2(5)$	2.37E-09	-8.57E+01	1.89E+02
$N_2(7) + N_2(6) \rightarrow N_2(8) + N_2(5)$	2.89E-09	-8.60E+01	1.83E+02
$N_2(8) + N_2(6) \rightarrow N_2(9) + N_2(5)$	3.49E-09	-8.63E+01	1.75E+02
$N_2(9) + N_2(6) \rightarrow N_2(10) + N_2(5)$	3.92E-09	-8.67E+01	1.67E+02
$N_2(10) + N_2(6) \rightarrow N_2(11) + N_2(5)$	4.41E-09	-8.73E+01	1.60E+02
$N_2(11) + N_2(6) \rightarrow N_2(12) + N_2(5)$	4.96E-09	-8.80E+01	1.52E+02
$N_2(12) + N_2(6) \rightarrow N_2(13) + N_2(5)$	5.55E-09	-8.88E+01	1.46E+02
$N_2(13) + N_2(6) \rightarrow N_2(14) + N_2(5)$	6.19E-09	-8.98E+01	1.39E+02
$N_2(14) + N_2(6) \rightarrow N_2(15) + N_2(5)$	6.89E-09	-9.08E+01	1.33E+02
$N_2(15) + N_2(6) \rightarrow N_2(16) + N_2(5)$	7.64E-09	-9.19E+01	1.27E+02
$N_2(16) + N_2(6) \rightarrow N_2(17) + N_2(5)$	8.44E-09	-9.31E+01	1.21E+02
$N_2(17) + N_2(6) \rightarrow N_2(18) + N_2(5)$	9.29E-09	-9.43E+01	1.16E+02
$N_2(18) + N_2(6) \rightarrow N_2(19) + N_2(5)$	1.02E-08	-9.55E+01	1.11E+02
$N_2(19) + N_2(6) \rightarrow N_2(20) + N_2(5)$	1.11E-08	-9.68E+01	1.06E+02
$N_2(6) + N_2(7) \rightarrow N_2(7) + N_2(6)$	2.77E-09	-8.53E+01	1.94E+02
$N_2(7) + N_2(7) \rightarrow N_2(8) + N_2(6)$	3.39E-09	-8.57E+01	1.89E+02
$N_2(8) + N_2(7) \rightarrow N_2(9) + N_2(6)$	4.08E-09	-8.60E+01	1.83E+02
$N_2(9) + N_2(7) \rightarrow N_2(10) + N_2(6)$	4.55E-09	-8.63E+01	1.75E+02
$N_2(10) + N_2(7) \rightarrow N_2(11) + N_2(6)$	5.10E-09	-8.67E+01	1.67E+02
$N_2(11) + N_2(7) \rightarrow N_2(12) + N_2(6)$	5.69E-09	-8.73E+01	1.60E+02
$N_2(12) + N_2(7) \rightarrow N_2(13) + N_2(6)$	6.34E-09	-8.80E+01	1.52E+02
$N_2(13) + N_2(7) \rightarrow N_2(14) + N_2(6)$	7.05E-09	-8.88E+01	1.46E+02
$N_2(14) + N_2(7) \rightarrow N_2(15) + N_2(6)$	7.82E-09	-8.98E+01	1.39E+02
$N_2(15) + N_2(7) \rightarrow N_2(16) + N_2(6)$	1.62E-09	-5.77E+01	-2.02E+01
$N_2(16) + N_2(7) \rightarrow N_2(17) + N_2(6)$	9.55E-09	-9.19E+01	1.27E+02
$N_2(17) + N_2(7) \rightarrow N_2(18) + N_2(6)$	1.05E-08	-9.31E+01	1.21E+02
$N_2(18) + N_2(7) \rightarrow N_2(19) + N_2(6)$	1.15E-08	-9.43E+01	1.16E+02
$N_2(19) + N_2(7) \rightarrow N_2(20) + N_2(6)$	7.58E-10	-4.03E+01	-1.43E+02
$N_2(7) + N_2(8) \rightarrow N_2(8) + N_2(7)$	3.88E-09	-8.53E+01	1.94E+02
$N_2(8) + N_2(8) \rightarrow N_2(9) + N_2(7)$	4.68E-09	-8.57E+01	1.89E+02
$N_2(9) + N_2(8) \rightarrow N_2(10) + N_2(7)$	5.20E-09	-8.60E+01	1.83E+02
$N_2(10) + N_2(8) \rightarrow N_2(11) + N_2(7)$	5.79E-09	-8.63E+01	1.75E+02
$N_2(11) + N_2(8) \rightarrow N_2(12) + N_2(7)$	6.43E-09	-8.67E+01	1.67E+02
$N_2(12) + N_2(8) \rightarrow N_2(13) + N_2(7)$	7.13E-09	-8.73E+01	1.60E+02
$N_2(13) + N_2(8) \rightarrow N_2(14) + N_2(7)$	7.90E-09	-8.80E+01	1.52E+02

$N_2(14) + N_2(8) \rightarrow N_2(15) + N_2(7)$	8.73E-09	-8.88E+01	1.46E+02
$N_2(15) + N_2(8) \rightarrow N_2(16) + N_2(7)$	9.63E-09	-8.98E+01	1.39E+02
$N_2(16) + N_2(8) \rightarrow N_2(17) + N_2(7)$	1.06E-08	-9.08E+01	1.33E+02
$N_2(17) + N_2(8) \rightarrow N_2(18) + N_2(7)$	1.16E-08	-9.19E+01	1.27E+02
$N_2(18) + N_2(8) \rightarrow N_2(19) + N_2(7)$	1.27E-08	-9.31E+01	1.21E+02
$N_2(19) + N_2(8) \rightarrow N_2(20) + N_2(7)$	1.39E-08	-9.43E+01	1.16E+02
$N_2(8) + N_2(9) \rightarrow N_2(9) + N_2(8)$	5.28E-09	-8.53E+01	1.94E+02
$N_2(9) + N_2(9) \rightarrow N_2(10) + N_2(8)$	5.88E-09	-8.57E+01	1.89E+02
$N_2(10) + N_2(9) \rightarrow N_2(11) + N_2(8)$	6.52E-09	-8.60E+01	1.83E+02
$N_2(11) + N_2(9) \rightarrow N_2(12) + N_2(8)$	7.20E-09	-8.63E+01	1.75E+02
$N_2(12) + N_2(9) \rightarrow N_2(13) + N_2(8)$	7.94E-09	-8.67E+01	1.67E+02
$N_2(13) + N_2(9) \rightarrow N_2(14) + N_2(8)$	8.74E-09	-8.73E+01	1.60E+02
$N_2(14) + N_2(9) \rightarrow N_2(15) + N_2(8)$	9.62E-09	-8.80E+01	1.52E+02
$N_2(15) + N_2(9) \rightarrow N_2(16) + N_2(8)$	1.06E-08	-8.88E+01	1.46E+02
$N_2(16) + N_2(9) \rightarrow N_2(17) + N_2(8)$	1.16E-08	-8.98E+01	1.39E+02
$N_2(17) + N_2(9) \rightarrow N_2(18) + N_2(8)$	1.27E-08	-9.08E+01	1.33E+02
$N_2(18) + N_2(9) \rightarrow N_2(19) + N_2(8)$	1.39E-08	-9.19E+01	1.27E+02
$N_2(19) + N_2(9) \rightarrow N_2(20) + N_2(8)$	1.51E-08	-9.31E+01	1.21E+02
$N_2(9) + N_2(10) \rightarrow N_2(10) + N_2(9)$	6.55E-09	-8.53E+01	1.94E+02
$N_2(10) + N_2(10) \rightarrow N_2(11) + N_2(9)$	7.28E-09	-8.57E+01	1.89E+02
$N_2(11) + N_2(10) \rightarrow N_2(12) + N_2(9)$	8.01E-09	-8.60E+01	1.83E+02
$N_2(12) + N_2(10) \rightarrow N_2(13) + N_2(9)$	8.78E-09	-8.63E+01	1.75E+02
$N_2(13) + N_2(10) \rightarrow N_2(14) + N_2(9)$	9.61E-09	-8.67E+01	1.67E+02
$N_2(14) + N_2(10) \rightarrow N_2(15) + N_2(9)$	1.05E-08	-8.73E+01	1.60E+02
$N_2(15) + N_2(10) \rightarrow N_2(16) + N_2(9)$	1.15E-08	-8.80E+01	1.52E+02
$N_2(16) + N_2(10) \rightarrow N_2(17) + N_2(9)$	1.26E-08	-8.88E+01	1.46E+02
$N_2(17) + N_2(10) \rightarrow N_2(18) + N_2(9)$	1.38E-08	-8.98E+01	1.39E+02
$N_2(18) + N_2(10) \rightarrow N_2(19) + N_2(9)$	1.50E-08	-9.08E+01	1.33E+02
$N_2(19) + N_2(10) \rightarrow N_2(20) + N_2(9)$	1.63E-08	-9.19E+01	1.27E+02
$N_2(10) + N_2(11) \rightarrow N_2(11) + N_2(10)$	8.03E-09	-8.53E+01	1.94E+02
$N_2(11) + N_2(11) \rightarrow N_2(12) + N_2(10)$	8.85E-09	-8.57E+01	1.89E+02
$N_2(12) + N_2(11) \rightarrow N_2(13) + N_2(10)$	9.66E-09	-8.60E+01	1.83E+02
$N_2(13) + N_2(11) \rightarrow N_2(14) + N_2(10)$	1.05E-08	-8.63E+01	1.75E+02
$N_2(14) + N_2(11) \rightarrow N_2(15) + N_2(10)$	1.15E-08	-8.67E+01	1.67E+02
$N_2(15) + N_2(11) \rightarrow N_2(16) + N_2(10)$	1.25E-08	-8.73E+01	1.60E+02
$N_2(16) + N_2(11) \rightarrow N_2(17) + N_2(10)$	1.36E-08	-8.80E+01	1.52E+02
$N_2(17) + N_2(11) \rightarrow N_2(18) + N_2(10)$	1.48E-08	-8.88E+01	1.46E+02

$N_2(18) + N_2(11) \rightarrow N_2(19) + N_2(10)$	1.61E-08	-8.98E+01	1.39E+02
$N_2(19) + N_2(11) \rightarrow N_2(20) + N_2(10)$	1.74E-08	-9.08E+01	1.33E+02
$N_2(11) + N_2(12) \rightarrow N_2(12) + N_2(11)$	9.68E-09	-8.53E+01	1.94E+02
$N_2(12) + N_2(12) \rightarrow N_2(13) + N_2(11)$	1.06E-08	-8.57E+01	1.89E+02
$N_2(13) + N_2(12) \rightarrow N_2(14) + N_2(11)$	1.15E-08	-8.60E+01	1.83E+02
$N_2(14) + N_2(12) \rightarrow N_2(15) + N_2(11)$	1.24E-08	-8.63E+01	1.75E+02
$N_2(15) + N_2(12) \rightarrow N_2(16) + N_2(11)$	1.35E-08	-8.67E+01	1.67E+02
$N_2(16) + N_2(12) \rightarrow N_2(17) + N_2(11)$	1.46E-08	-8.73E+01	1.60E+02
$N_2(17) + N_2(12) \rightarrow N_2(18) + N_2(11)$	1.58E-08	-8.80E+01	1.52E+02
$N_2(18) + N_2(12) \rightarrow N_2(19) + N_2(11)$	1.71E-08	-8.88E+01	1.46E+02
$N_2(19) + N_2(12) \rightarrow N_2(20) + N_2(11)$	1.85E-08	-8.98E+01	1.39E+02
$N_2(12) + N_2(13) \rightarrow N_2(13) + N_2(12)$	1.15E-08	-8.53E+01	1.94E+02
$N_2(13) + N_2(13) \rightarrow N_2(14) + N_2(12)$	1.25E-08	-8.57E+01	1.89E+02
$N_2(14) + N_2(13) \rightarrow N_2(15) + N_2(12)$	1.35E-08	-8.60E+01	1.83E+02
$N_2(15) + N_2(13) \rightarrow N_2(16) + N_2(12)$	1.45E-08	-8.63E+01	1.75E+02
$N_2(16) + N_2(13) \rightarrow N_2(17) + N_2(12)$	1.56E-08	-8.67E+01	1.67E+02
$N_2(17) + N_2(13) \rightarrow N_2(18) + N_2(12)$	1.69E-08	-8.73E+01	1.60E+02
$N_2(18) + N_2(13) \rightarrow N_2(19) + N_2(12)$	1.82E-08	-8.80E+01	1.52E+02
$N_2(19) + N_2(13) \rightarrow N_2(20) + N_2(12)$	1.96E-08	-8.88E+01	1.46E+02
$N_2(13) + N_2(14) \rightarrow N_2(14) + N_2(13)$	1.35E-08	-8.53E+01	1.94E+02
$N_2(14) + N_2(14) \rightarrow N_2(15) + N_2(13)$	1.46E-08	-8.57E+01	1.89E+02
$N_2(15) + N_2(14) \rightarrow N_2(16) + N_2(13)$	1.56E-08	-8.60E+01	1.83E+02
$N_2(16) + N_2(14) \rightarrow N_2(17) + N_2(13)$	1.68E-08	-8.63E+01	1.75E+02
$N_2(17) + N_2(14) \rightarrow N_2(18) + N_2(13)$	1.80E-08	-8.67E+01	1.67E+02
$N_2(18) + N_2(14) \rightarrow N_2(19) + N_2(13)$	1.93E-08	-8.73E+01	1.60E+02
$N_2(19) + N_2(14) \rightarrow N_2(20) + N_2(13)$	2.07E-08	-8.80E+01	1.52E+02
$N_2(14) + N_2(15) \rightarrow N_2(15) + N_2(14)$	1.57E-08	-8.53E+01	1.94E+02
$N_2(15) + N_2(15) \rightarrow N_2(16) + N_2(14)$	1.69E-08	-8.57E+01	1.89E+02
$N_2(16) + N_2(15) \rightarrow N_2(17) + N_2(14)$	1.80E-08	-8.60E+01	1.83E+02
$N_2(17) + N_2(15) \rightarrow N_2(18) + N_2(14)$	1.92E-08	-8.63E+01	1.75E+02
$N_2(18) + N_2(15) \rightarrow N_2(19) + N_2(14)$	2.04E-08	-8.67E+01	1.67E+02
$N_2(19) + N_2(15) \rightarrow N_2(20) + N_2(14)$	2.18E-08	-8.73E+01	1.60E+02
$N_2(15) + N_2(16) \rightarrow N_2(16) + N_2(15)$	1.80E-08	-8.53E+01	1.94E+02
$N_2(16) + N_2(16) \rightarrow N_2(17) + N_2(15)$	1.93E-08	-8.57E+01	1.89E+02
$N_2(17) + N_2(16) \rightarrow N_2(18) + N_2(15)$	2.05E-08	-8.60E+01	1.83E+02
$N_2(18) + N_2(16) \rightarrow N_2(19) + N_2(15)$	2.17E-08	-8.63E+01	1.75E+02
$N_2(19) + N_2(16) \rightarrow N_2(20) + N_2(15)$	2.30E-08	-8.67E+01	1.67E+02

N_2(16) + N_2(17) → N_2(17) + N_2(16)	2.05E-08	-8.53E+01	1.94E+02
N_2(17) + N_2(17) → N_2(18) + N_2(16)	2.18E-08	-8.57E+01	1.89E+02
N_2(18) + N_2(17) → N_2(19) + N_2(16)	2.31E-08	-8.60E+01	1.83E+02
N_2(19) + N_2(17) → N_2(20) + N_2(16)	2.44E-08	-8.63E+01	1.75E+02
N_2(17) + N_2(18) → N_2(18) + N_2(17)	2.32E-08	-8.53E+01	1.94E+02
N_2(18) + N_2(18) → N_2(19) + N_2(17)	2.46E-08	-8.57E+01	1.89E+02
N_2(19) + N_2(18) → N_2(20) + N_2(17)	2.58E-08	-8.60E+01	1.83E+02
N_2(18) + N_2(19) → N_2(19) + N_2(18)	2.60E-08	-8.53E+01	1.94E+02
N_2(19) + N_2(19) → N_2(20) + N_2(18)	2.74E-08	-8.57E+01	1.89E+02
N_2(19) + N_2(20) → N_2(20) + N_2(19)	2.89E-08	-8.53E+01	1.94E+02

Table A.5: Internal vibration exchanges in N_2

A.2.2 V-V exchanges $CO_2(v)$ + $CO_2(w) \rightleftharpoons$ $CO_2(v')$ + $CO_2(w')$

Expression:

$$k(v, T_g) = 1.66 \times 10^{-24} \exp^{A(v)+B(v)T_g^{-1/3}+C(v)T_g^{-2/3}}$$

Table A.6 for A, B and C:

Reaction	A	B	C
CO_2(0,0,0,1,1) + CO_2(0,0,0,0,1) → CO_2(0,2,2,0,1) + CO_2(0,1,1,0,1)	4.40E+01	-2.42E+02	6.33E+02
CO_2(0,0,0,1,1) + CO_2(0,0,0,0,1) → CO_2(1,0,0,0,2) + CO_2(0,1,1,0,1)	4.40E+01	-2.42E+02	6.33E+02
CO_2(0,0,0,1,1) + CO_2(0,0,0,1,1) → CO_2(0,0,0,0,1) + CO_2(0,0,0,2,1)	2.98E+01	2.21E+01	-4.03E+01
CO_2(0,0,0,1,1) + CO_2(0,0,0,2,1) → CO_2(0,0,0,0,1) + CO_2(0,0,0,3,1)	2.72E+01	2.21E+01	-4.03E+01
CO_2(0,0,0,1,1) + CO_2(0,0,0,3,1) → CO_2(0,0,0,0,1) + CO_2(0,0,0,4,1)	2.46E+01	2.21E+01	-4.03E+01
CO_2(0,0,0,1,1) + CO_2(0,0,0,4,1) → CO_2(0,0,0,0,1) + CO_2(0,0,0,5,1)	2.20E+01	2.21E+01	-4.03E+01
CO_2(0,0,0,2,1) + CO_2(0,0,0,0,1) → CO_2(0,1,1,1,1) + CO_2(0,2,2,0,1)	4.47E+01	-2.41E+02	6.37E+02
CO_2(0,0,0,2,1) + CO_2(0,0,0,0,1) → CO_2(0,1,1,1,1) + CO_2(1,0,0,0,2)	4.47E+01	-2.41E+02	6.37E+02
CO_2(0,0,0,2,1) + CO_2(0,0,0,0,1) → CO_2(0,2,2,1,1) + CO_2(0,1,1,0,1)	4.47E+01	-2.42E+02	6.35E+02
CO_2(0,0,0,2,1) + CO_2(0,0,0,0,1) → CO_2(1,0,0,1,2) + CO_2(0,1,1,0,1)	4.47E+01	-2.42E+02	6.35E+02
CO_2(0,0,0,2,1) + CO_2(0,0,0,2,1) → CO_2(0,0,0,1,1) + CO_2(0,0,0,3,1)	3.09E+01	2.21E+01	-4.03E+01
CO_2(0,0,0,2,1) + CO_2(0,0,0,3,1) → CO_2(0,0,0,1,1) + CO_2(0,0,0,4,1)	2.71E+01	2.21E+01	-4.03E+01
CO_2(0,0,0,2,1) + CO_2(0,0,0,4,1) → CO_2(0,0,0,1,1) + CO_2(0,0,0,5,1)	2.45E+01	2.21E+01	-4.03E+01
CO_2(0,0,0,3,1) + CO_2(0,0,0,0,1) → CO_2(0,1,1,2,1) + CO_2(0,2,2,0,1)	4.51E+01	-2.40E+02	6.41E+02
CO_2(0,0,0,3,1) + CO_2(0,0,0,0,1) → CO_2(0,1,1,2,1) + CO_2(1,0,0,0,2)	4.51E+01	-2.40E+02	6.41E+02
CO_2(0,0,0,3,1) + CO_2(0,0,0,0,1) → CO_2(0,2,2,2,1) + CO_2(0,1,1,0,1)	4.51E+01	-2.41E+02	6.36E+02
CO_2(0,0,0,3,1) + CO_2(0,0,0,0,1) → CO_2(1,0,0,2,2) + CO_2(0,1,1,0,1)	4.51E+01	-2.41E+02	6.36E+02
CO_2(0,0,0,3,1) + CO_2(0,0,0,1,1) → CO_2(0,0,0,2,1) + CO_2(0,0,0,2,1)	2.98E+01	2.21E+01	-4.03E+01
CO_2(0,0,0,3,1) + CO_2(0,0,0,3,1) → CO_2(0,0,0,2,1) + CO_2(0,0,0,4,1)	3.09E+01	2.21E+01	-4.03E+01
CO_2(0,0,0,3,1) + CO_2(0,0,0,4,1) → CO_2(0,0,0,2,1) + CO_2(0,0,0,5,1)	2.71E+01	2.21E+01	-4.03E+01

$CO_2(0,0,0,4,1) + CO_2(0,0,0,0,1) \rightarrow CO_2(0,1,1,3,1) + CO_2(0,2,2,0,1)$	4.53E+01	-2.38E+02	6.45E+02
$CO_2(0,0,0,4,1) + CO_2(0,0,0,0,1) \rightarrow CO_2(0,1,1,3,1) + CO_2(1,0,0,0,2)$	4.53E+01	-2.38E+02	6.45E+02
$CO_2(0,0,0,4,1) + CO_2(0,0,0,0,1) \rightarrow CO_2(0,2,2,3,1) + CO_2(0,1,1,0,1)$	4.54E+01	-2.41E+02	6.38E+02
$CO_2(0,0,0,4,1) + CO_2(0,0,0,0,1) \rightarrow CO_2(1,0,0,3,2) + CO_2(0,1,1,0,1)$	4.54E+01	-2.41E+02	6.38E+02
$CO_2(0,0,0,4,1) + CO_2(0,0,0,1,1) \rightarrow CO_2(0,0,0,3,1) + CO_2(0,0,0,2,1)$	2.82E+01	2.21E+01	-4.03E+01
$CO_2(0,0,0,4,1) + CO_2(0,0,0,2,1) \rightarrow CO_2(0,0,0,3,1) + CO_2(0,0,0,3,1)$	2.98E+01	2.21E+01	-4.03E+01
$CO_2(0,0,0,4,1) + CO_2(0,0,0,4,1) \rightarrow CO_2(0,0,0,3,1) + CO_2(0,0,0,5,1)$	3.09E+01	2.21E+01	-4.03E+01
$CO_2(0,0,0,5,1) + CO_2(0,0,0,0,1) \rightarrow CO_2(0,1,1,4,1) + CO_2(0,2,2,0,1)$	4.56E+01	-2.37E+02	6.49E+02
$CO_2(0,0,0,5,1) + CO_2(0,0,0,0,1) \rightarrow CO_2(0,1,1,4,1) + CO_2(1,0,0,0,2)$	4.56E+01	-2.37E+02	6.49E+02
$CO_2(0,0,0,5,1) + CO_2(0,0,0,0,1) \rightarrow CO_2(0,2,2,4,1) + CO_2(0,1,1,0,1)$	4.56E+01	-2.40E+02	6.39E+02
$CO_2(0,0,0,5,1) + CO_2(0,0,0,0,1) \rightarrow CO_2(1,0,0,4,2) + CO_2(0,1,1,0,1)$	4.56E+01	-2.40E+02	6.39E+02
$CO_2(0,0,0,5,1) + CO_2(0,0,0,1,1) \rightarrow CO_2(0,0,0,4,1) + CO_2(0,0,0,2,1)$	2.59E+01	2.21E+01	-4.03E+01
$CO_2(0,0,0,5,1) + CO_2(0,0,0,2,1) \rightarrow CO_2(0,0,0,4,1) + CO_2(0,0,0,3,1)$	2.98E+01	2.21E+01	-4.03E+01
$CO_2(0,0,0,5,1) + CO_2(0,0,0,3,1) \rightarrow CO_2(0,0,0,4,1) + CO_2(0,0,0,4,1)$	2.98E+01	2.21E+01	-4.03E+01
$CO_2(0,1,1,1,1) + CO_2(0,0,0,0,1) \rightarrow CO_2(0,0,0,1,1) + CO_2(0,1,1,0,1)$	3.41E+01	-8.77E+01	2.30E+02
$CO_2(0,1,1,1,1) + CO_2(0,1,1,0,1) \rightarrow CO_2(0,0,0,1,1) + CO_2(0,2,2,0,1)$	3.48E+01	-8.80E+01	2.33E+02
$CO_2(0,1,1,1,1) + CO_2(0,1,1,0,1) \rightarrow CO_2(0,0,0,1,1) + CO_2(1,0,0,0,2)$	3.48E+01	-8.80E+01	2.33E+02
$CO_2(0,1,1,1,1) + CO_2(0,2,2,0,1) \rightarrow CO_2(0,0,0,1,1) + CO_2(0,3,3,0,1)$	3.52E+01	-8.80E+01	2.33E+02
$CO_2(0,1,1,1,1) + CO_2(0,2,2,0,1) \rightarrow CO_2(0,0,0,1,1) + CO_2(1,1,1,0,2)$	3.52E+01	-8.80E+01	2.33E+02
$CO_2(0,1,1,1,1) + CO_2(0,3,3,0,1) \rightarrow CO_2(0,0,0,1,1) + CO_2(0,2,2,0,1)$	3.52E+01	-8.80E+01	2.33E+02
$CO_2(0,1,1,1,1) + CO_2(1,0,0,0,2) \rightarrow CO_2(0,0,0,1,1) + CO_2(1,1,1,0,2)$	3.55E+01	-8.80E+01	2.33E+02
$CO_2(0,1,1,1,1) + CO_2(1,1,1,0,2) \rightarrow CO_2(0,0,0,1,1) + CO_2(1,2,2,0,2)$	3.59E+01	-8.80E+01	2.33E+02
$CO_2(0,1,1,1,1) + CO_2(1,1,1,0,2) \rightarrow CO_2(0,0,0,1,1) + CO_2(2,0,0,0,3)$	3.59E+01	-8.80E+01	2.33E+02
$CO_2(0,1,1,2,1) + CO_2(0,0,0,1,1) \rightarrow CO_2(0,0,0,2,1) + CO_2(0,1,1,1,1)$	3.41E+01	-8.77E+01	2.30E+02
$CO_2(0,1,1,2,1) + CO_2(0,1,1,1,1) \rightarrow CO_2(0,0,0,2,1) + CO_2(0,2,2,1,1)$	3.48E+01	-8.80E+01	2.33E+02
$CO_2(0,1,1,2,1) + CO_2(0,1,1,1,1) \rightarrow CO_2(0,0,0,2,1) + CO_2(1,0,0,1,2)$	3.48E+01	-8.80E+01	2.33E+02
$CO_2(0,1,1,2,1) + CO_2(0,2,2,1,1) \rightarrow CO_2(0,0,0,2,1) + CO_2(0,3,3,1,1)$	3.52E+01	-8.80E+01	2.33E+02
$CO_2(0,1,1,2,1) + CO_2(0,2,2,1,1) \rightarrow CO_2(0,0,0,2,1) + CO_2(1,1,1,1,2)$	3.52E+01	-8.80E+01	2.33E+02
$CO_2(0,1,1,2,1) + CO_2(0,3,3,1,1) \rightarrow CO_2(0,0,0,2,1) + CO_2(0,2,2,1,1)$	3.52E+01	-8.80E+01	2.33E+02
$CO_2(0,1,1,2,1) + CO_2(1,0,0,1,2) \rightarrow CO_2(0,0,0,2,1) + CO_2(1,1,1,1,2)$	3.55E+01	-8.80E+01	2.33E+02
$CO_2(0,1,1,2,1) + CO_2(1,1,1,1,2) \rightarrow CO_2(0,0,0,2,1) + CO_2(1,2,2,1,2)$	3.59E+01	-8.80E+01	2.33E+02
$CO_2(0,1,1,2,1) + CO_2(1,1,1,1,2) \rightarrow CO_2(0,0,0,2,1) + CO_2(2,0,0,1,3)$	3.59E+01	-8.80E+01	2.33E+02
$CO_2(0,1,1,3,1) + CO_2(0,0,0,2,1) \rightarrow CO_2(0,0,0,3,1) + CO_2(0,1,1,2,1)$	3.41E+01	-8.77E+01	2.30E+02
$CO_2(0,1,1,3,1) + CO_2(0,1,1,2,1) \rightarrow CO_2(0,0,0,3,1) + CO_2(0,2,2,2,1)$	3.48E+01	-8.80E+01	2.33E+02
$CO_2(0,1,1,3,1) + CO_2(0,1,1,2,1) \rightarrow CO_2(0,0,0,3,1) + CO_2(1,0,0,2,2)$	3.48E+01	-8.80E+01	2.33E+02
$CO_2(0,1,1,3,1) + CO_2(0,2,2,2,1) \rightarrow CO_2(0,0,0,3,1) + CO_2(0,3,3,2,1)$	3.52E+01	-8.80E+01	2.33E+02
$CO_2(0,1,1,3,1) + CO_2(0,2,2,2,1) \rightarrow CO_2(0,0,0,3,1) + CO_2(1,1,1,2,2)$	3.52E+01	-8.80E+01	2.33E+02
$CO_2(0,1,1,3,1) + CO_2(0,3,3,2,1) \rightarrow CO_2(0,0,0,3,1) + CO_2(0,2,2,2,1)$	3.52E+01	-8.80E+01	2.33E+02
$CO_2(0,1,1,3,1) + CO_2(1,0,0,2,2) \rightarrow CO_2(0,0,0,3,1) + CO_2(1,1,1,2,2)$	3.55E+01	-8.80E+01	2.33E+02
$CO_2(0,1,1,3,1) + CO_2(1,1,1,2,2) \rightarrow CO_2(0,0,0,3,1) + CO_2(1,2,2,2,2)$	3.59E+01	-8.80E+01	2.33E+02

$CO_2(0,1,1,3,1) + CO_2(1,1,1,2,2) \rightarrow CO_2(0,0,0,3,1) + CO_2(2,0,0,2,3)$	3.59E+01	-8.80E+01	2.33E+02
$CO_2(0,1,1,4,1) + CO_2(0,0,0,3,1) \rightarrow CO_2(0,0,0,4,1) + CO_2(0,1,1,3,1)$	3.41E+01	-8.77E+01	2.30E+02
$CO_2(0,1,1,4,1) + CO_2(0,1,1,3,1) \rightarrow CO_2(0,0,0,4,1) + CO_2(0,2,2,3,1)$	3.48E+01	-8.80E+01	2.33E+02
$CO_2(0,1,1,4,1) + CO_2(0,1,1,3,1) \rightarrow CO_2(0,0,0,4,1) + CO_2(1,0,0,3,2)$	3.48E+01	-8.80E+01	2.33E+02
$CO_2(0,1,1,4,1) + CO_2(0,2,2,3,1) \rightarrow CO_2(0,0,0,4,1) + CO_2(0,3,3,3,1)$	3.52E+01	-8.80E+01	2.33E+02
$CO_2(0,1,1,4,1) + CO_2(0,2,2,3,1) \rightarrow CO_2(0,0,0,4,1) + CO_2(1,1,1,3,2)$	3.52E+01	-8.80E+01	2.33E+02
$CO_2(0,1,1,4,1) + CO_2(0,3,3,3,1) \rightarrow CO_2(0,0,0,4,1) + CO_2(0,2,2,3,1)$	3.52E+01	-8.80E+01	2.33E+02
$CO_2(0,1,1,4,1) + CO_2(1,0,0,3,2) \rightarrow CO_2(0,0,0,4,1) + CO_2(1,1,1,3,2)$	3.55E+01	-8.80E+01	2.33E+02
$CO_2(0,1,1,4,1) + CO_2(1,1,1,3,2) \rightarrow CO_2(0,0,0,4,1) + CO_2(1,2,2,3,2)$	3.59E+01	-8.80E+01	2.33E+02
$CO_2(0,1,1,4,1) + CO_2(1,1,1,3,2) \rightarrow CO_2(0,0,0,4,1) + CO_2(2,0,0,3,3)$	3.59E+01	-8.80E+01	2.33E+02
$CO_2(0,1,1,5,1) + CO_2(0,0,0,4,1) \rightarrow CO_2(0,0,0,5,1) + CO_2(0,1,1,4,1)$	3.41E+01	-8.77E+01	2.30E+02
$CO_2(0,1,1,5,1) + CO_2(0,1,1,4,1) \rightarrow CO_2(0,0,0,5,1) + CO_2(0,2,2,4,1)$	3.48E+01	-8.80E+01	2.33E+02
$CO_2(0,1,1,5,1) + CO_2(0,1,1,4,1) \rightarrow CO_2(0,0,0,5,1) + CO_2(1,0,0,4,2)$	3.48E+01	-8.80E+01	2.33E+02
$CO_2(0,1,1,5,1) + CO_2(0,2,2,4,1) \rightarrow CO_2(0,0,0,5,1) + CO_2(0,3,3,4,1)$	3.52E+01	-8.80E+01	2.33E+02
$CO_2(0,1,1,5,1) + CO_2(0,2,2,4,1) \rightarrow CO_2(0,0,0,5,1) + CO_2(1,1,1,4,2)$	3.52E+01	-8.80E+01	2.33E+02
$CO_2(0,1,1,5,1) + CO_2(0,3,3,4,1) \rightarrow CO_2(0,0,0,5,1) + CO_2(0,2,2,4,1)$	3.52E+01	-8.80E+01	2.33E+02
$CO_2(0,1,1,5,1) + CO_2(1,0,0,4,2) \rightarrow CO_2(0,0,0,5,1) + CO_2(1,1,1,4,2)$	3.55E+01	-8.80E+01	2.33E+02
$CO_2(0,1,1,5,1) + CO_2(1,1,1,4,2) \rightarrow CO_2(0,0,0,5,1) + CO_2(1,2,2,4,2)$	3.59E+01	-8.80E+01	2.33E+02
$CO_2(0,1,1,5,1) + CO_2(1,1,1,4,2) \rightarrow CO_2(0,0,0,5,1) + CO_2(2,0,0,4,3)$	3.59E+01	-8.80E+01	2.33E+02
$CO_2(0,2,2,0,1) + CO_2(0,0,0,0,1) \rightarrow CO_2(0,1,1,0,1) + CO_2(0,1,1,0,1)$	3.48E+01	-8.80E+01	2.33E+02
$CO_2(0,2,2,1,1) + CO_2(0,0,0,1,1) \rightarrow CO_2(0,1,1,1,1) + CO_2(0,1,1,1,1)$	3.48E+01	-8.80E+01	2.33E+02
$CO_2(0,2,2,2,1) + CO_2(0,0,0,2,1) \rightarrow CO_2(0,1,1,2,1) + CO_2(0,1,1,2,1)$	3.48E+01	-8.80E+01	2.33E+02
$CO_2(0,2,2,3,1) + CO_2(0,0,0,3,1) \rightarrow CO_2(0,1,1,3,1) + CO_2(0,1,1,3,1)$	3.48E+01	-8.80E+01	2.33E+02
$CO_2(0,2,2,4,1) + CO_2(0,0,0,4,1) \rightarrow CO_2(0,1,1,4,1) + CO_2(0,1,1,4,1)$	3.48E+01	-8.80E+01	2.33E+02
$CO_2(0,2,2,5,1) + CO_2(0,0,0,5,1) \rightarrow CO_2(0,1,1,5,1) + CO_2(0,1,1,5,1)$	3.48E+01	-8.80E+01	2.33E+02
$CO_2(0,3,3,0,1) + CO_2(0,0,0,0,1) \rightarrow CO_2(0,2,2,0,1) + CO_2(0,1,1,0,1)$	3.59E+01	-8.80E+01	2.33E+02
$CO_2(0,3,3,0,1) + CO_2(0,1,1,0,1) \rightarrow CO_2(0,2,2,0,1) + CO_2(0,2,2,0,1)$	3.59E+01	-8.80E+01	2.33E+02
$CO_2(0,3,3,0,1) + CO_2(0,1,1,0,1) \rightarrow CO_2(0,2,2,0,1) + CO_2(1,0,0,0,2)$	3.59E+01	-8.80E+01	2.33E+02
$CO_2(0,3,3,1,1) + CO_2(0,0,0,1,1) \rightarrow CO_2(0,2,2,1,1) + CO_2(0,1,1,1,1)$	3.59E+01	-8.80E+01	2.33E+02
$CO_2(0,3,3,1,1) + CO_2(0,1,1,1,1) \rightarrow CO_2(0,2,2,1,1) + CO_2(0,2,2,1,1)$	3.59E+01	-8.80E+01	2.33E+02
$CO_2(0,3,3,1,1) + CO_2(0,1,1,1,1) \rightarrow CO_2(0,2,2,1,1) + CO_2(1,0,0,1,2)$	3.59E+01	-8.80E+01	2.33E+02
$CO_2(0,3,3,2,1) + CO_2(0,0,0,2,1) \rightarrow CO_2(0,2,2,2,1) + CO_2(0,1,1,2,1)$	3.59E+01	-8.80E+01	2.33E+02
$CO_2(0,3,3,2,1) + CO_2(0,1,1,2,1) \rightarrow CO_2(0,2,2,2,1) + CO_2(0,2,2,2,1)$	3.59E+01	-8.80E+01	2.33E+02
$CO_2(0,3,3,2,1) + CO_2(0,1,1,2,1) \rightarrow CO_2(0,2,2,2,1) + CO_2(1,0,0,2,2)$	3.59E+01	-8.80E+01	2.33E+02
$CO_2(0,3,3,3,1) + CO_2(0,0,0,3,1) \rightarrow CO_2(0,2,2,3,1) + CO_2(0,1,1,3,1)$	3.59E+01	-8.80E+01	2.33E+02
$CO_2(0,3,3,3,1) + CO_2(0,1,1,3,1) \rightarrow CO_2(0,2,2,3,1) + CO_2(0,2,2,3,1)$	3.59E+01	-8.80E+01	2.33E+02
$CO_2(0,3,3,3,1) + CO_2(0,1,1,3,1) \rightarrow CO_2(0,2,2,3,1) + CO_2(1,0,0,3,2)$	3.59E+01	-8.80E+01	2.33E+02
$CO_2(0,3,3,4,1) + CO_2(0,0,0,4,1) \rightarrow CO_2(0,2,2,4,1) + CO_2(0,1,1,4,1)$	3.59E+01	-8.80E+01	2.33E+02
$CO_2(0,3,3,4,1) + CO_2(0,1,1,4,1) \rightarrow CO_2(0,2,2,4,1) + CO_2(0,2,2,4,1)$	3.59E+01	-8.80E+01	2.33E+02
$CO_2(0,3,3,4,1) + CO_2(0,1,1,4,1) \rightarrow CO_2(0,2,2,4,1) + CO_2(1,0,0,4,2)$	3.59E+01	-8.80E+01	2.33E+02

$CO_2(0,3,3,5,1) + CO_2(0,0,0,5,1) \rightarrow CO_2(0,2,2,5,1) + CO_2(0,1,1,5,1)$	3.59E+01	-8.80E+01	2.33E+02
$CO_2(0,3,3,5,1) + CO_2(0,1,1,5,1) \rightarrow CO_2(0,2,2,5,1) + CO_2(0,2,2,5,1)$	3.59E+01	-8.80E+01	2.33E+02
$CO_2(0,3,3,5,1) + CO_2(0,1,1,5,1) \rightarrow CO_2(0,2,2,5,1) + CO_2(1,0,0,5,2)$	3.59E+01	-8.80E+01	2.33E+02
$CO_2(0,4,4,0,1) + CO_2(0,0,0,0,1) \rightarrow CO_2(0,3,3,0,1) + CO_2(0,1,1,0,1)$	3.55E+01	-8.80E+01	2.33E+02
$CO_2(0,4,4,0,1) + CO_2(0,1,1,0,1) \rightarrow CO_2(0,3,3,0,1) + CO_2(0,2,2,0,1)$	3.62E+01	-8.80E+01	2.33E+02
$CO_2(0,4,4,0,1) + CO_2(0,1,1,0,1) \rightarrow CO_2(0,3,3,0,1) + CO_2(1,0,0,0,2)$	3.62E+01	-8.80E+01	2.33E+02
$CO_2(0,4,4,0,1) + CO_2(0,2,2,0,1) \rightarrow CO_2(0,3,3,0,1) + CO_2(0,3,3,0,1)$	3.66E+01	-8.80E+01	2.33E+02
$CO_2(0,4,4,0,1) + CO_2(0,2,2,0,1) \rightarrow CO_2(0,3,3,0,1) + CO_2(1,1,1,0,2)$	3.66E+01	-8.80E+01	2.33E+02
$CO_2(0,4,4,0,1) + CO_2(1,0,0,0,2) \rightarrow CO_2(0,3,3,0,1) + CO_2(1,1,1,0,2)$	3.69E+01	-8.80E+01	2.34E+02
$CO_2(0,4,4,1,1) + CO_2(0,0,0,1,1) \rightarrow CO_2(0,3,3,1,1) + CO_2(0,1,1,1,1)$	3.55E+01	-8.80E+01	2.33E+02
$CO_2(0,4,4,1,1) + CO_2(0,1,1,1,1) \rightarrow CO_2(0,3,3,1,1) + CO_2(0,2,2,1,1)$	3.62E+01	-8.80E+01	2.33E+02
$CO_2(0,4,4,1,1) + CO_2(0,1,1,1,1) \rightarrow CO_2(0,3,3,1,1) + CO_2(1,0,0,1,2)$	3.62E+01	-8.80E+01	2.33E+02
$CO_2(0,4,4,1,1) + CO_2(0,2,2,1,1) \rightarrow CO_2(0,3,3,1,1) + CO_2(0,3,3,1,1)$	3.66E+01	-8.80E+01	2.33E+02
$CO_2(0,4,4,1,1) + CO_2(0,2,2,1,1) \rightarrow CO_2(0,3,3,1,1) + CO_2(1,1,1,1,2)$	3.66E+01	-8.80E+01	2.33E+02
$CO_2(0,4,4,1,1) + CO_2(1,0,0,1,2) \rightarrow CO_2(0,3,3,1,1) + CO_2(1,1,1,1,2)$	3.69E+01	-8.80E+01	2.34E+02
$CO_2(0,4,4,2,1) + CO_2(0,0,0,2,1) \rightarrow CO_2(0,3,3,2,1) + CO_2(0,1,1,2,1)$	3.55E+01	-8.80E+01	2.33E+02
$CO_2(0,4,4,2,1) + CO_2(0,1,1,2,1) \rightarrow CO_2(0,3,3,2,1) + CO_2(0,2,2,2,1)$	3.62E+01	-8.80E+01	2.33E+02
$CO_2(0,4,4,2,1) + CO_2(0,1,1,2,1) \rightarrow CO_2(0,3,3,2,1) + CO_2(1,0,0,2,2)$	3.62E+01	-8.80E+01	2.33E+02
$CO_2(0,4,4,2,1) + CO_2(0,2,2,2,1) \rightarrow CO_2(0,3,3,2,1) + CO_2(0,3,3,2,1)$	3.66E+01	-8.80E+01	2.33E+02
$CO_2(0,4,4,2,1) + CO_2(0,2,2,2,1) \rightarrow CO_2(0,3,3,2,1) + CO_2(1,1,1,2,2)$	3.66E+01	-8.80E+01	2.33E+02
$CO_2(0,4,4,2,1) + CO_2(1,0,0,2,2) \rightarrow CO_2(0,3,3,2,1) + CO_2(1,1,1,2,2)$	3.69E+01	-8.80E+01	2.34E+02
$CO_2(0,4,4,3,1) + CO_2(0,0,0,3,1) \rightarrow CO_2(0,3,3,3,1) + CO_2(0,1,1,3,1)$	3.55E+01	-8.80E+01	2.33E+02
$CO_2(0,4,4,3,1) + CO_2(0,1,1,3,1) \rightarrow CO_2(0,3,3,3,1) + CO_2(0,2,2,3,1)$	3.62E+01	-8.80E+01	2.33E+02
$CO_2(0,4,4,3,1) + CO_2(0,1,1,3,1) \rightarrow CO_2(0,3,3,3,1) + CO_2(1,0,0,3,2)$	3.62E+01	-8.80E+01	2.33E+02
$CO_2(0,4,4,3,1) + CO_2(0,2,2,3,1) \rightarrow CO_2(0,3,3,3,1) + CO_2(0,3,3,3,1)$	3.66E+01	-8.80E+01	2.33E+02
$CO_2(0,4,4,3,1) + CO_2(0,2,2,3,1) \rightarrow CO_2(0,3,3,3,1) + CO_2(1,1,1,3,2)$	3.66E+01	-8.80E+01	2.33E+02
$CO_2(0,4,4,3,1) + CO_2(1,0,0,3,2) \rightarrow CO_2(0,3,3,3,1) + CO_2(1,1,1,3,2)$	3.69E+01	-8.80E+01	2.34E+02
$CO_2(0,4,4,4,1) + CO_2(0,0,0,4,1) \rightarrow CO_2(0,3,3,4,1) + CO_2(0,1,1,4,1)$	3.55E+01	-8.80E+01	2.33E+02
$CO_2(0,4,4,4,1) + CO_2(0,1,1,4,1) \rightarrow CO_2(0,3,3,4,1) + CO_2(0,2,2,4,1)$	3.62E+01	-8.80E+01	2.33E+02
$CO_2(0,4,4,4,1) + CO_2(0,1,1,4,1) \rightarrow CO_2(0,3,3,4,1) + CO_2(1,0,0,4,2)$	3.62E+01	-8.80E+01	2.33E+02
$CO_2(0,4,4,4,1) + CO_2(0,2,2,4,1) \rightarrow CO_2(0,3,3,4,1) + CO_2(0,3,3,4,1)$	3.66E+01	-8.80E+01	2.33E+02
$CO_2(0,4,4,4,1) + CO_2(0,2,2,4,1) \rightarrow CO_2(0,3,3,4,1) + CO_2(1,1,1,4,2)$	3.66E+01	-8.80E+01	2.33E+02
$CO_2(0,4,4,4,1) + CO_2(1,0,0,4,2) \rightarrow CO_2(0,3,3,4,1) + CO_2(1,1,1,4,2)$	3.69E+01	-8.80E+01	2.34E+02
$CO_2(0,4,4,5,1) + CO_2(0,0,0,5,1) \rightarrow CO_2(0,3,3,5,1) + CO_2(0,1,1,5,1)$	3.55E+01	-8.80E+01	2.33E+02
$CO_2(0,4,4,5,1) + CO_2(0,1,1,5,1) \rightarrow CO_2(0,3,3,5,1) + CO_2(0,2,2,5,1)$	3.62E+01	-8.80E+01	2.33E+02
$CO_2(0,4,4,5,1) + CO_2(0,1,1,5,1) \rightarrow CO_2(0,3,3,5,1) + CO_2(1,0,0,5,2)$	3.62E+01	-8.80E+01	2.33E+02
$CO_2(0,4,4,5,1) + CO_2(0,2,2,5,1) \rightarrow CO_2(0,3,3,5,1) + CO_2(0,3,3,5,1)$	3.66E+01	-8.80E+01	2.33E+02
$CO_2(0,4,4,5,1) + CO_2(0,2,2,5,1) \rightarrow CO_2(0,3,3,5,1) + CO_2(1,1,1,5,2)$	3.66E+01	-8.80E+01	2.33E+02
$CO_2(0,4,4,5,1) + CO_2(1,0,0,5,2) \rightarrow CO_2(0,3,3,5,1) + CO_2(1,1,1,5,2)$	3.69E+01	-8.80E+01	2.34E+02
$CO_2(0,5,5,0,1) + CO_2(0,0,0,0,1) \rightarrow CO_2(0,4,4,0,1) + CO_2(0,1,1,0,1)$	3.57E+01	-8.80E+01	2.33E+02

$CO_2(0,5,5,0,1) + CO_2(0,1,1,0,1) \rightarrow CO_2(0,4,4,0,1) + CO_2(0,2,2,0,1)$	3.64E+01	-8.80E+01	2.33E+02
$CO_2(0,5,5,0,1) + CO_2(0,1,1,0,1) \rightarrow CO_2(0,4,4,0,1) + CO_2(1,0,0,0,2)$	3.64E+01	-8.80E+01	2.33E+02
$CO_2(0,5,5,0,1) + CO_2(0,2,2,0,1) \rightarrow CO_2(0,4,4,0,1) + CO_2(0,3,3,0,1)$	3.69E+01	-8.80E+01	2.33E+02
$CO_2(0,5,5,0,1) + CO_2(0,2,2,0,1) \rightarrow CO_2(0,4,4,0,1) + CO_2(1,1,1,0,2)$	3.63E+01	-8.80E+01	2.33E+02
$CO_2(0,5,5,0,1) + CO_2(1,0,0,0,2) \rightarrow CO_2(0,4,4,0,1) + CO_2(1,1,1,0,2)$	3.71E+01	-8.80E+01	2.33E+02
$CO_2(0,5,5,1,1) + CO_2(0,0,0,1,1) \rightarrow CO_2(0,4,4,1,1) + CO_2(0,1,1,1,1)$	3.57E+01	-8.80E+01	2.33E+02
$CO_2(0,5,5,1,1) + CO_2(0,1,1,1,1) \rightarrow CO_2(0,4,4,1,1) + CO_2(0,2,2,1,1)$	3.64E+01	-8.80E+01	2.33E+02
$CO_2(0,5,5,1,1) + CO_2(0,1,1,1,1) \rightarrow CO_2(0,4,4,1,1) + CO_2(1,0,0,1,2)$	3.64E+01	-8.80E+01	2.33E+02
$CO_2(0,5,5,1,1) + CO_2(0,2,2,1,1) \rightarrow CO_2(0,4,4,1,1) + CO_2(0,3,3,1,1)$	3.69E+01	-8.80E+01	2.33E+02
$CO_2(0,5,5,1,1) + CO_2(0,2,2,1,1) \rightarrow CO_2(0,4,4,1,1) + CO_2(1,1,1,1,2)$	3.63E+01	-8.80E+01	2.33E+02
$CO_2(0,5,5,1,1) + CO_2(1,0,0,1,2) \rightarrow CO_2(0,4,4,1,1) + CO_2(1,1,1,1,2)$	3.71E+01	-8.80E+01	2.33E+02
$CO_2(0,5,5,2,1) + CO_2(0,0,0,2,1) \rightarrow CO_2(0,4,4,2,1) + CO_2(0,1,1,2,1)$	3.57E+01	-8.80E+01	2.33E+02
$CO_2(0,5,5,2,1) + CO_2(0,1,1,2,1) \rightarrow CO_2(0,4,4,2,1) + CO_2(0,2,2,2,1)$	3.64E+01	-8.80E+01	2.33E+02
$CO_2(0,5,5,2,1) + CO_2(0,1,1,2,1) \rightarrow CO_2(0,4,4,2,1) + CO_2(1,0,0,2,2)$	3.64E+01	-8.80E+01	2.33E+02
$CO_2(0,5,5,2,1) + CO_2(0,2,2,2,1) \rightarrow CO_2(0,4,4,2,1) + CO_2(0,3,3,2,1)$	3.69E+01	-8.80E+01	2.33E+02
$CO_2(0,5,5,2,1) + CO_2(0,2,2,2,1) \rightarrow CO_2(0,4,4,2,1) + CO_2(1,1,1,2,2)$	3.63E+01	-8.80E+01	2.33E+02
$CO_2(0,5,5,2,1) + CO_2(1,0,0,2,2) \rightarrow CO_2(0,4,4,2,1) + CO_2(1,1,1,2,2)$	3.71E+01	-8.80E+01	2.33E+02
$CO_2(0,5,5,3,1) + CO_2(0,0,0,3,1) \rightarrow CO_2(0,4,4,3,1) + CO_2(0,1,1,3,1)$	3.57E+01	-8.80E+01	2.33E+02
$CO_2(0,5,5,3,1) + CO_2(0,1,1,3,1) \rightarrow CO_2(0,4,4,3,1) + CO_2(0,2,2,3,1)$	3.64E+01	-8.80E+01	2.33E+02
$CO_2(0,5,5,3,1) + CO_2(0,1,1,3,1) \rightarrow CO_2(0,4,4,3,1) + CO_2(1,0,0,3,2)$	3.64E+01	-8.80E+01	2.33E+02
$CO_2(0,5,5,3,1) + CO_2(0,2,2,3,1) \rightarrow CO_2(0,4,4,3,1) + CO_2(0,3,3,3,1)$	3.69E+01	-8.80E+01	2.33E+02
$CO_2(0,5,5,3,1) + CO_2(0,2,2,3,1) \rightarrow CO_2(0,4,4,3,1) + CO_2(1,1,1,3,2)$	3.63E+01	-8.80E+01	2.33E+02
$CO_2(0,5,5,3,1) + CO_2(1,0,0,3,2) \rightarrow CO_2(0,4,4,3,1) + CO_2(1,1,1,3,2)$	3.71E+01	-8.80E+01	2.33E+02
$CO_2(0,5,5,4,1) + CO_2(0,0,0,4,1) \rightarrow CO_2(0,4,4,4,1) + CO_2(0,1,1,4,1)$	3.57E+01	-8.80E+01	2.33E+02
$CO_2(0,5,5,4,1) + CO_2(0,1,1,4,1) \rightarrow CO_2(0,4,4,4,1) + CO_2(0,2,2,4,1)$	3.64E+01	-8.80E+01	2.33E+02
$CO_2(0,5,5,4,1) + CO_2(0,1,1,4,1) \rightarrow CO_2(0,4,4,4,1) + CO_2(1,0,0,4,2)$	3.64E+01	-8.80E+01	2.33E+02
$CO_2(0,5,5,4,1) + CO_2(0,2,2,4,1) \rightarrow CO_2(0,4,4,4,1) + CO_2(0,3,3,4,1)$	3.69E+01	-8.80E+01	2.33E+02
$CO_2(0,5,5,4,1) + CO_2(0,2,2,4,1) \rightarrow CO_2(0,4,4,4,1) + CO_2(1,1,1,4,2)$	3.63E+01	-8.80E+01	2.33E+02
$CO_2(0,5,5,4,1) + CO_2(1,0,0,4,2) \rightarrow CO_2(0,4,4,4,1) + CO_2(1,1,1,4,2)$	3.71E+01	-8.80E+01	2.33E+02
$CO_2(0,5,5,5,1) + CO_2(0,0,0,5,1) \rightarrow CO_2(0,4,4,5,1) + CO_2(0,1,1,5,1)$	3.57E+01	-8.80E+01	2.33E+02
$CO_2(0,5,5,5,1) + CO_2(0,1,1,5,1) \rightarrow CO_2(0,4,4,5,1) + CO_2(0,2,2,5,1)$	3.64E+01	-8.80E+01	2.33E+02
$CO_2(0,5,5,5,1) + CO_2(0,1,1,5,1) \rightarrow CO_2(0,4,4,5,1) + CO_2(1,0,0,5,2)$	3.64E+01	-8.80E+01	2.33E+02
$CO_2(0,5,5,5,1) + CO_2(0,2,2,5,1) \rightarrow CO_2(0,4,4,5,1) + CO_2(0,3,3,5,1)$	3.69E+01	-8.80E+01	2.33E+02
$CO_2(0,5,5,5,1) + CO_2(0,2,2,5,1) \rightarrow CO_2(0,4,4,5,1) + CO_2(1,1,1,5,2)$	3.63E+01	-8.80E+01	2.33E+02
$CO_2(0,5,5,5,1) + CO_2(1,0,0,5,2) \rightarrow CO_2(0,4,4,5,1) + CO_2(1,1,1,5,2)$	3.71E+01	-8.80E+01	2.33E+02
$CO_2(1,0,0,0,2) + CO_2(0,0,0,0,1) \rightarrow CO_2(0,1,1,0,1) + CO_2(0,1,1,0,1)$	3.48E+01	-8.80E+01	2.33E+02
$CO_2(1,0,0,0,2) + CO_2(0,1,1,0,1) \rightarrow CO_2(0,1,1,0,1) + CO_2(0,2,2,0,1)$	3.55E+01	-8.80E+01	2.33E+02
$CO_2(1,0,0,1,2) + CO_2(0,0,0,1,1) \rightarrow CO_2(0,1,1,1,1) + CO_2(0,1,1,1,1)$	3.48E+01	-8.80E+01	2.33E+02
$CO_2(1,0,0,1,2) + CO_2(0,1,1,1,1) \rightarrow CO_2(0,1,1,1,1) + CO_2(0,2,2,1,1)$	3.55E+01	-8.80E+01	2.33E+02
$CO_2(1,0,0,2,2) + CO_2(0,0,0,2,1) \rightarrow CO_2(0,1,1,2,1) + CO_2(0,1,1,2,1)$	3.48E+01	-8.80E+01	2.33E+02

$CO_2(1,0,0,2,2) + CO_2(0,1,1,2,1) \rightarrow CO_2(0,1,1,2,1) + CO_2(0,2,2,2,1)$	3.55E+01	-8.80E+01	2.33E+02
$CO_2(1,0,0,3,2) + CO_2(0,0,0,3,1) \rightarrow CO_2(0,1,1,3,1) + CO_2(0,1,1,3,1)$	3.48E+01	-8.80E+01	2.33E+02
$CO_2(1,0,0,3,2) + CO_2(0,1,1,3,1) \rightarrow CO_2(0,1,1,3,1) + CO_2(0,2,2,3,1)$	3.55E+01	-8.80E+01	2.33E+02
$CO_2(1,0,0,4,2) + CO_2(0,0,0,4,1) \rightarrow CO_2(0,1,1,4,1) + CO_2(0,1,1,4,1)$	3.48E+01	-8.80E+01	2.33E+02
$CO_2(1,0,0,4,2) + CO_2(0,1,1,4,1) \rightarrow CO_2(0,1,1,4,1) + CO_2(0,2,2,4,1)$	3.55E+01	-8.80E+01	2.33E+02
$CO_2(1,0,0,5,2) + CO_2(0,0,0,5,1) \rightarrow CO_2(0,1,1,5,1) + CO_2(0,1,1,5,1)$	3.48E+01	-8.80E+01	2.33E+02
$CO_2(1,0,0,5,2) + CO_2(0,1,1,5,1) \rightarrow CO_2(0,1,1,5,1) + CO_2(0,2,2,5,1)$	3.55E+01	-8.80E+01	2.33E+02
$CO_2(1,1,1,0,2) + CO_2(0,0,0,0,1) \rightarrow CO_2(0,2,2,0,1) + CO_2(0,1,1,0,1)$	3.52E+01	-8.80E+01	2.33E+02
$CO_2(1,1,1,0,2) + CO_2(0,0,0,0,1) \rightarrow CO_2(1,0,0,0,2) + CO_2(0,1,1,0,1)$	3.57E+01	-8.82E+01	2.33E+02
$CO_2(1,1,1,0,2) + CO_2(0,0,0,0,1) \rightarrow CO_2(1,0,0,0,2) + CO_2(1,0,0,0,2)$	3.57E+01	-8.80E+01	2.33E+02
$CO_2(1,1,1,0,2) + CO_2(0,1,1,0,1) \rightarrow CO_2(0,2,2,0,1) + CO_2(0,2,2,0,1)$	3.59E+01	-8.80E+01	2.33E+02
$CO_2(1,1,1,0,2) + CO_2(0,1,1,0,1) \rightarrow CO_2(1,0,0,0,2) + CO_2(1,0,0,0,2)$	3.62E+01	-8.80E+01	2.33E+02
$CO_2(1,1,1,0,2) + CO_2(0,2,2,0,1) \rightarrow CO_2(0,2,2,0,1) + CO_2(0,3,3,0,1)$	3.63E+01	-8.80E+01	2.33E+02
$CO_2(1,1,1,0,2) + CO_2(0,2,2,0,1) \rightarrow CO_2(1,0,0,0,2) + CO_2(1,1,1,0,2)$	3.66E+01	-8.80E+01	2.33E+02
$CO_2(1,1,1,0,2) + CO_2(1,0,0,0,2) \rightarrow CO_2(0,2,2,0,1) + CO_2(1,1,1,0,2)$	3.63E+01	-8.80E+01	2.33E+02
$CO_2(1,1,1,0,2) + CO_2(1,1,1,0,2) \rightarrow CO_2(1,0,0,0,2) + CO_2(0,3,3,0,1)$	3.66E+01	-8.80E+01	2.33E+02
$CO_2(1,1,1,1,2) + CO_2(0,0,0,1,1) \rightarrow CO_2(0,2,2,1,1) + CO_2(0,1,1,1,1)$	3.52E+01	-8.80E+01	2.33E+02
$CO_2(1,1,1,1,2) + CO_2(0,0,0,1,1) \rightarrow CO_2(1,0,0,1,2) + CO_2(0,1,1,1,1)$	3.57E+01	-8.82E+01	2.33E+02
$CO_2(1,1,1,1,2) + CO_2(0,0,0,1,1) \rightarrow CO_2(1,0,0,1,2) + CO_2(1,0,0,1,2)$	3.57E+01	-8.80E+01	2.33E+02
$CO_2(1,1,1,1,2) + CO_2(0,1,1,1,1) \rightarrow CO_2(0,2,2,1,1) + CO_2(0,2,2,1,1)$	3.59E+01	-8.80E+01	2.33E+02
$CO_2(1,1,1,1,2) + CO_2(0,1,1,1,1) \rightarrow CO_2(1,0,0,1,2) + CO_2(1,0,0,1,2)$	3.62E+01	-8.80E+01	2.33E+02
$CO_2(1,1,1,1,2) + CO_2(0,2,2,1,1) \rightarrow CO_2(0,2,2,1,1) + CO_2(0,3,3,1,1)$	3.63E+01	-8.80E+01	2.33E+02
$CO_2(1,1,1,1,2) + CO_2(0,2,2,1,1) \rightarrow CO_2(1,0,0,1,2) + CO_2(1,1,1,1,2)$	3.66E+01	-8.80E+01	2.33E+02
$CO_2(1,1,1,1,2) + CO_2(1,0,0,1,2) \rightarrow CO_2(0,2,2,1,1) + CO_2(1,1,1,1,2)$	3.63E+01	-8.80E+01	2.33E+02
$CO_2(1,1,1,1,2) + CO_2(1,1,1,1,2) \rightarrow CO_2(1,0,0,1,2) + CO_2(0,3,3,1,1)$	3.66E+01	-8.80E+01	2.33E+02
$CO_2(1,1,1,2,2) + CO_2(0,0,0,2,1) \rightarrow CO_2(0,2,2,2,1) + CO_2(0,1,1,2,1)$	3.52E+01	-8.80E+01	2.33E+02
$CO_2(1,1,1,2,2) + CO_2(0,0,0,2,1) \rightarrow CO_2(1,0,0,2,2) + CO_2(0,1,1,2,1)$	3.57E+01	-8.82E+01	2.33E+02
$CO_2(1,1,1,2,2) + CO_2(0,0,0,2,1) \rightarrow CO_2(1,0,0,2,2) + CO_2(1,0,0,2,2)$	3.57E+01	-8.80E+01	2.33E+02
$CO_2(1,1,1,2,2) + CO_2(0,1,1,2,1) \rightarrow CO_2(0,2,2,2,1) + CO_2(0,2,2,2,1)$	3.59E+01	-8.80E+01	2.33E+02
$CO_2(1,1,1,2,2) + CO_2(0,1,1,2,1) \rightarrow CO_2(1,0,0,2,2) + CO_2(1,0,0,2,2)$	3.62E+01	-8.80E+01	2.33E+02
$CO_2(1,1,1,2,2) + CO_2(0,2,2,2,1) \rightarrow CO_2(0,2,2,2,1) + CO_2(0,3,3,2,1)$	3.63E+01	-8.80E+01	2.33E+02
$CO_2(1,1,1,2,2) + CO_2(0,2,2,2,1) \rightarrow CO_2(1,0,0,2,2) + CO_2(1,1,1,2,2)$	3.66E+01	-8.80E+01	2.33E+02
$CO_2(1,1,1,2,2) + CO_2(1,0,0,2,2) \rightarrow CO_2(0,2,2,2,1) + CO_2(1,1,1,2,2)$	3.63E+01	-8.80E+01	2.33E+02
$CO_2(1,1,1,2,2) + CO_2(1,1,1,2,2) \rightarrow CO_2(1,0,0,2,2) + CO_2(0,3,3,2,1)$	3.66E+01	-8.80E+01	2.33E+02
$CO_2(1,1,1,3,2) + CO_2(0,0,0,3,1) \rightarrow CO_2(0,2,2,3,1) + CO_2(0,1,1,3,1)$	3.52E+01	-8.80E+01	2.33E+02
$CO_2(1,1,1,3,2) + CO_2(0,0,0,3,1) \rightarrow CO_2(1,0,0,3,2) + CO_2(0,1,1,3,1)$	3.57E+01	-8.82E+01	2.33E+02
$CO_2(1,1,1,3,2) + CO_2(0,0,0,3,1) \rightarrow CO_2(1,0,0,3,2) + CO_2(1,0,0,3,2)$	3.57E+01	-8.80E+01	2.33E+02
$CO_2(1,1,1,3,2) + CO_2(0,1,1,3,1) \rightarrow CO_2(0,2,2,3,1) + CO_2(0,2,2,3,1)$	3.59E+01	-8.80E+01	2.33E+02
$CO_2(1,1,1,3,2) + CO_2(0,1,1,3,1) \rightarrow CO_2(1,0,0,3,2) + CO_2(1,0,0,3,2)$	3.62E+01	-8.80E+01	2.33E+02
$CO_2(1,1,1,3,2) + CO_2(0,2,2,3,1) \rightarrow CO_2(0,2,2,3,1) + CO_2(0,3,3,3,1)$	3.63E+01	-8.80E+01	2.33E+02

$CO_2(1,1,1,3,2) + CO_2(0,2,2,3,1) \rightarrow CO_2(1,0,0,3,2) + CO_2(1,1,1,3,2)$	3.66E+01	-8.80E+01	2.33E+02
$CO_2(1,1,1,3,2) + CO_2(1,0,0,3,2) \rightarrow CO_2(0,2,2,3,1) + CO_2(1,1,1,3,2)$	3.63E+01	-8.80E+01	2.33E+02
$CO_2(1,1,1,3,2) + CO_2(1,1,1,3,2) \rightarrow CO_2(1,0,0,3,2) + CO_2(0,3,3,3,1)$	3.66E+01	-8.80E+01	2.33E+02
$CO_2(1,1,1,4,2) + CO_2(0,0,0,4,1) \rightarrow CO_2(0,2,2,4,1) + CO_2(0,1,1,4,1)$	3.52E+01	-8.80E+01	2.33E+02
$CO_2(1,1,1,4,2) + CO_2(0,0,0,4,1) \rightarrow CO_2(1,0,0,4,2) + CO_2(0,1,1,4,1)$	3.57E+01	-8.82E+01	2.33E+02
$CO_2(1,1,1,4,2) + CO_2(0,0,0,4,1) \rightarrow CO_2(1,0,0,4,2) + CO_2(1,0,0,4,2)$	3.57E+01	-8.80E+01	2.33E+02
$CO_2(1,1,1,4,2) + CO_2(0,1,1,4,1) \rightarrow CO_2(0,2,2,4,1) + CO_2(0,2,2,4,1)$	3.59E+01	-8.80E+01	2.33E+02
$CO_2(1,1,1,4,2) + CO_2(0,1,1,4,1) \rightarrow CO_2(1,0,0,4,2) + CO_2(1,0,0,4,2)$	3.62E+01	-8.80E+01	2.33E+02
$CO_2(1,1,1,4,2) + CO_2(0,2,2,4,1) \rightarrow CO_2(0,2,2,4,1) + CO_2(0,3,3,4,1)$	3.63E+01	-8.80E+01	2.33E+02
$CO_2(1,1,1,4,2) + CO_2(0,2,2,4,1) \rightarrow CO_2(1,0,0,4,2) + CO_2(1,1,1,4,2)$	3.66E+01	-8.80E+01	2.33E+02
$CO_2(1,1,1,4,2) + CO_2(1,0,0,4,2) \rightarrow CO_2(0,2,2,4,1) + CO_2(1,1,1,4,2)$	3.63E+01	-8.80E+01	2.33E+02
$CO_2(1,1,1,4,2) + CO_2(1,1,1,4,2) \rightarrow CO_2(1,0,0,4,2) + CO_2(0,3,3,4,1)$	3.66E+01	-8.80E+01	2.33E+02
$CO_2(1,1,1,5,2) + CO_2(0,0,0,5,1) \rightarrow CO_2(0,2,2,5,1) + CO_2(0,1,1,5,1)$	3.52E+01	-8.80E+01	2.33E+02
$CO_2(1,1,1,5,2) + CO_2(0,0,0,5,1) \rightarrow CO_2(1,0,0,5,2) + CO_2(0,1,1,5,1)$	3.57E+01	-8.82E+01	2.33E+02
$CO_2(1,1,1,5,2) + CO_2(0,0,0,5,1) \rightarrow CO_2(1,0,0,5,2) + CO_2(1,0,0,5,2)$	3.57E+01	-8.80E+01	2.33E+02
$CO_2(1,1,1,5,2) + CO_2(0,1,1,5,1) \rightarrow CO_2(0,2,2,5,1) + CO_2(0,2,2,5,1)$	3.59E+01	-8.80E+01	2.33E+02
$CO_2(1,1,1,5,2) + CO_2(0,1,1,5,1) \rightarrow CO_2(1,0,0,5,2) + CO_2(1,0,0,5,2)$	3.62E+01	-8.80E+01	2.33E+02
$CO_2(1,1,1,5,2) + CO_2(0,2,2,5,1) \rightarrow CO_2(0,2,2,5,1) + CO_2(0,3,3,5,1)$	3.63E+01	-8.80E+01	2.33E+02
$CO_2(1,1,1,5,2) + CO_2(0,2,2,5,1) \rightarrow CO_2(1,0,0,5,2) + CO_2(1,1,1,5,2)$	3.66E+01	-8.80E+01	2.33E+02
$CO_2(1,1,1,5,2) + CO_2(1,0,0,5,2) \rightarrow CO_2(0,2,2,5,1) + CO_2(1,1,1,5,2)$	3.63E+01	-8.80E+01	2.33E+02
$CO_2(1,1,1,5,2) + CO_2(1,1,1,5,2) \rightarrow CO_2(1,0,0,5,2) + CO_2(0,3,3,5,1)$	3.66E+01	-8.80E+01	2.33E+02
$CO_2(1,2,2,0,2) + CO_2(0,0,0,0,1) \rightarrow CO_2(0,2,2,0,1) + CO_2(1,0,0,0,2)$	3.38E+01	-8.80E+01	2.33E+02
$CO_2(1,2,2,0,2) + CO_2(0,0,0,0,1) \rightarrow CO_2(0,3,3,0,1) + CO_2(0,1,1,0,1)$	3.55E+01	-8.80E+01	2.33E+02
$CO_2(1,2,2,0,2) + CO_2(0,0,0,0,1) \rightarrow CO_2(1,1,1,0,2) + CO_2(0,1,1,0,1)$	3.59E+01	-8.80E+01	2.33E+02
$CO_2(1,2,2,0,2) + CO_2(0,1,1,0,1) \rightarrow CO_2(1,1,1,0,2) + CO_2(0,2,2,0,1)$	3.66E+01	-8.80E+01	2.33E+02
$CO_2(1,2,2,0,2) + CO_2(0,1,1,0,1) \rightarrow CO_2(1,1,1,0,2) + CO_2(1,0,0,0,2)$	3.66E+01	-8.80E+01	2.33E+02
$CO_2(1,2,2,0,2) + CO_2(0,2,2,0,1) \rightarrow CO_2(0,3,3,0,1) + CO_2(0,3,3,0,1)$	3.66E+01	-8.80E+01	2.33E+02
$CO_2(1,2,2,0,2) + CO_2(0,2,2,0,1) \rightarrow CO_2(1,1,1,0,2) + CO_2(0,3,3,0,1)$	3.75E+01	-8.80E+01	2.33E+02
$CO_2(1,2,2,0,2) + CO_2(0,2,2,0,1) \rightarrow CO_2(1,1,1,0,2) + CO_2(1,1,1,0,2)$	3.70E+01	-8.80E+01	2.33E+02
$CO_2(1,2,2,0,2) + CO_2(0,3,3,0,1) \rightarrow CO_2(0,3,3,0,1) + CO_2(0,4,4,0,1)$	3.69E+01	-8.80E+01	2.33E+02
$CO_2(1,2,2,0,2) + CO_2(0,3,3,0,1) \rightarrow CO_2(1,1,1,0,2) + CO_2(0,4,4,0,1)$	3.73E+01	-8.80E+01	2.30E+01
$CO_2(1,2,2,0,2) + CO_2(0,3,3,0,1) \rightarrow CO_2(1,1,1,0,2) + CO_2(1,2,2,0,2)$	3.73E+01	-8.80E+01	2.33E+02
$CO_2(1,2,2,0,2) + CO_2(1,0,0,0,2) \rightarrow CO_2(0,2,2,0,1) + CO_2(2,0,0,0,3)$	3.49E+01	-8.90E+01	2.34E+02
$CO_2(1,2,2,0,2) + CO_2(1,0,0,0,2) \rightarrow CO_2(0,3,3,0,1) + CO_2(1,1,1,0,2)$	3.69E+01	-8.80E+01	2.33E+02
$CO_2(1,2,2,0,2) + CO_2(1,0,0,0,2) \rightarrow CO_2(1,1,1,0,2) + CO_2(1,1,1,0,2)$	3.73E+01	-8.80E+01	2.33E+02
$CO_2(1,2,2,0,2) + CO_2(1,1,1,0,2) \rightarrow CO_2(0,3,3,0,1) + CO_2(1,0,0,0,2)$	3.73E+01	-8.80E+01	2.33E+02
$CO_2(1,2,2,0,2) + CO_2(1,1,1,0,2) \rightarrow CO_2(0,3,3,0,1) + CO_2(1,2,2,0,2)$	3.73E+01	-8.80E+01	2.33E+02
$CO_2(1,2,2,1,2) + CO_2(0,0,0,1,1) \rightarrow CO_2(0,2,2,1,1) + CO_2(1,0,0,1,2)$	3.38E+01	-8.80E+01	2.33E+02
$CO_2(1,2,2,1,2) + CO_2(0,0,0,1,1) \rightarrow CO_2(0,3,3,1,1) + CO_2(0,1,1,1,1)$	3.55E+01	-8.80E+01	2.33E+02
$CO_2(1,2,2,1,2) + CO_2(0,0,0,1,1) \rightarrow CO_2(1,1,1,1,2) + CO_2(0,1,1,1,1)$	3.59E+01	-8.80E+01	2.33E+02

$CO_2(1,2,2,1,2) + CO_2(0,1,1,1,1) \rightarrow CO_2(1,1,1,1,2) + CO_2(0,2,2,1,1)$	3.66E+01	-8.80E+01	2.33E+02
$CO_2(1,2,2,1,2) + CO_2(0,1,1,1,1) \rightarrow CO_2(1,1,1,1,2) + CO_2(1,0,0,1,2)$	3.66E+01	-8.80E+01	2.33E+02
$CO_2(1,2,2,1,2) + CO_2(0,2,2,1,1) \rightarrow CO_2(0,3,3,1,1) + CO_2(0,3,3,1,1)$	3.66E+01	-8.80E+01	2.33E+02
$CO_2(1,2,2,1,2) + CO_2(0,2,2,1,1) \rightarrow CO_2(1,1,1,1,2) + CO_2(0,3,3,1,1)$	3.75E+01	-8.80E+01	2.33E+02
$CO_2(1,2,2,1,2) + CO_2(0,2,2,1,1) \rightarrow CO_2(1,1,1,1,2) + CO_2(1,1,1,1,2)$	3.70E+01	-8.80E+01	2.33E+02
$CO_2(1,2,2,1,2) + CO_2(0,3,3,1,1) \rightarrow CO_2(0,3,3,1,1) + CO_2(0,4,4,1,1)$	3.69E+01	-8.80E+01	2.33E+02
$CO_2(1,2,2,1,2) + CO_2(0,3,3,1,1) \rightarrow CO_2(1,1,1,1,2) + CO_2(0,4,4,1,1)$	3.73E+01	-8.80E+01	2.30E+01
$CO_2(1,2,2,1,2) + CO_2(0,3,3,1,1) \rightarrow CO_2(1,1,1,1,2) + CO_2(1,2,2,1,2)$	3.73E+01	-8.80E+01	2.33E+02
$CO_2(1,2,2,1,2) + CO_2(1,0,0,1,2) \rightarrow CO_2(0,2,2,1,1) + CO_2(2,0,0,1,3)$	3.49E+01	-8.90E+01	2.34E+02
$CO_2(1,2,2,1,2) + CO_2(1,0,0,1,2) \rightarrow CO_2(0,3,3,1,1) + CO_2(1,1,1,1,2)$	3.69E+01	-8.80E+01	2.33E+02
$CO_2(1,2,2,1,2) + CO_2(1,0,0,1,2) \rightarrow CO_2(1,1,1,1,2) + CO_2(1,1,1,1,2)$	3.73E+01	-8.80E+01	2.33E+02
$CO_2(1,2,2,1,2) + CO_2(1,1,1,1,2) \rightarrow CO_2(0,3,3,1,1) + CO_2(1,0,0,1,2)$	3.73E+01	-8.80E+01	2.33E+02
$CO_2(1,2,2,1,2) + CO_2(1,1,1,1,2) \rightarrow CO_2(0,3,3,1,1) + CO_2(1,2,2,1,2)$	3.73E+01	-8.80E+01	2.33E+02
$CO_2(1,2,2,2,2) + CO_2(0,0,0,2,1) \rightarrow CO_2(0,2,2,2,1) + CO_2(1,0,0,2,2)$	3.38E+01	-8.80E+01	2.33E+02
$CO_2(1,2,2,2,2) + CO_2(0,0,0,2,1) \rightarrow CO_2(0,3,3,2,1) + CO_2(0,1,1,2,1)$	3.55E+01	-8.80E+01	2.33E+02
$CO_2(1,2,2,2,2) + CO_2(0,0,0,2,1) \rightarrow CO_2(1,1,1,2,2) + CO_2(0,1,1,2,1)$	3.59E+01	-8.80E+01	2.33E+02
$CO_2(1,2,2,2,2) + CO_2(0,1,1,2,1) \rightarrow CO_2(1,1,1,2,2) + CO_2(0,2,2,2,1)$	3.66E+01	-8.80E+01	2.33E+02
$CO_2(1,2,2,2,2) + CO_2(0,1,1,2,1) \rightarrow CO_2(1,1,1,2,2) + CO_2(1,0,0,2,2)$	3.66E+01	-8.80E+01	2.33E+02
$CO_2(1,2,2,2,2) + CO_2(0,2,2,2,1) \rightarrow CO_2(0,3,3,2,1) + CO_2(0,3,3,2,1)$	3.66E+01	-8.80E+01	2.33E+02
$CO_2(1,2,2,2,2) + CO_2(0,2,2,2,1) \rightarrow CO_2(1,1,1,2,2) + CO_2(0,3,3,2,1)$	3.75E+01	-8.80E+01	2.33E+02
$CO_2(1,2,2,2,2) + CO_2(0,2,2,2,1) \rightarrow CO_2(1,1,1,2,2) + CO_2(1,1,1,2,2)$	3.70E+01	-8.80E+01	2.33E+02
$CO_2(1,2,2,2,2) + CO_2(0,3,3,2,1) \rightarrow CO_2(0,3,3,2,1) + CO_2(0,4,4,2,1)$	3.69E+01	-8.80E+01	2.33E+02
$CO_2(1,2,2,2,2) + CO_2(0,3,3,2,1) \rightarrow CO_2(1,1,1,2,2) + CO_2(0,4,4,2,1)$	3.73E+01	-8.80E+01	2.30E+01
$CO_2(1,2,2,2,2) + CO_2(0,3,3,2,1) \rightarrow CO_2(1,1,1,2,2) + CO_2(1,2,2,2,2)$	3.73E+01	-8.80E+01	2.33E+02
$CO_2(1,2,2,2,2) + CO_2(1,0,0,2,2) \rightarrow CO_2(0,2,2,2,1) + CO_2(2,0,0,2,3)$	3.49E+01	-8.90E+01	2.34E+02
$CO_2(1,2,2,2,2) + CO_2(1,0,0,2,2) \rightarrow CO_2(0,3,3,2,1) + CO_2(1,1,1,2,2)$	3.69E+01	-8.80E+01	2.33E+02
$CO_2(1,2,2,2,2) + CO_2(1,0,0,2,2) \rightarrow CO_2(1,1,1,2,2) + CO_2(1,1,1,2,2)$	3.73E+01	-8.80E+01	2.33E+02
$CO_2(1,2,2,2,2) + CO_2(1,1,1,2,2) \rightarrow CO_2(0,3,3,2,1) + CO_2(1,0,0,2,2)$	3.73E+01	-8.80E+01	2.33E+02
$CO_2(1,2,2,2,2) + CO_2(1,1,1,2,2) \rightarrow CO_2(0,3,3,2,1) + CO_2(1,2,2,2,2)$	3.73E+01	-8.80E+01	2.33E+02
$CO_2(1,2,2,3,2) + CO_2(0,0,0,3,1) \rightarrow CO_2(0,2,2,3,1) + CO_2(1,0,0,3,2)$	3.38E+01	-8.80E+01	2.33E+02
$CO_2(1,2,2,3,2) + CO_2(0,0,0,3,1) \rightarrow CO_2(0,3,3,3,1) + CO_2(0,1,1,3,1)$	3.55E+01	-8.80E+01	2.33E+02
$CO_2(1,2,2,3,2) + CO_2(0,0,0,3,1) \rightarrow CO_2(1,1,1,3,2) + CO_2(0,1,1,3,1)$	3.59E+01	-8.80E+01	2.33E+02
$CO_2(1,2,2,3,2) + CO_2(0,1,1,3,1) \rightarrow CO_2(1,1,1,3,2) + CO_2(0,2,2,3,1)$	3.66E+01	-8.80E+01	2.33E+02
$CO_2(1,2,2,3,2) + CO_2(0,1,1,3,1) \rightarrow CO_2(1,1,1,3,2) + CO_2(1,0,0,3,2)$	3.66E+01	-8.80E+01	2.33E+02
$CO_2(1,2,2,3,2) + CO_2(0,2,2,3,1) \rightarrow CO_2(0,3,3,3,1) + CO_2(0,3,3,3,1)$	3.66E+01	-8.80E+01	2.33E+02
$CO_2(1,2,2,3,2) + CO_2(0,2,2,3,1) \rightarrow CO_2(1,1,1,3,2) + CO_2(0,3,3,3,1)$	3.75E+01	-8.80E+01	2.33E+02
$CO_2(1,2,2,3,2) + CO_2(0,2,2,3,1) \rightarrow CO_2(1,1,1,3,2) + CO_2(1,1,1,3,2)$	3.70E+01	-8.80E+01	2.33E+02
$CO_2(1,2,2,3,2) + CO_2(0,3,3,3,1) \rightarrow CO_2(0,3,3,3,1) + CO_2(0,4,4,3,1)$	3.69E+01	-8.80E+01	2.33E+02
$CO_2(1,2,2,3,2) + CO_2(0,3,3,3,1) \rightarrow CO_2(1,1,1,3,2) + CO_2(0,4,4,3,1)$	3.73E+01	-8.80E+01	2.30E+01
$CO_2(1,2,2,3,2) + CO_2(0,3,3,3,1) \rightarrow CO_2(1,1,1,3,2) + CO_2(1,2,2,3,2)$	3.73E+01	-8.80E+01	2.33E+02

$CO_2(1,2,2,3,2) + CO_2(1,0,0,3,2) \rightarrow CO_2(0,2,2,3,1) + CO_2(2,0,0,3,3)$	3.49E+01	-8.90E+01	2.34E+02
$CO_2(1,2,2,3,2) + CO_2(1,0,0,3,2) \rightarrow CO_2(0,3,3,3,1) + CO_2(1,1,1,3,2)$	3.69E+01	-8.80E+01	2.33E+02
$CO_2(1,2,2,3,2) + CO_2(1,0,0,3,2) \rightarrow CO_2(1,1,1,3,2) + CO_2(1,1,1,3,2)$	3.73E+01	-8.80E+01	2.33E+02
$CO_2(1,2,2,3,2) + CO_2(1,1,1,3,2) \rightarrow CO_2(0,3,3,3,1) + CO_2(1,0,0,3,2)$	3.73E+01	-8.80E+01	2.33E+02
$CO_2(1,2,2,3,2) + CO_2(1,1,1,3,2) \rightarrow CO_2(0,3,3,3,1) + CO_2(1,2,2,3,2)$	3.73E+01	-8.80E+01	2.33E+02
$CO_2(1,2,2,4,2) + CO_2(0,0,0,4,1) \rightarrow CO_2(0,2,2,4,1) + CO_2(1,0,0,4,2)$	3.38E+01	-8.80E+01	2.33E+02
$CO_2(1,2,2,4,2) + CO_2(0,0,0,4,1) \rightarrow CO_2(0,3,3,4,1) + CO_2(0,1,1,4,1)$	3.55E+01	-8.80E+01	2.33E+02
$CO_2(1,2,2,4,2) + CO_2(0,0,0,4,1) \rightarrow CO_2(1,1,1,4,2) + CO_2(0,1,1,4,1)$	3.59E+01	-8.80E+01	2.33E+02
$CO_2(1,2,2,4,2) + CO_2(0,1,1,4,1) \rightarrow CO_2(1,1,1,4,2) + CO_2(0,2,2,4,1)$	3.66E+01	-8.80E+01	2.33E+02
$CO_2(1,2,2,4,2) + CO_2(0,1,1,4,1) \rightarrow CO_2(1,1,1,4,2) + CO_2(1,0,0,4,2)$	3.66E+01	-8.80E+01	2.33E+02
$CO_2(1,2,2,4,2) + CO_2(0,2,2,4,1) \rightarrow CO_2(0,3,3,4,1) + CO_2(0,3,3,4,1)$	3.66E+01	-8.80E+01	2.33E+02
$CO_2(1,2,2,4,2) + CO_2(0,2,2,4,1) \rightarrow CO_2(1,1,1,4,2) + CO_2(0,3,3,4,1)$	3.75E+01	-8.80E+01	2.33E+02
$CO_2(1,2,2,4,2) + CO_2(0,2,2,4,1) \rightarrow CO_2(1,1,1,4,2) + CO_2(1,1,1,4,2)$	3.70E+01	-8.80E+01	2.33E+02
$CO_2(1,2,2,4,2) + CO_2(0,3,3,4,1) \rightarrow CO_2(0,3,3,4,1) + CO_2(0,4,4,4,1)$	3.69E+01	-8.80E+01	2.33E+02
$CO_2(1,2,2,4,2) + CO_2(0,3,3,4,1) \rightarrow CO_2(1,1,1,4,2) + CO_2(0,4,4,4,1)$	3.73E+01	-8.80E+01	2.30E+01
$CO_2(1,2,2,4,2) + CO_2(0,3,3,4,1) \rightarrow CO_2(1,1,1,4,2) + CO_2(1,2,2,4,2)$	3.73E+01	-8.80E+01	2.33E+02
$CO_2(1,2,2,4,2) + CO_2(1,0,0,4,2) \rightarrow CO_2(0,2,2,4,1) + CO_2(2,0,0,4,3)$	3.49E+01	-8.90E+01	2.34E+02
$CO_2(1,2,2,4,2) + CO_2(1,0,0,4,2) \rightarrow CO_2(0,3,3,4,1) + CO_2(1,1,1,4,2)$	3.69E+01	-8.80E+01	2.33E+02
$CO_2(1,2,2,4,2) + CO_2(1,0,0,4,2) \rightarrow CO_2(1,1,1,4,2) + CO_2(1,1,1,4,2)$	3.73E+01	-8.80E+01	2.33E+02
$CO_2(1,2,2,4,2) + CO_2(1,1,1,4,2) \rightarrow CO_2(0,3,3,4,1) + CO_2(1,0,0,4,2)$	3.73E+01	-8.80E+01	2.33E+02
$CO_2(1,2,2,4,2) + CO_2(1,1,1,4,2) \rightarrow CO_2(0,3,3,4,1) + CO_2(1,2,2,4,2)$	3.73E+01	-8.80E+01	2.33E+02
$CO_2(1,2,2,5,2) + CO_2(0,0,0,5,1) \rightarrow CO_2(0,2,2,5,1) + CO_2(1,0,0,5,2)$	3.38E+01	-8.80E+01	2.33E+02
$CO_2(1,2,2,5,2) + CO_2(0,0,0,5,1) \rightarrow CO_2(0,3,3,5,1) + CO_2(0,1,1,5,1)$	3.55E+01	-8.80E+01	2.33E+02
$CO_2(1,2,2,5,2) + CO_2(0,0,0,5,1) \rightarrow CO_2(1,1,1,5,2) + CO_2(0,1,1,5,1)$	3.59E+01	-8.80E+01	2.33E+02
$CO_2(1,2,2,5,2) + CO_2(0,1,1,5,1) \rightarrow CO_2(1,1,1,5,2) + CO_2(0,2,2,5,1)$	3.66E+01	-8.80E+01	2.33E+02
$CO_2(1,2,2,5,2) + CO_2(0,1,1,5,1) \rightarrow CO_2(1,1,1,5,2) + CO_2(1,0,0,5,2)$	3.66E+01	-8.80E+01	2.33E+02
$CO_2(1,2,2,5,2) + CO_2(0,2,2,5,1) \rightarrow CO_2(0,3,3,5,1) + CO_2(0,3,3,5,1)$	3.66E+01	-8.80E+01	2.33E+02
$CO_2(1,2,2,5,2) + CO_2(0,2,2,5,1) \rightarrow CO_2(1,1,1,5,2) + CO_2(0,3,3,5,1)$	3.75E+01	-8.80E+01	2.33E+02
$CO_2(1,2,2,5,2) + CO_2(0,2,2,5,1) \rightarrow CO_2(1,1,1,5,2) + CO_2(1,1,1,5,2)$	3.70E+01	-8.80E+01	2.33E+02
$CO_2(1,2,2,5,2) + CO_2(0,3,3,5,1) \rightarrow CO_2(0,3,3,5,1) + CO_2(0,4,4,5,1)$	3.69E+01	-8.80E+01	2.33E+02
$CO_2(1,2,2,5,2) + CO_2(0,3,3,5,1) \rightarrow CO_2(1,1,1,5,2) + CO_2(0,4,4,5,1)$	3.73E+01	-8.80E+01	2.30E+01
$CO_2(1,2,2,5,2) + CO_2(0,3,3,5,1) \rightarrow CO_2(1,1,1,5,2) + CO_2(1,2,2,5,2)$	3.73E+01	-8.80E+01	2.33E+02
$CO_2(1,2,2,5,2) + CO_2(1,0,0,5,2) \rightarrow CO_2(0,2,2,5,1) + CO_2(2,0,0,5,3)$	3.49E+01	-8.90E+01	2.34E+02
$CO_2(1,2,2,5,2) + CO_2(1,0,0,5,2) \rightarrow CO_2(0,3,3,5,1) + CO_2(1,1,1,5,2)$	3.69E+01	-8.80E+01	2.33E+02
$CO_2(1,2,2,5,2) + CO_2(1,0,0,5,2) \rightarrow CO_2(1,1,1,5,2) + CO_2(1,1,1,5,2)$	3.73E+01	-8.80E+01	2.33E+02
$CO_2(1,2,2,5,2) + CO_2(1,1,1,5,2) \rightarrow CO_2(0,3,3,5,1) + CO_2(1,0,0,5,2)$	3.73E+01	-8.80E+01	2.33E+02
$CO_2(1,2,2,5,2) + CO_2(1,1,1,5,2) \rightarrow CO_2(0,3,3,5,1) + CO_2(1,2,2,5,2)$	3.73E+01	-8.80E+01	2.33E+02
$CO_2(1,3,3,0,2) + CO_2(0,0,0,0,1) \rightarrow CO_2(0,4,4,0,1) + CO_2(0,1,1,0,1)$	3.57E+01	-8.80E+01	2.33E+02
$CO_2(1,3,3,0,2) + CO_2(0,0,0,0,1) \rightarrow CO_2(1,2,2,0,2) + CO_2(0,1,1,0,1)$	3.62E+01	-8.80E+01	2.33E+02
$CO_2(1,3,3,0,2) + CO_2(0,1,1,0,1) \rightarrow CO_2(0,4,4,0,1) + CO_2(0,2,2,0,1)$	3.64E+01	-8.80E+01	2.33E+02

CO_2(1,3,3,0,2) + CO_2(0,1,1,0,1) → CO_2(0,4,4,0,1) + CO_2(1,0,0,0,2)	3.64E+01	-8.80E+01	2.33E+02
CO_2(1,3,3,0,2) + CO_2(0,1,1,0,1) → CO_2(1,2,2,0,2) + CO_2(0,2,2,0,1)	3.69E+01	-8.80E+01	2.33E+02
CO_2(1,3,3,0,2) + CO_2(0,1,1,0,1) → CO_2(1,2,2,0,2) + CO_2(1,0,0,0,2)	3.69E+01	-8.80E+01	2.33E+02
CO_2(1,3,3,0,2) + CO_2(0,2,2,0,1) → CO_2(0,4,4,0,1) + CO_2(0,3,3,0,1)	3.68E+01	-8.80E+01	2.33E+02
CO_2(1,3,3,0,2) + CO_2(0,2,2,0,1) → CO_2(0,4,4,0,1) + CO_2(1,1,1,0,2)	3.68E+01	-8.80E+01	2.33E+02
CO_2(1,3,3,0,2) + CO_2(0,2,2,0,1) → CO_2(1,2,2,0,2) + CO_2(0,3,3,0,1)	3.75E+01	-8.80E+01	2.33E+02
CO_2(1,3,3,0,2) + CO_2(0,2,2,0,1) → CO_2(1,2,2,0,2) + CO_2(1,1,1,0,2)	3.73E+01	-8.80E+01	2.33E+02
CO_2(1,3,3,0,2) + CO_2(1,0,0,0,2) → CO_2(0,4,4,0,1) + CO_2(1,1,1,0,2)	3.64E+01	-8.80E+01	2.33E+02
CO_2(1,3,3,0,2) + CO_2(1,0,0,0,2) → CO_2(1,2,2,0,2) + CO_2(1,1,1,0,2)	3.76E+01	-8.80E+01	2.33E+02
CO_2(1,3,3,1,2) + CO_2(0,0,0,1,1) → CO_2(0,4,4,1,1) + CO_2(0,1,1,1,1)	3.57E+01	-8.80E+01	2.33E+02
CO_2(1,3,3,1,2) + CO_2(0,0,0,1,1) → CO_2(1,2,2,1,2) + CO_2(0,1,1,1,1)	3.62E+01	-8.80E+01	2.33E+02
CO_2(1,3,3,1,2) + CO_2(0,1,1,1,1) → CO_2(0,4,4,1,1) + CO_2(0,2,2,1,1)	3.64E+01	-8.80E+01	2.33E+02
CO_2(1,3,3,1,2) + CO_2(0,1,1,1,1) → CO_2(0,4,4,1,1) + CO_2(1,0,0,1,2)	3.64E+01	-8.80E+01	2.33E+02
CO_2(1,3,3,1,2) + CO_2(0,1,1,1,1) → CO_2(1,2,2,1,2) + CO_2(0,2,2,1,1)	3.69E+01	-8.80E+01	2.33E+02
CO_2(1,3,3,1,2) + CO_2(0,1,1,1,1) → CO_2(1,2,2,1,2) + CO_2(1,0,0,1,2)	3.69E+01	-8.80E+01	2.33E+02
CO_2(1,3,3,1,2) + CO_2(0,2,2,1,1) → CO_2(0,4,4,1,1) + CO_2(0,3,3,1,1)	3.68E+01	-8.80E+01	2.33E+02
CO_2(1,3,3,1,2) + CO_2(0,2,2,1,1) → CO_2(0,4,4,1,1) + CO_2(1,1,1,1,2)	3.68E+01	-8.80E+01	2.33E+02
CO_2(1,3,3,1,2) + CO_2(0,2,2,1,1) → CO_2(1,2,2,1,2) + CO_2(0,3,3,1,1)	3.75E+01	-8.80E+01	2.33E+02
CO_2(1,3,3,1,2) + CO_2(0,2,2,1,1) → CO_2(1,2,2,1,2) + CO_2(1,1,1,1,2)	3.73E+01	-8.80E+01	2.33E+02
CO_2(1,3,3,1,2) + CO_2(1,0,0,1,2) → CO_2(0,4,4,1,1) + CO_2(1,1,1,1,2)	3.64E+01	-8.80E+01	2.33E+02
CO_2(1,3,3,1,2) + CO_2(1,0,0,1,2) → CO_2(1,2,2,1,2) + CO_2(1,1,1,1,2)	3.76E+01	-8.80E+01	2.33E+02
CO_2(1,3,3,2,2) + CO_2(0,0,0,2,1) → CO_2(0,4,4,2,1) + CO_2(0,1,1,2,1)	3.57E+01	-8.80E+01	2.33E+02
CO_2(1,3,3,2,2) + CO_2(0,0,0,2,1) → CO_2(1,2,2,2,2) + CO_2(0,1,1,2,1)	3.62E+01	-8.80E+01	2.33E+02
CO_2(1,3,3,2,2) + CO_2(0,1,1,2,1) → CO_2(0,4,4,2,1) + CO_2(0,2,2,2,1)	3.64E+01	-8.80E+01	2.33E+02
CO_2(1,3,3,2,2) + CO_2(0,1,1,2,1) → CO_2(0,4,4,2,1) + CO_2(1,0,0,2,2)	3.64E+01	-8.80E+01	2.33E+02
CO_2(1,3,3,2,2) + CO_2(0,1,1,2,1) → CO_2(1,2,2,2,2) + CO_2(0,2,2,2,1)	3.69E+01	-8.80E+01	2.33E+02
CO_2(1,3,3,2,2) + CO_2(0,1,1,2,1) → CO_2(1,2,2,2,2) + CO_2(1,0,0,2,2)	3.69E+01	-8.80E+01	2.33E+02
CO_2(1,3,3,2,2) + CO_2(0,2,2,2,1) → CO_2(0,4,4,2,1) + CO_2(0,3,3,2,1)	3.68E+01	-8.80E+01	2.33E+02
CO_2(1,3,3,2,2) + CO_2(0,2,2,2,1) → CO_2(0,4,4,2,1) + CO_2(1,1,1,2,2)	3.68E+01	-8.80E+01	2.33E+02
CO_2(1,3,3,2,2) + CO_2(0,2,2,2,1) → CO_2(1,2,2,2,2) + CO_2(0,3,3,2,1)	3.75E+01	-8.80E+01	2.33E+02
CO_2(1,3,3,2,2) + CO_2(0,2,2,2,1) → CO_2(1,2,2,2,2) + CO_2(1,1,1,2,2)	3.73E+01	-8.80E+01	2.33E+02
CO_2(1,3,3,2,2) + CO_2(1,0,0,2,2) → CO_2(0,4,4,2,1) + CO_2(1,1,1,2,2)	3.64E+01	-8.80E+01	2.33E+02
CO_2(1,3,3,2,2) + CO_2(1,0,0,2,2) → CO_2(1,2,2,2,2) + CO_2(1,1,1,2,2)	3.76E+01	-8.80E+01	2.33E+02
CO_2(1,3,3,3,2) + CO_2(0,0,0,3,1) → CO_2(0,4,4,3,1) + CO_2(0,1,1,3,1)	3.57E+01	-8.80E+01	2.33E+02
CO_2(1,3,3,3,2) + CO_2(0,0,0,3,1) → CO_2(1,2,2,3,2) + CO_2(0,1,1,3,1)	3.62E+01	-8.80E+01	2.33E+02
CO_2(1,3,3,3,2) + CO_2(0,1,1,3,1) → CO_2(0,4,4,3,1) + CO_2(0,2,2,3,1)	3.64E+01	-8.80E+01	2.33E+02
CO_2(1,3,3,3,2) + CO_2(0,1,1,3,1) → CO_2(0,4,4,3,1) + CO_2(1,0,0,3,2)	3.64E+01	-8.80E+01	2.33E+02
CO_2(1,3,3,3,2) + CO_2(0,1,1,3,1) → CO_2(1,2,2,3,2) + CO_2(0,2,2,3,1)	3.69E+01	-8.80E+01	2.33E+02
CO_2(1,3,3,3,2) + CO_2(0,1,1,3,1) → CO_2(1,2,2,3,2) + CO_2(1,0,0,3,2)	3.69E+01	-8.80E+01	2.33E+02
CO_2(1,3,3,3,2) + CO_2(0,2,2,3,1) → CO_2(0,4,4,3,1) + CO_2(0,3,3,3,1)	3.68E+01	-8.80E+01	2.33E+02

$CO_2(1,3,3,3,2) + CO_2(0,2,2,3,1) \rightarrow CO_2(0,4,4,3,1) + CO_2(1,1,1,3,2)$	3.68E+01	-8.80E+01	2.33E+02
$CO_2(1,3,3,3,2) + CO_2(0,2,2,3,1) \rightarrow CO_2(1,2,2,3,2) + CO_2(0,3,3,3,1)$	3.75E+01	-8.80E+01	2.33E+02
$CO_2(1,3,3,3,2) + CO_2(0,2,2,3,1) \rightarrow CO_2(1,2,2,3,2) + CO_2(1,1,1,3,2)$	3.73E+01	-8.80E+01	2.33E+02
$CO_2(1,3,3,3,2) + CO_2(1,0,0,3,2) \rightarrow CO_2(0,4,4,3,1) + CO_2(1,1,1,3,2)$	3.64E+01	-8.80E+01	2.33E+02
$CO_2(1,3,3,3,2) + CO_2(1,0,0,3,2) \rightarrow CO_2(1,2,2,3,2) + CO_2(1,1,1,3,2)$	3.76E+01	-8.80E+01	2.33E+02
$CO_2(1,3,3,4,2) + CO_2(0,0,0,4,1) \rightarrow CO_2(0,4,4,4,1) + CO_2(0,1,1,4,1)$	3.57E+01	-8.80E+01	2.33E+02
$CO_2(1,3,3,4,2) + CO_2(0,0,0,4,1) \rightarrow CO_2(1,2,2,4,2) + CO_2(0,1,1,4,1)$	3.62E+01	-8.80E+01	2.33E+02
$CO_2(1,3,3,4,2) + CO_2(0,1,1,4,1) \rightarrow CO_2(0,4,4,4,1) + CO_2(0,2,2,4,1)$	3.64E+01	-8.80E+01	2.33E+02
$CO_2(1,3,3,4,2) + CO_2(0,1,1,4,1) \rightarrow CO_2(0,4,4,4,1) + CO_2(1,0,0,4,2)$	3.64E+01	-8.80E+01	2.33E+02
$CO_2(1,3,3,4,2) + CO_2(0,1,1,4,1) \rightarrow CO_2(1,2,2,4,2) + CO_2(0,2,2,4,1)$	3.69E+01	-8.80E+01	2.33E+02
$CO_2(1,3,3,4,2) + CO_2(0,1,1,4,1) \rightarrow CO_2(1,2,2,4,2) + CO_2(1,0,0,4,2)$	3.69E+01	-8.80E+01	2.33E+02
$CO_2(1,3,3,4,2) + CO_2(0,2,2,4,1) \rightarrow CO_2(0,4,4,4,1) + CO_2(0,3,3,4,1)$	3.68E+01	-8.80E+01	2.33E+02
$CO_2(1,3,3,4,2) + CO_2(0,2,2,4,1) \rightarrow CO_2(0,4,4,4,1) + CO_2(1,1,1,4,2)$	3.68E+01	-8.80E+01	2.33E+02
$CO_2(1,3,3,4,2) + CO_2(0,2,2,4,1) \rightarrow CO_2(1,2,2,4,2) + CO_2(0,3,3,4,1)$	3.75E+01	-8.80E+01	2.33E+02
$CO_2(1,3,3,4,2) + CO_2(0,2,2,4,1) \rightarrow CO_2(1,2,2,4,2) + CO_2(1,1,1,4,2)$	3.73E+01	-8.80E+01	2.33E+02
$CO_2(1,3,3,4,2) + CO_2(1,0,0,4,2) \rightarrow CO_2(0,4,4,4,1) + CO_2(1,1,1,4,2)$	3.64E+01	-8.80E+01	2.33E+02
$CO_2(1,3,3,4,2) + CO_2(1,0,0,4,2) \rightarrow CO_2(1,2,2,4,2) + CO_2(1,1,1,4,2)$	3.76E+01	-8.80E+01	2.33E+02
$CO_2(1,3,3,5,2) + CO_2(0,0,0,5,1) \rightarrow CO_2(0,4,4,5,1) + CO_2(0,1,1,5,1)$	3.57E+01	-8.80E+01	2.33E+02
$CO_2(1,3,3,5,2) + CO_2(0,0,0,5,1) \rightarrow CO_2(1,2,2,5,2) + CO_2(0,1,1,5,1)$	3.62E+01	-8.80E+01	2.33E+02
$CO_2(1,3,3,5,2) + CO_2(0,1,1,5,1) \rightarrow CO_2(0,4,4,5,1) + CO_2(0,2,2,5,1)$	3.64E+01	-8.80E+01	2.33E+02
$CO_2(1,3,3,5,2) + CO_2(0,1,1,5,1) \rightarrow CO_2(0,4,4,5,1) + CO_2(1,0,0,5,2)$	3.64E+01	-8.80E+01	2.33E+02
$CO_2(1,3,3,5,2) + CO_2(0,1,1,5,1) \rightarrow CO_2(1,2,2,5,2) + CO_2(0,2,2,5,1)$	3.69E+01	-8.80E+01	2.33E+02
$CO_2(1,3,3,5,2) + CO_2(0,1,1,5,1) \rightarrow CO_2(1,2,2,5,2) + CO_2(1,0,0,5,2)$	3.69E+01	-8.80E+01	2.33E+02
$CO_2(1,3,3,5,2) + CO_2(0,2,2,5,1) \rightarrow CO_2(0,4,4,5,1) + CO_2(0,3,3,5,1)$	3.68E+01	-8.80E+01	2.33E+02
$CO_2(1,3,3,5,2) + CO_2(0,2,2,5,1) \rightarrow CO_2(0,4,4,5,1) + CO_2(1,1,1,5,2)$	3.68E+01	-8.80E+01	2.33E+02
$CO_2(1,3,3,5,2) + CO_2(0,2,2,5,1) \rightarrow CO_2(1,2,2,5,2) + CO_2(0,3,3,5,1)$	3.75E+01	-8.80E+01	2.33E+02
$CO_2(1,3,3,5,2) + CO_2(0,2,2,5,1) \rightarrow CO_2(1,2,2,5,2) + CO_2(1,1,1,5,2)$	3.73E+01	-8.80E+01	2.33E+02
$CO_2(1,3,3,5,2) + CO_2(1,0,0,5,2) \rightarrow CO_2(0,4,4,5,1) + CO_2(1,1,1,5,2)$	3.64E+01	-8.80E+01	2.33E+02
$CO_2(1,3,3,5,2) + CO_2(1,0,0,5,2) \rightarrow CO_2(1,2,2,5,2) + CO_2(1,1,1,5,2)$	3.76E+01	-8.80E+01	2.33E+02
$CO_2(2,0,0,0,3) + CO_2(0,0,0,0,1) \rightarrow CO_2(1,0,0,0,2) + CO_2(1,0,0,0,2)$	3.49E+01	-8.90E+01	2.34E+02
$CO_2(2,0,0,0,3) + CO_2(0,0,0,0,1) \rightarrow CO_2(1,1,1,0,2) + CO_2(0,1,1,0,1)$	3.59E+01	-8.80E+01	2.33E+02
$CO_2(2,0,0,0,3) + CO_2(0,1,1,0,1) \rightarrow CO_2(1,1,1,0,2) + CO_2(0,2,2,0,1)$	3.66E+01	-8.80E+01	2.33E+02
$CO_2(2,0,0,0,3) + CO_2(0,1,1,0,1) \rightarrow CO_2(1,1,1,0,2) + CO_2(1,0,0,0,2)$	3.67E+01	-8.82E+01	2.33E+02
$CO_2(2,0,0,0,3) + CO_2(0,2,2,0,1) \rightarrow CO_2(1,1,1,0,2) + CO_2(0,3,3,0,1)$	3.70E+01	-8.80E+01	2.33E+02
$CO_2(2,0,0,0,3) + CO_2(0,2,2,0,1) \rightarrow CO_2(1,1,1,0,2) + CO_2(1,1,1,0,2)$	3.70E+01	-8.80E+01	2.33E+02
$CO_2(2,0,0,0,3) + CO_2(0,3,3,0,1) \rightarrow CO_2(1,1,1,0,2) + CO_2(0,4,4,0,1)$	3.73E+01	-8.80E+01	2.33E+02
$CO_2(2,0,0,0,3) + CO_2(1,0,0,0,2) \rightarrow CO_2(1,1,1,0,2) + CO_2(1,1,1,0,2)$	3.73E+01	-8.80E+01	2.33E+02
$CO_2(2,0,0,0,3) + CO_2(1,1,1,0,2) \rightarrow CO_2(1,1,1,0,2) + CO_2(1,2,2,0,2)$	3.77E+01	-8.80E+01	2.33E+02
$CO_2(2,0,0,1,3) + CO_2(0,0,0,1,1) \rightarrow CO_2(1,0,0,1,2) + CO_2(1,0,0,1,2)$	3.49E+01	-8.90E+01	2.34E+02
$CO_2(2,0,0,1,3) + CO_2(0,0,0,1,1) \rightarrow CO_2(1,1,1,1,2) + CO_2(0,1,1,1,1)$	3.59E+01	-8.80E+01	2.33E+02

$CO_2(2,0,0,1,3) + CO_2(0,1,1,1,1) \rightarrow CO_2(1,1,1,1,2) + CO_2(0,2,2,1,1)$	3.66E+01	-8.80E+01	2.33E+02
$CO_2(2,0,0,1,3) + CO_2(0,1,1,1,1) \rightarrow CO_2(1,1,1,1,2) + CO_2(1,0,0,1,2)$	3.67E+01	-8.82E+01	2.33E+02
$CO_2(2,0,0,1,3) + CO_2(0,2,2,1,1) \rightarrow CO_2(1,1,1,1,2) + CO_2(0,3,3,1,1)$	3.70E+01	-8.80E+01	2.33E+02
$CO_2(2,0,0,1,3) + CO_2(0,2,2,1,1) \rightarrow CO_2(1,1,1,1,2) + CO_2(1,1,1,1,2)$	3.70E+01	-8.80E+01	2.33E+02
$CO_2(2,0,0,1,3) + CO_2(0,3,3,1,1) \rightarrow CO_2(1,1,1,1,2) + CO_2(0,4,4,1,1)$	3.73E+01	-8.80E+01	2.33E+02
$CO_2(2,0,0,1,3) + CO_2(1,0,0,1,2) \rightarrow CO_2(1,1,1,1,2) + CO_2(1,1,1,1,2)$	3.73E+01	-8.80E+01	2.33E+02
$CO_2(2,0,0,1,3) + CO_2(1,1,1,1,2) \rightarrow CO_2(1,1,1,1,2) + CO_2(1,2,2,1,2)$	3.77E+01	-8.80E+01	2.33E+02
$CO_2(2,0,0,2,3) + CO_2(0,0,0,2,1) \rightarrow CO_2(1,0,0,2,2) + CO_2(1,0,0,2,2)$	3.49E+01	-8.90E+01	2.34E+02
$CO_2(2,0,0,2,3) + CO_2(0,0,0,2,1) \rightarrow CO_2(1,1,1,2,2) + CO_2(0,1,1,2,1)$	3.59E+01	-8.80E+01	2.33E+02
$CO_2(2,0,0,2,3) + CO_2(0,1,1,2,1) \rightarrow CO_2(1,1,1,2,2) + CO_2(0,2,2,2,1)$	3.66E+01	-8.80E+01	2.33E+02
$CO_2(2,0,0,2,3) + CO_2(0,1,1,2,1) \rightarrow CO_2(1,1,1,2,2) + CO_2(1,0,0,2,2)$	3.67E+01	-8.82E+01	2.33E+02
$CO_2(2,0,0,2,3) + CO_2(0,2,2,2,1) \rightarrow CO_2(1,1,1,2,2) + CO_2(0,3,3,2,1)$	3.70E+01	-8.80E+01	2.33E+02
$CO_2(2,0,0,2,3) + CO_2(0,2,2,2,1) \rightarrow CO_2(1,1,1,2,2) + CO_2(1,1,1,2,2)$	3.70E+01	-8.80E+01	2.33E+02
$CO_2(2,0,0,2,3) + CO_2(0,3,3,2,1) \rightarrow CO_2(1,1,1,2,2) + CO_2(0,4,4,2,1)$	3.73E+01	-8.80E+01	2.33E+02
$CO_2(2,0,0,2,3) + CO_2(1,0,0,2,2) \rightarrow CO_2(1,1,1,2,2) + CO_2(1,1,1,2,2)$	3.73E+01	-8.80E+01	2.33E+02
$CO_2(2,0,0,2,3) + CO_2(1,1,1,2,2) \rightarrow CO_2(1,1,1,2,2) + CO_2(1,2,2,2,2)$	3.77E+01	-8.80E+01	2.33E+02
$CO_2(2,0,0,3,3) + CO_2(0,0,0,3,1) \rightarrow CO_2(1,0,0,3,2) + CO_2(1,0,0,3,2)$	3.49E+01	-8.90E+01	2.34E+02
$CO_2(2,0,0,3,3) + CO_2(0,0,0,3,1) \rightarrow CO_2(1,1,1,3,2) + CO_2(0,1,1,3,1)$	3.59E+01	-8.80E+01	2.33E+02
$CO_2(2,0,0,3,3) + CO_2(0,1,1,3,1) \rightarrow CO_2(1,1,1,3,2) + CO_2(0,2,2,3,1)$	3.66E+01	-8.80E+01	2.33E+02
$CO_2(2,0,0,3,3) + CO_2(0,1,1,3,1) \rightarrow CO_2(1,1,1,3,2) + CO_2(1,0,0,3,2)$	3.67E+01	-8.82E+01	2.33E+02
$CO_2(2,0,0,3,3) + CO_2(0,2,2,3,1) \rightarrow CO_2(1,1,1,3,2) + CO_2(0,3,3,3,1)$	3.70E+01	-8.80E+01	2.33E+02
$CO_2(2,0,0,3,3) + CO_2(0,2,2,3,1) \rightarrow CO_2(1,1,1,3,2) + CO_2(1,1,1,3,2)$	3.70E+01	-8.80E+01	2.33E+02
$CO_2(2,0,0,3,3) + CO_2(0,3,3,3,1) \rightarrow CO_2(1,1,1,3,2) + CO_2(0,4,4,3,1)$	3.73E+01	-8.80E+01	2.33E+02
$CO_2(2,0,0,3,3) + CO_2(1,0,0,3,2) \rightarrow CO_2(1,1,1,3,2) + CO_2(1,1,1,3,2)$	3.73E+01	-8.80E+01	2.33E+02
$CO_2(2,0,0,3,3) + CO_2(1,1,1,3,2) \rightarrow CO_2(1,1,1,3,2) + CO_2(1,2,2,3,2)$	3.77E+01	-8.80E+01	2.33E+02
$CO_2(2,0,0,4,3) + CO_2(0,0,0,4,1) \rightarrow CO_2(1,0,0,4,2) + CO_2(1,0,0,4,2)$	3.49E+01	-8.90E+01	2.34E+02
$CO_2(2,0,0,4,3) + CO_2(0,0,0,4,1) \rightarrow CO_2(1,1,1,4,2) + CO_2(0,1,1,4,1)$	3.59E+01	-8.80E+01	2.33E+02
$CO_2(2,0,0,4,3) + CO_2(0,1,1,4,1) \rightarrow CO_2(1,1,1,4,2) + CO_2(0,2,2,4,1)$	3.66E+01	-8.80E+01	2.33E+02
$CO_2(2,0,0,4,3) + CO_2(0,1,1,4,1) \rightarrow CO_2(1,1,1,4,2) + CO_2(1,0,0,4,2)$	3.67E+01	-8.82E+01	2.33E+02
$CO_2(2,0,0,4,3) + CO_2(0,2,2,4,1) \rightarrow CO_2(1,1,1,4,2) + CO_2(0,3,3,4,1)$	3.70E+01	-8.80E+01	2.33E+02
$CO_2(2,0,0,4,3) + CO_2(0,2,2,4,1) \rightarrow CO_2(1,1,1,4,2) + CO_2(1,1,1,4,2)$	3.70E+01	-8.80E+01	2.33E+02
$CO_2(2,0,0,4,3) + CO_2(0,3,3,4,1) \rightarrow CO_2(1,1,1,4,2) + CO_2(0,4,4,4,1)$	3.73E+01	-8.80E+01	2.33E+02
$CO_2(2,0,0,4,3) + CO_2(1,0,0,4,2) \rightarrow CO_2(1,1,1,4,2) + CO_2(1,1,1,4,2)$	3.73E+01	-8.80E+01	2.33E+02
$CO_2(2,0,0,4,3) + CO_2(1,1,1,4,2) \rightarrow CO_2(1,1,1,4,2) + CO_2(1,2,2,4,2)$	3.77E+01	-8.80E+01	2.33E+02
$CO_2(2,0,0,5,3) + CO_2(0,0,0,5,1) \rightarrow CO_2(1,0,0,5,2) + CO_2(1,0,0,5,2)$	3.49E+01	-8.90E+01	2.34E+02
$CO_2(2,0,0,5,3) + CO_2(0,0,0,5,1) \rightarrow CO_2(1,1,1,5,2) + CO_2(0,1,1,5,1)$	3.59E+01	-8.80E+01	2.33E+02
$CO_2(2,0,0,5,3) + CO_2(0,1,1,5,1) \rightarrow CO_2(1,1,1,5,2) + CO_2(0,2,2,5,1)$	3.66E+01	-8.80E+01	2.33E+02
$CO_2(2,0,0,5,3) + CO_2(0,1,1,5,1) \rightarrow CO_2(1,1,1,5,2) + CO_2(1,0,0,5,2)$	3.67E+01	-8.82E+01	2.33E+02
$CO_2(2,0,0,5,3) + CO_2(0,2,2,5,1) \rightarrow CO_2(1,1,1,5,2) + CO_2(0,3,3,5,1)$	3.70E+01	-8.80E+01	2.33E+02
$CO_2(2,0,0,5,3) + CO_2(0,2,2,5,1) \rightarrow CO_2(1,1,1,5,2) + CO_2(1,1,1,5,2)$	3.70E+01	-8.80E+01	2.33E+02

$CO_2(2,0,0,5,3) + CO_2(0,3,3,5,1) \rightarrow CO_2(1,1,1,5,2) + CO_2(0,4,4,5,1)$	3.73E+01	-8.80E+01	2.33E+02
$CO_2(2,0,0,5,3) + CO_2(1,0,0,5,2) \rightarrow CO_2(1,1,1,5,2) + CO_2(1,1,1,5,2)$	3.73E+01	-8.80E+01	2.33E+02
$CO_2(2,0,0,5,3) + CO_2(1,1,1,5,2) \rightarrow CO_2(1,1,1,5,2) + CO_2(1,2,2,5,2)$	3.77E+01	-8.80E+01	2.33E+02
$CO_2(2,1,1,0,3) + CO_2(0,0,0,0,1) \rightarrow CO_2(1,2,2,0,2) + CO_2(0,1,1,0,1)$	3.62E+01	-8.80E+01	2.33E+02
$CO_2(2,1,1,0,3) + CO_2(0,0,0,0,1) \rightarrow CO_2(2,0,0,0,3) + CO_2(0,1,1,0,1)$	3.63E+01	-8.80E+01	2.33E+02
$CO_2(2,1,1,0,3) + CO_2(0,1,1,0,1) \rightarrow CO_2(1,2,2,0,2) + CO_2(0,2,2,0,1)$	3.69E+01	-8.80E+01	2.33E+02
$CO_2(2,1,1,0,3) + CO_2(0,1,1,0,1) \rightarrow CO_2(1,2,2,0,2) + CO_2(1,0,0,0,2)$	3.69E+01	-8.80E+01	2.33E+02
$CO_2(2,1,1,0,3) + CO_2(0,1,1,0,1) \rightarrow CO_2(2,0,0,0,3) + CO_2(0,2,2,0,1)$	3.70E+01	-8.80E+01	2.33E+02
$CO_2(2,1,1,0,3) + CO_2(0,1,1,0,1) \rightarrow CO_2(2,0,0,0,3) + CO_2(1,0,0,0,2)$	3.70E+01	-9.80E+01	2.33E+02
$CO_2(2,1,1,0,3) + CO_2(0,2,2,0,1) \rightarrow CO_2(1,2,2,0,2) + CO_2(0,2,2,0,1)$	3.73E+01	-8.80E+01	2.33E+02
$CO_2(2,1,1,0,3) + CO_2(0,2,2,0,1) \rightarrow CO_2(1,2,2,0,2) + CO_2(1,1,1,0,2)$	3.75E+01	-8.80E+01	2.33E+02
$CO_2(2,1,1,0,3) + CO_2(0,2,2,0,1) \rightarrow CO_2(2,0,0,0,3) + CO_2(0,3,3,0,1)$	3.74E+01	-8.80E+01	2.33E+02
$CO_2(2,1,1,0,3) + CO_2(0,2,2,0,1) \rightarrow CO_2(2,0,0,0,3) + CO_2(0,4,4,0,1)$	3.77E+01	-8.80E+01	2.33E+02
$CO_2(2,1,1,0,3) + CO_2(0,2,2,0,1) \rightarrow CO_2(2,0,0,0,3) + CO_2(1,1,1,0,2)$	3.74E+01	-8.80E+01	2.33E+02
$CO_2(2,1,1,0,3) + CO_2(0,3,3,0,1) \rightarrow CO_2(1,2,2,0,2) + CO_2(1,2,2,0,2)$	3.76E+01	-8.80E+01	2.33E+02
$CO_2(2,1,1,0,3) + CO_2(1,0,0,0,2) \rightarrow CO_2(1,2,2,0,2) + CO_2(1,1,1,0,2)$	3.76E+01	-8.80E+01	2.33E+02
$CO_2(2,1,1,0,3) + CO_2(1,0,0,0,2) \rightarrow CO_2(2,0,0,0,3) + CO_2(1,1,1,0,2)$	3.78E+01	-8.80E+01	2.33E+02
$CO_2(2,1,1,0,3) + CO_2(1,1,1,0,2) \rightarrow CO_2(2,0,0,0,3) + CO_2(1,2,2,0,2)$	3.81E+01	-8.80E+01	2.33E+02
$CO_2(2,1,1,0,3) + CO_2(1,1,1,0,2) \rightarrow CO_2(2,0,0,0,3) + CO_2(2,0,0,0,3)$	3.81E+01	-8.80E+01	2.33E+02
$CO_2(2,1,1,1,3) + CO_2(0,0,0,1,1) \rightarrow CO_2(1,2,2,1,2) + CO_2(0,1,1,1,1)$	3.62E+01	-8.80E+01	2.33E+02
$CO_2(2,1,1,1,3) + CO_2(0,0,0,1,1) \rightarrow CO_2(2,0,0,1,3) + CO_2(0,1,1,1,1)$	3.63E+01	-8.80E+01	2.33E+02
$CO_2(2,1,1,1,3) + CO_2(0,1,1,1,1) \rightarrow CO_2(1,2,2,1,2) + CO_2(0,2,2,1,1)$	3.69E+01	-8.80E+01	2.33E+02
$CO_2(2,1,1,1,3) + CO_2(0,1,1,1,1) \rightarrow CO_2(1,2,2,1,2) + CO_2(1,0,0,1,2)$	3.69E+01	-8.80E+01	2.33E+02
$CO_2(2,1,1,1,3) + CO_2(0,1,1,1,1) \rightarrow CO_2(2,0,0,1,3) + CO_2(0,2,2,1,1)$	3.70E+01	-8.80E+01	2.33E+02
$CO_2(2,1,1,1,3) + CO_2(0,1,1,1,1) \rightarrow CO_2(2,0,0,1,3) + CO_2(1,0,0,1,2)$	3.70E+01	-9.80E+01	2.33E+02
$CO_2(2,1,1,1,3) + CO_2(0,2,2,1,1) \rightarrow CO_2(1,2,2,1,2) + CO_2(0,2,2,1,1)$	3.73E+01	-8.80E+01	2.33E+02
$CO_2(2,1,1,1,3) + CO_2(0,2,2,1,1) \rightarrow CO_2(1,2,2,1,2) + CO_2(1,1,1,1,2)$	3.75E+01	-8.80E+01	2.33E+02
$CO_2(2,1,1,1,3) + CO_2(0,2,2,1,1) \rightarrow CO_2(2,0,0,1,3) + CO_2(0,3,3,1,1)$	3.74E+01	-8.80E+01	2.33E+02
$CO_2(2,1,1,1,3) + CO_2(0,2,2,1,1) \rightarrow CO_2(2,0,0,1,3) + CO_2(0,4,4,1,1)$	3.77E+01	-8.80E+01	2.33E+02
$CO_2(2,1,1,1,3) + CO_2(0,2,2,1,1) \rightarrow CO_2(2,0,0,1,3) + CO_2(1,1,1,1,2)$	3.74E+01	-8.80E+01	2.33E+02
$CO_2(2,1,1,1,3) + CO_2(0,3,3,1,1) \rightarrow CO_2(1,2,2,1,2) + CO_2(1,2,2,1,2)$	3.76E+01	-8.80E+01	2.33E+02
$CO_2(2,1,1,1,3) + CO_2(1,0,0,1,2) \rightarrow CO_2(1,2,2,1,2) + CO_2(1,1,1,1,2)$	3.76E+01	-8.80E+01	2.33E+02
$CO_2(2,1,1,1,3) + CO_2(1,0,0,1,2) \rightarrow CO_2(2,0,0,1,3) + CO_2(1,1,1,1,2)$	3.78E+01	-8.80E+01	2.33E+02
$CO_2(2,1,1,1,3) + CO_2(1,1,1,1,2) \rightarrow CO_2(2,0,0,1,3) + CO_2(1,2,2,1,2)$	3.81E+01	-8.80E+01	2.33E+02
$CO_2(2,1,1,1,3) + CO_2(1,1,1,1,2) \rightarrow CO_2(2,0,0,1,3) + CO_2(2,0,0,1,3)$	3.81E+01	-8.80E+01	2.33E+02
$CO_2(2,1,1,2,3) + CO_2(0,0,0,2,1) \rightarrow CO_2(1,2,2,2,2) + CO_2(0,1,1,2,1)$	3.62E+01	-8.80E+01	2.33E+02
$CO_2(2,1,1,2,3) + CO_2(0,0,0,2,1) \rightarrow CO_2(2,0,0,2,3) + CO_2(0,1,1,2,1)$	3.63E+01	-8.80E+01	2.33E+02
$CO_2(2,1,1,2,3) + CO_2(0,1,1,2,1) \rightarrow CO_2(1,2,2,2,2) + CO_2(0,2,2,2,1)$	3.69E+01	-8.80E+01	2.33E+02
$CO_2(2,1,1,2,3) + CO_2(0,1,1,2,1) \rightarrow CO_2(1,2,2,2,2) + CO_2(1,0,0,2,2)$	3.69E+01	-8.80E+01	2.33E+02
$CO_2(2,1,1,2,3) + CO_2(0,1,1,2,1) \rightarrow CO_2(2,0,0,2,3) + CO_2(0,2,2,2,1)$	3.70E+01	-8.80E+01	2.33E+02

$CO_2(2,1,1,2,3) + CO_2(0,1,1,2,1) \rightarrow CO_2(2,0,0,2,3) + CO_2(1,0,0,2,2)$	3.70E+01	-9.80E+01	2.33E+02
$CO_2(2,1,1,2,3) + CO_2(0,2,2,2,1) \rightarrow CO_2(1,2,2,2,2) + CO_2(0,2,2,2,1)$	3.73E+01	-8.80E+01	2.33E+02
$CO_2(2,1,1,2,3) + CO_2(0,2,2,2,1) \rightarrow CO_2(1,2,2,2,2) + CO_2(1,1,1,2,2)$	3.75E+01	-8.80E+01	2.33E+02
$CO_2(2,1,1,2,3) + CO_2(0,2,2,2,1) \rightarrow CO_2(2,0,0,2,3) + CO_2(0,3,3,2,1)$	3.74E+01	-8.80E+01	2.33E+02
$CO_2(2,1,1,2,3) + CO_2(0,2,2,2,1) \rightarrow CO_2(2,0,0,2,3) + CO_2(0,4,4,2,1)$	3.77E+01	-8.80E+01	2.33E+02
$CO_2(2,1,1,2,3) + CO_2(0,2,2,2,1) \rightarrow CO_2(2,0,0,2,3) + CO_2(1,1,1,2,2)$	3.74E+01	-8.80E+01	2.33E+02
$CO_2(2,1,1,2,3) + CO_2(0,3,3,2,1) \rightarrow CO_2(1,2,2,2,2) + CO_2(1,2,2,2,2)$	3.76E+01	-8.80E+01	2.33E+02
$CO_2(2,1,1,2,3) + CO_2(1,0,0,2,2) \rightarrow CO_2(1,2,2,2,2) + CO_2(1,1,1,2,2)$	3.76E+01	-8.80E+01	2.33E+02
$CO_2(2,1,1,2,3) + CO_2(1,0,0,2,2) \rightarrow CO_2(2,0,0,2,3) + CO_2(1,1,1,2,2)$	3.78E+01	-8.80E+01	2.33E+02
$CO_2(2,1,1,2,3) + CO_2(1,1,1,2,2) \rightarrow CO_2(2,0,0,2,3) + CO_2(1,2,2,2,2)$	3.81E+01	-8.80E+01	2.33E+02
$CO_2(2,1,1,2,3) + CO_2(1,1,1,2,2) \rightarrow CO_2(2,0,0,2,3) + CO_2(2,0,0,2,3)$	3.81E+01	-8.80E+01	2.33E+02
$CO_2(2,1,1,3,3) + CO_2(0,0,0,3,1) \rightarrow CO_2(1,2,2,3,2) + CO_2(0,1,1,3,1)$	3.62E+01	-8.80E+01	2.33E+02
$CO_2(2,1,1,3,3) + CO_2(0,0,0,3,1) \rightarrow CO_2(2,0,0,3,3) + CO_2(0,1,1,3,1)$	3.63E+01	-8.80E+01	2.33E+02
$CO_2(2,1,1,3,3) + CO_2(0,1,1,3,1) \rightarrow CO_2(1,2,2,3,2) + CO_2(0,2,2,3,1)$	3.69E+01	-8.80E+01	2.33E+02
$CO_2(2,1,1,3,3) + CO_2(0,1,1,3,1) \rightarrow CO_2(1,2,2,3,2) + CO_2(1,0,0,3,2)$	3.69E+01	-8.80E+01	2.33E+02
$CO_2(2,1,1,3,3) + CO_2(0,1,1,3,1) \rightarrow CO_2(2,0,0,3,3) + CO_2(0,2,2,3,1)$	3.70E+01	-8.80E+01	2.33E+02
$CO_2(2,1,1,3,3) + CO_2(0,1,1,3,1) \rightarrow CO_2(2,0,0,3,3) + CO_2(1,0,0,3,2)$	3.70E+01	-9.80E+01	2.33E+02
$CO_2(2,1,1,3,3) + CO_2(0,2,2,3,1) \rightarrow CO_2(1,2,2,3,2) + CO_2(0,2,2,3,1)$	3.73E+01	-8.80E+01	2.33E+02
$CO_2(2,1,1,3,3) + CO_2(0,2,2,3,1) \rightarrow CO_2(1,2,2,3,2) + CO_2(1,1,1,3,2)$	3.75E+01	-8.80E+01	2.33E+02
$CO_2(2,1,1,3,3) + CO_2(0,2,2,3,1) \rightarrow CO_2(2,0,0,3,3) + CO_2(0,3,3,3,1)$	3.74E+01	-8.80E+01	2.33E+02
$CO_2(2,1,1,3,3) + CO_2(0,2,2,3,1) \rightarrow CO_2(2,0,0,3,3) + CO_2(0,4,4,3,1)$	3.77E+01	-8.80E+01	2.33E+02
$CO_2(2,1,1,3,3) + CO_2(0,2,2,3,1) \rightarrow CO_2(2,0,0,3,3) + CO_2(1,1,1,3,2)$	3.74E+01	-8.80E+01	2.33E+02
$CO_2(2,1,1,3,3) + CO_2(0,3,3,3,1) \rightarrow CO_2(1,2,2,3,2) + CO_2(1,2,2,3,2)$	3.76E+01	-8.80E+01	2.33E+02
$CO_2(2,1,1,3,3) + CO_2(1,0,0,3,2) \rightarrow CO_2(1,2,2,3,2) + CO_2(1,1,1,3,2)$	3.76E+01	-8.80E+01	2.33E+02
$CO_2(2,1,1,3,3) + CO_2(1,0,0,3,2) \rightarrow CO_2(2,0,0,3,3) + CO_2(1,1,1,3,2)$	3.78E+01	-8.80E+01	2.33E+02
$CO_2(2,1,1,3,3) + CO_2(1,1,1,3,2) \rightarrow CO_2(2,0,0,3,3) + CO_2(1,2,2,3,2)$	3.81E+01	-8.80E+01	2.33E+02
$CO_2(2,1,1,3,3) + CO_2(1,1,1,3,2) \rightarrow CO_2(2,0,0,3,3) + CO_2(2,0,0,3,3)$	3.81E+01	-8.80E+01	2.33E+02
$CO_2(2,1,1,4,3) + CO_2(0,0,0,4,1) \rightarrow CO_2(1,2,2,4,2) + CO_2(0,1,1,4,1)$	3.62E+01	-8.80E+01	2.33E+02
$CO_2(2,1,1,4,3) + CO_2(0,0,0,4,1) \rightarrow CO_2(2,0,0,4,3) + CO_2(0,1,1,4,1)$	3.63E+01	-8.80E+01	2.33E+02
$CO_2(2,1,1,4,3) + CO_2(0,1,1,4,1) \rightarrow CO_2(1,2,2,4,2) + CO_2(0,2,2,4,1)$	3.69E+01	-8.80E+01	2.33E+02
$CO_2(2,1,1,4,3) + CO_2(0,1,1,4,1) \rightarrow CO_2(1,2,2,4,2) + CO_2(1,0,0,4,2)$	3.69E+01	-8.80E+01	2.33E+02
$CO_2(2,1,1,4,3) + CO_2(0,1,1,4,1) \rightarrow CO_2(2,0,0,4,3) + CO_2(0,2,2,4,1)$	3.70E+01	-8.80E+01	2.33E+02
$CO_2(2,1,1,4,3) + CO_2(0,1,1,4,1) \rightarrow CO_2(2,0,0,4,3) + CO_2(1,0,0,4,2)$	3.70E+01	-9.80E+01	2.33E+02
$CO_2(2,1,1,4,3) + CO_2(0,2,2,4,1) \rightarrow CO_2(1,2,2,4,2) + CO_2(0,2,2,4,1)$	3.73E+01	-8.80E+01	2.33E+02
$CO_2(2,1,1,4,3) + CO_2(0,2,2,4,1) \rightarrow CO_2(1,2,2,4,2) + CO_2(1,1,1,4,2)$	3.75E+01	-8.80E+01	2.33E+02
$CO_2(2,1,1,4,3) + CO_2(0,2,2,4,1) \rightarrow CO_2(2,0,0,4,3) + CO_2(0,3,3,4,1)$	3.74E+01	-8.80E+01	2.33E+02
$CO_2(2,1,1,4,3) + CO_2(0,2,2,4,1) \rightarrow CO_2(2,0,0,4,3) + CO_2(0,4,4,4,1)$	3.77E+01	-8.80E+01	2.33E+02
$CO_2(2,1,1,4,3) + CO_2(0,2,2,4,1) \rightarrow CO_2(2,0,0,4,3) + CO_2(1,1,1,4,2)$	3.74E+01	-8.80E+01	2.33E+02
$CO_2(2,1,1,4,3) + CO_2(0,3,3,4,1) \rightarrow CO_2(1,2,2,4,2) + CO_2(1,2,2,4,2)$	3.76E+01	-8.80E+01	2.33E+02
$CO_2(2,1,1,4,3) + CO_2(1,0,0,4,2) \rightarrow CO_2(1,2,2,4,2) + CO_2(1,1,1,4,2)$	3.76E+01	-8.80E+01	2.33E+02

CO_2(2,1,1,4,3) + CO_2(1,0,0,4,2) → CO_2(2,0,0,4,3) + CO_2(1,1,1,4,2)	3.78E+01	-8.80E+01	2.33E+02
CO_2(2,1,1,4,3) + CO_2(1,1,1,4,2) → CO_2(2,0,0,4,3) + CO_2(1,2,2,4,2)	3.81E+01	-8.80E+01	2.33E+02
CO_2(2,1,1,4,3) + CO_2(1,1,1,4,2) → CO_2(2,0,0,4,3) + CO_2(2,0,0,4,3)	3.81E+01	-8.80E+01	2.33E+02
CO_2(2,1,1,5,3) + CO_2(0,0,0,5,1) → CO_2(1,2,2,5,2) + CO_2(0,1,1,5,1)	3.62E+01	-8.80E+01	2.33E+02
CO_2(2,1,1,5,3) + CO_2(0,0,0,5,1) → CO_2(2,0,0,5,3) + CO_2(0,1,1,5,1)	3.63E+01	-8.80E+01	2.33E+02
CO_2(2,1,1,5,3) + CO_2(0,1,1,5,1) → CO_2(1,2,2,5,2) + CO_2(0,2,2,5,1)	3.69E+01	-8.80E+01	2.33E+02
CO_2(2,1,1,5,3) + CO_2(0,1,1,5,1) → CO_2(1,2,2,5,2) + CO_2(1,0,0,5,2)	3.69E+01	-8.80E+01	2.33E+02
CO_2(2,1,1,5,3) + CO_2(0,1,1,5,1) → CO_2(2,0,0,5,3) + CO_2(0,2,2,5,1)	3.70E+01	-8.80E+01	2.33E+02
CO_2(2,1,1,5,3) + CO_2(0,1,1,5,1) → CO_2(2,0,0,5,3) + CO_2(1,0,0,5,2)	3.70E+01	-9.80E+01	2.33E+02
CO_2(2,1,1,5,3) + CO_2(0,2,2,5,1) → CO_2(1,2,2,5,2) + CO_2(0,2,2,5,1)	3.73E+01	-8.80E+01	2.33E+02
CO_2(2,1,1,5,3) + CO_2(0,2,2,5,1) → CO_2(1,2,2,5,2) + CO_2(1,1,1,5,2)	3.75E+01	-8.80E+01	2.33E+02
CO_2(2,1,1,5,3) + CO_2(0,2,2,5,1) → CO_2(2,0,0,5,3) + CO_2(0,3,3,5,1)	3.74E+01	-8.80E+01	2.33E+02
CO_2(2,1,1,5,3) + CO_2(0,2,2,5,1) → CO_2(2,0,0,5,3) + CO_2(0,4,4,5,1)	3.77E+01	-8.80E+01	2.33E+02
CO_2(2,1,1,5,3) + CO_2(0,2,2,5,1) → CO_2(2,0,0,5,3) + CO_2(1,1,1,5,2)	3.74E+01	-8.80E+01	2.33E+02
CO_2(2,1,1,5,3) + CO_2(0,3,3,5,1) → CO_2(1,2,2,5,2) + CO_2(1,2,2,5,2)	3.76E+01	-8.80E+01	2.33E+02
CO_2(2,1,1,5,3) + CO_2(1,0,0,5,2) → CO_2(1,2,2,5,2) + CO_2(1,1,1,5,2)	3.76E+01	-8.80E+01	2.33E+02
CO_2(2,1,1,5,3) + CO_2(1,0,0,5,2) → CO_2(2,0,0,5,3) + CO_2(1,1,1,5,2)	3.78E+01	-8.80E+01	2.33E+02
CO_2(2,1,1,5,3) + CO_2(1,1,1,5,2) → CO_2(2,0,0,5,3) + CO_2(1,2,2,5,2)	3.81E+01	-8.80E+01	2.33E+02
CO_2(2,1,1,5,3) + CO_2(1,1,1,5,2) → CO_2(2,0,0,5,3) + CO_2(2,0,0,5,3)	3.81E+01	-8.80E+01	2.33E+02

Table A.6: Internal vibration exchanges in CO_2

A.2.3 V-V exchanges $N_2(v)$ + $CO_2(0, 0^0, w) \rightleftharpoons N_2(v-1)$ + $CO_2(0, 0^0, w+1)$

No scaling was applied: for $v \in [1; 10]$ and $w \in [0; 4]$ all the rate coefficients are equal. Expression:

$$k(v, T_g) = \exp^{A+BT_g^{-1/3}+CT_g^{-2/3}} \times \exp^{-\Delta E/T_g}$$

Table A.7 for A, B and C:

Reaction	A	B	C	ΔE (K)
CO_2(0,0,0,0,1)+N_2(1) → CO_2(0,0,0,1,1)+N_2(0)	2.57E+01	-1.01E+00	4.58E+01	43

Table A.7: Vibration exchanges between CO_2 and N_2

Appendix B

Additional figures about the 37-varying SA

This part of the Appendix presents additional figures displaying the absolute mean μ^*, for each of the 12 outputs considered, obtained for the 37-varying SA with the restricted kinetic scheme (see section 5.7 in chapter 5).

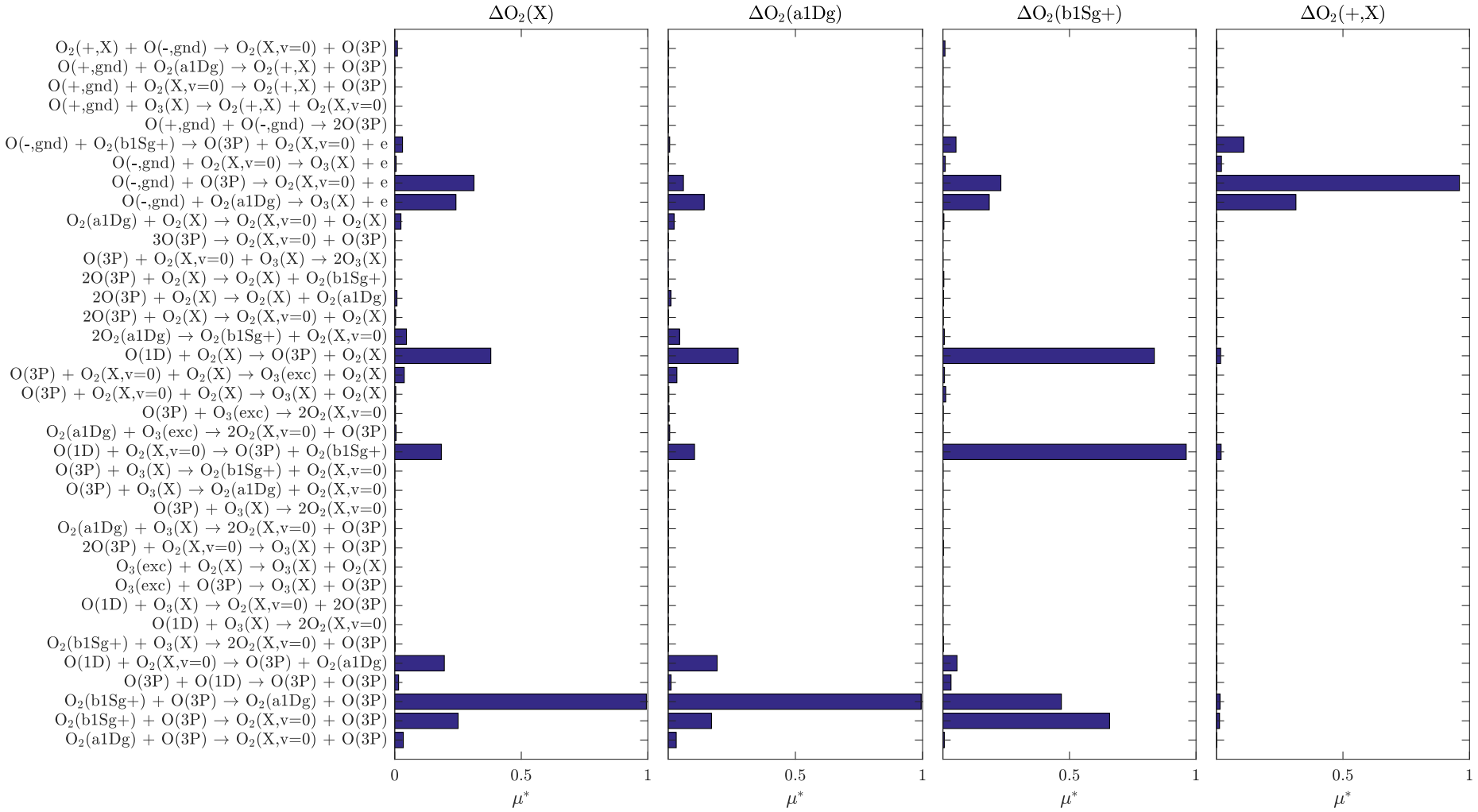

Figure B.1: Absolute means μ^* for 37 reactions, relative to O_2 variations, from the SA with the restricted kinetic scheme.

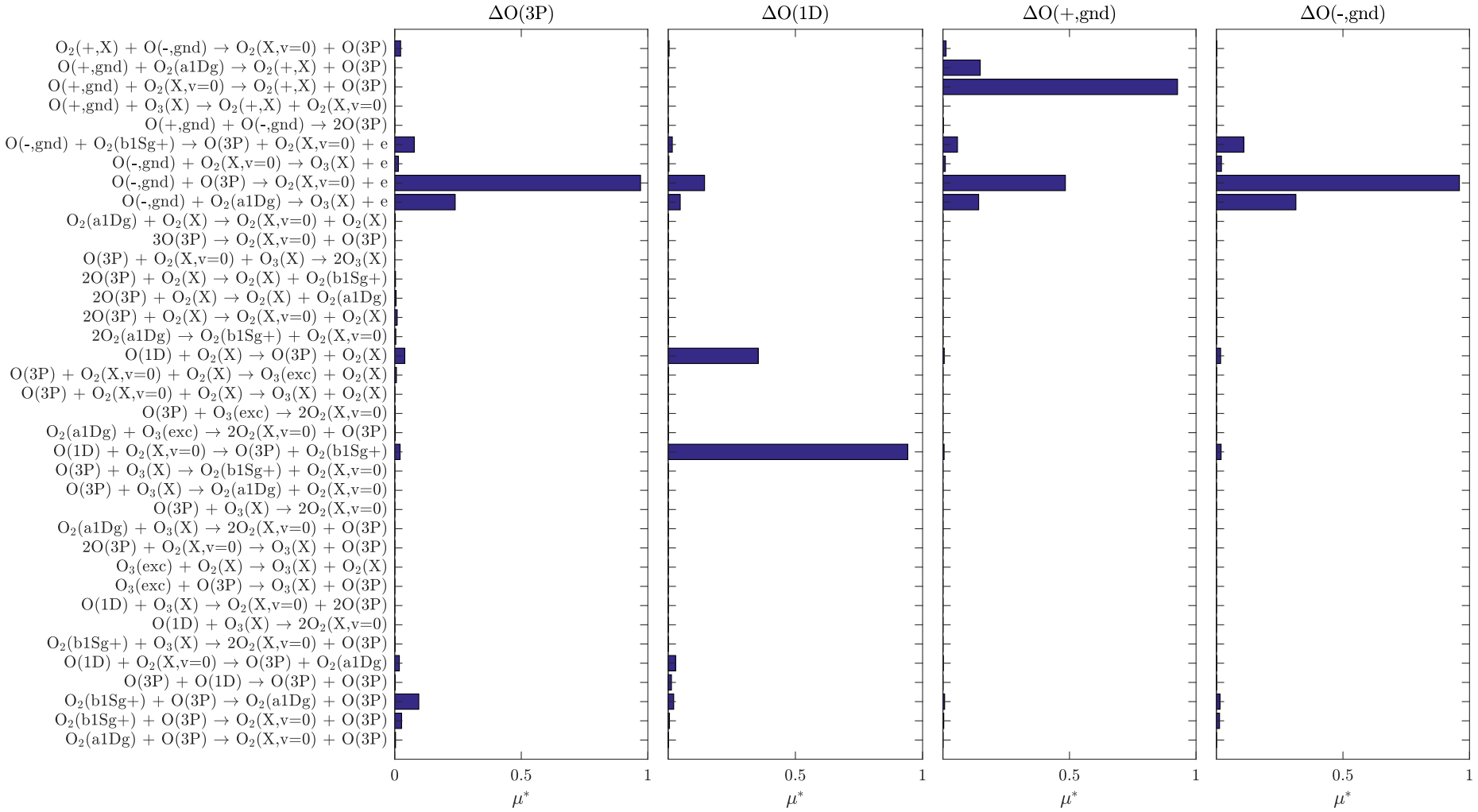

Figure B.2: Absolute means μ^* for 37 reactions, relative to O variations, from the SA with the restricted kinetic scheme.

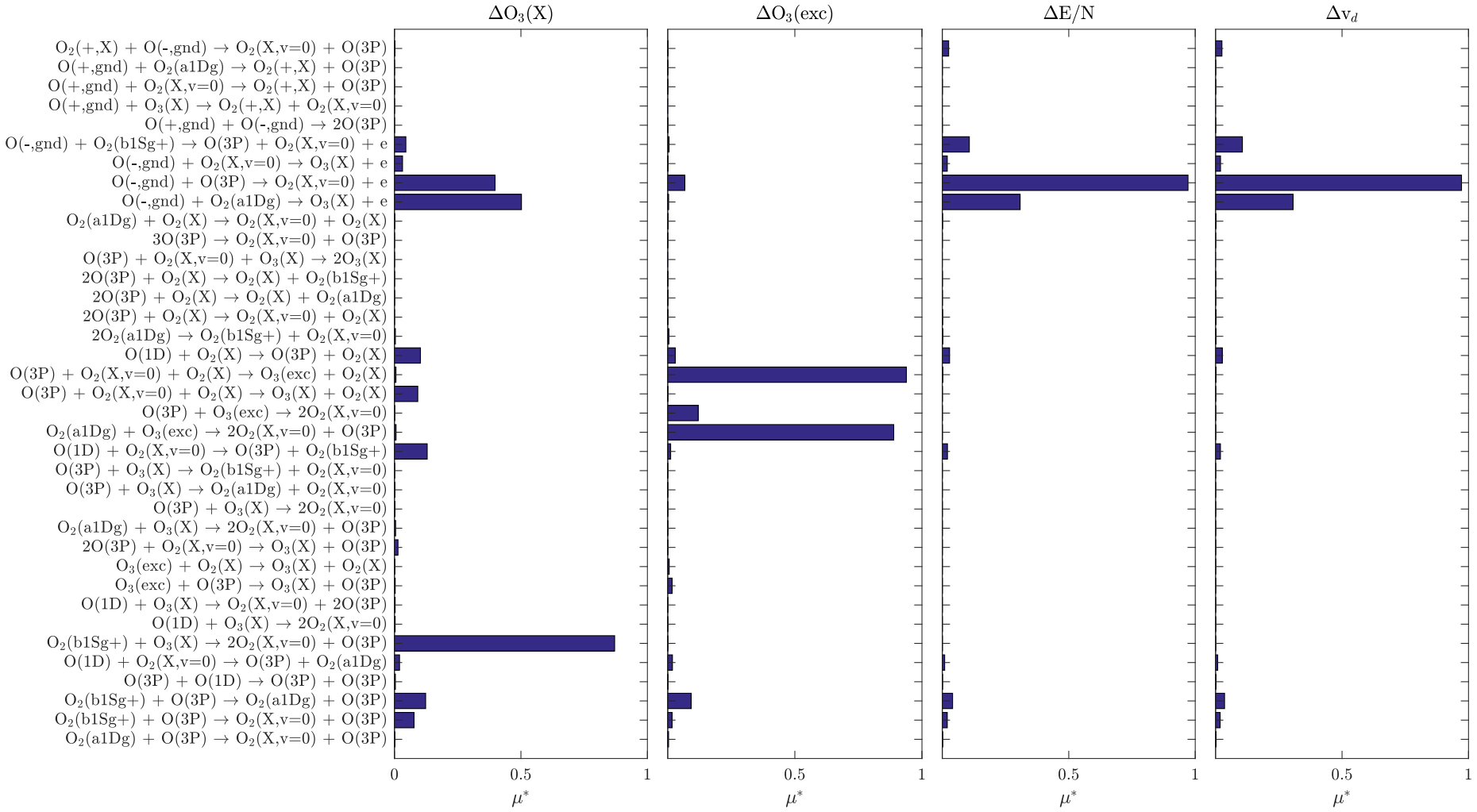

Figure B.3: Absolute means μ^* for 37 reactions, relative to O_3 and swarm parameters variations, from the SA with the restricted kinetic scheme.

Appendix C

Rate coefficient functions in the Lisbon KInetics (LoKI) code

This chapter intends to describe the rate coefficient functions utilized in LoKI code for oxygen plasmas, as well as to give all the necessary references for the rate coefficient functions that are too complex to write explicitly. For the sake of clarity, all the names of the functions used to derive the reaction rate coefficients are written in **bold blue** in this chapter. As mentioned in section 5.3, two cases are studied for the full-varying SA: a low pressure regime and a moderate pressure regime.

Differences between the 40 mTorr case (low pressure) and the 1 Torr case (moderate pressure)

There are only two modifications in the set of inputs between the low pressure and the moderate pressure cases. The changes take place in the **.chem** file of LoKI's inputs (see Appendix D):

- **Ion transport:** reactions O_2(+,X) + wall $\rightarrow$ O_2(X,v=0) and O(+,gnd) + wall $\rightarrow$ O(3P) use different functions
  - 40 mTorr case: the reaction rate coefficients are computed from the **LiebermanDiff** function. Other versions of these reactions have to be commented.
  - 1 Torr case: the reaction rate coefficients are computed from the **classicalAmbipolarDiff** function. Other versions of these reactions have to be commented.
- **Neutral transport:** reactions O_2(a1Dg) + wall $\rightarrow$ O_2(X,v=0), O(3P) + wall $\rightarrow$ 0.5O_2(X,v=0) and O_3(exc) + wall $\rightarrow$ O_3(X) (*i.e.* 3 over 5 reactions) use different coefficients for the **gasOnGasDiffOxygen** function
  - 40 mTorr case: the coefficients for the 3 reactions are, respectively: 5e-5, 0.15 and 0.01.
  - 1 Torr case: the coefficients for the 3 reactions are, respectively: 2e-5, 4.6e-4 and 0.1.

The different diffusion functions are briefly described below.

Electronic reactions

Most of the electronic reactions, with the exceptions of the group **Electron dissociative recombination** and the group **Electron impact processes considered from O_2(X, v>0)**, have their rate coefficients calculated directly from cross-sections. The function called by LoKI in this case is labeled **eedf** in the **.chem** file (cf. Appendix D). Most of the cross-sections are available on the open access LXCat website, in the database 'IST-Lisbon' (see [161]). The cross-sections for the group **Vibrational excitation by electron impact** are available in the database of the Phys4Entry website (see [152]). Note that not all the reactions for this group were directly taken from this database: see [62] for details.

Simple reaction rate coefficient functions used in LoKI

Table C.1 is extracted from the User manual of the LoKI tool suite. The functions are simple enough to have their explicit expression written here. The parameters a, b and c correspond to the input coefficients in the last columns of the **.chem** input file (cf. Appendix D). The variables T_e and T_g correspond to the electron temperature and the gas temperature, respectively. The rate coefficients present in the file can be found in [70].

Table C.1: Simple rate coefficient functions

Function name	Expression	Parameters and variables [units]
powerElectronTemp	aT_e^b	a [S.I.], T_e [eV], b [ ]
constantRateCoeff	a	a [S.I.]
arrheniusGasTemp	$a\exp(b/T_g)$	a [S.I.], b [K]
modifiedArrheniusGasTemp	$aT_g^b\exp(c/T_g)$	a [S.I.], T_g [K], b [ ], c [K]
expGasTemp	$a\exp(T_g/b)$	a [S.I.], T_g [K], b [K]
powerGasTemp	aT_g^b	a [S.I.], T_g [K], b [ ]

C.1 Complex reaction rate coefficient functions used in LoKI

The functions listed hereafter cannot be easily detailed in this document, as their expression is not simple, or because they depend on data tables for fitting purposes. The corresponding publication, if applicable, is referenced with the function name.

- **LiebermanDiff** Diffusion of O_2^+ and O^+ towards the walls. See [105] as modified by [70] based on [106].
- **classicalAmbipolarDiff** Classical ambipolar diffusion. See [62].
- **gasOnGasDiffOxygen** Deexcitation of neutral molecules/atoms of the walls [63].

- **rateCoeffCopy** This function copies the rate coefficient calculated for the reaction passed as a parameter. For instance, in the **.chem** input file: the reaction e + O_2(X,v=1:41) $\rightarrow$ 2e + O_2(+,X) is assumed to have the same rate coefficient as the reaction e + O_2(X,v=0) $\rightarrow$ 2e + O_2(+,X).
- **laportaScalingLaw** The reactions and the scaling are described in [70]. The parameter EID1 corresponds to Electron Impact Dissociation and the parameter DEA corresponds to Dissociative Electron Attachment.
- **oxygenMolecularVT** The reactions and rate coefficients are described in detail in [70].
- **oxygenMolecularVTDiss** The reactions and rate coefficients are described in detail in [70].
- **oxygenAtomicVT** The tables are given in [162]
- **oxygenMolecularVV** The reactions and rate coefficients are described in detail in [70].
- **oxygenVibDeExcWall** The reactions and rate coefficients are described in detail in [70].

Appendix D

Typical oxygen chemistry input file for the code LoKI

This part of the Appendix presents an example of a typical chemistry input file, for oxygen plasmas, to run the Lisbon KInetics (LoKI) tool suite. The **.chem** file presented here corresponds to the reference case of the *Moderate pressure case* described in chapter 5 and in C. Note that the input file needs to respect a specific format, not shown here. Basically, each column separation in the table below corresponds to a separator '|' in the original file. Contrarily to the default chemistry file, the example below has an extra column representing the efficiency factor Φ, used to vary the reaction rate coefficients during a Sensitivity Analysis (SA). By default, all the efficiency factors are set to 1. The function **eedfFactor** was created to allow the classic **eedf** function's results to be multiplied by an efficiency factor.

Reactions	Function	Φ	A	B	C
%— electron impact excitation —-					
e + O2(X,v=0) <->e + O2(a1Dg)	eedfFactor	1			
e + O2(X,v=0) <->e + O2(b1Sg+)	eedfFactor	1			
e + O2(a1Dg) <->e + O2(b1Sg+)	eedfFactor	1			
e + O(3P) <->e + O(1D)	eedfFactor	1			
%— electron impact dissociation —-					
e + O2(X,v=0) ->e + 2O(3P)	eedfFactor	1			
e + O2(X,v=0) ->e + O(3P) + O(1D)	eedfFactor	1			
e + O2(a1Dg) ->e + 2O(3P)	eedfFactor	1			
e + O2(a1Dg) ->e + O(3P) + O(1D)	eedfFactor	1			
e + O2(b1Sg+) ->e + 2O(3P)	eedfFactor	1			
e + O2(b1Sg+) ->e + O(3P) + O(1D)	eedfFactor	1			
e + O3(X) ->e + O(3P) + O2(X,v=0)	eedfFactor	1			
%— electron impact ionisation —-					
e + O2(X,v=0) ->2e + O2(+,X)	eedfFactor	1			
e + O2(a1Dg) ->2e + O2(+,X)	eedfFactor	1			
e + O(3P) ->2e + O(+,gnd)	eedfFactor	1			
e + O(-,gnd) ->2e + O(3P)	eedfFactor	1			
%— electron impact dissociative ionisation —-					
e + O2(X,v=0) ->2e + O(3P) + O(+,gnd)	eedfFactor	1			
e + O2(a1Dg) ->2e + O(3P) + O(+,gnd)	eedfFactor	1			

Table D.1 continued from previous page

Reactions	Function	Φ	A	B	C
%— electron dissociative attachment —-					
e + O2(X,v=0) ->O(-,gnd) + O(3P)	eedfFactor	1			
e + O2(a1Dg) ->O(-,gnd) + O(3P)	eedfFactor	1			
%— electron dissociative recombination —					
e + O2(+,X) ->2O(3P)	powerElectronTemp	1	5.1704E-15	-1	
e + O2(+,X) ->O(3P) + O(1D)	powerElectronTemp	1	1.50932E-14	-0.7	
%— heavy species collisions —					
O2(a1Dg) + O(3P) ->O2(X,v=0) + O(3P)	constantRateCoeff	1	7.00E-23		
O2(b1Sg+) + O(3P) ->O2(X,v=0) + O(3P)	constantRateCoeff	1	4.00E-20		
O2(b1Sg+) + O(3P) ->O2(a1Dg) + O(3P)	constantRateCoeff	1	4.00E-20		
O(3P) + O(1D) ->O(3P) + O(3P)	constantRateCoeff	1	8.00E-18		
O(1D) + O2(X,v=0) ->O(3P) + O2(a1Dg)	constantRateCoeff	1	1.00E-18		
O2(b1Sg+) + O3(X) ->2O2(X,v=0) + O(3P)	constantRateCoeff	1	1.50E-17		
O(1D) + O3(X) ->2O2(X,v=0)	constantRateCoeff	1	1.20E-16		
O(1D) + O3(X) ->O2(X,v=0) + 2O(3P)	constantRateCoeff	1	1.20E-16		
O3(exc) + O(3P) ->O3(X) + O(3P)	constantRateCoeff	1	2.00E-19		
O3(exc) + O2(X) ->O3(X) + O2(X)	constantRateCoeff	1	3.00E-21		
2O(3P) + O2(X,v=0) ->O3(X) + O(3P)	arrheniusGasTemp	1	2.10E-46	345	
O2(a1Dg) + O3(X) ->2O2(X,v=0) + O(3P)	arrheniusGasTemp	1	5.20E-17	-2840	
O(3P) + O3(X) ->2O2(X,v=0)	arrheniusGasTemp	1	9E-18	-2300	

Table D.1 continued from previous page

Reactions	Function	Φ	A	B	C
O(3P) + O3(X) ->O2(a1Dg) + O2(X,v=0)	arrheniusGasTemp	1	5.94E-18	-2300	
O(3P) + O3(X) ->O2(b1Sg+) + O2(X,v=0)	arrheniusGasTemp	1	3.06E-18	-2300	
O(1D) + O2(X,v=0) ->O(3P) + O2(b1Sg+)	arrheniusGasTemp	1	2.56E-17	67	
O2(a1Dg) + O3(exc) ->2O2(X,v=0) + O(3P)	arrheniusGasTemp	1	2.6E-16	-1287	
O(3P) + O3(exc) ->2O2(X,v=0)	arrheniusGasTemp	1	8.00E-18	-507	
O(3P) + O2(X,v=0) + O2(X) ->O3(X) + O2(X)	arrheniusGasTemp	1	2.112E-47	663	
O(3P) + O2(X,v=0) + O2(X) ->O3(exc) + O2(X)	arrheniusGasTemp	1	4.288E-47	663	
O(1D) + O2(X) ->O(3P) + O2(X)	arrheniusGasTemp	1	7.00E-18	67	
2O2(a1Dg) ->O2(b1Sg+) + O2(X,v=0)	modifiedArrheniusGasTemp	1	6.99226E-34	3.8	700
2O(3P) + O2(X) ->O2(X,v=0) + O2(X)	modifiedArrheniusGasTemp	1	1.905E-42	-1	-170
2O(3P) + O2(X) ->O2(X) + O2(a1Dg)	modifiedArrheniusGasTemp	1	1.2573E-42	-1	-170
2O(3P) + O2(X) ->O2(X) + O2(b1Sg+)	modifiedArrheniusGasTemp	1	6.477E-43	-1	-170
O(3P) + O2(X,v=0) + O3(X) ->2O3(X)	expGasTemp	1	1.66E-46	300	
3O(3P) ->O2(X,v=0) + O(3P)	powerGasTemp	1	3.60E-44	-0.63	
O2(a1Dg) + O2(X) ->O2(X,v=0) + O2(X)	powerGasTemp	1	2.2947E-26	0.8	
O(-,gnd) + O2(a1Dg) ->O3(X) + e	constantRateCoeff	1	1.425E-16		
O(-,gnd) + O(3P) ->O2(X,v=0) + e	constantRateCoeff	1	1.30E-15		
O(-,gnd) + O2(X,v=0) ->O3(X) + e	constantRateCoeff	1	1.00E-18		
O(-,gnd) + O2(b1Sg+) ->O(3P) + O2(X,v=0) + e	constantRateCoeff	1	6.90E-16		
O(+,gnd) + O(-,gnd) ->2O(3P)	constantRateCoeff	1	2.80E-13		
O(+,gnd) + O3(X) ->O2(+,X) + O2(X,v=0)	constantRateCoeff	1	1.00E-16		
O(+,gnd) + O2(X,v=0) ->O2(+,X) + O(3P)	powerGasTemp	1	3.4641E-16	-0.5	
O(+,gnd) + O2(a1Dg) ->O2(+,X) + O(3P)	powerGasTemp	1	3.4641E-16	-0.5	

Table D.1 continued from previous page

Reactions	Function	Φ	A	B	C
O2(+,X) + O(-,gnd) ->O2(X,v=0) + O(3P)	powerGasTemp	1	1.66277E-12	-0.5	
%— Ion transport —-					
O2(+,X) + wall ->O2(X,v=0)	classicalAmbipolarDiff	1	1		
O(+,gnd) + wall ->O(3P)	classicalAmbipolarDiff	1	1		
%— Neutral transport —-					
O2(a1Dg) + wall ->O2(X,v=0)	gasOnGasDiffOxygen	1	2.00E-05		
O2(b1Sg+) + wall ->O2(X,v=0)	gasOnGasDiffOxygen	1	2.00E-02		
O(3P) + wall ->0.5O2(X,v=0)	gasOnGasDiffOxygen	1	4.60E-04		
O(1D) + wall ->O(3P)	gasOnGasDiffOxygen	1	1.00E+00		
O3(exc) + wall ->O3(X)	gasOnGasDiffOxygen	1	1.00E-01		
%— Electron impact processes considered from O2(X, v>0) —					
e + O2(X,v=1:41) ->2e + O2(+,X)	rateCoeffCopy	e + O2(X,v=0) ->2e + O2(+,X)			
e + O2(X,v=1:41) ->e + 2O(3P)	laportaScalingLaw	EID1			
e + O2(X,v=1:41) ->e + O(3P) + O(1D)	rateCoeffCopy	e + O2(X,v=0) ->e + O(3P) + O(1D)			
e + O2(X,v=1:6) ->e + O2(a1Dg)	eedfFactor	1			
e + O2(X,v=1:8) ->e + O2(b1Sg+)	eedfFactor	1			
e + O2(X,v=1:41) ->O(3P) + O(-,gnd)	laportaScalingLaw	DEA			
%— Vibrational excitation by electron impact —					
e + O2(X,v=0:40) <->e + O2(X,v=41)	eedfFactor	1			

Table D.1 continued from previous page

Reactions	Function	Φ	A	B	C
e + O2(X,v=0:39) <->e + O2(X,v=40)	eedfFactor	1			
e + O2(X,v=0:38) <->e + O2(X,v=39)	eedfFactor	1			
e + O2(X,v=0:37) <->e + O2(X,v=38)	eedfFactor	1			
e + O2(X,v=0:36) <->e + O2(X,v=37)	eedfFactor	1			
e + O2(X,v=0:35) <->e + O2(X,v=36)	eedfFactor	1			
e + O2(X,v=0:34) <->e + O2(X,v=35)	eedfFactor	1			
e + O2(X,v=0:33) <->e + O2(X,v=34)	eedfFactor	1			
e + O2(X,v=0:32) <->e + O2(X,v=33)	eedfFactor	1			
e + O2(X,v=0:31) <->e + O2(X,v=32)	eedfFactor	1			
e + O2(X,v=0:30) <->e + O2(X,v=31)	eedfFactor	1			
e + O2(X,v=0:29) <->e + O2(X,v=30)	eedfFactor	1			
e + O2(X,v=0:28) <->e + O2(X,v=29)	eedfFactor	1			
e + O2(X,v=0:27) <->e + O2(X,v=28)	eedfFactor	1			
e + O2(X,v=0:26) <->e + O2(X,v=27)	eedfFactor	1			
e + O2(X,v=0:25) <->e + O2(X,v=26)	eedfFactor	1			
e + O2(X,v=0:24) <->e + O2(X,v=25)	eedfFactor	1			
e + O2(X,v=0:23) <->e + O2(X,v=24)	eedfFactor	1			
e + O2(X,v=0:22) <->e + O2(X,v=23)	eedfFactor	1			
e + O2(X,v=0:21) <->e + O2(X,v=22)	eedfFactor	1			
e + O2(X,v=0:20) <->e + O2(X,v=21)	eedfFactor	1			
e + O2(X,v=0:19) <->e + O2(X,v=20)	eedfFactor	1			
e + O2(X,v=0:18) <->e + O2(X,v=19)	eedfFactor	1			
e + O2(X,v=0:17) <->e + O2(X,v=18)	eedfFactor	1			

Table D.1 continued from previous page

Reactions	Function	Φ	A	B	C
e + O2(X,v=0:16) <->e + O2(X,v=17)	eedfFactor	1			
e + O2(X,v=0:15) <->e + O2(X,v=16)	eedfFactor	1			
e + O2(X,v=0:14) <->e + O2(X,v=15)	eedfFactor	1			
e + O2(X,v=0:13) <->e + O2(X,v=14)	eedfFactor	1			
e + O2(X,v=0:12) <->e + O2(X,v=13)	eedfFactor	1			
e + O2(X,v=0:11) <->e + O2(X,v=12)	eedfFactor	1			
e + O2(X,v=0:10) <->e + O2(X,v=11)	eedfFactor	1			
e + O2(X,v=0:9) <->e + O2(X,v=10)	eedfFactor	1			
e + O2(X,v=0:8) <->e + O2(X,v=9)	eedfFactor	1			
e + O2(X,v=0:7) <->e + O2(X,v=8)	eedfFactor	1			
e + O2(X,v=0:6) <->e + O2(X,v=7)	eedfFactor	1			
e + O2(X,v=0:5) <->e + O2(X,v=6)	eedfFactor	1			
e + O2(X,v=0:4) <->e + O2(X,v=5)	eedfFactor	1			
e + O2(X,v=0:3) <->e + O2(X,v=4)	eedfFactor	1			
e + O2(X,v=0:2) <->e + O2(X,v=3)	eedfFactor	1			
e + O2(X,v=0:1) <->e + O2(X,v=2)	eedfFactor	1			
e + O2(X,v=0) <->e + O2(X,v=1)	eedfFactor	1			
%— Molecular V-T processes —					
O2(X,v=1:41) + O2(X) <->O2(X,v=v-1) + O2(X)	oxygenMolecularVT	1			
O2(X,v=41) + O2(X) ->2O(1D) + O2(X)	oxygenMolecularVTDiss	1			
%— Atomic V-T processes —					

Table D.1 continued from previous page

Reactions	Function	Φ	A	B	C
O2(X,v=1:41) + O(3P) <->O2(X,w=v-1) + O(3P)	oxygenAtomicVT	1			
O2(X,v=2:41) + O(3P) <->O2(X,w=v-2) + O(3P)	oxygenAtomicVT	1			
O2(X,v=3:41) + O(3P) <->O2(X,w=v-3) + O(3P)	oxygenAtomicVT	1			
O2(X,v=4:41) + O(3P) <->O2(X,w=v-4) + O(3P)	oxygenAtomicVT	1			
O2(X,v=5:41) + O(3P) <->O2(X,w=v-5) + O(3P)	oxygenAtomicVT	1			
O2(X,v=6:41) + O(3P) <->O2(X,w=v-6) + O(3P)	oxygenAtomicVT	1			
O2(X,v=7:41) + O(3P) <->O2(X,w=v-7) + O(3P)	oxygenAtomicVT	1			
O2(X,v=8:41) + O(3P) <->O2(X,w=v-8) + O(3P)	oxygenAtomicVT	1			
O2(X,v=9:41) + O(3P) <->O2(X,w=v-9) + O(3P)	oxygenAtomicVT	1			
O2(X,v=10:41) + O(3P) <->O2(X,w=v-10) + O(3P)	oxygenAtomicVT	1			
O2(X,v=11:41) + O(3P) <->O2(X,w=v-11) + O(3P)	oxygenAtomicVT	1			
O2(X,v=12:41) + O(3P) <->O2(X,w=v-12) + O(3P)	oxygenAtomicVT	1			
O2(X,v=13:41) + O(3P) <->O2(X,w=v-13) + O(3P)	oxygenAtomicVT	1			
O2(X,v=14:41) + O(3P) <->O2(X,w=v-14) + O(3P)	oxygenAtomicVT	1			
O2(X,v=15:41) + O(3P) <->O2(X,w=v-15) + O(3P)	oxygenAtomicVT	1			
O2(X,v=16:41) + O(3P) <->O2(X,w=v-16) + O(3P)	oxygenAtomicVT	1			
O2(X,v=17:41) + O(3P) <->O2(X,w=v-17) + O(3P)	oxygenAtomicVT	1			
O2(X,v=18:41) + O(3P) <->O2(X,w=v-18) + O(3P)	oxygenAtomicVT	1			
O2(X,v=19:41) + O(3P) <->O2(X,w=v-19) + O(3P)	oxygenAtomicVT	1			
O2(X,v=20:41) + O(3P) <->O2(X,w=v-20) + O(3P)	oxygenAtomicVT	1			
O2(X,v=21:41) + O(3P) <->O2(X,w=v-21) + O(3P)	oxygenAtomicVT	1			
O2(X,v=22:41) + O(3P) <->O2(X,w=v-22) + O(3P)	oxygenAtomicVT	1			
O2(X,v=23:41) + O(3P) <->O2(X,w=v-23) + O(3P)	oxygenAtomicVT	1			

Table D.1 continued from previous page

Reactions	Function	Φ	A	B	C
O2(X,v=24:41) + O(3P) <->O2(X,w=v-24) + O(3P)	oxygenAtomicVT	1			
O2(X,v=25:41) + O(3P) <->O2(X,w=v-25) + O(3P)	oxygenAtomicVT	1			
O2(X,v=26:41) + O(3P) <->O2(X,w=v-26) + O(3P)	oxygenAtomicVT	1			
O2(X,v=27:41) + O(3P) <->O2(X,w=v-27) + O(3P)	oxygenAtomicVT	1			
O2(X,v=28:41) + O(3P) <->O2(X,w=v-28) + O(3P)	oxygenAtomicVT	1			
O2(X,v=29:41) + O(3P) <->O2(X,w=v-29) + O(3P)	oxygenAtomicVT	1			
O2(X,v=30:41) + O(3P) <->O2(X,w=v-30) + O(3P)	oxygenAtomicVT	1			
O2(X,v=1:41) + O(1D) <->O2(X,w=v-1) + O(1D)	oxygenAtomicVT	1			
O2(X,v=2:41) + O(1D) <->O2(X,w=v-2) + O(1D)	oxygenAtomicVT	1			
O2(X,v=3:41) + O(1D) <->O2(X,w=v-3) + O(1D)	oxygenAtomicVT	1			
O2(X,v=4:41) + O(1D) <->O2(X,w=v-4) + O(1D)	oxygenAtomicVT	1			
O2(X,v=5:41) + O(1D) <->O2(X,w=v-5) + O(1D)	oxygenAtomicVT	1			
O2(X,v=6:41) + O(1D) <->O2(X,w=v-6) + O(1D)	oxygenAtomicVT	1			
O2(X,v=7:41) + O(1D) <->O2(X,w=v-7) + O(1D)	oxygenAtomicVT	1			
O2(X,v=8:41) + O(1D) <->O2(X,w=v-8) + O(1D)	oxygenAtomicVT	1			
O2(X,v=9:41) + O(1D) <->O2(X,w=v-9) + O(1D)	oxygenAtomicVT	1			
O2(X,v=10:41) + O(1D) <->O2(X,w=v-10) + O(1D)	oxygenAtomicVT	1			
O2(X,v=11:41) + O(1D) <->O2(X,w=v-11) + O(1D)	oxygenAtomicVT	1			
O2(X,v=12:41) + O(1D) <->O2(X,w=v-12) + O(1D)	oxygenAtomicVT	1			
O2(X,v=13:41) + O(1D) <->O2(X,w=v-13) + O(1D)	oxygenAtomicVT	1			
O2(X,v=14:41) + O(1D) <->O2(X,w=v-14) + O(1D)	oxygenAtomicVT	1			
O2(X,v=15:41) + O(1D) <->O2(X,w=v-15) + O(1D)	oxygenAtomicVT	1			
O2(X,v=16:41) + O(1D) <->O2(X,w=v-16) + O(1D)	oxygenAtomicVT	1			

Table D.1 continued from previous page

Reactions	Function	Φ	A	B	C
O2(X,v=17:41) + O(1D) <->O2(X,w=v-17) + O(1D)	oxygenAtomicVT	1			
O2(X,v=18:41) + O(1D) <->O2(X,w=v-18) + O(1D)	oxygenAtomicVT	1			
O2(X,v=19:41) + O(1D) <->O2(X,w=v-19) + O(1D)	oxygenAtomicVT	1			
O2(X,v=20:41) + O(1D) <->O2(X,w=v-20) + O(1D)	oxygenAtomicVT	1			
O2(X,v=21:41) + O(1D) <->O2(X,w=v-21) + O(1D)	oxygenAtomicVT	1			
O2(X,v=22:41) + O(1D) <->O2(X,w=v-22) + O(1D)	oxygenAtomicVT	1			
O2(X,v=23:41) + O(1D) <->O2(X,w=v-23) + O(1D)	oxygenAtomicVT	1			
O2(X,v=24:41) + O(1D) <->O2(X,w=v-24) + O(1D)	oxygenAtomicVT	1			
O2(X,v=25:41) + O(1D) <->O2(X,w=v-25) + O(1D)	oxygenAtomicVT	1			
O2(X,v=26:41) + O(1D) <->O2(X,w=v-26) + O(1D)	oxygenAtomicVT	1			
O2(X,v=27:41) + O(1D) <->O2(X,w=v-27) + O(1D)	oxygenAtomicVT	1			
O2(X,v=28:41) + O(1D) <->O2(X,w=v-28) + O(1D)	oxygenAtomicVT	1			
O2(X,v=29:41) + O(1D) <->O2(X,w=v-29) + O(1D)	oxygenAtomicVT	1			
O2(X,v=30:41) + O(1D) <->O2(X,w=v-30) + O(1D)	oxygenAtomicVT	1			
O2(X,v=12:41) + O(3P) ->2O(1D) + O(3P)	oxygenAtomicVT	1			
O2(X,v=12:41) + O(1D) ->3O(1D)	oxygenAtomicVT	1			
%— Molecular V-V processes —					
O2(X,v=1:40) + O2(X,w=v:40) <->O2(X,v=v-1) + O2(X,v=w+1)	oxygenMolecularVV	1			
O2(X,v=1:40) + O2(X,w=41) ->O2(X,v=v-1) + 2O(1D)	oxygenMolecularVV	1			
%— Wall vibrational de-excitation —					
O2(X,v=1:41) + wall ->O2(X,v=v-1)	oxygenVibDeExcWall	1			

List of Tables

List of Figures